Acoustic Classification of Zooplankton

by

Linda V. Martin Traykovski

B.A.Sc. Systems Design Engineering, University of Waterloo, 1990

Submitted in Partial Fulfillment of the Requirements for the Degree of

DOCTOR OF PHILOSOPHY

at the

Massachusetts Institute of Technology
and the
Woods Hole Oceanographic Institution

February 1998

Signature of Author.....

Joint Program in Biological Oceanography
Massachusetts Institute of Technology and
Woods Hole Oceanographic Institution

Certified by.....

.....
Timothy K. Stanton, Chairman
Department of Applied Ocean Physics and Engineering
Woods Hole Oceanographic Institution
Thesis Advisor

Certified by.....

.....
Peter H. Wiebe
Biology Department
Woods Hole Oceanographic Institution
Thesis Advisor

Accepted by.....

Mark E. Hahn, Chairman
Joint Committee in Biological Oceanography
MIT/WHOI Joint Program in Oceanography and Oceanographic Engineering

Acoustic Classification of Zooplankton

by

Linda V. Martin Traykovski

Submitted on December 19, 1997 in Partial Fulfillment of
the Requirements for the Degree of Doctor of Philosophy

ABSTRACT

Work on the forward problem in zooplankton bioacoustics has resulted in the identification of three categories of acoustic scatterers: elastic-shelled (e.g. pteropods), fluid-like (e.g. euphausiids), and gas-bearing (e.g. siphonophores). The relationship between backscattered energy and animal biomass has been shown to vary by a factor of ~19,000 across these categories, so that to make accurate estimates of zooplankton biomass from acoustic backscatter measurements of the ocean, the acoustic characteristics of the species of interest must be well-understood. This thesis describes the development of both feature based and model based classification techniques to invert broadband acoustic echoes from individual zooplankton for scatterer type, as well as for particular parameters such as animal orientation. The feature based Empirical Orthogonal Function Classifier (EOFC) discriminates scatterer types by identifying characteristic modes of variability in the echo spectra, exploiting only the inherent characteristic structure of the acoustic signatures. The model based Model Parameterisation Classifier (MPC) classifies based on correlation of observed echo spectra with simplified parameterisations of theoretical scattering models for the three classes. The Covariance Mean Variance Classifiers (CMVC) are a set of advanced model based techniques which exploit the full complexity of the theoretical models by searching the entire physical model parameter space without employing simplifying parameterisations. Three different CMVC algorithms were developed: the Integrated Score Classifier (ISC), the Pairwise Score Classifier (PSC) and the Bayesian Probability Classifier (BPC); these classifiers assign observations to a class based on similarities in covariance, mean, and variance, while accounting for model ambiguity and validity. These feature based and model based inversion techniques were successfully applied to several thousand echoes acquired from broadband (~350 kHz - 750 kHz) insonifications of live zooplankton collected on Georges Bank and the Gulf of Maine to determine scatterer class. CMVC techniques were also applied to echoes from fluid-like zooplankton (Antarctic krill) to invert for angle of orientation using generic and animal-specific theoretical and empirical models. Application of these inversion techniques *in situ* will allow correct apportionment of backscattered energy to animal biomass, significantly improving estimates of zooplankton biomass based on acoustic surveys.

TABLE OF CONTENTS

LIST OF FIGURES

CHAPTER 1

THE CLASSIFICATION PROBLEM

Accurate acoustic characterisation of zooplankton species is essential if reliable estimates of zooplankton biomass are to be made from acoustic backscatter measurements of the water column. Much work has recently been done on the forward problem, where scattering predictions have been made based on animal morphology. Three categories of scatterers (Figure 1-1), represented by theoretical scattering models, have been identified by Stanton *et al.* (1994a):

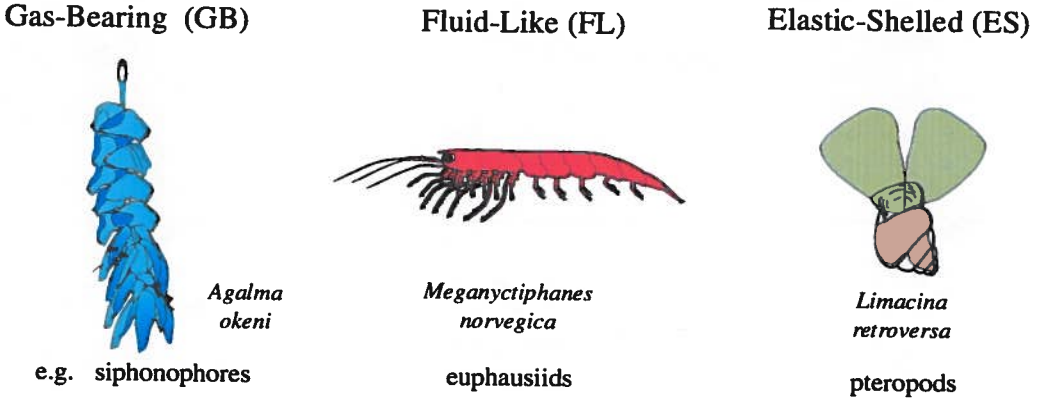

Figure 1-1 Examples of three acoustic scattering types, each represented by a theoretical scattering model.

The characteristic acoustic signature of each of these classes of zooplankton is unique. As a result, it is possible to invert acoustic backscatter data for the class of scatterer. The material properties of species within a scattering class are similar, leading to a relationship between scattering class and animal biomass. Solving the "inverse problem" of identifying a scatterer from its acoustic signature will enable biological oceanographers to make more reliable estimates of zooplankton biomass from acoustic backscatter data.

The thesis work described herein encompasses the development of a classification scheme for inverting acoustic backscatter data for organism type, leading to the identification of marine zooplankton by their acoustic signatures (Figure 1-2). Central to this objective is the development of classification algorithms that exploit unique features of the acoustic signatures for each class. To ensure the development of robust classifiers, an investigation of the effect of animal orientation on acoustic signature is undertaken. The product of this thesis research is an assemblage of classification techniques evaluated in terms of their performance with experimental data, as well as a brief outline of some guidelines for classifier implementation and indications for future work.

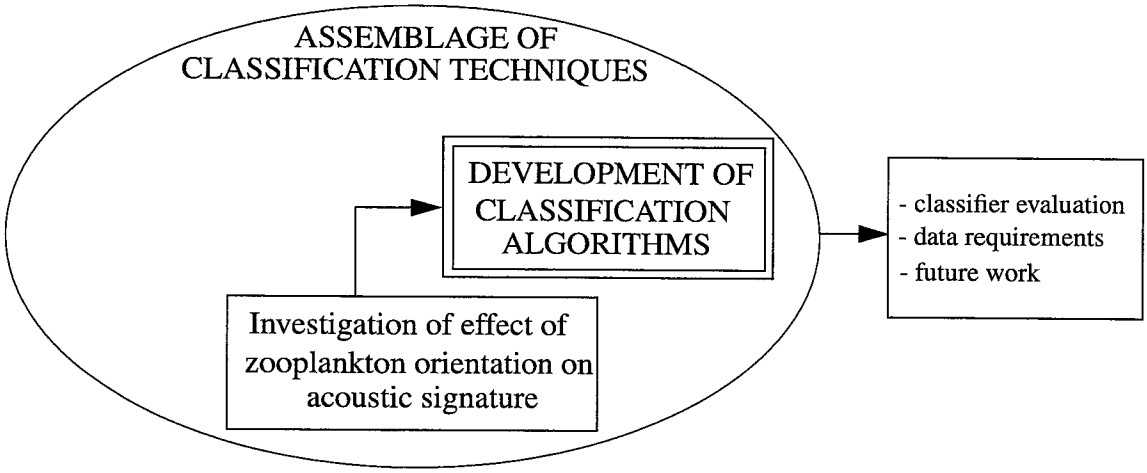

Figure 1-2 Scope of this thesis work.

1.1 BACKGROUND

1.1.1 ZOOPLANKTON BIOMASS ESTIMATION

Marine zooplankton influence the global carbon cycle since they play a critical role in determining the flux of nutrients and carbon from the upper mixed layer to depth (Smith *et al.* 1992). They also serve as a principal food source for most of the commercially important fish species, particularly during the larval stages (Turner 1984). Consequently, accurate knowledge of zooplankton distribution, abundance and production is necessary in order to understand the global biological pump as well as to characterise the trophic interactions between commercial fish species and their prey. For example, to quantitatively assess the amount of food available to a particular fish stock, accurate estimates of zooplankton biomass are essential. Conventional methods for estimating zooplankton biomass include measurement of displacement volume (Yentsch and Hebard 1957 cited in Wiebe *et al.* 1975), wet weight (Nakai and Honjo 1962 cited in Wiebe *et al.* 1975), dry weight (Lovegrove 1966 cited in Wiebe *et al.* 1975) or carbon (Curl 1962 cited in Wiebe *et al.* 1975) from net (e.g. MOCNESS - Wiebe *et al.* 1985) or pump (Miller and Judkins 1981) samples. As a result of the spatial patchiness of zooplankton populations in the ocean and extreme temporal variability in their abundance, it is estimated that biomass can vary over seven orders of magnitude on the spatial and temporal scales important for populations of macrozooplankton (Huntley and Lopez 1992). This magnitude of spatial and temporal variability is particularly troublesome, since conventional techniques for biomass estimation (nets, pumps, trawls) are not suited for simultaneous sampling of the entire water column over the relevant scales. To make more accurate

biomass estimates, high resolution instruments (~1 m) capable of mapping variation in zooplankton biomass on large vertical (10 - 100 m), horizontal (1 - 10 km) and temporal (days to months) scales are required. The use of high-frequency acoustics to make volume backscatter measurements of the water column has recently made it possible to do rapid, high-resolution, broad-scale synoptic surveys of zooplankton abundance over the time and space scales of interest (Greenlaw 1979).

The acoustic characterisation of various species of zooplankton is essential if biologists wish to use volume backscatter measurements of the ocean as indicators of zooplankton biomass. Traditional acoustic biomass estimation methods have employed an empirical conversion from acoustic scattering strength (at a single frequency) to biomass, relying on regression relationships between the acoustic backscatter data and the biomass collected in simultaneous net samples. For example, Flagg and Smith (1989a, 1989b) used data from a 307 kHz (1989a, 1989b) or a 150 kHz (1989b) ADCP (Acoustic Doppler Current Profiler) in correlation with simultaneously acquired MOCNESS (Multiple Opening / Closing Net and Environmental Sensing System) data to make biomass estimates of New England Shelf zooplankton populations; they claim these estimates are accurate to within ~ 15 mg/m^3 (10 - 40%). Greenlaw (1979) pointed out that biomass estimates made in this manner are subject to all the shortcomings of the net sampling technique (size and species specificity, avoidance, inability to sample over relevant scales). For a single, known size class of animals, or for a monospecific population of known size distribution, single-frequency acoustic measures have been used in conjunction with the fluid sphere model to make biomass estimates (Greenlaw 1979). However, observations of the biota will be largely influenced by the choice of acoustic frequency (Holliday 1980). In addition, oceanic zooplankton populations often consist of multiple-species assemblages of different sized organisms with drastically different acoustic scattering properties. For these reasons, biomass estimates based on simple regression curves to net data or single-frequency echo energy measurements will be subject to large errors. For example, Wiebe *et al.* (1996) found that although the volume backscattering was 4 to 7 times higher at two stratified sites as compared with a mixed site on Georges Bank, MOCNESS-collected biovolumes at these sites were not significantly different. Greenlaw (1979) noted that the volume scattering from a region containing a single 22 mm fish, which has a gas inclusion, is the same as that from a region containing 260 similar-sized euphausiids, which are fluid-like, weak scatterers. In fact, Stanton *et al.* (1994a) observed that the relative echo energy per unit of biomass measured from a variety of animals ranging from elastic-shelled gastropods to fluid-like salps

varies by a factor of ~19,000 to 1. This huge species-dependent variability in echo energy per unit biomass has important implications for the interpretation of acoustic survey data. Attempts to equate larger acoustic returns to the presence of more or larger animals and thereby conclude that the higher the echo energy, the greater the biomass in the insonified region, could lead to gross errors in biomass estimates by several orders of magnitude (Stanton *et al.* 1994a).

Much effort has been put toward characterising the acoustic target strength of zooplankton for the purposes of species identification, animal size classification, abundance estimation and acoustic signal separation. In fact, the echo integration method for acoustic biomass estimation, which measures the acoustic backscatter from a volume of water which may contain multiple scatterers, relies on accurate knowledge of the species of scatterers in the insonified volume and their respective scattering characteristics. Some attempts have been made to bridge the gap between acoustic backscatter measurements of the water column and the animal biomass present, while accounting for the vast species differences in scattering strength per unit biomass. Stanton *et al.* (1987) used existing theoretical and empirical scattering models for different classes of zooplankton in combination with the species composition in net tows to predict the expected acoustic backscatter over a transect in the Gulf Stream, and compared this prediction to the measured acoustic backscatter; the predictions were to within an order of magnitude of the measured values for samples with lower volume scattering strengths, but the agreement was poor for samples with higher scattering strengths, probably as a result of net avoidance and/or failure to account for the poorly sampled siphonophore biomass. Wiebe *et al.* (1996) performed a similar analysis on data from Georges Bank using more recently developed theoretical scattering models, and found reasonable agreement between observed and predicted values, to within about 4 dB. These studies have demonstrated that a solid understanding of the dependence of zooplankton target strength on animal size, shape, material properties and orientation is necessary to convert integrated backscattered energy to numerical densities and apportion these densities to individual species of zooplankton, thereby obtaining an estimate of biomass in the water column.

1.1.2 THE FORWARD PROBLEM

The solution to the **forward problem** involves **predicting the properties of the acoustic return from a scatterer** based on knowledge of the physical and geometric properties of the scatterer as well as the specifications of the sonar system used to insonify it. Most of the progress in zooplankton bioacoustics has been made in this area, via the development of both theoretical and

empirical models which describe the scattering from these animals in terms of their morphology and material properties. Various theoretical models have been developed to predict acoustic scattering from zooplankton based on animal morphology. Initially, scattering from all zooplankton (including elongated and elastic-shelled organisms) was modelled using the Anderson fluid sphere model (Anderson 1950). Greenlaw (1977, 1979) used the Johnson (1977) fluid sphere model (a simplified version of the Anderson model) for euphausiids and sergestid shrimp at dorsal, ventral and side aspects. Alternatively, Penrose and Kaye (1979) used a Love empirical formula, originally developed to model the backscattering cross-section of fish (Love 1977), to describe the scattering from elongated zooplankton. Comparison of backscatter data with the predictions of these models led to the conclusion that the fluid-sphere model does not adequately describe the scattering from elongated zooplankton such as euphausiids and shrimp (Stanton 1990a). The first scattering model to account for the elongate and deformable morphology of some of the crustacean zooplankton was developed by Stanton (1988a,b and 1989a). These models are based on the modal series solution for an incident plane wave, and describe the scattering of sound by arbitrarily deformed cylinders of finite length. To overcome the computational difficulties of calculating the exact scattered field via the modal series solution, Stanton (1989b) refined and generalised Johnson's (1977) approach of combining the low- and high-frequency asymptotic limits of the modal series to provide a continuous juncture of the two solutions, thereby obtaining simple closed form solutions for the sphere, prolate spheroid, straight finite cylinder and bent finite cylinder.

Although these "high-pass" models were useful for making quick estimates of target strength for objects of various geometries (including zooplankton), and could roughly model some of the null structure via empirical adjustment of certain parameters, these were not exact solutions and failed to accurately account for the modal interferences in the geometric region ($ka>1$). For zooplankton such as siphonophores (which have an approximately spherical gas inclusion) the full modal series solution for a gas-filled sphere described in Stanton *et al.* (in press b) is a better descriptor of the scattering from the siphonophore gas inclusion than is the gas sphere high-pass model. Another shortcoming of the high-pass models is that they are only applicable for normal or near-normal incidence of the sound wave (broadside incidence) for the elongated geometries (Stanton 1989b). Recently, Chu *et al.* (1993) and Stanton *et al.* (1993b) developed the deformed finite cylinder model for a distribution of animal orientations using the DWBA (distorted wave Born approximation). Since many crustacean zooplankton behave acoustically as weakly scattering bent fluid cylinders, Stanton *et al.* (1993a,b and 1994b) described them acoustically at normal incidence

and at a distribution of orientations using a ray summation model. This ray-based solution is approximate, but it accounts for the null structure observed in empirically collected data for ka>1. It was demonstrated that a simple solution including a summation of only two rays (which models the constructive and destructive interference between the rays reflected from the front and back interfaces of the weakly scattering target) agrees very well with the exact modal series solution, accounts for empirically observed null structure (particularly when the target is near broadside incidence), and has the advantage of being computationally manageable (Stanton *et al.* 1993a,b). Stanton *et al.* (1994b) included six rays (which can account for scattering contributions from other parts of the animal) in the summation to better model pings exhibiting more erratic null structures. It was determined that even a chaotic signal (e.g. white noise or that due to turbulence microstructure) can be adequately modelled by as few as six randomised rays (Stanton *et al.* 1994b).

For hard elastic-shelled organisms (e.g. gastropods), the exact modal series solution is outlined in Stanton (1990b) with coefficients specific to the material composition, as specified by Goodman and Stern (1962 *cited in* Stanton 1990b). To simplify the numerical computations, Stanton *et al.* (1994a) applied a high-pass model for dense fluid spheres to describe the scattering from spherical elastic-shelled organisms. This model assumes that scattering from the organism is dominated by the echo from the front interface of the body. Since the body is irregular with discontinuities, this formulation is not sufficient to explain the scattering of these organisms at all angles of incidence. Furthermore, it is not capable of predicting echo spectrum structure resulting from sound incident on the elastic shell. For the case where the incident sound hits the shell, Stanton *et al.* (in press b) have developed a ray-based formulation based on Marston (1988) that accounts for both the direct return and one type of Lamb wave, as well as shell roughness and discontinuities. The Lamb wave travels circumferentially around the shell and sheds energy in all directions. This model accounts for the interference between the direct-return ray from the body and the energy shed in the backscatter direction from the circumferential wave.

To develop and corroborate scattering models, target strength measurements have been made of zooplankton, both experimentally constrained (e.g. Greenlaw 1977, Kristensen and Dalen 1986, Wiebe *et al.* 1990, Foote *et al.* 1990, Demer and Martin 1995) and *in situ* (e.g. Hewitt and Demer 1991, Foote 1991). Most of these measurements were taken at a single frequency, or a small number of discrete frequencies, and although they provide information about the scattering

strength of the organisms, it was not possible to quantify the frequency dependence of the scattering over a continuous range of frequencies with these types of measurements. Recently, Chu *et al.* (1992) were able to insonify the decapod shrimp (*Palaemonetes vulgaris*) with a broad spectrum of frequencies simultaneously using a broadband chirp sonar. Analysis of the broadband echoes from these fluid-like animals revealed a pronounced structure in the frequency response of the target strength, with deep nulls (30 dB) at certain frequencies. Following this work, Stanton *et al.* (1994a) have been making target strength measurements of single organisms over a broad range of frequencies simultaneously by insonifying tethered zooplankton with broadband chirps. Several representatives from each of three scattering classes have been insonified in this manner, demonstrating that the frequency response is characteristic of the scatterer class.

1.1.3 THE INVERSE PROBLEM

The **inverse problem** is concerned with **predicting the properties of the scatterer** based on knowledge of the acoustic return from that object. The solution to this inverse problem has been investigated for several applications within the discipline of acoustical oceanography. The geoacoustic properties of the ocean bottom have been deduced by inverting both narrow-band and broadband acoustic returns in the water column for the compressional wave speed in the bottom (e.g. Lynch *et al.* 1991), using an inverse technique described by Rajan *et al.* (1987). Undersea seismic activity (volcanic eruptions, earthquakes) has been detected and analysed, using acoustic signals to solve the inverse problem (Fox *et al.* 1994). Munk and Wunsch (1979) proposed a scheme for monitoring the mesoscale variability of the ocean basins using an acoustic tomographic inverse. With this type of inverse, the physical properties of the water column (e.g. temperature) can be measured by inverting acoustic wave travel time perturbations for sound speed in the ocean (Brown 1984). Chiu *et al.* (1987) used acoustic tomographic inverses to elucidate the dynamics of ocean circulation by resolving mesoscale eddies in the marginal ice zone. Preliminary work on the inversion of acoustic data for the temperature field of turbulence microstructure has been carried out in a laboratory tank setting by Goodman *et al.* (1992). In bioacoustical oceanography, work is beginning to identify and track baleen whales remotely by inverting received acoustic signals for species, and in some cases, individual animal identification (Nishimura and Conlon 1994). Some work has been done on identifying individual fish and fish schools from both single-frequency and multiple frequency acoustic returns (e.g. Deuser *et al.* 1979, Zakharia and Sessarego 1982, Vray *et al.* 1990, Lebourges 1990, Scalabrin *et al.* 1996,

Simmonds *et al.* 1996). Holliday *et al.* (1989) have estimated the size distribution of a zooplankton assemblage based on volume scattering data from a multi-frequency sonar system using several discrete frequencies.

If the solution to the forward problem is known, the inverse problem for a linear system may be solved using a standard general inversion technique that has been described in several works on inverse theory (Backus and Gilbert 1967, Aki and Richards 1980, Menke 1989). The general formulation for a linear system expresses the observed data as a linear combination of the model parameters weighted by the kernel, which represents the solution to the forward problem. The solution to the inverse problem involves solving for the model parameters that, once weighted by the kernel, best predict the observed data. There exist other means by which acoustic backscatter data may be inverted for scatterer class identification. For example, the features of the acoustic signatures of each scattering class can be exploited in a pattern recognition scheme, which matches the features of a novel dataset to known features of a scattering class.

To perform an inversion of an acoustic return for the scatterer properties (Figure 1-3), acoustic sampling of the ocean must be broadband. This can be accomplished either by using many discrete frequencies, e.g. MAPS (Multifrequency Acoustic Profiling System), which uses 21 frequencies from 0.1-10 MHz (Pieper *et al.* 1990), or a broadband chirp (Chu *et al.* 1992). *A priori* information may be obtained via simultaneous net samples, which can provide species composition and size class information, and/or VPR (Video Plankton Recorder) samples, which can provide some species composition data as well as orientational information. The echoes obtained from the acoustic sampling are initially represented as a time series of voltage levels. Echo integration may be performed to determine the volume backscattered energy and obtain a calibrated echogram.

If the range of sampling frequencies brackets the turning point between the Rayleigh regime and the geometric regime for the particular sample, then a non-linear NNLS (Non-Negative Least Squares (Holliday *et al.* 1989)) inverse can be performed yielding a histogram of the absolute number of scatterers in each size class. This type of inversion, where the model parameters are the number of individuals in each size class, lends itself to the classical inversion formulation described in (EQ 3.8). Holliday *et al.* (1989), Pieper *et al.* (1990), Holliday (1980), Holliday and Pieper (1980 cited in Pieper *et al.* 1990) and Pieper (1983 cited in Pieper *et al.* 1990) used this technique on MAPS data to make biomass estimates of zooplankton; the accuracy of these estimates not known. Their NNLS algorithm assumes that the scattering by the targets is described

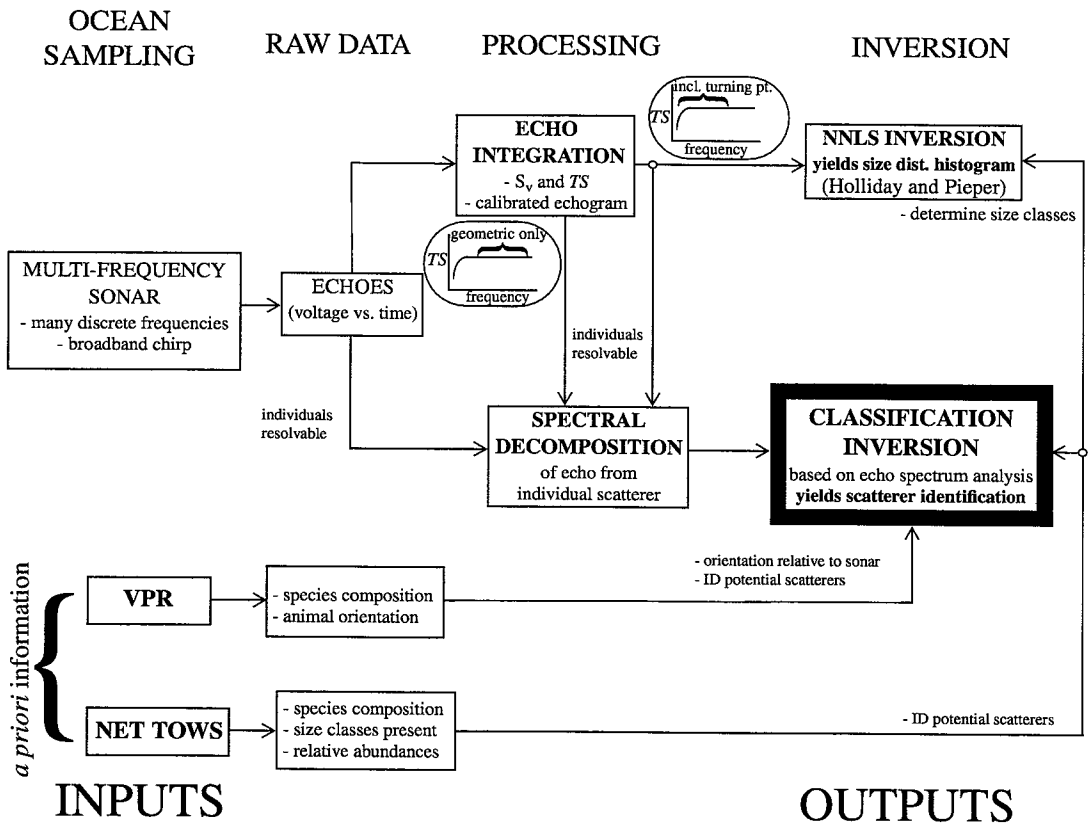

Figure 1-3 Some approaches to solving the inverse problem for zooplankton, based on ideas from Stanton.

by a truncated version of Anderson's fluid sphere model (Holliday *et al.* 1989), so that the size-distribution histogram is in terms of the equivalent spherical radii of the zooplankton; this assumption is not valid for predicting scattering from elongated zooplankton. Holliday (1977) presents a mathematical formulation of the NNLS inversion that can account for animals of different scattering properties and possibly geometries, but notes that the available scattering models upon which this type of inversion is based will often be inadequate. The results of the Holliday/Pieper NNLS inversion are also very sensitive to the choice of size classes used in the inversion, and accurate *a priori* information from net or pump samples (which may be subject to avoidance and size- and species- selectivity (Holliday *et al.* 1989)) is important for choosing the appropriate size classes for a given dataset. If individual scatterers are not resolvable in the dataset, this type of inversion may be the only possibility.

In the case where the echoes from individual zooplankton are resolvable and the acoustic sampling includes a broadband signal with a continuous (or virtually continuous) range of frequencies, a different type of inversion is possible. A spectral decomposition may be performed on the echo

time series from each individual scatterer, and the zooplankton may be classified according to their frequency-dependent scattering characteristics. This type of classification inversion aims to identify individual scatterers from their acoustic signatures, and can be carried out with or without relying on theoretical scattering models. The development of a classification inversion of marine zooplankton based on single-ping broadband insonifications is the basis for this thesis work.

1.2 APPROACH

The principal objective of this thesis work is to develop a classification scheme that will identify marine zooplankton by their acoustic signatures, allowing biologists to correctly apportion backscattered acoustic energy to individual scattering classes of zooplankton, thereby obtaining an accurate estimate of biomass in the water column. Central to this objective is the development of classification algorithms that exploit unique features of the acoustic signatures of zooplankton. This has been accomplished employing both feature based and theoretical model based approaches. To ensure the robustness of the classifications, the inherent variability in the acoustic signatures was examined, and in particular the effect of zooplankton orientation on the acoustic signature was investigated. The product of this thesis research is an assemblage of classification techniques evaluated in terms of their performance with experimental data. The relative performance of the classifiers is discussed, leading to specifications for their use, as well as recommendations concerning requirements for field data collection.

The balance of Chapter 1 (Section 1.3) is devoted to outlining the data collection techniques for acquiring the dataset used to develop and test the classifiers. The experimental setup is detailed, and the processing steps for the acoustic data are outlined. Since the video data were employed primarily to investigate the effect of animal orientation on acoustic signature, acquisition and processing details for the video portion of the dataset are described separately (Chapter 5). The thesis consists of two main parts: three chapters (Chapters 2, 3 and 4) are dedicated to detailing the development of several classification algorithms, and a separate chapter (Chapter 5) is devoted to an exploration of the effects of zooplankton orientation on acoustic signature, including the application of classification techniques to invert broadband acoustic echoes for animal orientation.

1.2.1 DEVELOPMENT OF CLASSIFICATION ALGORITHMS

The development of an automatic classification scheme for zooplankton described herein essentially involves the inversion of the return spectrum of a broadband acoustic insonification of an individual zooplankter for scatterer type. An inversion of this type can produce several different

results. An individual may be assigned to a category based on the classification of a single return echo from that animal. Alternatively, an animal may be assigned a score or probability that it is a member of a given class based on a single echo. In addition, it is feasible to invert for some of the physical properties (e.g. size, orientation etc.) of the animal. If several return echoes are available for a particular organism, then it is possible to obtain the proportion of echoes assigned to each class, or the average score or probability associated with each class, based on the ensemble of echoes.

Inversion schemes can be of two general types, those based on intrinsic features in the data and those based on an empirical or theoretical forward model of the scattering process. Both feature based and theoretical model based classifiers have been developed. Several approaches, all concentrated on exploiting the spectral characteristics of the acoustic returns, have been investigated. Feature based classification operates independently of the theoretical models, exploiting only the inherent characteristics of the signals. The Empirical Orthogonal Function Classifier (Chapter 2) discriminates scatterer types based on differences in the variability in the signals, and does not rely on theoretical model predictions.

The emphasis of this thesis work has been on developing and refining model based approaches in order to best exploit the existing set of theoretical forward models. These models express the relationship between the observed acoustic backscattered spectra from individual zooplankton and the physical model parameters. As a result, a model based approach not only allows inversion for scatterer class, it also has the potential to invert for certain physical characteristics of the scatterer represented by the model parameters (e.g. size, shape). The Model Parameterisation Classifier (Chapter 3) depends on comparison of the acoustic signatures with simplifying parameterisations of the theoretical scattering models for each class, assigning a given acoustic return to one of the three classes. The Covariance Mean Variance Classifiers (Chapter 4) are a set of more advanced model based techniques which exploit the full complexity of the theoretical models by searching the entire physical model parameter space without employing simplifying parameterisations. This more sophisticated approach incorporates weighting functions to account for the ambiguity between the model spaces for different scattering classes as well as to quantify the validity of each theoretical model in predicting acoustic returns from known scatterers. The result of the inversion is expressed as a certainty or probability that a given acoustic return belongs to each class.

The sensitivity of some of the classification algorithms to the effects of signal degradation as well as signal variability was investigated. In particular, simulated acoustic signals representing returns from scatterers in each class were degraded through the addition of synthetic noise as well as by decreasing the signal bandwidth, and the ability of the Empirical Orthogonal Function Classifier (EOFC) and the Model Parameterisation Classifier (MPC) to discriminate these degraded signatures was measured (Sections 2.4 and 3.4). The sensitivity of the MPC to the ping-to-ping and animal-to-animal variability inherent in the acoustic returns from individuals in the same scattering class was also evaluated using simulated datasets (Section 3.5).

Some of the work on MPC development (portions of Sections 2.1, 2.2 and 2.3) has been published together with part of the EOFC development (portions of Sections 3.1, 3.2 and 3.3) in Martin *et. al* (1996). The development of the Covariance Mean Variance Classifiers (Chapter 4) is presented here as a manuscript to be submitted for publication (Martin Traykovski *et al.* submitted a); consequently, some repetition of the contents of previous chapters will be necessary to ensure the completeness of this manuscript.

1.2.2 INVESTIGATION OF EFFECT OF ZOOPLANKTON ORIENTATION

To determine the effect of zooplankton orientation on acoustic signature, video data of each animal (acquired simultaneously with the acoustic returns) was analysed in conjunction with the acoustic data for individuals in the fluid-like scattering class (Chapter 5). For different animal orientations, a preliminary look at the time series data led to a detailed examination of the frequency responses (spectra of the returns) to provide information on how the acoustic signature of this scattering class can be expected to change versus angle of orientation. The angle of orientation of the animal at the time of insonification was compared on a ping-by-ping basis with the frequency spectrum of the corresponding acoustic return, giving an indication of the variability in the acoustic returns for a given orientation. The acoustic returns observed from tethered zooplankton were compared to the spectra predicted by the distorted wave Born approximation theoretical model for the angle of orientation, size, and shape of the measured animal. Finally, the classification algorithms were employed to invert the observed spectra for angle of orientation, and a comparison of experimentally-measured and classifier-predicted orientations was made.

To render the results of this analysis of the effect of orientation on zooplankton acoustic returns applicable to *in situ* acoustic surveys, it is important to establish the animals' natural (untethered) orientation during feeding, swimming and resting. A preliminary investigation of the *in situ*

orientation of those species of zooplankton for which we have acoustic data was carried out, and a brief summary of the findings is summarised (Section 5.1); sources of information included the literature as well as video footage taken by SCUBA divers, submersibles, and the Video Plankton Recorder (VPR). The results of this analysis have increased our *a priori* knowledge-base, and in the future, this type of information can assist in placing bounds on some model parameter values as well as in helping to constrain the acceptable tethered-animal dataset to include only "reasonable" animal orientations.

A portion of the work on the investigation of the effect of animal orientation on acoustic signature is presented here as a manuscript to be submitted for publication. In particular, the comparison of experimental results with theoretical model predictions and the results of the classification inversion for orientation angle (Section 5.3) are presented in manuscript form. This manuscript (Martin Traykovski *et al.* submitted b) includes a brief summary of other work detailed in Chapter 5, so that some overlap is inevitable. It is one of two papers co-authored with D.E. McGehee and R.L. O'Driscoll (see also McGehee *et al.* accepted) and is included here with the co-authors' permission.

Finally, the various classification techniques developed are compared, some implementation guidelines are given, considerations for the collection of field data are discussed, recommendations for future research based on this thesis work are outlined, and the contributions of this thesis are summarised (Chapter 6).

1.3 SOURCES OF DATA

The data used in classifier development were collected on two separate cruises to Georges Bank and the Gulf of Maine: the Oceanus cruise 262 (27 September - 6 October 1993) and the Endeavor cruise 253 (18 September - 29 September 1994). Data used in the investigation of the effects of animal orientation on acoustic signature were collected at the Second Bioacoustics Workshop in Santa Cruz, CA (1 August - 25 August 1995).

1.3.1 METHODS OF DATA COLLECTION

On the two cruises, organisms were captured in both vertical and oblique tows in the slope water, the Gulf of Maine and over Georges Bank with a meter net (335 μm mesh) with a cod-end bucket (32 cm diameter by 46 cm tall), and sorted into large containers for short-term storage under refrigeration to maintain seawater temperature. The animals for the workshop were captured in the Southern Ocean in February 1995 and kept alive under refrigeration at 2°C in the absence of food until the experiments in August 1995. A detailed sketch was made of each animal before or after insonification, and various measurements were taken:

1. siphonophores: total length, size of gas inclusion
2. euphausiids: - total length and width of carapace (1993 and 1994 cruises)
   - 5 length measures, carapace width, depth (1995 workshop)
3. shelled pteropods, gastropods: length and width of shell
4. salps: length and width of mucous house, diameter of gut
5. ctenophores: length, width
6. naked pteropods: length and width of body, size of "feet"
7. amphipods: relaxed and extended length and width of thorax

Individual organisms were tethered with an acoustically transparent monofilament strand, and suspended in a 2.44 m diameter by 1.52 m high tank filled with filtered (through 64 μm mesh) sea water on-board the ship (1993 and 1994 cruises) or a 2 m by 0.75 m by 0.8 m deep insulated tank filled with filtered, chilled seawater (1995 workshop). Extreme care was taken to ensure that no air bubbles were present on the animal or the tether during insonification. Acoustic experiments included broadband insonification (center frequency 500 kHz, ~350 kHz - 750 kHz) of each live animal, as well as narrowband insonification at several other frequencies. Only the 500 kHz broadband data were used in this thesis work. The return echoes from several thousand acoustic transmissions (pings) were collected. Insonifications were made with a pulse-echo acoustic data acquisition system (Figure 1-4).

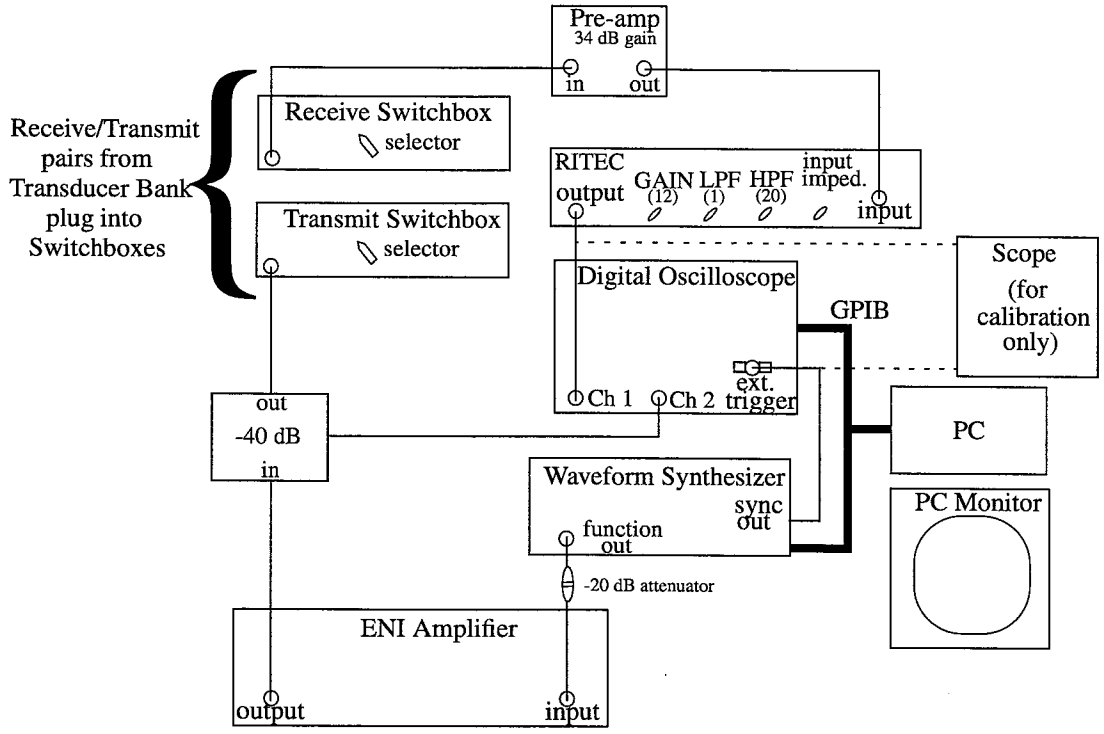

Figure 1-4 Pulse-echo acoustic data acquisition system used to insonify several species of zooplankton.

The transmit/receive transducer pair was mounted in an upward-looking transducer bank (1993 and 1994 cruises) sitting on the bottom of the experimental tank (Figure 1-5) or in a horizontally-aimed configuration (1995 workshop), looking across the tank (Figure 5-8). To allow investigation of correlations between the acoustic scattering of an organism and its orientation, each animal was filmed during insonification with a high-magnification underwater video system (1994 cruise and 1995 workshop only). Each insonification was marked with an acoustic pulse recorded on the audio track of the Hi-8 video tape.

After the experiment, excess water was removed from each organism and the specimens were frozen. Wet weight of the samples was measured on land following the cruises, and after insonification (before freezing) during the workshop. Several organisms from each of the three scattering classes were insonified (Table 1-1). On the cruises, 11 individuals (all of one species) from the elastic-shelled class and 14 individuals (representing 2 species) from the gas-bearing class were insonified. A total of 24 zooplankters of 3 different species were insonified from the fluid-like class during the cruises and the workshop. In addition to using animals from the three scattering classes, data from several other unmodelled zooplankton were also collected.

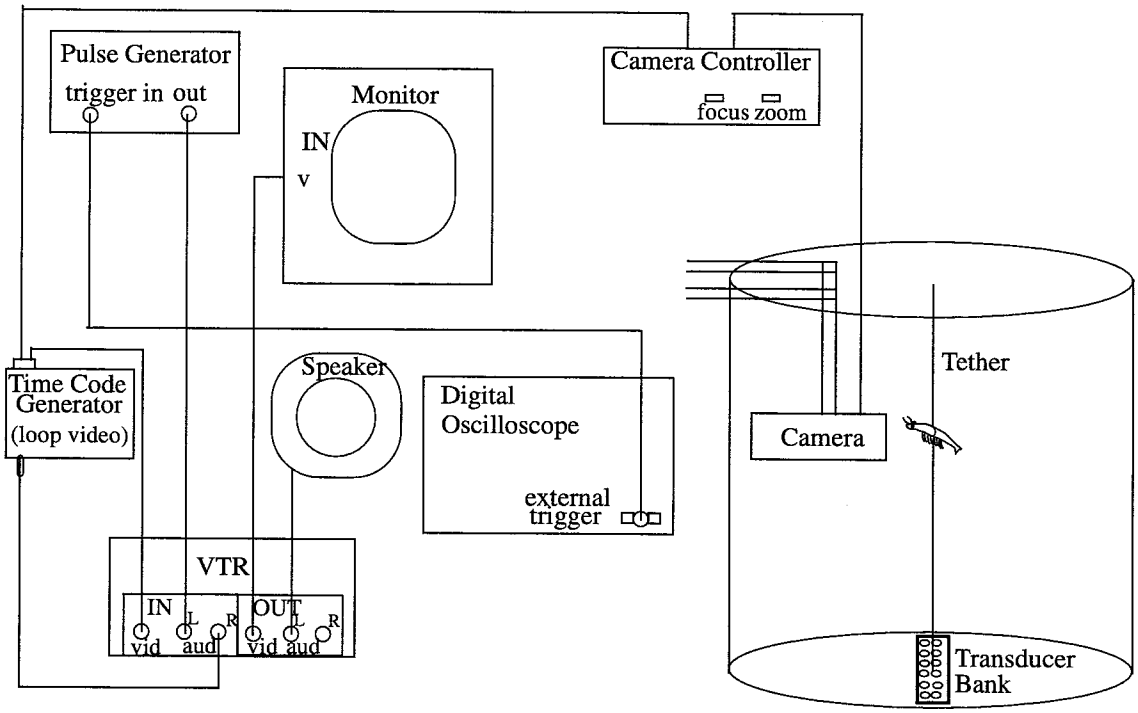

Figure 1-5 Experimental setup for insonifying zooplankton, including underwater video system.

Table 1-1 Animals insonified from the three scattering classes; 1993 and 1994 cruises, 1995 workshop.

scattering class	species and number	# pings
gas-bearing (**GB**)	9 *Agalma okeni* (1993) 3 *Agalma okeni* (1994) 2 *Nanomia cara* (1994)	50 each 1200/1200/800 1000/600
fluid-like (**FL**)	1 *Meganyctiphanes norvegica* (1993) 7 *Meganyctiphanes norvegica* (1994) 2 *Euphausia croni* (1994) 14 *Euphausia superba* (1995)	1000 1000/1200/1200/600/3200/1600/200 200 each 1000 each
hard elastic-shelled (**ES**)	8 *Limacina retroversa* (1993) 3 *Limacina retroversa* (1994)	50 each 4600/4400/2400
not modelled	1 *Clione limacina* (1993) 1 *Clio pyramidata* (1993) 2 Hyperiid amphipod (1994) 1 *Parathimisto* sp. (1994) 1 *Pelagia noctiluca* (1994) 1 *Cavolinia inflexa* (1994) 8 *Creseis* sp. (1994)	50 50 1000 each 1000 200 200 250/250/200/1000/1000/600/1200/1000

1.3.2 ACOUSTIC DATA PROCESSING

For the pulse-echo system used in these experiments, the frequency response of the return echo received from the animal during insonification may be expressed using the sonar equation in terms of logarithmic quantities as follows:

$$VR_S = VT_S + GT_S + ST_S - TL_S + ES - TL_S + SR_S + GR_S \quad \textbf{(EQ 1.1)}$$

where VR_S represents the voltage signal level received while scattering from the animal, VT_S represents the voltage signal level transmitted to scatter from the animal, GT_S and GR_S are the transmitter and receiver gains, ST_S and SR_S are the transmitter and receiver sensitivities, TL_S is the transmission loss $20\log(r_S)$ due to the distance r_S between the transducer faces and the animal, which appears twice to account for two-way transmission loss, and ES represents the echo spectrum of the acoustic target strength of the animal.

To obtain the calibrated echo spectrum, the results of the calibration measurements must be incorporated. During calibration, the transmit and receive transducers are focused on each other with no target in the beam, and a calibration signal is transmitted. Writing the calibration equation in the same manner as (EQ 1.1):

$$VR_C = VT_C + GT_C + ST_C - TL_C + SR_C + GR_C \quad \textbf{(EQ 1.2)}$$

where VR_C represents the voltage signal level received during calibration, VT_C represents the voltage signal level transmitted for calibration (of much lower amplitude than the signal used in the scattering experiment), GT_C and GR_C are the transmitter and receiver gains, ST_C and SR_C are the transmitter and receiver sensitivities, and TL_C is the transmission loss $20\log(r_C)$ due to the distance r_C between the transmitter and receiver when they are in the calibration configuration. Assuming that $(ST,\ SR,\ GR)_S = (ST,\ SR,\ GR)_C$, subtracting (EQ 1.2) from (EQ 1.1) yields an expression for the echo spectrum of the animal in terms of the transmitted and received signal levels, the transmission losses, and the transmitter gains for both scattering and calibration:

$$ES = VR_S - VR_C + (VT_C + GT_C) - (VT_S + GT_S) + 2TL_S - TL_C \quad \textbf{(EQ 1.3)}$$

This is equivalent to:

$$20\log(F_{bs}) = 20(\log Vrec_S - \log Vrec_C + \log Vxmit_C - \log Vxmit_S + \log r_s^2 - \log r_C) \quad \textbf{(EQ 1.4)}$$

with

$Vrec_S = 10^{(VR_S/20)}$, $Vrec_C = 10^{(VR_C/20)}$, $Vxmit_C = 10^{(VT_C + GT_C)/20}$ and $Vxmit_S = 10^{(VT_S + GT_S)/20}$.

Here ES is represented in terms of F_{bs} (= $|f_{bs}|$) where f_{bs} is the backscattering amplitude, and is a measure of the efficiency with which an object scatters sound back toward the sound source (f_{bs} is related to σ_{bs}, the differential backscattering cross section, by $\sigma_{bs} = |f_{bs}|^2$).

(EQ 1.4) leads to an explicit expression for $|f_{bs}|$, the absolute value of the acoustic backscattering amplitude of the animal:

$$|f_{bs}| = \left(\frac{Vrec_S}{Vrec_C}\right) \cdot \left(\frac{Vxmit_C}{Vxmit_S}\right) \cdot \left(\frac{r^2_S}{r_C}\right) \qquad \textbf{(EQ 1.5)}$$

In this equation, f_{bs} is expressed in terms of measurable quantities. $Vrec_C$ and $Vxmit_C$ are computed by taking the absolute value of the FFT of the received and transmitted voltage time series for calibration, measured at the beginning and again at the end of the experiments each year. $Vxmit_S$ is computed as the absolute value of the FFT of the transmitted voltage time series for scattering measured at the end of each run (every 50 or 200 pings). To compute $Vrec_S$, a fixed rectangular window is applied to the received voltage time series for each ping (to capture only the echo from the animal) before applying the FFT. The scattering and calibration distances were $r_S \approx 51$ cm and $r_C \approx 60$ cm respectively.

The acoustic returns of the zooplankton studied exhibit a very large dynamic range over the frequency band, and are often characterised by the occurrence of deep nulls at certain frequencies (where σ_{bs} is ~1/1000 of peak values). The echo spectrum, conventionally represented by TS (where $TS = 20\log|f_{bs}|$) on a logarithmic scale, is a convenient and widely-accepted means of compressing this huge dynamic range. This representation has the advantage of emphasising the peak-and-null structure in the acoustic signatures, and the dynamic range compression also improves the suitability of the signals for numerical classification inversion schemes (other data transformations are also possible; a single choice may not be optimal for every classification application (Fukunaga 1972)). The echo spectrum ($ES = 20\log|f_{bs}|$) of each acoustic return was sampled at 241 points between 348.33 kHz and 748.33 kHz (1993 data), or at 152 points between 348.33 kHz and 600 kHz (1994 data) or at 203 points between 348.33 kHz and 685 kHz (1995 data). The reduced bandwidth of the 1994 and 1995 data is due to the use of a different transducer with a different frequency response over the 350-750 kHz band. It is this sampled version of the echo spectrum that is used as the basis for classifier development and evaluation.

CHAPTER 2

FEATURE BASED CLASSIFICATION:

EMPIRICAL ORTHOGONAL FUNCTION CLASSIFIER (EOFC)

2.1 RATIONALE

One approach to the classification problem is the application of techniques that capitalise on measurable features of the data belonging to each class, and seek to exploit class-specific differences in these features. Feature based inversion approaches do not rely on any theoretical or empirical models which may exist to predict the data in each class; they are based only on the inherent characteristics of the observed data. For inversion problems where the theoretical or empirical basis from which to construct a relationship between observed data and model parameters is not well-characterised, it is necessary to adopt a feature based formulation, which can operate independently of a forward model. Feature based techniques are often the first approach used to attack a classification problem since they allow a direct exploration of the data in terms of its intrinsic characteristics, and are not complicated by the details of sophisticated theoretical models. An important advantage of feature based inversion schemes is that they are not subject to assumptions and potential errors in model structure. For this reason, it may be desirable to design an inverse formulation independent of theoretical models, even in cases where there exist well-developed theoretical forward models with which to predict the data, as is the case for the zooplankton acoustic classification problem. In addition, the application of feature based techniques yields unique insights into the problem by identifying discriminating features, providing a solid basis for model based inversions. Although these feature based approaches are independent of an explicit model, it is possible to relate features to biologically relevant parameters, thereby illuminating the bases of class separation, and providing insights into the underlying processes which contribute to the expression of the discriminating features.

The objective is to develop a general acoustic classification technique for zooplankton based on single-ping broadband insonifications which does not depend on scatterer-specific or species-specific assumptions to identify scattering type, but instead relies on the empirical separation of scatterers based on the unique spectral signatures of each scatterer type. One approach to a feature based classification scheme is the implementation of a statistical distance based classifier, which categorises observations based on metrics or distances in "feature space". An alternative forward

model-independent approach involves the construction of a library of "signatures" against which observational data may be compared, ultimately leading to a categorisation of the observations. To invert broadband acoustic backscatter data for zooplankton scatterer type using this approach, unique characteristics of the echo spectra of each scatterer type can be exploited in a pattern recognition scheme, which matches the signatures of a novel zooplankter to known signatures characteristic of a particular scattering class. The emphasis of the feature based portion of this thesis work has been on developing an approach based on such a signature library (e.g. the EOFC). A short discussion of the distance based classification approach, accompanied by a preliminary clustering analysis of the 1993 data, is included for completeness. The potential of the distance based approaches has not been fully explored herein.

2.1.1 DISTANCE BASED CLASSIFICATION

Distance based classification schemes operate independently of theoretical model predictions, and assign a data point to a class based on its projection in feature space. In this implementation, a subset of n features of the spectral signatures are identified which best discriminate the different scatterer types of interest. Known scatterer types are then projected in n-dimensional space as a function of these discriminating features, and class boundaries are delineated (e.g. via eigenvalue decomposition or Fisher Pairwise Projection (Fukunaga 1972)) to separate scatterer type domains. Novel observations of unknown zooplankton may then be projected onto this feature space, and various statistical decision rules applied to classify the observations into particular domains.

Distance based classification involves identifying and extracting the relevant characteristics or features of the data that uniquely identify a particular scattering class, thereby allowing retrieval of the properties of interest. These features may consist of direct measurements, as well as properties derived or calculated from these direct measurements. The goal is to identify and select features which are the best delineators of the scattering classes. A sensitivity analysis can be carried out on these features, using *a priori* information to place bounds on the feature values. Features that are most discriminating are then selected to be used in the classification. Means of feature selection include the Karhunen-Loève Expansion, which decomposes the features into a basis set, thereby expanding them in terms of the eigenvectors of the covariance matrix (Fukunaga 1972). This technique yields features which are optimal in terms of representing the data, but may not be the best features for discriminating between scattering classes. Other discriminators in combination with the K-L expansion may yield features with greater class-separability potential (Tang and Stewart 1994). The presence of contaminating noise can make feature extraction more difficult.

Once the relevant feature set is identified, it can then be employed to identify classes or categories which share common properties or attributes. This is accomplished by projecting data from known scatterers in feature space as a function of the relevant discriminating features. Possible projection techniques include eigenvalue decomposition, in which the data are projected onto a plane in which the principle axes are the first two eigenvectors of the covariance matrix, and the Optimal Discriminant Projection (Fisher Pairwise Projection), in which all the data are projected onto the plane that optimally discriminates a particular pair of classes. The delineation of class boundaries is accomplished by means of statistical decision rules based on discriminant functions or metrics, such as minimum Euclidean distance, minimum intra-class distance, maximum inter-class distance and minimum mean-squared error. Statistical decision theory can be used to derive an optimum classification rule if multivariate probability density functions are known for each class or if an empirical probability model can be obtained by statistical estimation. Alternatively, a decision rule may be derived directly from the distribution of samples in feature space. Once class boundaries are determined, novel observations may subsequently be projected in feature space and classified into categories based on the discriminating features and the statistical decision rules. Distance based classification is also possible where no *a priori* information is available, through exploitation of naturally occurring groupings or clusters in the data. Features can then be empirically related to scatterer type.

Preliminary Clustering Analysis

In order to better characterise the zooplankton scatterer types, a preliminary analysis of some of the potentially discriminating features was undertaken. Some statistics were compiled on various features of the spectra from animals of known scatterer type from the 1850-ping 1993 dataset. An average level (mean *TS* in dB) was computed for each ping. Null spacing (the distance between successive peaks or nulls in the spectra, measured in frequency units) was also estimated for each ping, as was the frequency shift (translation of the spectra along the frequency axis relative to some zero-reference spectrum). The mean *TS* feature did not appear to be a good discriminator between animals in the **FL** class (e.g. *Meganyctiphanes norvegica)* and those in the **ES** class (e.g. *Limacina retroversa)*, but may be a good way to distinguish the **GB** class (e.g. *Agalma okeni)*, since average levels for animals in this class seem to be higher than those observed for the other two classes, based on this limited dataset. In addition to considering features based only on individual pings, features based on ensembles of pings have potential to discriminate the classes.

For example, the distribution (variance) of mean *TS* (based on ensembles of n = 50 pings) may be a good discriminator, since it appears to be much tighter for animals from the **ES** class than it is for the other two classes. The distributions of null spacing and frequency shift also appear much tighter for ensembles of pings from the **ES** class than for the **FL** class. Ensemble type features are promising discriminators, since they are based on statistical analysis of several echoes from the same animal. The practical utility of ensemble-based discriminators depends on the feasibility of acquiring many insonifications of a single animal or several animals in a given class.

An initial clustering analysis was performed (Figure 2-1) to view the 1993 data in terms of three individual ping features that were thought to have good class-discriminating potential: mean *TS*, null spacing, and SSR (sum of squares of the residuals: $SSR = \Sigma (y(i) - SPEC(i))^2$, where y represents the straight line fit through the echo spectrum SPEC). These three features were extracted from all 1850 echo spectra from the 1993 cruise dataset. Although there is overlap between the feature spaces of pings in the three classes, some separability is evident. For example, many of the 400 pings from the *Limacina retroversa* individuals (**ES** class) are clustered tightly around a particular null spacing and over a small range of SSR. Even though the 450 Agalma *okeni* pings (**GB** class) appear quite spread out in terms of the null spacing feature, they are clustered toward the lower end of the SSR range for all the pings, with a very tight grouping in the upper left-hand corner, a region of low SSR and high mean *TS*. As a possible result of the fact that the *Meganyctiphanes norvegica* specimens (**FL** class) were permitted to assume a wide range of orientations during insonification, these 1000 pings are distributed widely along the null spacing axis. However, *M. norvegica* pings tend to exhibit a higher SSR than do *A. okeni* pings, and may be discriminable from members of the **GB** class by this feature alone.

Further insight into potential class separability using these same three individual ping features may be gained by employing alternative projections. The highest SNR subset of 150 pings (93-18, 93-33e (run5) and 93-29) was extracted from the 1993 data, containing 50 pings from a single individual from each of the 3 classes. This subset was clustered using a Fisher Pairwise Projection, in which the data are projected onto a two-dimensional plane that optimally discriminates a particular pair of classes (in this case, **FL** and **ES**) by maximising the between-class distance and minimising the within-class distance between the class pair (Figure 2-2). This projection reveals that the *L. retroversa* data (**ES**) is very tightly clustered, but the *M. norvegica* data (**FL**), even for only 50 pings from 1 animal, is spread over the feature space occupied by the other two classes.

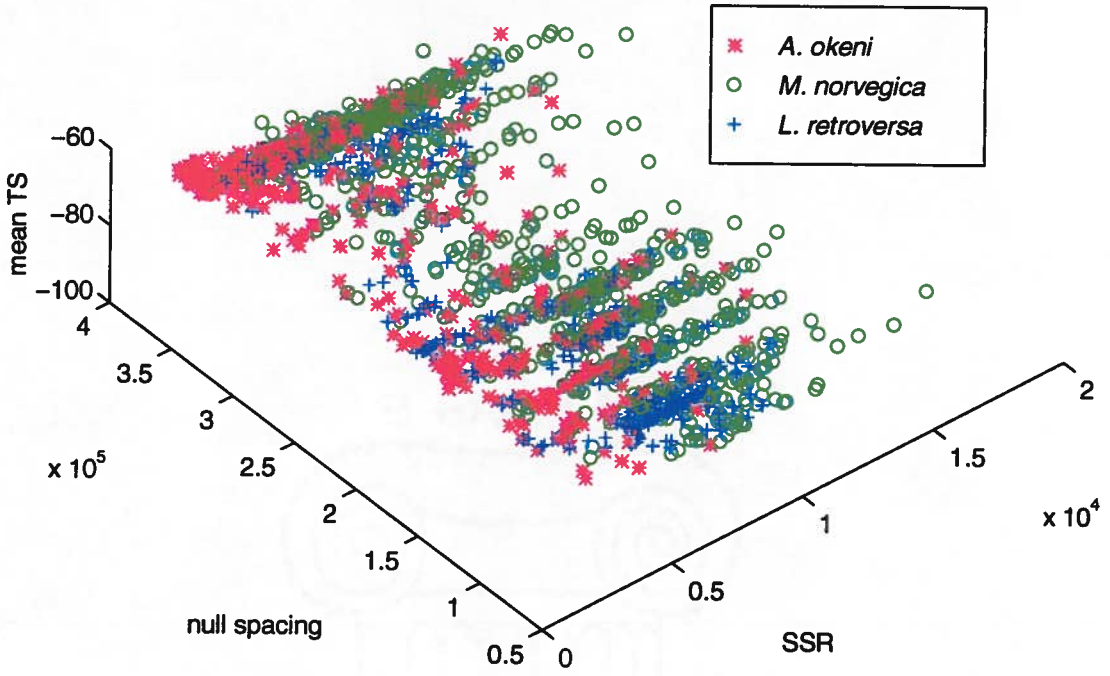

Figure 2-1 Preliminary clustering analysis for 1850 echo spectra (1993) from 3 scattering classes.

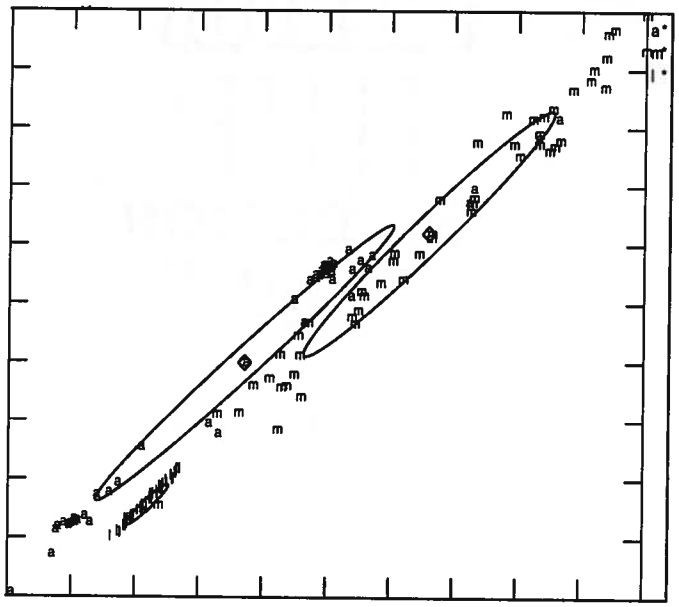

Figure 2-2 Fisher Pairwise Projection for the high SNR subset of the 1993 data. Data are projected onto the 2-D plane which optimally discriminates the **ES** and the **FL** classes from each other; class means shown as diamonds, ellipses are standard deviations. Data point labels: l = *Limacina retroversa* 93-29 (**ES** class), m = *Meganyctiphanes norvegica* 93-33e (**FL** class), a = *Agalma okeni* 93-18 (**GB** class). In this projection, "l" data is tightly clustered, forming a very tight **ES** grouping, whereas "m" data is shows much higher variability, spreading over the feature space occupied by the other two classes.

2.1.2 MODES OF VARIABILITY AS FEATURES

The individual ping features used in the clustering analysis (e.g. mean *TS*, null spacing) are each single metrics that capture a certain aspect of the echo spectra. There is considerable overlap in the cluster diagram (Figure 2-1) between the three classes, and distinct clusters are not immediately evident. Even when only 50 echo spectra from one individual from each class are considered (Figure 2-2), the classes are not completely distinct. This may be because the individual ping features chosen here are not the best discriminators of the three classes. It is likely that an exhaustive search of all possible features, followed by a detailed feature selection analysis, would yield an optimally-discriminating feature set, allowing better separation of the classes. Another possibility is that these individual ping metrics are unable to exploit the richness of information contained in the broadband spectra of the acoustic returns.

The distance based approach described in Section 2.1.1 is well-suited to problems in which the available information content of the data is limited. For example, the inversion of satellite remotely sensed ocean colour data from the Coastal Zone Color Scanner (CZCS) for water properties or phytoplankton bloom taxa is a classification problem that lends itself well to a distance based approach. For a given area of ocean surface, only water-leaving radiances at 443, 520 and 550 nm (three samples over the entire optical spectrum) are measured; projection in a three-dimensional feature space can exploit all the available information. In fact, different water types, as well as waters containing different phytoplankton species, are readily distinguishable in this feature space (Martin Traykovski and Sosik in prep.). The 241-point sample of the echo spectra resulting from broadband insonifications of individual animals that provide the data basis for the zooplankton acoustic classification inversion problem may contain much more information than can be exploited in a distance based classifier. Consequently, an alternative to individual ping metric distance based classification was developed, and will be the focus of the remainder of this chapter.

To design a robust feature based classification scheme, features were sought that were better able to exploit the full information content of the broadband echo spectra than were the individual ping features. A promising approach is to classify the echo spectra based on the variability they exhibit. A feature that can capture that variability will be derived from the entire frequency response, and will be based on more than one acoustic return from a particular animal. In the case of the Empirical Orthogonal Function Classifier (EOFC) developed herein, the discriminating features are the modes of variability present in the frequency responses of the acoustic returns from animals

in each class. An EOF decomposition of the echo spectral data from scatterers belonging to each class reveals that the mode shapes present in the data are characteristic of the scattering classes. These mode shapes serve as the basis for classification. The EOFC is able to discriminate the scattering classes by identifying characteristic modes of variability in the echo spectra for each class, thereby creating a library of modal signatures. Classification of a novel observation involves matching the observed mode shape to the library, and identifying the class to which the best-fit modal signature belongs.

2.2 ALGORITHM

The EOFC matches an observed echo spectrum (ping) to a scattering class based on an empirical orthogonal function decomposition. The frequency spectra of echoes from scatterers in each class are decomposed into modes that represent the variation of the data from the mean value. This is accomplished by computing the eigenvalues and eigenvectors (EOFs) via a singular value decomposition (see Menke 1989) of the covariance matrix (**K**) of the data:

$$\mathbf{K} = \mathbf{A}^{\mathrm{T}} \cdot \mathbf{A} \qquad \text{(EQ 2.1)}$$

where A is a matrix in which each row represents a mean-subtracted ping. The modal decomposition hinges on the fact that:

$$\mathbf{K} \cdot \varphi_i = \lambda_i \cdot \varphi_i \qquad \text{(EQ 2.2)}$$

where φ_i represent the eigenvectors or EOFs, and λ_i are the eigenvalues. The eigenvector corresponding to the maximum eigenvalue is the dominant mode. For example, for the 1993 dataset (in which the echo spectra are sampled at 241 points between 348.33 kHz and 748.33 kHz), a total of 241 EOFs (modes of variability) can be calculated. To classify echo spectra, the EOFC employs any of the modes, alone or in summation, weighted by the corresponding eigenvalues:

$$\sum_{i=n}^{N} \lambda_i \cdot \varphi_i \qquad \text{(EQ 2.3)}$$

Here n is the initial mode number and N is the final mode number of the modes used in the weighted sum. To build a library of modal signatures against which novel observations may be classified, the appropriate weighted sum of modes was computed for each individual insonified in the 1993 experiment. For example, creation of the dominant mode (M1) library for the M1-EOFC

involves setting $n = 1$ and $N = 1$ in (EQ 2.3). In this M1 library, the "modal space" of a given scattering class is represented by the dominant mode (based on 50-ping datasets) weighted by the dominant eigenvector of each individual insonified from that class. For the M2-EOFC, the M2 library is constructed in a similar manner ($n = 2$ and $N = 2$), using only the second-to-dominant mode (M2), so that the modal space for a given scattering class is represented by the second mode weighted by the second eigenvalue of each individual of that class. In general, the WN-EOFC classifies using a WN library constructed from the weighted sum of the first N modes, and the modal space for each scattering class is represented by the weighted sum of a number of modes. For example, in the W2-EOFC, a W2 library is built using the weighted sum of the first 2 modes ($n = 1$ and $N = 2$ in (EQ 2.3)).

Once the libraries are constructed and the modal spaces for each scattering class are delineated, echo spectra from a novel scatterer may be classified. Since the EOF decomposition characterises the modes of variability of the returns, the EOFC classifies based on multiple pings from a particular scatterer. Although thousands of returns can be acquired from a single individual in a tank experiment, practical considerations dictate the number of pings that can reasonably be collected for field applications. For example, it is unlikely that individual animals can be insonified even 50 times in the field on a regular basis. However, five insonifications of a single animal seems a reasonable number, given the speed at which the echosounder is towed, and the velocity of the swimming plankton (for a moored system). The EOFC was therefore evaluated on the basis of five pings collected from an individual animal. To classify a novel scatterer, an EOF decomposition is performed on an ensemble of five acoustic returns from that scatterer. For the M1-EOFC, for example, the five-ping-ensemble dominant mode is then correlated to the M1 library (containing the M1 modal spaces for all scattering classes). Classification involves determining to which modal space the best-fit dominant mode belongs.

2.3 PERFORMANCE

The EOFC modal libraries were developed based on 37 50-ping datasets collected from 18 animals insonified on the 1993 cruise. Initially, a 150-ping sub-sample (representing the highest signal-to-noise ratio (SNR) data) consisting of 10 five-ping ensembles from one animal in each of the three classes (Animals 93-18 *Agalma okeni*, 93-33e *Meganyctiphanes norvegica* (run 5) and 93-29 *Limacina retroversa*) was classified with the M1-EOFC to assess classifier performance with the best quality data. M1-EOFC success rate with this high SNR dataset was about 93% (Figure 2-3).

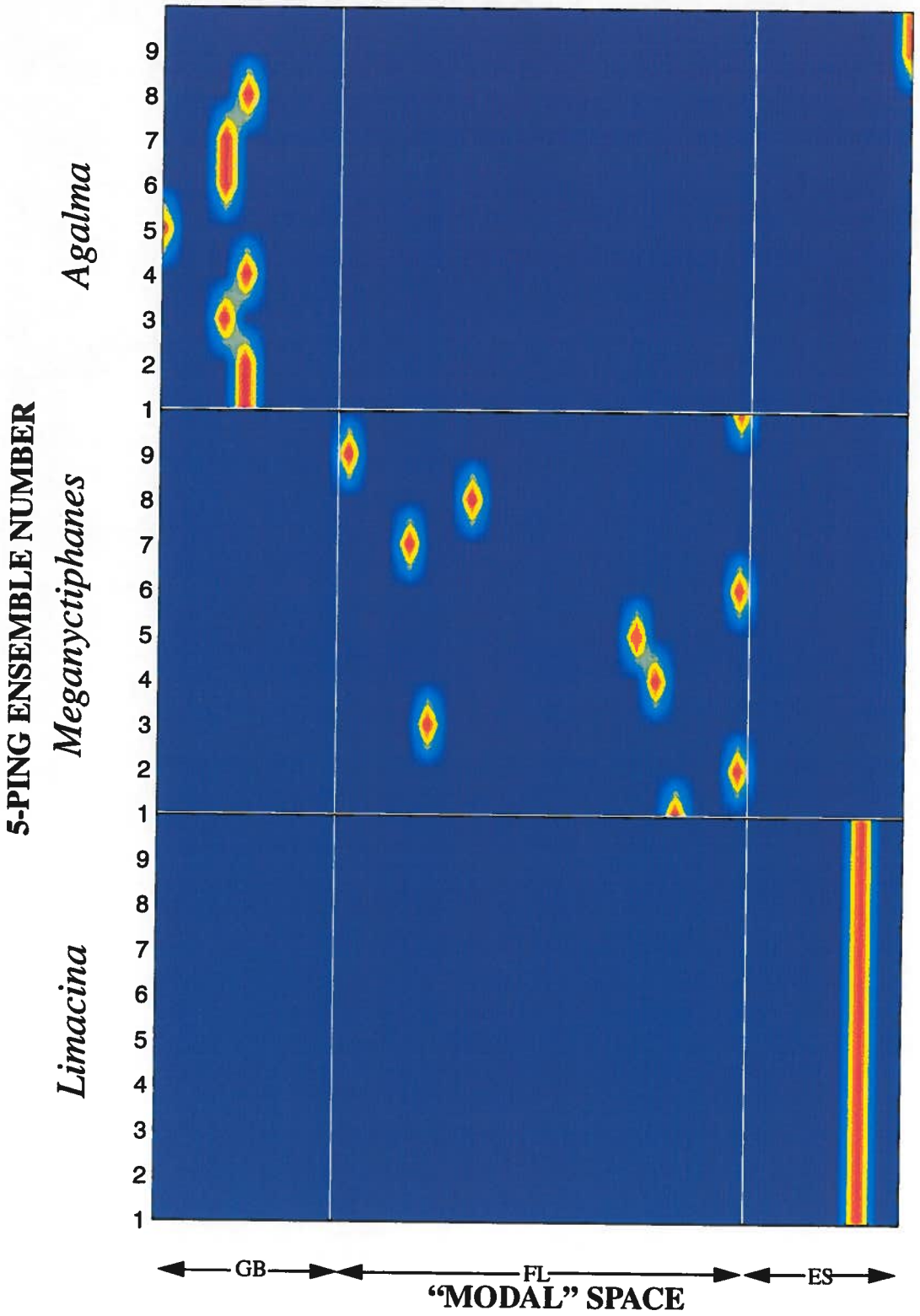

Figure 2-3 M1-EOFC classification results for the high SNR subset (1993 cruise). Success rate was ~93%. Five-ping ensembles of echo spectra for each class are numbered up the y-axis.

The M1-EOFC average success rate over the entire 1993 dataset of 1850 pings was about 86%, with excellent performance for euphausiid (**FL** class) and gastropod (**ES** class) data (Table 2-1).

Table 2-1 M1, M2 and W2-EOFC results for 370 5-ping ensembles (1993). "*" indicates high SNR data.

				% CORRECTLY CLASSIFIED		
species	Animal #	run #	n	M1-EOFC	M2-EOFC	W2-EOFC
Agalma okeni	93-13	1	10	70%	60%	70%
	93-14	1	10	80%	50%	60%
	93-16	1	10	100%	60%	80%
	93-17	1	10	100%	60%	90%
*	93-18	1	10	80%	70%	80%
	93-19	1	10	40%	40%	30%
	93-20	1	10	70%	30%	30%
	93-21	1	10	60%	40%	50%
	93-22	1	10	60%	50%	40%
	TOTAL		90	73%	51%	59%
Meganyctiphanes norvegica	93-33a	1	10	80%	80%	60%
	93-33b	2	60	83%	70%	78%
	93-33c	3	60	87%	72%	88%
	93-33d	4	60	92%	60%	93%
*	93-33e	5	10	100%	90%	90%
	TOTAL		200	88%	69%	86%
Limacina retroversa	93-23	1	10	100%	70%	100%
	93-24	1	10	100%	80%	100%
	93-26	1	10	90%	30%	90%
	93-27	1	10	100%	100%	100%
	93-28	1	10	90%	60%	60%
*	93-29	1	10	100%	70%	100%
	93-30	1	10	90%	40%	70%
	93-31	1	10	90%	80%	90%
	TOTAL		80	95%	66%	89%
ALL ANIMALS	TOTAL		370	86%	64%	80%

Although the second mode shows some discriminating power, particularly for identifying echo spectra from the **FL** class, the overall performance of the M1 classifier is substantially better than the M2 classifier. This indicates that the dominant mode is a better discriminating feature than is M2 for the data classified here (1993 cruise). The W2 classifier, which discriminates based on the weighted sum of the first two modes, performs better than the M2 classifier overall, but not as well as the M1-EOFC, which classifies based on the dominant mode alone. To evaluate whether better results could be achieved through the inclusion of additional modes in the weighted sum, classifications were carried out for the entire 1993 dataset using the W3-EOFC (n = 1 and N = 3 in (EQ 2.3)) through the W10-EOFC (n = 1 and N = 10) as well as with the W241-EOFC (Figure 2-4). The W3 classifier, in which the third mode is included in the weighted sum, performs slightly better than the W2 classifier for the *L. retroversa* and *A. okeni* data, but considerably worse for the *M. norvegica* data. Inclusion of up to 10 modes in the weighted sum does not improve the overall performance of the EOFC. In fact, including all the modes (W241-EOFC) results in overall performance similar to that achieved with only 3 modes, and in all cases, using M1 alone yields the best results. For a signal with contaminating noise present, the higher order modes tend to represent the variability contributed by the noise. This may explain the degradation in performance as higher order modes are added to the dominant mode. In general, the M1-EOFC appears most robust to noise contamination, although it may be desirable to use the W2 classifier in cases where M2 demonstrates good discriminating power (e.g. for the *M. norvegica* data). The performance of the EOFC relative to that of the other classifiers developed in this thesis work is discussed briefly in Section 6.1.

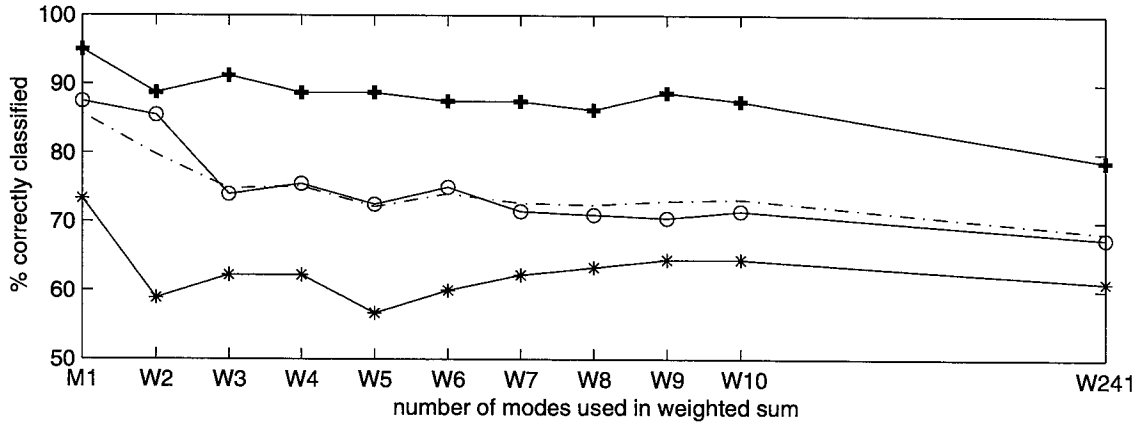

Figure 2-4 Average classification results for the 370 5-ping ensembles (1993) using M1, W2 through W10, and W241-EOFC. + = *L. retroversa* (**ES** class), o = *M. norvegica* (**FL** class), * = *A. okeni* (**GB** class). Dashed line is overall average.

2.4 SENSITIVITY TO SIGNAL DEGRADATION

To classify zooplankton based on their acoustic signatures, return echoes from broadband insonifications of individuals must be acquired, either in an experimental tank from tethered (constrained) animals, or ideally, *in situ* from free-swimming zooplankton. In either case, the presence of contaminating noise in the echo spectra of the acoustic returns could present an obstacle to the classification process. Depending on the nature and level of noise present, noise contamination could cause the classification inversion to be non-unique.

The sources and nature of noise contamination in the echo spectra of the broadband acoustic returns from individual zooplankton are varied, and may depend to a great extent on whether the data are collected in a tank or *in situ*. Even for the tank experiments described in Section 1.3, from which all the data used to develop the classifiers was collected, specific sources of noise differ between ship-board tank experiments and a land-based experimental setup. Potential sources of contaminating noise for both tank and *in situ* data collection include system noise (e.g. pre-amplifier noise), background noise (e.g. for shipboard experiments, reverberation due to the tank enclosure, to sea state, or to ambient noise such as electrical noise from other functions of the research vessel), the presence of other acoustic scatterers other than the target of interest (e.g. temperature microstructure in the tank water, or the presence of multiple zooplankton scatterers in an *in situ* insonified volume), and calibration error or drift. System noise and background noise are generally simple additive noise, but noise from other scatterers could be complex and have a "signature" of its own. In addition, noise contamination observed in data collected in a tank experiment is not necessarily representative of the noise likely to be present in field-collected data.

The presence of noise can contaminate both the signature information in the echo spectra and the inversion process itself. For example, for echo spectra characterised by a pronounced undulating structure with deep nulls (30 dB) at certain frequencies (e.g. returns from fluid-like animals at broadside incidence), uncorrelated additive noise will add proportionately more energy to the nulls than to the peaks. This simple form of noise addition can degrade the signature by making the null and peak structure less pronounced. On the other hand, correlated additive noise may exhibit a spectrum possessing pronounced structure itself. The structure in the noise spectrum could resemble the acoustic return of the scatterer of interest, but in the additive process, it could markedly alter the scatterer signature. Alternatively, the noise spectrum structure could differ significantly from the scatterer spectra, thereby confounding or degrading the scatterer signature

and/or resulting in classification of the noise signature instead of the scatterer signature. Simple offset-type multiplicative noise introduces a gain factor which shifts the entire echo spectrum, altering the average level of the return but leaving the structure of the scatterer signature intact This form of multiplicative noise can confound classification approaches that discriminate based on the average level of the echo spectra. Other forms of multiplicative noise (e.g. frequency-dependent spectral amplitude drift) could significantly alter the features of the scatterer echo spectra, blurring or distorting the signature of the scatterer.

Several strategies may be adopted to mitigate the effects of contaminating noise on the classification process. Standard procedures include pre-processing the collected data to remove noise, either via time-windowing or frequency domain filtering. These approaches are particularly effective if the noise characteristics are well-understood, which may be more likely for a controlled tank experiment than for a field data collection system. For field data applications, range-gating is an effective technique to avoid scattering from multiple targets, and is used extensively in current echosounder applications. In the case of both tank and *in situ* data collections, reduction of incoherent noise may be achieved by averaging over several returns from a particular scatterer. This may also result in a degradation of the structure in the scatterer echo spectrum, so that there exists a trade-off between noise reduction and scatterer signature preservation, both of which will affect classifier performance.

In addition, the usable bandwidth of the collected data is an important consideration for the success of the classification inversion, since signal degradation through bandwidth reduction results in information loss. Significant loss of bandwidth could lead to data which contain insufficient information for robust classification. Reduction in usable bandwidth may arise from filtering out contaminating noise in a particular spectral band. In this case, the trade-off between scatterer signature degradation due to the presence of noise and information loss due to bandwidth reduction must be considered. Bandwidth reduction can also result from the frequency response characteristics of the acoustic transducer used to make the measurements. The operational characteristics of different transducers are variable; one device may exhibit a flat frequency response across the spectral band of interest, whereas another may possess a non-ideal frequency response over part of the band, yielding data with a reduced usable bandwidth.

Successful classification is possible in the presence of contaminating noise as well as with signals of reduced bandwidth, and may be achieved through the simultaneous application of alternative

classification techniques. Different classification approaches will differ in their sensitivities to the effects of noise contamination or the impact of information loss through bandwidth reduction. By taking into account the differential performance of each technique with noisy signals and bandwidth-reduced signals, overall classification performance can be improved. This requires a solid understanding of the sensitivity of the classifiers to signal degradation. To better understand the strengths and shortcomings of each classification approach, the EOFC (this Chapter) and the MPC (Chapter 3) have been evaluated in terms of their sensitivity to both noise contamination and signal bandwidth reduction. Based on the good performance of the EOFC in classifying the 1993 dataset (which included both reasonably high SNR data and some much noisier data), it is expected that this feature based classifier will prove robust in the presence of contaminating noise. EOFC performance with reduced bandwidth signals is also expected to be robust in the face of considerable bandwidth reduction. For the spectral signatures characteristic of the three classes, successful EOFC classification will likely be possible until bandwidth reduction results in the elimination of the signature information in the spectra.

2.4.1 EFFECT OF CONTAMINATING NOISE ADDITION

To explore the impact of noise contamination on the success of the different classification approaches (EOFC, MPC), simulations were carried out in which synthetic noise was added to simulated, noise-free acoustic returns for scatterers belonging to each of the three classes. To generate clean (noise-free) signals for the three scatterer types, the theoretical models detailed in Section 3.1.1 (Figure 3-1) were employed. These models are capable of generating a wide range of signals for each scattering class, but only a small subset of these signals was chosen as a basis for this noise sensitivity analysis, so that sensitivity to signal variability was not confounded with sensitivity to contaminating noise. For this analysis, animals in the gas-bearing class (**GB**) were modelled as a spherical gas bubble plus a contribution from fluid-like tissue, with the echo from the gas bubble dominating the return ((EQ 3.1) with $b_j = 0$). Returns from the fluid-like class (**FL**) were modelled as a ray summation including two rays, which represent scattering from the front and back interfaces of the animal (EQ 3.4). Similarly, noise-free elastic-shelled returns (**ES**) were modelled by a summation of the contributions of two rays, one from the direct return from a hard elastic sphere and the other from scattering due to a circumferential Lamb wave with the series truncated to include only the first partial circumnavigation (EQ 3.6).

To simulate a wide range of noise contamination conditions, varying quantities of synthetic noise were combined with these clean signals. Noise contamination was modelled as Gaussian-distributed white noise (GDWN). Many physical processes are well-modelled by Gaussian distributions, and GDWN is a reasonably good approximation to many of the potential noise sources in both tank experiments and field data collections. To consider the effects of additive, uncorrelated noise contamination on classifier performance, increasing quantities of synthesised GDWN were added to the clean signatures characteristic of each class, and classifier performance under these different signal-to-noise-ratio (SNR) conditions was monitored. Some other noise effects, including the effects of ensemble-averaged noise and multiplicative noise contamination, were also explored. These effects do not represent expected forms of noise contamination, but were investigated to isolate the effects on the classifiers of specific aspects of signal degradation.

Some noise contamination is apparent in the data collected in the ship-board tank (1993, 1994 cruise) as well as the land-based tank experiments (1995 workshop). A rough estimate of the degree of noise contamination can be made by determining the approximate range of SNR observed in the datasets. For the 1993 cruise datasets, the time series from 50 acoustic returns from each scatterer type (Animals 93-18 *Agalma okeni*, 93-33e *Meganyctiphanes norvegica* (run 5) and 93-29 *Limacina retroversa*) were examined. Assuming noise stationarity, time-windowing each return made it possible to isolate the experimental noise by looking at the portion of the return after the echo from the scatterer was received. The SNR (in dB) was computed by taking the logarithm of the ratio of the mean squared signal $\langle s^2(t)\rangle$ to the mean squared noise $\langle n^2(t)\rangle$:

$$SNR = 10\log(snr) = 10\log\left(\frac{\langle s^2(t)\rangle}{\langle n^2(t)\rangle}\right) \qquad \textbf{(EQ 2.4)}$$

Using (EQ 2.4), the mean SNR ($10\log(\overline{snr})$) of the 50 *A. okeni* (**GB** class) returns was ~14 dB, ranging from 5.3 dB to 16.8 dB. For the 50 *M. norvegica* echoes, the mean SNR was ~7 dB, ranging between 6 dB and 8 dB. The *L. retroversa* returns also had a mean SNR of ~7 dB, but with a much greater variance, ranging between 1.75 dB and 12.9 dB.

Coherent addition of instantaneous sample of GDWN

To simulate the noise contamination present in the experimental data, an instantaneous sample of synthesised GDWN was added coherently to the clean (noise-free) theoretical-model-generated signals for each class. This addition of an instantaneous GDWN sample may be the best approximation of incoherent, additive noise contamination, particularly if the primary source of

the noise in the experimental data is pre-amplifier noise. Gaussian-distributed white noise may be represented as the sum of sinusoids with varying amplitude and phase as follows:

$$n(t) = \sum_{n=1}^{N} A_n \cdot \sin(\omega_n t + \phi_n) \qquad \textbf{(EQ 2.5)}$$

For white noise, ω_n and ϕ_n are uniformly distributed between 0 to 2π. This formulation has the advantage that it can be used to generate noise that has a spectrum differing from white noise (e.g. red noise, which is a low-pass version of white noise) simply by choosing different distributions for ω_n and ϕ_n (Shinozuka and Jan 1972). For white noise (ω_n and ϕ_n uniformly distributed), the sum in (EQ 2.5) itself converges to a Gaussian distribution by virtue of the Central Limit Theorem. Therefore, by choosing samples at random from a Gaussian distribution, a time series of the noise process described in (EQ 2.5) may be simulated. For this synthesised GDWN, the magnitude of the Fourier transform ($|N(\omega)|$, where $N(\omega)$ is the Fourier transform of $n(t)$) is Rayleigh-distributed whereas the phase of $N(\omega)$ is uniformly-distributed (Figure 2-5). This arises from the fact that the real and imaginary parts of the Fourier transform of GDWN are Gaussian-distributed. Since the magnitude and phase are statistically independent, the joint PDF of the magnitude and phase can be shown to be the product of a uniform distribution and a Rayleigh distribution (Haykin 1988).

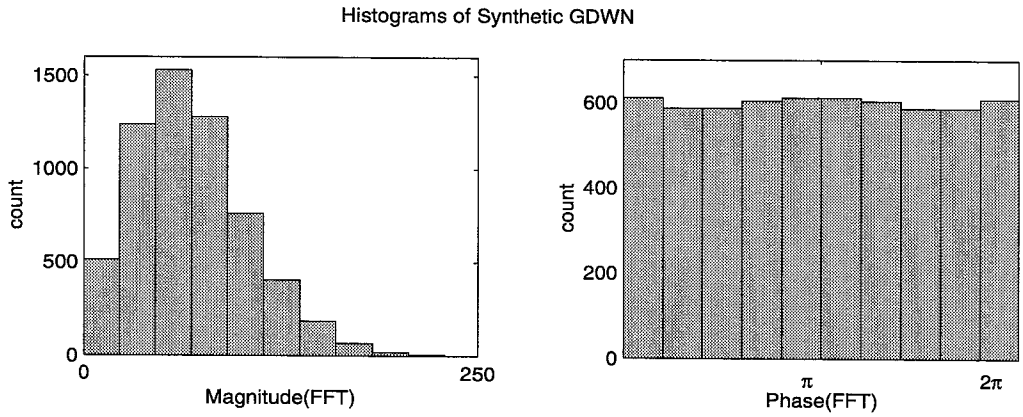

Figure 2-5 Histograms of the magnitude and phase of $N(\omega)$ (FFT of $n(t)$) reveal that the magnitude of the synthetic noise is Rayleigh-distributed while the phase is uniformly-distributed.

Coherent addition of the synthesised GDWN noise to the clean signals is accomplished by summing the real (Re) and imaginary (Im) parts of the spectra separately:

$$S(\omega) + N(\omega) = [\mathrm{Re}(S(\omega)) + \mathrm{Re}(N(\omega))] + i[\mathrm{Im}(S(\omega)) + \mathrm{Im}(N(\omega))] \qquad \textbf{(EQ 2.6)}$$

Where $S(\omega)$ and $N(\omega)$ are the Fourier transforms of $s(t)$ and $n(t)$ respectively.

An appreciation for the potential effects of noise addition to the theoretical-model generated clean signals can be gained through examination of the magnitude and phase, as well as the real and imaginary parts of the clean signals (Figure 2-6). In phase space, at a particular frequency, a single GDWN realisation will have a magnitude (length) drawn from a Rayleigh distribution and a phase (angle from the real axis) randomly sampled from a uniform distribution. Adding this noise phasor to the signal phasors will result in a "noisy" signal-like phasor, characterised by random deviations from the general shape of the signal phasor,

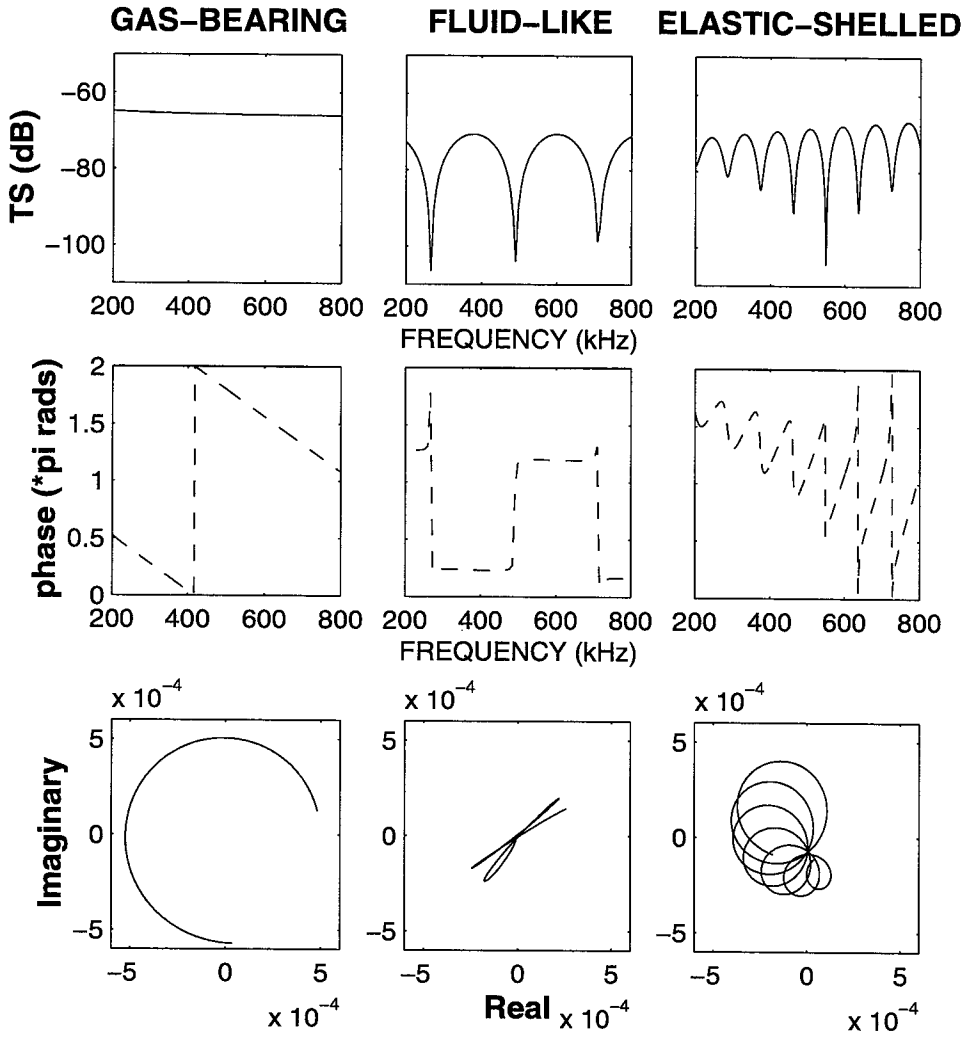

Figure 2-6 Characteristics of the theoretical-model-generated clean signals. Top row is $|S(\omega)|$, the magnitude of the Fourier transform of $s(t)$, plotted as target strength (TS) in dB. Second row is the phase of $S(\omega)$, computed as $\tan^{-1}(\mathrm{Re}[S(\omega)]/\mathrm{Im}[S(\omega)])$. Bottom row is the phasor diagram, showing plot of $\mathrm{Im}[S(\omega)]$ vs. $\mathrm{Re}[S(\omega)]$ over the frequency band 200 kHz - 800 kHz. Theoretical models plotted above are explicitly described in (EQ 3.1) with $b_j = 0$ (**GB**), (EQ 3.2) with $N = 2$ (**FL**) and (EQ 3.5) with the series truncated to include only the first partial circumnavigation (**ES**).

Since the classification algorithms are based on the magnitude of the frequency response of the echoes, only the effect of noise contamination on the resultant echo spectra is important. As noise contamination increases (decreasing SNR), the characteristic signature in the echo spectrum for each class becomes blurred due to random deviations from the signal shape introduced by the noise as well as a disproportionate addition of noise energy to the nulls as compared to the peaks (Figure 2-7). At an SNR of 0 (*snr* = 1), spectra from the three classes begin to resemble each other.

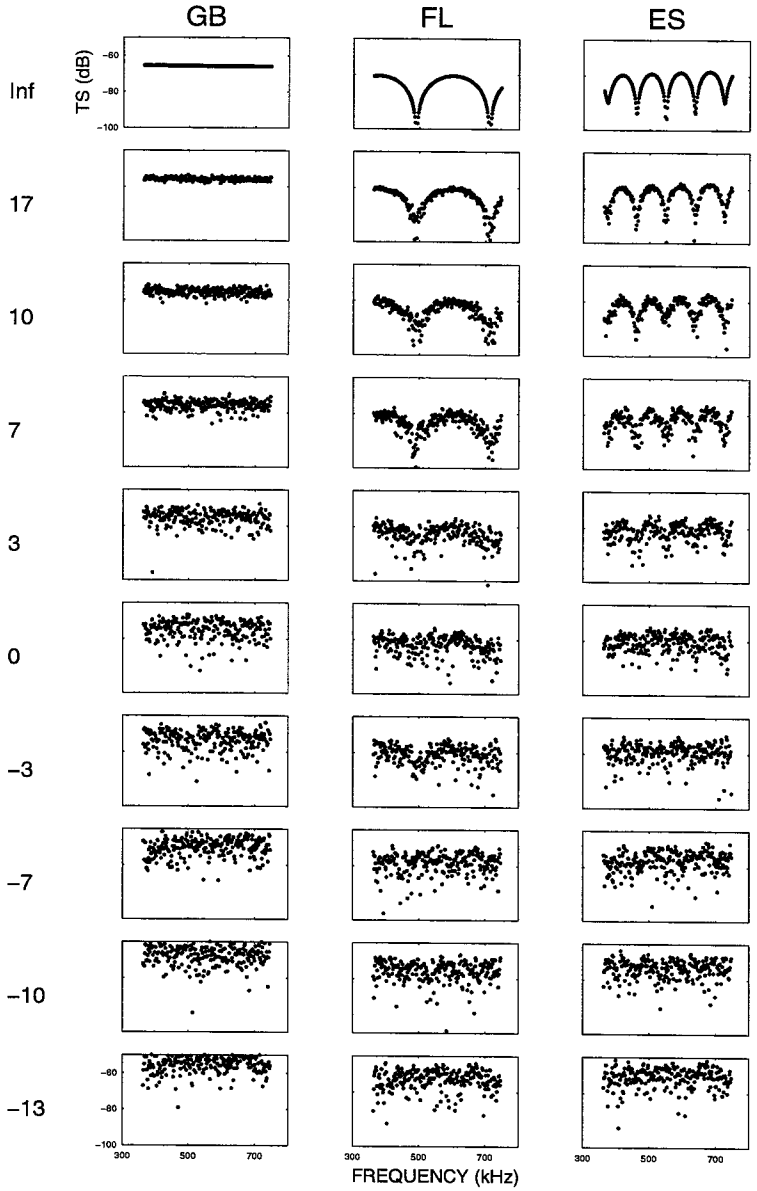

Figure 2-7 Effect of coherent addition of GDWN to clean signals (top row) on the magnitude of the Fourier transform (plotted as *TS* in dB). SNR (value to left of rows, in dB) decreases down the columns.

EOFC performance as a function of SNR was evaluated with 10 5-ping ensembles of simulated noise-contaminated signals. The M1-EOFC, which classifies the noisy 5-ping ensemble dominant mode (M1) against the M1 library for clean data, was fairly robust in the presence of GDWN. In particular, M1-EOFC performance began to deteriorate only once the SNR fell below -3 dB (noise energy twice as large as signal energy) for the **FL** and **ES** class realisations (Figure 2-8). For **GB** class realisations however, performance degraded at an SNR of as high as 17 dB (for which the signal energy is still 50 times the noise energy). This is not surprising, since the simulated clean signal for the **GB** class has no structure of its own. It is likely that even with the addition of very little noise energy, sufficient structure is added to the spectrum so that the dominant mode of variability of the noise-added signal becomes the noise mode. This will prevent the M1-EOFC from identifying it as the correct M1 library entry. In fact, the M21-EOFC results (for which M2 of the 5-ping ensembles of the noisy data were classified versus the M1 library) reveal that for some low SNR conditions, M2 of the noisy data is better identified versus the M1 library than is M1.

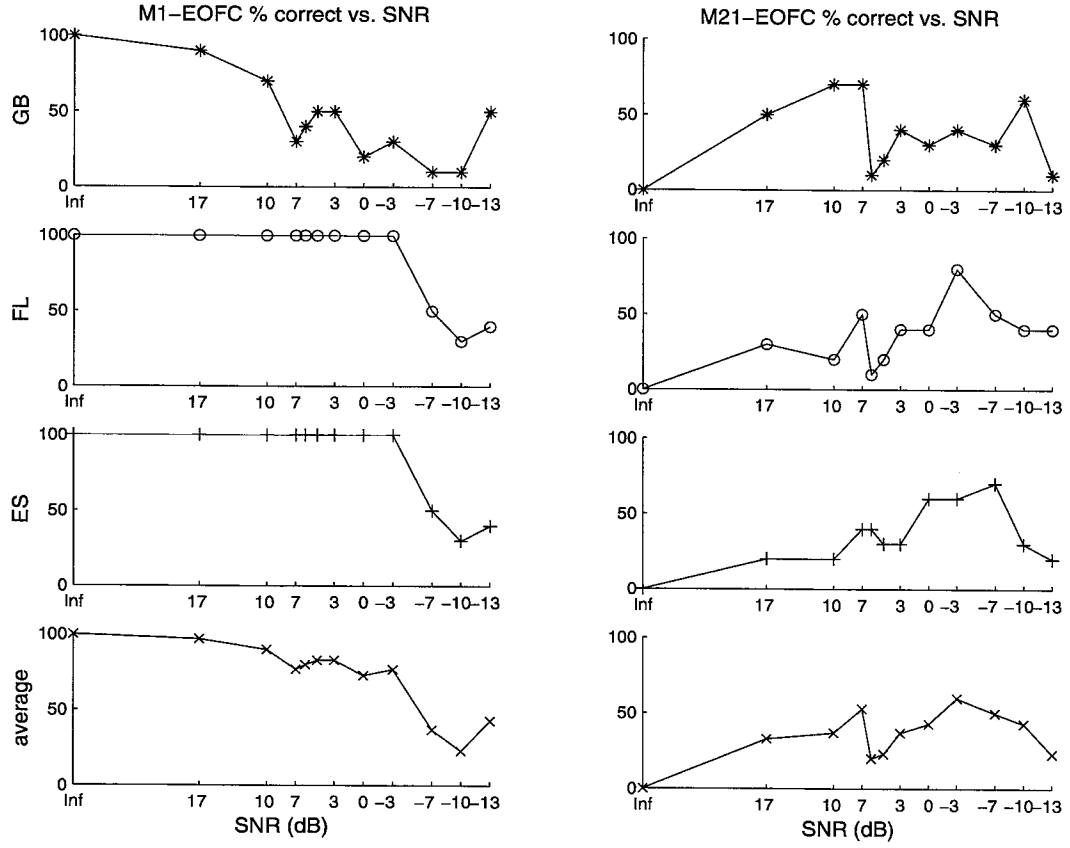

Figure 2-8 M1-EOFC and M21-EOFC performance (% correct, n=50) for GDWN contaminated signals.

Addition of ensemble-averaged noise

The effect of the coherent addition of clean signals to instantaneous samples of GDWN, which yields the spectra shown (Figure 2-7), can be thought of as a combination of two separate contributions. The effect of the first of these contributions will be considered here, and the effects of the second will be further explored subsequently (see **"Multiplicative noise contamination"**). With increasing noise addition (decreasing SNR), the structure in the echo spectra of the signals is degraded because the noise energy adds disproportionately to the nulls as compared to the peaks. If the noise simulation process were not confined to the addition of finite length, finite bandwidth, sampled instantaneous GDWN, the effect of this disproportionate addition of energy to the nulls of the echo spectra on the classifiers could be explored. In fact, ensemble-averaging an infinite number of realisations of instantaneous GDWN results in truly "white" time series. This averaged noise will be spectrally flat, with equal energy at all frequencies. By evaluating classifier performance on signals contaminated by the addition of this ensemble-averaged noise, the effects of structure degradation due to adding proportionately more energy to the nulls than to the peaks of the signal echo spectra may be explored in isolation. To simulate the effects of this type of noise contamination, increasing amounts of spectrally flat noise were added to the clean signals (Figure 2-9). This form of noise contamination affects the signal spectra for the three classes differently. For the **FL** and **ES** classes, increasing noise addition degrades the null and peak structure, making the spectral features progressively less pronounced. Since the ideal ensemble-averaged noise has a flat spectrum, as does the theoretical-model-generated clean signal used in this analysis to describe the **GB** class, the structure (or lack thereof) in the **GB** realisations remains intact once noise is added. However, the average level (*TS*) changes significantly with increasing noise addition. Similar to the case of the addition of instantaneous GDWN, at an SNR of 0 ($snr = 1$), the spectra from the three classes resemble each other considerably, both in the absence of any marked spectral structure, and in terms of average signal level (*TS*). For an SNR of 10, and perhaps even for SNR as low as 3, sufficient structure may remain in the spectra to allow class discrimination.

M1-EOFC performance (classification of the dominant modes (M1) of the noisy signals against M1 library for clean data) was outstanding for ideal noise-added realisations in all three classes (Table 2-2). The EOFC proved to be extremely robust to the effects of structure degradation alone. Even with noise contamination of same magnitude as signal (SNR=0), the M1-EOFC always correctly identified the dominant mode in the signal. This is a result of the fact that the EOFC does not depend directly on a pronounced structure in the spectra, but rather on the modes of variability

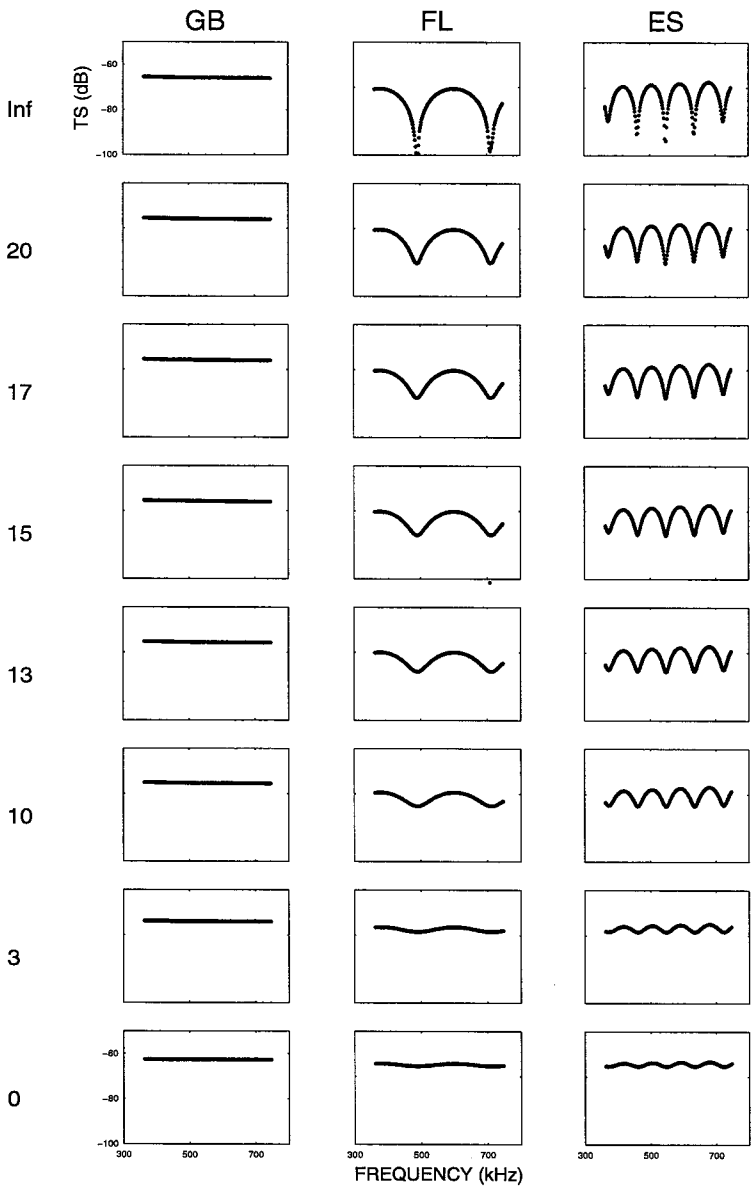

Figure 2-9 Effect of addition of ensemble-averaged noise to clean signals (top row) on the magnitude of the Fourier transform (plotted as *TS* in dB). SNR (in dB) decreases down the columns (value at left).

in the spectra. The addition of ensemble-averaged noise does not alter the modes of variability of the characteristic signatures of each class, it merely re-scales the energy of the signal by reducing the dynamic range so that the noise-contaminated realisations are easily identified. Since the performance of the EOFC under conditions of more severe noise contamination (SNR < 0) was not evaluated for this type of noise addition, the point at which performance degrades (if it does) is

unknown. It is certain that the EOFC will fail once the noise level exceeds the threshold at which the numerical quantisation of the spectral levels (in dB) becomes insufficient to resolve the variability which exists in the signal.

Table 2-2 M1-EOFC results (% correctly classified, n=50) with ensemble-averaged noise contamination.

	MAXIMUM SNR (dB)							
class	Inf	20	17	15	13	10	3	0
GB	100%	100%	100%	100%	100%	100%	100%	100%
FL	100%	100%	100%	100%	100%	100%	100%	100%
ES	100%	100%	100%	100%	100%	100%	100%	100%
AVERAGE	100%	100%	100%	100%	100%	100%	100%	100%

Multiplicative noise contamination

Examination of the echo spectra resulting from the coherent addition of instantaneous samples of GDWN (Figure 2-7) reveals that signature degradation occurs not only because of the disproportionate effects of noise addition on the nulls in the signal structure, but the characteristic signature in the echo spectrum for each class is also blurred due to random deviations from the signal shape introduced by the noise. In fact, complex scattering effects (from parts of the animal body not accounted for by the simplifying theoretical models, or from reverberation effects) can lead to returns that appear "spectrally noisy", where the spectra are characterised by signature-obscuring, seemingly random deviations. To isolate and investigate the effect of such random deviations in the spectra on classifier performance, simulations were carried out in which a form of multiplicative noise contamination was applied. Simulation of multiplicative noise was accomplished by adding the log-transformed noise spectra to the log-transformed spectra (*TS*) of the clean signals (Figure 2-10). This is equivalent to multiplying the non-log-transformed clean signals by the non-log-transformed noise. The noise spectra were simulated by choosing frequency samples at random from a normal distribution with a mean *TS* of 0 dB. Noise levels were altered by increasing the variance of the normal distribution from which the frequency samples were drawn. Since SNR is not a meaningful measure of multiplicative noise contamination, noise levels were measured in terms of this variance increase. With increasing noise variance, this form of noise contamination blurs the signature structure quite rapidly, in addition to widening the spread of the resultant echo spectrum. Applying multiplicative noise with a variance of 15 dB or greater results in the loss of all visible signature structure, so that the spectra from the three classes become indistinguishable to the eye.

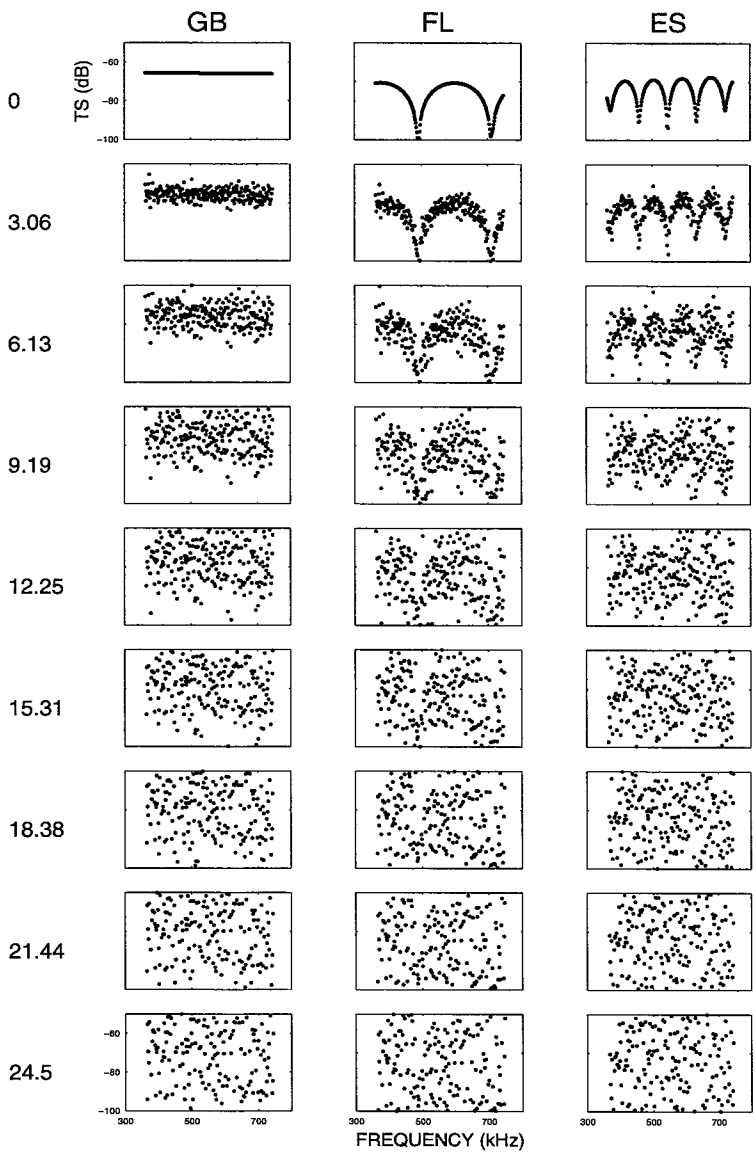

Figure 2-10 Effect of simulated multiplicative noise contamination on the magnitude of the Fourier transform of clean signals (top row). Log-transformed noise variance increases down the columns.

The EOFC was evaluated with a simulated dataset for each class (n=50) in which the noise variance was increased from 0 dB up to 24.5 dB. The M1-EOFC was highly sensitive to this form of multiplicative noise contamination, and was unable to correctly classify most of the spectrally noisy data, particularly for the **GB** and **FL** classes (Table 2-3). In contrast, the M21-EOFC showed considerable improvement over M1-EOFC performance. This indicates that as the noise variance

increased, the dominant mode became the noise mode (i.e. M1 represented the variability present in the noise, not the signal). The second-to-dominant mode (M2) then became the signal mode, and was readily identified vs. the M1 library. Although this mode switch (of M1 to noise mode and M2 to signal mode) occurred right away for **GB** realisations and at a noise variance of ~10 dB for **FL** realisations, it did not happen until higher noise variances for **ES** realisations. This is because the **ES** clean signal has higher variance than the **FL** signal, so that the **ES** signal mode remains the higher energy mode (M1) for higher levels of noise energy than does the **FL** signal mode under the same noise contamination conditions. An improvement in EOFC performance for the **ES** realisations can be achieved by using the weighted sum of the first 2 modes (W2-EOFC).

Table 2-3 EOFC results (% correct, n=50) with multiplicative noise contamination (max. variance=24.5 dB).

	M1-EOFC	M21-EOFC	W2-EOFC
GB	0%	100%	0%
FL	0%	100%	100%
ES	40%	60%	100%

2.4.2 EFFECT OF BANDWIDTH REDUCTION

Information loss through bandwidth reduction represents another important form of signal degradation. If classifier performance with reduced-bandwidth signals is well-understood, it is possible to optimise the trade-off between scatterer signature degradation due to the presence of noise, and information loss due to bandwidth reduction resulting from band-limited noise filtering. Even if filtering of band-limited noise is not performed, variability in the properties of transducer frequency responses can lead to bandwidth limitation issues. For example, the data collected in the three experiments (1993 cruise, 1994 cruise, 1995 workshop) differ in usable bandwidth due to differences in the transducer frequency responses for each experiment. The 1993 cruise data had a maximum usable bandwidth of between ~348 and 748 kHz, whereas the usable bandwidth for the 1994 cruise data was markedly reduced (~348 - 600 kHz) due to the poor high-end frequency response characteristics of the new transducer used on that cruise. Data from the 1995 workshop had an intermediate bandwidth, since a third transducer with a flatter high-end frequency response was employed. Regardless of the cause of bandwidth reduction, significant loss of bandwidth could lead to data which contain insufficient information for robust classification.

To assess the performance of the classifiers in the face of spectra with decreasing information content due to progressive bandwidth reduction, simulations were carried out in which clean

signals (described in Section 2.4.1, generated from theoretical models detailed in Section 3.1.1) were band-pass filtered using filters with pass-bands of decreasing width. This type of simulation not only allows characterisation of performance degradation with decreasing bandwidth, but the minimum required bandwidth for successful classification can also be determined in this manner. Clean signal bandwidth was reduced progressively from 241 sampled points representing the full spectrum between 348.33 - 748.55 kHz, down to a single point (Figure 2-11). For each bandwidth, the retained portion of the spectrum was varied by frequency-shifting the band-pass filter relative to the clean signal. This ensured that the classification results reflected the degree of bandwidth limitation and not the particular portion of the signal that was retained in a given realisation.

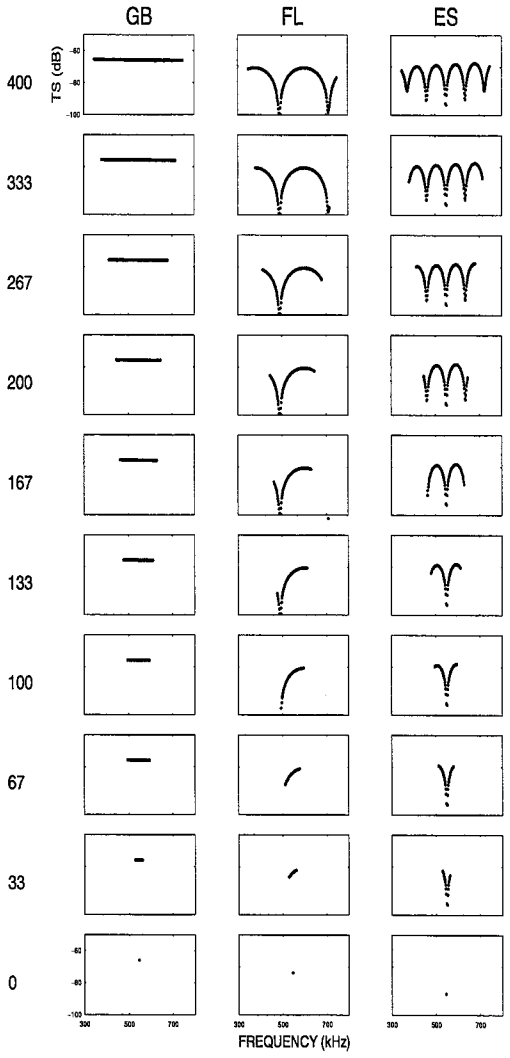

Figure 2-11 Effect of bandwidth reduction on the magnitude of the Fourier transform of clean signals (top row, plotted as *TS* in dB). For these realisations, the band-pass filter is centered at ~550 kHz. Remaining bandwidth (value to left of rows, in kHz) decreases down the columns.

M1-EOFC performance was remarkably robust with decreasing bandwidth (Figure 2-12). In particular, the modes of **GB** realisations appear to be insensitive to bandwidth reduction, with excellent results obtainable down to bandwidths just above 0 kHz. Classification success was also very high for the bandwidth reduced **ES** realisations. Good results were obtained down to a remaining bandwidth of only 125 kHz, which is approximately the bandwidth between successive nulls. On the other hand, performance with reduced-bandwidth **FL** realisations degraded much sooner. This is due to the fact that the bandwidth reduced **FL** modes are undersampled, resulting in aliasing and misclassification with as much as 300 kHz of remaining bandwidth.

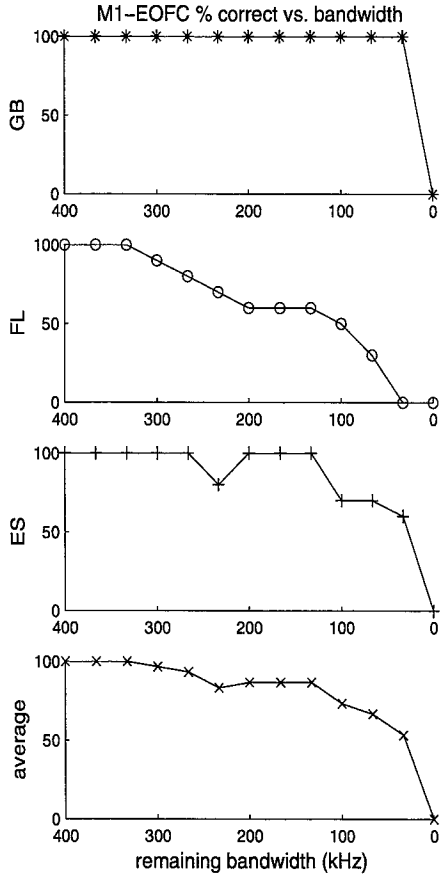

Figure 2-12 M1-EOFC performance (% correctly classified, n=50) for bandwidth reduced signals.

The time-bandwidth product is a frequently used guideline of discrimination power. It provides a measure of the number of orthogonal signals that can be resolved for a given length time series with a given bandwidth. For example, for the 200 μs duration echo time series collected in the experiments, in order to resolve 3 perfectly orthogonal model realisations (corresponding to the 3 classes), a bandwidth of only 15 kHz should be required ($3 = T \cdot BW = 2\times10^{-4}s \cdot 15\times10^{3}Hz$). This

measure provides an absolute lower bandwidth limit, assuming orthogonality. Since the clean signals used in this analysis to represent the 3 classes are not orthogonal, it is expected that a minimum bandwidth of significantly greater than 15 kHz will be necessary to resolve them. In the presence of contaminating noise, bandwidth requirements for successful classification will likely increase further, since depending on the noise characteristics, the information in a limited bandwidth spectra may become insufficient once confounded with a noise signal.

CHAPTER 3

THEORETICAL MODEL BASED CLASSIFICATION: MODEL PARAMETERISATION CLASSIFIER (MPC)

3.1 RATIONALE

The application of model based classification techniques is only possible if there exist theoretical or empirical forward models which express the relationship between the observed data and the model parameters. For inversion problems where the theoretical or empirical basis from which to construct such a relationship is well-characterised, a promising approach to the classification problem is the application of techniques that can capitalise on the predictive power of class-specific models. For the zooplankton classification problem, there are reasonably well-developed theoretical scattering models for the three classes (Section 1.1.2), providing a sound basis for a model based classification approach. The success of any model-based inversion scheme depends upon the degree to which the forward model adequately describes the relationship between the observed data and the model parameters, and whether features predicted by the model can be resolved in the data. Although the theoretical models for each scattering class will not accurately predict all possible observed echoes, these sophisticated models describe the general scattering characteristics of zooplankton in each class sufficiently to allow discrimination between classes.

A model based classification scheme that incorporates the full detail of the theoretical model predictions for each class can be designed, but such a design would be very complex due to the number of model parameters, and may not classify robustly, particularly in the case where the values of many of these parameters are unknown or unmeasurable. It may in fact be desirable to design a scheme that can exploit the predictive power of the theoretical models for echo classification without being encumbered by the details in the models. For example, it is possible to parameterise the theoretical model predictions into simpler forms and to establish a connection between the model parameters and the physical properties of the animal, so as to achieve a practical, working parameterisation that can be generalised to other animal types. The Model Parameterisation Classifier (MPC) described in this Chapter represents an initial approach to theoretical model based classification. The MPC involves the creation of several alternative parameterisations of the theoretical scattering models for each class. This parameterisation process was carried out in such a manner that the resulting simplified model realisations encompassed a range of predicted spectra for each class, but also allowed separability of the classes.

3.1.1 SUMMARY OF THEORETICAL MODELS

For gas-bearing (**GB**) fluid-like plankton (siphonophores) with a single gas inclusion, the general scattering properties are described by the spherical gas bubble plus fluid-like tissue model (modal series solution for bubble plus ray summation solution for tissue) as given in Stanton *et al.* (in press b):

$$TS_{GB} \cong 20\log\left|-\frac{i}{k}\sum_{m=0}^{\infty}(2m+1)\cdot(-1)^m\cdot b_m^{(f)} + \sum_{j=1}^{N} b_j \cdot e^{i2k\varepsilon_j}\right| \qquad \textbf{(EQ 3.1)}$$

The first term represents the scattering from the gas inclusion (which at high ka is dominated by the echo from the front interface), assuming the bubble can be modelled as a fluid sphere, whereas the second term represents the scattering from the body as a summation of the rays due to the major scattering features of the fluid-like tissue. The $b_m^{(f)}$ are the modal series coefficients for a sphere (Anderson 1950), ε_j is the displacement of the scattering feature from a zero-phase reference plane, thereby accounting for the phase shift of each ray, and the b_j are the amplitude coefficients for the rays. These amplitude coefficients are difficult to determine for the siphonophore body, which is composed of many bracts, gastrozooids and tentacles. The echo from the gas bubble is believed to dominate the scattering from siphonophores; however, echoes from the tissue (although many dB weaker) may contribute measurably in some cases.

Scattering from elongated fluid-like (**FL**) crustacean zooplankton (euphausiids, shrimp) in the geometric regime is described by a ray summation formula, from Stanton *et al.* (1994b, in press b):

$$TS_{FL} \cong 20\log\left|\sum_{j=1}^{N} b_j \cdot e^{i2k\varepsilon_j}\right| \qquad \textbf{(EQ 3.2)}$$

In much the same way as for the siphonophore tissue, each ray represents the scattering contribution from a different scattering feature of the fluid-like body. The phase shift of each ray is again accounted for by the ε_j, but for these elongated fluid-like animals, the amplitude coefficients b_j are more easily defined. For example, for the ray associated with the front interface of the animal $b_j = (1/2)\Re(\rho_j^{(1)} \cdot \rho_j^{(2)})^{1/2}$ where $\rho_j^{(1)}$ and $\rho_j^{(2)}$ are the local radii of curvature (in two $\perp$ planes, (1) and (2)) of the point of scatter. With this formulation, many rays (associated with different scattering features of the animal body) may be taken into account, and the resultant predicted signal is the summation of the scattering contributions from all these rays. Although this

formulation allows the incorporation of an infinite number of scattering features, the summation of more than two rays can lead to an erratic signal, and with as few as six rays, the frequency response can appear similar to that of noise. In fact, changing the relative locations and strengths of the scattering features drastically changes the predicted backscattered signal. In many cases, particularly when the animal is oriented near broadside relative to the transducer, the scattering from these elongated fluid-like crustacean zooplankton is well-described by a simpler two-ray summation, which models the constructive and destructive interference between the ray associated with scattering from the front interface of the animal and the ray associated with scattering from the back interface. This two-ray randomly oriented fluid bent cylinder model is expressed as follows, from Stanton *et al.* (1993a,b):

$$TS_{FL} \cong 20\log\left(\frac{1}{2}\sqrt{\rho_c a}\Re e^{-i2k_1 a} I_0 e^{-\alpha_B(2\theta\rho_c/L)^2}\right) \qquad \textbf{(EQ 3.3)}$$

where

$I_0 = 1 - T_{12}T_{21}e^{i4k_2 a}e^{i\mu(k_1 a)}$ with $T_{mn} = 2\frac{\rho_n c_n}{\rho_m c_m}/\left(1+\left(\frac{\rho_n c_n}{\rho_m c_m}\right)\right)$, $\mu(k_1 a) \cong -\frac{\pi}{2}\frac{k_1 a}{(k_1 a + 0.4)}$;

ρ_c is the radius of curvature along the longitudinal axis of the body; and

θ is the angle of orientation, with $\theta = 0$ indicating broadside incidence.

For a narrow range of lengths, and orientations including broadside incidence, (EQ 3.3) was used to derive an expression for the average backscattering cross-section (Stanton *et al.* 1993b), yielding:

$$TS_{FL} \cong 10\log\left(2A_{ij}\frac{\Re^2\bar{L}^2}{\beta}\left[1 - e^{-8(ka)^2 s^2}\cos\left(ka\left(4 - \frac{\pi}{2(ka+0.4)}\right)\right)\right]\right) \qquad \textbf{(EQ 3.4)}$$

where

$A_{ij} = \frac{T_B^2 C_B^2}{8\sqrt{2\pi}\sqrt{\alpha_B}}$ for angle of orientation uniformly-distributed;

$\beta = (L/a)$; and

$s = s_L/\bar{L}$, where s_L is the standard deviation of length.

Here $\alpha_B = 0.8$, $T_B = 1$, and $C_B = 1.2$ are empirically determined parameters (Stanton *et al.* in press b), with values adjusted to achieve a best fit to predictions using the more precise distorted wave Born approximation. Stanton *et al.* (1993b) also includes an expression for averaging over angle of orientation only, as well as an expression for A_{ij} for Gaussian-distributed orientations.

For spherical hard elastic-shelled (**ES**) organisms (e.g. pteropods) a ray-based model also applies (Stanton *et al.* in press b):

$$TS_{ES} \cong 20\log\left|F_{spec}\frac{a}{2}\Re e^{-i2ka} - F_l\frac{\bar{a}}{2}G_l e^{i\Phi_l}e^{-2(\pi-\theta_l)\beta_l}\cdot e^{i\eta_l}\sum_{m=0}^{n}(-1)^m\cdot e^{-2\pi m\beta_l}\cdot e^{im\phi}\cdot e^{-(1/2)\gamma^2\sigma^2}\right| \quad \textbf{(EQ 3.5)}$$

where

$$G_l = -8\pi\beta_l\left(\frac{c}{c_l}\right) \text{ with } \frac{c}{c_l} = \frac{8ka+0.5}{k\bar{a}};$$

$$\eta_l = 2k\bar{a}\left[\frac{c}{c_l}(\pi-\theta_l)-\cos\theta_l\right]-\frac{\pi}{2};$$

$$\phi = 2\pi k\bar{a}\left(\frac{c}{c_l}\right);$$

$$\theta_l = Re\{\operatorname{asin}(c/c_l)\};$$

$$\gamma = k\left\{2\left[\frac{c}{c_l}(\pi-\theta_l)-\cos\theta_l\right]+2\pi m\left(\frac{c}{c_l}\right)\right\}; \text{ and}$$

$$\beta_l = 0.002ka$$

Here $\Phi_l = -\pi/2$, $\sigma = 0.025\bar{a}$ and a is the average value of several samples from a Gaussian distribution with mean $\bar{a}$ and standard deviation σ. The first term represents the direct return (the echo from the front interface), assuming the body can be modelled as a fluid sphere, with F_{spec} indicating the relative contribution of this specular reflection. The second term represents the scattering from a circumferential, antisymmetric Lamb wave l travelling at subsonic speeds along the surface of the shell (Marston 1988), with F_l indicating the relative contribution of this return. If the animal is oriented in such a way that the opercular opening interferes with the propagation of the flexural wave, the scattering will be dominated by the direct return, and the second term may be neglected ($F_l = 0$). For these organisms, the zeroth-order Lamb wave (flexural wave) dominates (Stanton *et al.* in press a), and the series is truncated to include only the first partial circumnavigation (m=0 term), so that (EQ 3.5) becomes:

$$TS_{ES} \cong 20\log\left|F_{spec}\frac{a}{2}\Re e^{-i2ka} - F_l\frac{\bar{a}}{2}G_l e^{i\Phi_l}e^{-2(\pi-\theta_l)\beta_l}\cdot e^{i\eta_l}e^{-(1/2)\gamma^2\sigma^2}\right| \quad \textbf{(EQ 3.6)}$$

where γ is now:

$$\gamma = 2k\left(\frac{c}{c_l}(\pi-\theta_l)-\cos\theta_l\right).$$

In the expressions for all three scattering classes, a is the equivalent spherical or cylindrical radius of the animal in m, k is the acoustic wavenumber $k = 2\pi f/c$, f is the acoustic frequency in Hz, c is the sound speed in m/s, $\Re$ is the reflection coefficient $\Re = (gh-1)/(gh+1)$ where $g = \rho_2/\rho_1$ is the density contrast of the organism (subscript 2) relative to water (subscript 1), $h = c_2/c_1$ is its sound speed contrast, and L is the total length of the animal in m.

3.1.2 COMPARISON OF DATA AND THEORETICAL MODELS

In order to parameterise the theoretical models so that the resulting model realisations allow discrimination between classes while encompassing the range of echoes observed for each class, it is necessary to gain an understanding of the variability present in the echo spectra as well as to identify the features of the data and the theoretical predictions that will allow discrimination of the classes. To this end, some single-ping echo spectra collected from animals in each scattering class are compared to a theoretical model of *TS* versus frequency for that class (Figure 3-1).

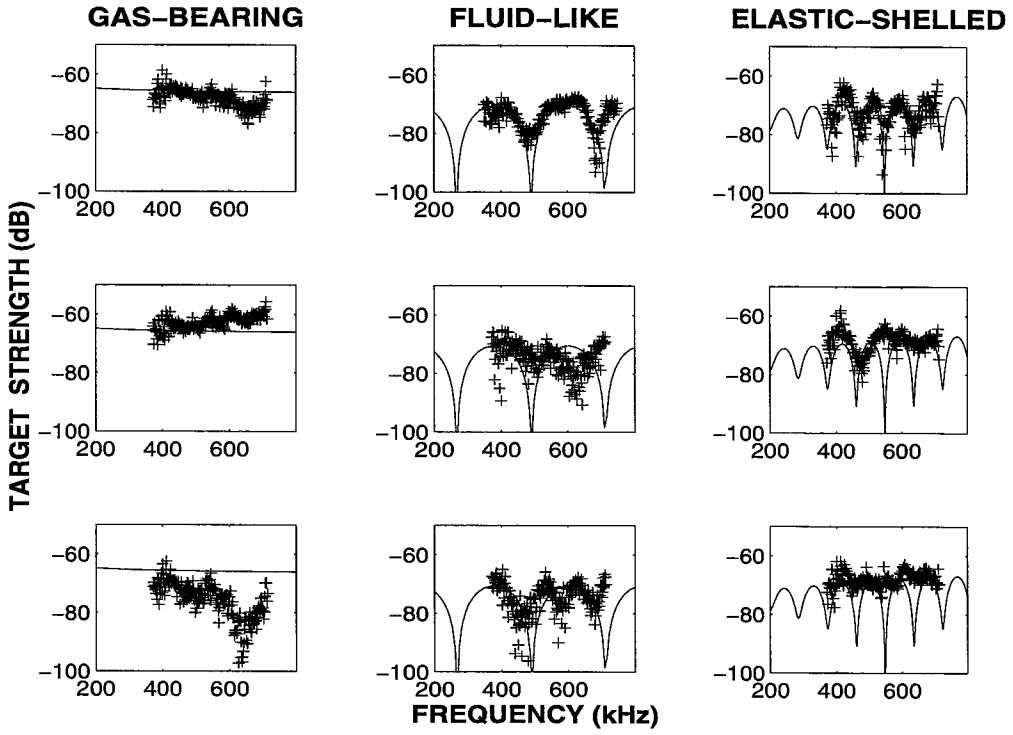

Figure 3-1 Echo spectra of a selected set of experimental data plotted with theoretical models for each class. **GB** model: spherical gas bubble plus fluid-like tissue model (EQ 3.1) with echo from gas dominating scattering; **GB** data: single siphonophore *Agalma okeni* (Animal 93-18). **FL** model: ray summation including two rays, one from front interface, one from back interface (EQ 3.4); **FL** data: decapod shrimp *Palaemonetes vulgaris* (top) and euphausiid *Meganyctiphanes norvegica*, (Animal 93-33). **ES** model: ray summation including only first partial circumnavigation of Lamb wave (EQ 3.6); **ES** data: two pteropods *Limacina retroversa* (Animals 93-29 (top) and 93-30).

For gas-bearing (**GB**) fluid-like plankton (siphonophores) with a single gas inclusion, selected echo spectra were compared to the spherical gas bubble plus fluid-like tissue model (modal series solution for bubble plus ray summation solution for tissue from Stanton *et al.* in press b) with the echo from the gas bubble dominating the scattering. For elongated fluid-like (**FL**) crustacean zooplankton (euphausiids, shrimp), pings were compared to the ray summation formula (Stanton *et al.* in press b), with two rays (those representing scattering from the front and back interface of the animal) included in the summation (from Stanton *et al.* 1993b). For spherical hard elastic-shelled (**ES**) organisms (pteropods), echo spectra were compared to the ray-based model that accounts for the direct return (the echo from the front interface), as well as the scattering from a circumferential Lamb wave travelling along the surface of the shell with the zeroth-order Lamb wave dominating and the series truncated to include only the first partial circumnavigation (Stanton *et al.* in press a). The experimentally collected echo spectra shown for the gas-bearing category (**GB**) are from a single siphonophore *Agalma okeni* insonified during the 1993 cruise (Animal 93-18). Pings from animals in the fluid-like (**FL**) class are from a euphausiid *Meganyctiphanes norvegica* insonified during the 1993 cruise (Animal 93-33) and a decapod shrimp *Palaemonetes vulgaris* insonified in a tank on land (see Chu *et al.* 1992, Stanton *et al.* 1994b). Data collected from animals in the elastic-shelled class (**ES**) include the echo spectra of two pteropods, *Limacina retroversa* insonified during the 1993 cruise (Animals 93-29 and 93-30).

The observed variability in the frequency spectra of the acoustic returns within and between individuals in a scattering class can be attributed to differences in the behaviour and morphology of the animals. Changes in the orientation of the animal during insonification may lead to ping-to-ping variability in the acoustic returns from a single target. For example, the spectra of elongated fluid-like zooplankton can exhibit different null-spacings depending on the animal's orientation relative to the acoustic beam (Figure 5-6). Additionally, when the animal is not near broadside incidence, it is possible that other scattering features contribute, leading to a more complicated interference pattern. Differences in orientation may explain why echoes from some elastic-shelled individuals contain several tightly spaced nulls, whereas echoes from others exhibit a flat spectrum. For certain orientations, Lamb (circumferential) waves may propagate and scatter back toward the receiver, yielding an oscillatory spectrum as a result of the interference between the direct return (from the front interface of the shell) and the Lamb wave. For other orientations, attenuation of the Lamb waves by the opercular opening may eliminate the interference pattern, and the spectrum may be flat (Stanton *et al.* 1996). Variability in the frequency response between

different animals of the same species or in the same scattering class can also be attributed to differences in apparent animal size (which may change as orientation changes). For fluid-like and elastic-shelled scatterers there is an inverse relationship between apparent animal size and null spacing in the frequency response (Figure 5-5). The size range of the elastic-shelled *Limacina retroversa* represented in the data is tight, resulting in fairly similar null spacings for different animals for this dataset. Although gas-bearing animals with a single gas inclusion dominating the scattering will exhibit predominantly flat spectra, individuals with multiple closely-spaced inclusions or animals in which the tissue contributes significantly to the backscattered signal can exhibit an interference pattern and a spectrum with nulls.

It is evident that some echo spectra fit the theoretical model predictions better than others. For example, although the top and middle echo spectra (Figure 3-1) for the gas-bearing category are fairly well-described by the bubble-dominated spherical gas bubble plus fluid-like tissue model, the bottom spectrum may be better described by a non-bubble-dominated version of this model (one in which the tissue contributes significantly to the scattering giving rise to an interference pattern with a deep null). In the fluid-like category, the top return is remarkably well-described by a two-ray summation model, the middle spectrum is adequately described by a frequency-shifted version of this same two-ray model, while the bottom ping may be better described by a two-ray summation for a scatterer with a larger apparent size (either because the animal has a larger girth thereby increasing the distance between its front and back interfaces, or the animal is oriented off-broadside, also leading to a greater apparent girth). Alternatively, inclusion of more than two rays in the summation due to possible contributions from other scattering features may lead to a better prediction of this bottom spectrum. In a similar manner, the top and middle echo spectra in the elastic-shelled category appear to be well-predicted by a model which includes significant contributions from both the specular return and the backscattered energy from the Lamb wave, whereas the bottom ping does not possess the same structure as do the other two, and would likely be better predicted by a direct-return dominated version of the model where the Lamb wave contribution is significantly reduced.

3.2 ALGORITHM

The theoretical models outlined in Section 3.1.1 describe a non-linear relationship between the many input parameters and the predicted acoustic returns from zooplankton in the three scattering classes. Classifying observed data based on these model parameters would involve a non-linear inversion, since the theoretical model parameters cannot be linearly combined to predict the observations. Instead of attempting to classify observed data by inverting for these theoretical model parameters, the Model Parameterisation Classifier (MPC) matches observations to **model realisations**, which are generated by employing simplifying parameterisations of the theoretical models. The MPC is based on the assumption that the data can be represented as a linear combination of these simplified model realisations. MPC classification consists of choosing the best match among all the model realisations, so that an observation is assigned to the model space (or class) which contains the model realisation with the highest contribution in the linear sum.

To build the model spaces (which consist of several alternative model realisations) from the theoretical models, a range of simplifying parameters was chosen for each scattering class that could encompass most of the variability present in the echoes from scatterers in that class, and at the same time allow for distinction between the 3 classes of scatterers. The MPC incorporates parameterisations of the subset of theoretical model predictions plotted in Figure 3-1: the bubble-dominated spherical gas bubble plus fluid-like tissue model for the **GB** class, the ray summation formula including the principal two rays for the **FL** class, and the specular return plus zeroth-order-Lamb-wave ray-based model (with the series truncated to include only the first partial circumnavigation) for the **ES** class. This subset of the theoretical model predictions can be parameterised to yield three unique model spaces. Attempts to incorporate other model parameterisations that are not unique to a particular scattering class will result in overlapping of the model spaces, leading to an inability to discriminate the classes. For example, the non-bubble-dominated spherical gas bubble plus fluid-like tissue model can predict **GB** echoes nearly identical to the **FL** echoes predicted by a multiple-ray summation. Clearly, including parameterisations of these in the **GB** and **FL** model spaces will result in the confounding of these model spaces and an ambiguous classification result.

The MPC involves two stages of classification (Figure 3-2). In the first stage (STAGE I), the gas-bearing model is parameterised as a straight line with slope (m) and intercept (b) parameters. A straight line is fit through each echo spectrum (SPEC) by linear regression ($y = mx + b$) and the

sum of squares of the residuals (SSR) is computed for each: $SSR = \Sigma (y(i) - SPEC(i))^2$. Echo spectra from scatterers that are well represented by a straight-line model will have considerably smaller SSR than echo spectra exhibiting deep nulls. All echo spectra are classed as either "**GB**" (gas-bearing) if $SSR \leq t$ or "not **GB**" if $SSR > t$, where t is an optimal threshold adjusted to give the best classification of a sample known dataset. The **GB** model space consists of 25 bins that quantify the SSR associated with each return. Echo spectra classed as "not **GB**" enter the second stage of classification.

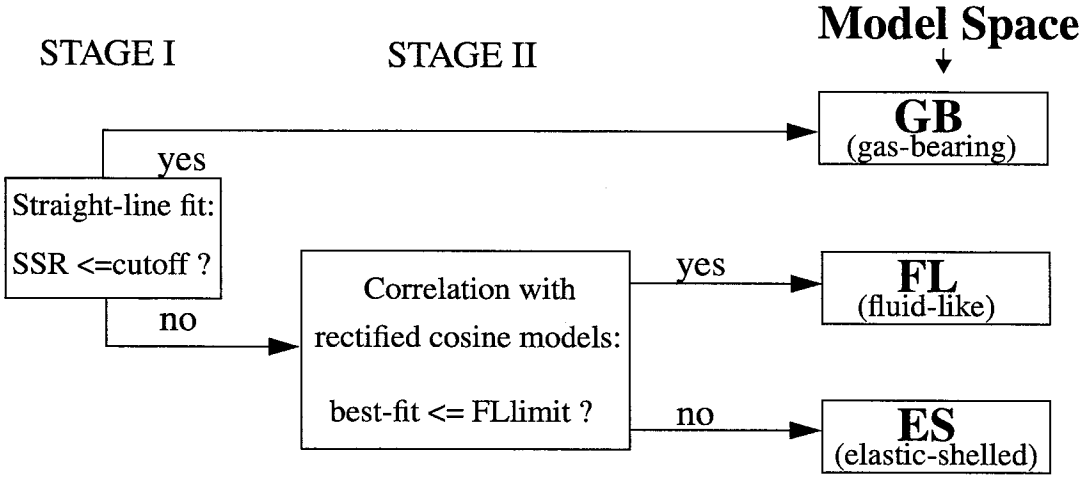

Figure 3-2 Summary of the MPC classification algorithm.

In STAGE II, the **FL** (fluid-like (EQ 3.3)) and **ES** (hard elastic-shelled (EQ 3.6)) theoretical models are simplified by parameterising them as rectified cosines. These sinusoidal realisations are fully described by only two features: null spacing and frequency shift. To construct each of the model spaces, several model realisations of rectified cosines, differing in null spacing and frequency shift, were created (Table 3-1). The ranges of these two parameters for fluid-like (**FL**) and hard elastic-shelled (**ES**) model realisations were determined by examining the appropriate theoretical model predictions as well as several dozen experimentally collected echo spectra for each scatterer type. To include the range of echo spectra observed in the datasets, nine different null spacings were chosen for the **FL** model realisations. For **ES**, 5 different null spacings were used. The possibility of frequency-shifted returns was also accounted for in the model spaces, resulting in 81 different **FL** model realisations and 25 different **ES** model realisations. These simplified model realisations are able to capture the structure in the echo spectra, differentiating the classes based only on differences in the null spacing. Other features of the echo spectra such as mean echo level, null depth and variance are not exploited in this preliminary classification scheme.

Table 3-1 Parameter values used in the simplifying parameterisations of the **FL** and **ES** theoretical models.

MODEL TYPE	null spacing	frequency shift
FL (fluid-like)	every 130 - 370 units	every $2\pi/9$
ES (hard elastic-shelled)	every 60 - 100 units	every $2\pi/5$

All pings classed as "not **GB**" pings after STAGE I of classification were examined to determine whether they were **FL** (fluid-like) or **ES** (hard elastic-shelled). The echo spectrum of each ping was correlated to each model realisation as follows:

$$\mathbf{x} = \mathbf{M}^{\mathrm{T}}\mathbf{y} \qquad \textbf{(EQ 3.7)}$$

where $\mathbf{y}$ is a matrix in which each column represents one mean-subtracted echo spectrum to be classified, $\mathbf{M}$ is a matrix in which each column represents a model realisation and $\mathbf{x}$ gives the degree of correlation of each ping to each model realisation. Maximum correlation (i.e. maximum value in each column of $\mathbf{x}$) reveals the best-correlated model realisation for a particular echo spectra, indicating best fit. Classification of a ping involves determining to which model space the best-fit model belongs. This correlation procedure, which identifies the largest contributing model realisation in the linear sum, follows from the least squares linear inverse solution.

The MPC as a Least Squares Linear Inverse

For a linear system, the inverse problem may be solved using a standard general inversion technique that has been described in several works on inverse theory (Backus and Gilbert 1967, Aki and Richards 1980, Menke 1989). In a linear inversion, the observed data can be expressed as a linear combination of the theoretical forward model parameters, so that the solution to the inverse problem involves solving for the model parameters that, once weighted by the kernel, best predict the observed data (Menke 1989). The general formula for a linear system is expressed as:

$$d_i = \sum_{j=1}^{M} G_{ij} m_j \qquad \textbf{(EQ 3.8)}$$

where d_i (i = 1, 2,..., N) are the data or observations of the system, G_{ij} is the kernel, and m_j are the model parameters for which we wish to invert. This equation can be written in matrix form as:

$$\mathbf{d} = \mathbf{Gm} \qquad \textbf{(EQ 3.9)}$$

For the zooplankton classification problem, this formulation of the linear inverse problem does not present a convenient form in which to invert observed data for theoretical model parameters, since

the theoretical models (Section 3.1.1) describe a non-linear relationship between the model parameters and the predicted acoustic returns from zooplankton in the three scattering classes. However, this linear inverse solution may be exploited by deriving simplifying parameterisations of the theoretical models to create model realisations for each scattering class, and assuming that the data can be represented as a linear combination of these simplified model realisations. The zooplankton classification problem can then be cast in the form of a generalised inverse solution in the following manner:

$$\mathbf{y} = \mathbf{M}\mathbf{x} \qquad \text{(EQ 3.10)}$$

Where $\mathbf{y}$ is either a vector or a matrix containing the data to be classified (in this case, the echo spectrum/spectra of the acoustic return(s) from an animal), $\mathbf{M}$ is a matrix containing the model realisations against which we want to classify the data (derived from parameterisations of the theoretical models), and $\mathbf{x}$ is a vector or matrix of weights which reveal the best classification for the input data. One approach to inverting for $\mathbf{x}$ (for an over-determined problem) involves looking at the model space:

$$\mathbf{x} = (\mathbf{M}^T\mathbf{M})^{-1}\mathbf{M}^T\mathbf{y} \qquad \text{(EQ 3.11)}$$

where $(\mathbf{M}^T\mathbf{M})^{-1}$ can be decomposed into its orthogonal basis functions:

$$(\mathbf{M}^T\mathbf{M})^{-1} = \varphi\Lambda^{-1}\varphi^T \qquad \text{(EQ 3.12)}$$

If the model realisations contained in $\mathbf{M}$ are all orthogonal, then φ would contain exactly these model realisations; in the case of non-orthogonal realisations, φ represents the basis set from which all the model realisations may be constructed. An alternative formulation (for an under-determined problem) of the generalised inverse given in (EQ 3.11) is as follows:

$$\mathbf{x} = \mathbf{M}^T(\mathbf{M}\mathbf{M}^T)^{-1}\mathbf{y} \qquad \text{(EQ 3.13)}$$

This formulation permits a more informative investigation of the data space. In a similar manner to (EQ 3.12) above, $(\mathbf{M}\mathbf{M}^T)^{-1}$ may be decomposed into it's orthogonal basis functions:

$$(\mathbf{M}\mathbf{M}^T)^{-1} = \phi\Lambda^{-1}\phi^T \qquad \text{(EQ 3.14)}$$

Substituting (EQ 3.14) into (EQ 3.13) yields:

$$\mathbf{x} = \mathbf{M}^T(\phi\Lambda^{-1}\phi^T)\mathbf{y} \qquad \text{(EQ 3.15)}$$

Thus the solution to the inverse problem $\mathbf{x}$ is arrived at by first projecting the model realisations onto their own orthogonal basis set ($\mathbf{M}^T\phi$) to determine how much of each orthogonal element

composes each of the model realisations. Similarly, the data for which we want to invert for scattering class is projected onto the orthogonal basis set of the model realisations ($\phi^T\mathbf{y}$) to determine how much of each component is required to describe the data. Finally, Λ^{-1} is a weighting function that gives the relationship between the two projections by normalising the energy content of each projection to yield an estimate of $\mathbf{x}$.

The representations in (EQ 3.11) through (EQ 3.15) allow for an adjustment of the resolution of the inverse. This may accomplished through a de-tuning of the Λ matrix which will decrease resolution, and depending upon the particular classification problem may lead to more accurate results than the highest resolution inversion. In fact, the trade-off between resolution and variance for this type of classifier is the key to ensuring robust classification. For the zooplankton classification problem, the primary goal of this preliminary classification scheme is not to be able to discriminate between the many similar but alternative model parameterisations within the model space for a given scattering class, but instead to make gross distinctions between one class and the other with very little error. Given this requirement, the most robust classification results will likely be obtained using the fully-damped least squares inverse, which sacrifices resolution in favour of low error/variance. This least squares inverse is arrived at by setting $(\mathbf{M}^T\mathbf{M})^{-1} = (\mathbf{M}\mathbf{M}^T)^{-1} = \mathbf{I}$ in (EQ 3.11) and/or (EQ 3.13), resulting in:

$$\mathbf{x} = \mathbf{M}^T\mathbf{y} \qquad \textbf{(EQ 3.16)}$$

Comparing (EQ 3.16) to (EQ 3.7), it becomes apparent that the MPC is simply the fully-damped least squares formulation of the generalised linear inverse. The MPC has very low resolution, but the level of resolving power is sufficient to discriminate between the three scattering classes, and with very low error. An increase in resolution may be unnecessary for the purposes of discriminating the scattering classes, and would lead to an increase in error (variance) in the classification results.

3.3 PERFORMANCE

In addition to the variability observed in the spectra, both between separate insonifications of a single zooplankter as well as between different individuals in the same scattering class, noise contamination was more evident in returns from some animals than others. Initially, MPC performance was evaluated against a 150-ping sub-sample (representing the highest signal-to-noise ratio (SNR) data) consisting of acoustic returns from one animal in each of the three classes. This high-quality dataset consisted of 50 echo spectra each of a siphonophore *Agalma okeni* (Animal 93-18), a euphausiid *Meganyctiphanes norvegica* (Animal 93-33e (run 5)), and a pteropod *Limacina retroversa* (Animal 93-29).

For this subset of data, MPC STAGE I correctly identified all *M. norvegica* and *L. retroversa* pings as "not **GB**" and 92% of the *A. okeni* pings as "**GB**", indicating that the parameterisations of the bubble-dominated theoretical model are adequate to classify these **GB** class returns (Figure 3-3).

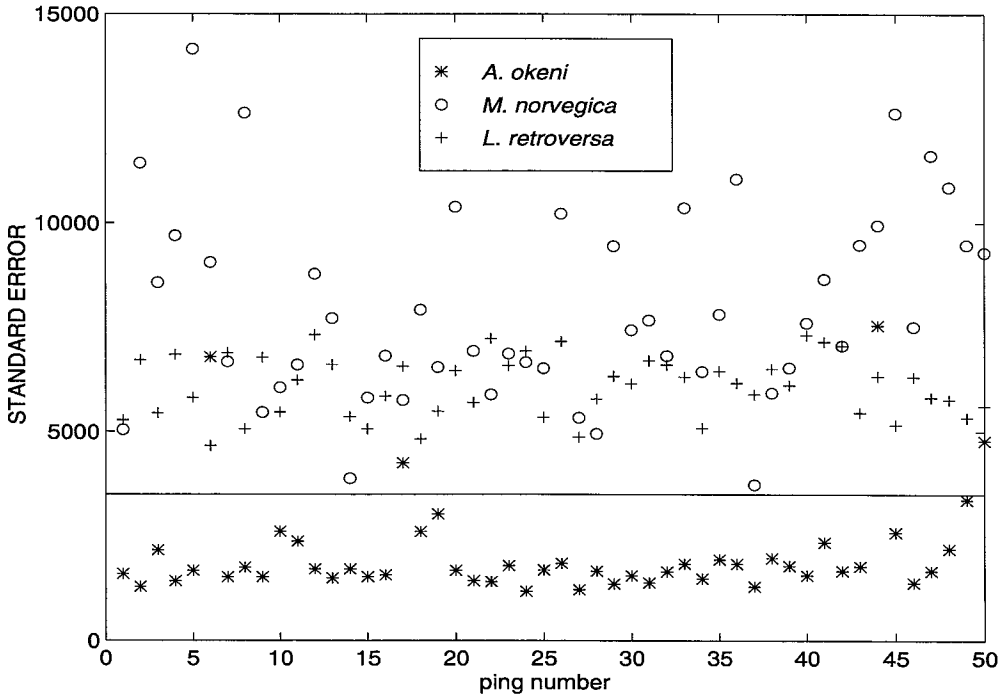

Figure 3-3 Results of MPC STAGE I with the high-SNR 150-ping sub-sample of the 1993 dataset. The optimal SSR threshold as estimated for this data is shown as a straight line.

After STAGE II, the MPC success rate for these three high SNR 50-ping datasets was about 95% (Figure 3-4). The parameterisations of the 2-ray model for the **FL** class and the direct-return-plus-Lamb-wave model for the ES class allow excellent discrimination of these echo spectra.

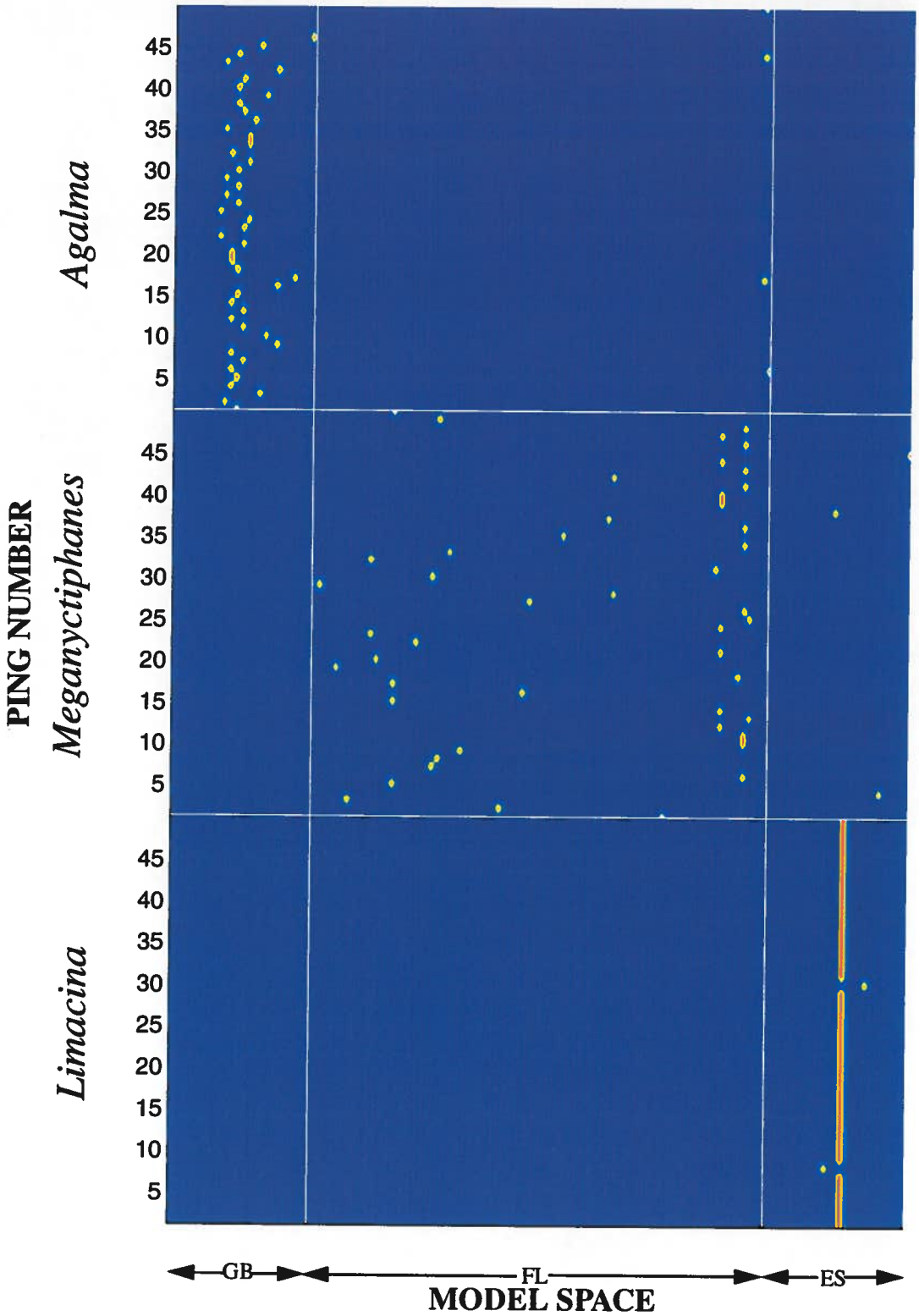

Figure 3-4 MPC classification results for the high SNR subset (1993 cruise). Success rate was ~95%. Individual echo spectra for each class are numbered up the y-axis.

The MPC was less successful in classifying many of the other datasets (Table 3-2). The MPC average success rate over the entire 1993 cruise dataset of 1850 echoes (37 50-ping ensembles) was approximately 64%.

Table 3-2 MPC results for 1850-ping (1993) dataset. "*" indicates high SNR data shown in (Figure 3-4).

species		Animal #	run #	n	% correct
Agalma okeni		93-13	1	50	58%
		93-14	1	50	50%
		93-16	1	50	10%
		93-17	1	50	66%
	*	93-18	1	50	92%
		93-19	1	50	10%
		93-20	1	50	12%
		93-21	1	50	48%
		93-22	1	50	12%
		TOTAL		450	40%
Meganyctiphanes norvegica		93-33a	1	50	92%
		93-33b	2	300	86%
		93-33c	3	300	79%
		93-33d	4	300	86%
	*	93-33e	5	50	94%
		TOTAL		1000	85%
Limacina retroversa		93-23	1	50	20%
		93-24	1	50	16%
		93-26	1	50	2%
		93-27	1	50	66%
		93-28	1	50	40%
	*	93-29	1	50	100%
		93-30	1	50	0%
		93-31	1	50	54%
		TOTAL		400	37%
ALL ANIMALS		TOTAL		1850	64%

Despite a very high success rate with the high SNR subset of the 1993 cruise data, the MPC was much less successful in classifying the balance of the 1993 dataset. This follows from the fact that acoustic returns that are not well-predicted by the parameterised theoretical models will not be correctly inverted for with this model based inversion scheme. Deviations from the model realisations could result from either noise contamination in the data or the presence of a wider range of signal variability in the data than is captured in the parameterised model realisations. Both the *Agalma okeni* and *Limacina retroversa* data were poorly classified due to variability in the observed echo spectra for these two scatterer types. Much of the *L. retroversa* data also had lower SNR than data from the other two species. Because the MPC relies on matching an observed acoustic return to the parameterised noise-free model realisations, noise contamination is likely to be particularly troublesome for this classifier. Sections 3.4 and 3.5 describe the results of a thorough investigation of the sensitivity of the MPC to signal degradation caused by noise contamination as well as a preliminary look at the effects of signal variability on this model based classifier. The performance of the MPC relative to the other classifiers developed in this thesis work is discussed briefly in Section 6.1.

All of the misclassified *A. okeni* returns were identified as "not **GB**" by MPC STAGE I, and most were subsequently classed as **FL**. STAGE I of the MPC relies on the fact that spectra from scatterers that are well represented by the straight-line parameterisation of the **GB** model will have considerably smaller SSR than spectra exhibiting deep nulls. Significant individual-to-individual variability in echo spectra was observed in the 1993 *A. okeni* data. This variability may have been due to the presence of multiple-bubble gas inclusions in some of the experimental animals, since individuals with multiple closely-spaced inclusions (as can result from embolism upon being removed from depth too quickly (Pugh and Harbison 1986, Pugh and Youngbluth 1988)) could exhibit a multiple-bubble interference pattern and a spectrum with nulls. Pre-insonification visual inspection of the siphonophores in this experiment revealed multiple bubbles in all but two individuals (Animals 17 and 20) whereas the majority of the specimens contained only one bubble after insonification. It is uncertain how many bubbles were present during insonification, or whether the presence of multiple bubbles is the sole mechanism for the observed oscillatory spectra. It is believed that even individuals with a single gas inclusion can exhibit both flat and oscillatory spectra (see (EQ 3.1)). If the tissue contributes significantly to the scattering, then the scattering from the bubble may no longer dominate and the interference between returns from the

tissue and the single bubble can introduce spectral oscillations (Stanton *et al.* in press b), which are not included in the theoretical model parameterisation used to create the **GB** model space.

In a similar manner, the model parameterisation used in the **ES** model space does not account for possible attenuation of the Lamb wave by the orientation of the opercular opening. Several *Limacina* returns, particularly those from Animal 93-30, were classified as **GB** because the echo spectra were more or less flat due to an insignificant Lamb wave contribution. Many *L. retroversa* returns were misclassified as **FL** (especially those from Animals 93-24, 93-26 and 93-28), either because they exhibited a wider null spacing due to a smaller apparent size, or some nulls were not as pronounced, possibly due to a smaller Lamb wave contribution. Although MPC success with the *Meganyctiphanes norvegica* data was generally high, most of the few misclassified echo spectra were assigned to the **ES** class, likely due to tighter null spacings resulting from changes in apparent animal size.

The simplifying parameterisations employed in the MPC provided a convenient basis from which to build model spaces for the three scattering classes, and inversion based on these model spaces is reasonably effective, particularly for high SNR data and datasets with low intra- and inter-individual variability. For datasets which include gas-bearing animals with differing scattering contributions from the tissue, fluid-like zooplankton which assume a broad range of orientations, or elastic-shelled animals with variable Lamb wave contributions, these simple parameterisations may not be adequate to account for the extent of signal variability present in the data. It is uncertain to what degree the wide range of variability observed in some of the experimentally collected acoustic returns is an artifact of the experimental procedure itself, particularly since much of the variability is orientation dependent. The natural orientation distribution of these zooplankton is not well-understood; Section 5.1 contains a summary of what is known about the *in situ* orientation of zooplankton in the three scattering classes from the literature and observations. Even if experimental artifacts were eliminated, it is possible that model spaces consisting of simple parameterisations of a subset of the theoretical model predictions for each class may not be sufficient to correctly classify all echoes from these zooplankton. Building model spaces which incorporate the full breadth of echoes predictable by the theoretical models for each scattering class will result in a classification scheme better able to classify data exhibiting a high degree of variability in the acoustic returns of zooplankton within a class, providing that the confounding effects of inter-class ambiguity due to overlapping model spaces can be overcome (see Chapter 4).

3.4 SENSITIVITY TO SIGNAL DEGRADATION

To better understand the limitations of the classifiers, the effects of several different forms of signal degradation on the classification success of the MPC were explored. In particular, the characteristic acoustic signatures of each scattering class were subjected to various forms of noise contamination and bandwidth reduction, and the performance of the MPC was evaluated under these conditions. This investigation sought to simulate several possible types of signal degradation, including system noise, background noise, the presence of other scatterers, calibration error/drift, and a non-ideal transducer frequency response over the band of interest. A detailed discussion of the sources and various effects of these forms of signal degradation is included in Section 2.4. Possible strategies to minimise the effects of processes contributing to signal degradation include pre-processing to remove noise, range-gating to avoid scattering from multiple targets, and averaging over several returns to reduce the incoherent noise. Once the differential performance of the classification approaches with degraded signals is well-understood, additional classification success with degraded signals can be achieved through the simultaneous application of several different classification techniques.

3.4.1 EFFECT OF CONTAMINATING NOISE ADDITION

To understand the effect of contaminating noise on MPC performance, simulations were undertaken in which different types of synthetic noise were added to simulated noise-free (clean) signals and classifier performance was evaluated. As outlined in Section 2.4.1, a limited set of clean signals were generated using the theoretical models detailed in Section 3.1.1. To investigate the effects of additive, uncorrelated noise, MPC performance under different SNR conditions (computed using (EQ 2.4)) was evaluated by adding increasing quantities of synthesised GDWN to the clean signatures characteristic of each class. The effects of ensemble-averaged noise addition and multiplicative noise contamination were also explored.

Coherent addition of instantaneous sample of GDWN

In this analysis, instantaneous samples of synthesised GDWN (EQ 2.5) were added coherently to the clean theoretical-model-generated signals for each class using (EQ 2.6), yielding realisations with increasing noise levels (Figure 2-7). The amplitude and phase characteristics of the clean signals, and the properties of GDWN and its appropriateness for this analysis, are discussed in detail in Section 2.4.1. For example, addition of an instantaneous GDWN sample is a good approximation of the incoherent, additive pre-amplifier noise contamination suspected in the tank experiments.

The performance of the MPC was fairly robust in the presence of GDWN, with deterioration beginning only once the SNR fell below 0 dB (noise energy same as signal energy) for the **FL** and **ES** class realisations (Figure 3-5). For **GB** class realisations however, performance degraded at an SNR of as high as 7 dB (for which the signal energy is 5 times the noise energy). Since the simulated clean signal for the **GB** class has no structure of its own, the addition of relatively small quantities of noise energy adds sufficient structure to the spectrum so that the SSR exceeds the **GB** classification threshold for the **GB** class. This prevents the MPC from identifying it as a **GB** realisation, and classification success goes immediately to 0 once this threshold is exceeded. For the other two classes, MPC performance degrades gracefully with increasing SNR.

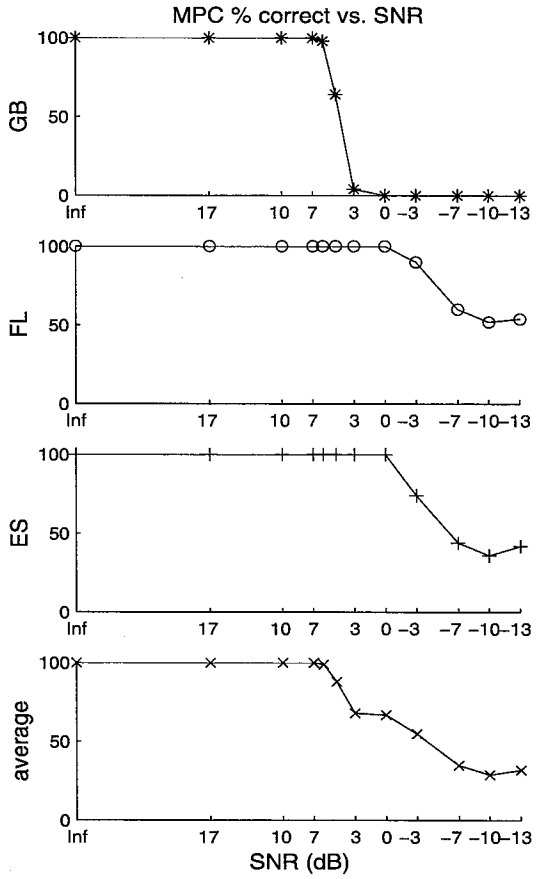

Figure 3-5 MPC performance vs. SNR (in dB) for GDWN contaminated signals.

Addition of ensemble-averaged noise

As described in Section 2.4.1, to decompose the effects of the instantaneous GDWN contamination explored above into two separate contributions, the impact of ensemble-averaged (spectrally-flat) additive noise on MPC performance was investigated in isolation. This form of

additive noise contamination affects the spectra for the three classes somewhat differently (Figure 2-9): the null and peak structures are degraded for the **FL** and **ES** classes, whereas only the average level is changed for the **GB** class.

The MPC performs well with ideal noise-added **GB** realisations (Table 3-3), but its performance quickly deteriorates as noise is added for the other 2 classes (**FL, ES**). This is not surprising, since the MPC relies heavily on matching the structure of the signal to the structure of the theoretical model parameterisations. This form of noise contamination adds energy disproportionately to the nulls relative to the peaks, thereby narrowing the dynamic range of the spectra by progressively shallowing the nulls. Any noise contamination that degrades the spectral structure in this manner will be particularly problematic for the MPC. In fact, adding a maximum of only 5% noise (SNR=13 dB) significantly decreased the success probability of the MPC for **FL** and **ES** class realisations.

Table 3-3 MPC results (% correctly classified, n=50) with ensemble-averaged GDWN contamination.

	MAXIMUM SNR (dB)							
class	Inf	20	17	15	13	10	3	0
GB	100%	100%	100%	100%	100%	100%	100%	100%
FL	100%	100%	98%	64%	40%	20%	4%	2%
ES	100%	100%	100%	100%	60%	30%	6%	4%
AVERAGE	100%	100%	99%	89%	67%	50%	37%	35%

Multiplicative noise contamination

The second noise effect (as discussed in Section 2.4.1) that was investigated in isolation was the blurring of the characteristic echo spectra of each class due to random deviations from the signal shape introduced by the noise. To determine the effect on MPC performance of this spectral blurring and of the accompanying increase in spectral dynamic range, varying levels of multiplicative noise contamination (measured by the variance of the noise in dB) were applied to the clean signals for each class (Figure 2-10).

MPC STAGE I (the SSR decision threshold) was found to be very sensitive to multiplicative noise contamination (Table 3-4). This follows from the fact that increasing levels of multiplicative noise contamination applied to even the lowest variance clean signals (e.g. clean **GB** realisation) drastically increase the value of the spectral SSR, so that the optimal classification threshold is rapidly exceeded. A decision threshold-based rule is bound to fail in the presence of the levels of

multiplicative noise contamination tested herein. It should be noted that the SSR threshold may be optimised for different signal-to-noise conditions, within a reasonable range that will allow the **FL** and **ES** pings to be distinguished from the **GB** pings. MPC STAGE II on the other hand is extremely robust in the presence of multiplicative noise contamination. Classification results for the **FL** and **ES** class realisations were perfect, even when the noise variance reached 24.5 dB. MPC STAGE II is based on correlation of the data spectra to parameterised model realisations. Since the multiplicative noise spectrum is completely uncorrelated (each frequency sample was chosen at random from a normal distribution), the STAGE II correlation process is unaffected by the presence of even large quantities of this type of noise. For this reason, the MPC is able to correctly identify the maximum correlation model realisation for even highly noise contaminated spectra.

Table 3-4 MPC results (% correct, n=50) with 2 levels of multiplicative noise contamination.

	MAXIMUM NOISE VARIANCE (dB)	
	12.25	24.5
GB	32%	16%
FL	100%	100%
ES	100%	100%

3.4.2 EFFECT OF BANDWIDTH REDUCTION

As discussed in Section 2.4.2, signal degradation through bandwidth reduction can arise due to filtering of band-limited noise or as a result of non-ideal transducer frequency response characteristics. In fact, the data from the three experiments (1993 cruise, 1994 cruise, 1995 workshop) differs in usable bandwidth due to differences in the frequency response of the transducer used for each experiment. To understand MPC performance capabilities with reduced bandwidth signals, a simulated dataset of progressively narrower-band signals was created for each class (Figure 2-11). For a given bandwidth reduction, the band-pass filter was frequency-shifted relative to the clean signal so that the retained portion of the spectrum was varied. MPC performance with these bandwidth-reduced signals was evaluated.

The MPC was able to correctly classify the reduced bandwidth realisations quite well down to a remaining bandwidth of 200 - 220 kHz (Figure 3-6). It was found that MPC STAGE I (the SSR decision threshold) is somewhat sensitive to bandwidth reduction, particularly for **FL** and **ES** realisations. For a given bandwidth reduction, the SSR varies considerably depending on which

portion of the band is retained. In some cases, the remaining portion of the bandwidth for the **FL** and **ES** realisations had an SSR below the optimal SSR decision threshold, leading to mis-classification of these realisations as **GB**. The MPC proved most robust with reduced bandwidth **GB** realisations, since bandwidth reduction does not affect SSR for these signals. Even with the **FL** and **ES** signals, a good portion of the spectrum can be filtered out (depending on which portion of the band remains) before classification performance degrades. Interestingly, MPC STAGE II results reveal that the bandwidth-reduced signals correlate best with different frequency-shifted model realisations in the correct class. It is not surprising that the MPC results with reduced bandwidth **ES** realisations are slightly better than with **FL** realisations, since more structure is contained in the signature per unit of bandwidth for the **ES** signals relative to the **FL** signals,

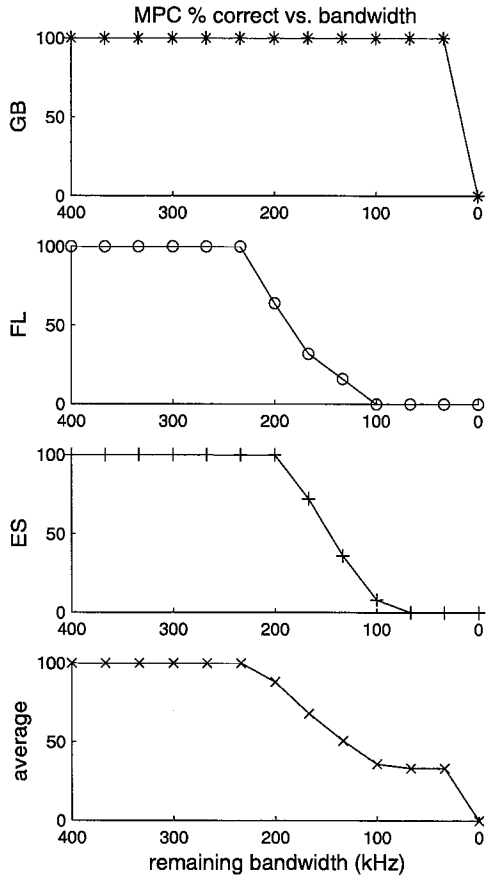

Figure 3-6 MPC performance vs. remaining bandwidth (in kHz) for bandwidth reduced signals.

3.5 SENSITIVITY TO SIGNAL VARIABILITY

The simulations described in Sections 2.4 and 3.4 to assess the sensitivity of the classifiers to signal degradation made use of the theoretical models detailed in Section 3.1.1 to generate clean (noise-free) signals characteristic of the three scatterer types. Varying the parameter values of these theoretical models generates a wide range of possible signals for each scattering class. Only a limited subset of these possible predicted echoes (Section 2.4.1) was employed in the sensitivity analyses so that classifier sensitivity to signal variability was not confounded with sensitivity to signal degradation. This allowed the effects of noise contamination and bandwidth reduction on the classifiers to be explored in isolation. However, not only do the theoretical models predict a wide range of signals for each class, significant variability in the observed echo spectra is evident both between different returns from the same individual as well as across different individuals in a given scattering class (Figure 3-1). In addition, the MPC classification algorithm is based on matching observed echo spectra to parameterised versions of a subset of the full range of signals predictable by the theoretical models. As a result, the sensitivity of the MPC to variability in the acoustic returns within a given class was investigated in order to better characterise the limitations of this classifier.

Acoustic signature variability exists both between distinct echoes from a single individual as well as between the returns from different individuals within a particular scattering class. Some sources of intra-individual signature variability include changes in the orientation of the individual, differences in its material properties due to changes in physiological state (e.g. starving vs. replete) or changes in season (e.g. molting, over-wintering), and alterations of individual body geometry/ morphometry (changes in gas inclusion size with depth, tentacle extension for feeding or tentacle contraction for swimming, etc.). Changes in orientation alone can drastically modify the amount of acoustic energy scattered by a particular zooplankter, as well as the apparent size of the individual (particularly for non-spherical, elongated animals). These orientation-dependent effects result in differences in the level (*TS*) of the acoustic returns from a single animal as well as variability in the structure of the echo spectra; changes in apparent size of the animal alter the null spacing of the signature (Figure 5-6). Additional orientational effects include fundamental changes in the physical scattering characteristics of the animal, manifested as changes in the relative contribution of different rays to the total scattered energy. For example, for a pteropod oriented in such a way that the opercular opening interferes with the propagation of the circumferential wave, the direct return ray can dominate the scattering, dwarfing any contribution from the

circumferential ray. Variability in the acoustic signatures of different individuals within the same scattering class can result from inter-individual differences in animal size or from differences in animal morphometry (i.e. the relative proportions of the animal, its radius of curvature etc.) between individuals of the same species, as well as between animals of different species within the same scattering class. In addition to size-dependent effects on the echo spectra (variability in echo level and null spacing), morphometric differences could have complex scattering effects, contributing to significant variability in signature structure through the possible introduction of additional scattering features.

The presence of acoustic signature variability within each of the three scattering classes poses some challenges to the classification process. Signature variability broadens the range of average echo levels and signature structures that must be identified with a particular scattering class. A successful classifier must encompass this range of possibilities in the model spaces for each class in order to correctly recognise animals exhibiting variable signatures. However, this broadening of possible signatures within each class could result in an overlap or ambiguity between the model spaces of different classes (at least in terms of certain aspects of the structure), so that simply broadening the model spaces for each class will not ensure successful classification. For example, given the possible range of sizes and orientations for animals in the **FL** and **ES** classes, the observable range of null-spacings could overlap, and the echo spectra of animals in these two classes will not be unambiguously distinguishable on the basis of null-spacing alone (Figure 3-7). In a similar manner, the range of SSR for the **GB** and **ES** classes could overlap for **GB** animals whose scattering is dominated by their gas inclusion and **ES** animals whose scattering is direct-return dominated, so that discrimination based on SSR alone will be confounded. Animals in the **GB** class whose scattering is influenced by significant contributions from the tissue could exhibit spectra with null-spacings that overlap with those observed in **FL** or **ES** echoes. In these cases, successful classification will depend heavily upon the ability of the classifier to resolve these ambiguities.

One strategy that can be adopted to overcome the confounding effects of signature variability on the classifiers is the incorporation of *a priori* information into the classification process. For field applications, this includes information about the species or taxa present in the water and their respective size ranges (obtainable from direct water sampling by net or pump), as well as the orientation of the animals (obtained directly using video cameras, or estimated as expected

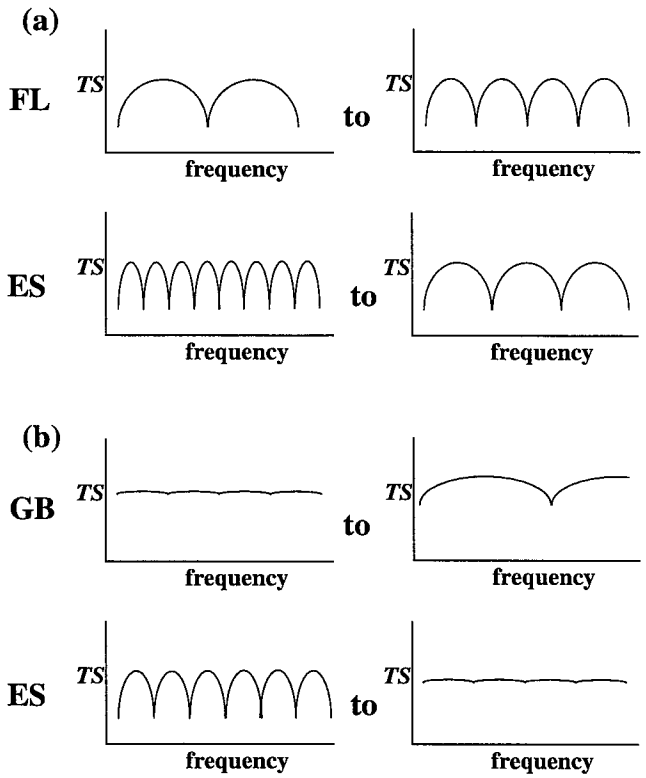

Figure 3-7 Diagram illustrating the potential for signature ambiguity between classes due to intra- and inter-individual variability in the acoustic returns within a class. In (a), variability in animal size and/or orientation leads to an overlap in the observed null-spacing of the echo spectra for animals in the **FL** and **ES** classes. In (b), the SSR-overlap between the **GB** and **ES** classes due to variability in scattering-feature contributions for these two animal types also leads to signature ambiguity.

orientations corresponding with suspected activities). For a given dataset, this *a priori* information may be used to place bounds on the set of possible species, sizes, and orientations, thereby constraining the range of feature values (e.g. null-spacing, SSR) and combinations of feature values (particularly for co-dependent features) used in the classification. This information can also serve to constrain the classification itself, since in the known absence of a particular scattering class, that class may be ruled out as a possibility entirely. Another strategy to combat the effects of variability might be to classify an animal based on several echoes, computing the moments of the feature values (e.g. mean, variance). These statistical measures may prove to be better discriminating features since they take into account the information contained in several acoustic returns from the same animal, thereby capturing the inherent variability in these returns. Finally, the simultaneous implementation of several different classification approaches that have differing sensitivities to signature variability will increase classification success. This requires a solid understanding of the relative affect of signature variability on classifier performance.

A preliminary investigation of the impact of within-class acoustic signature variability on MPC performance was undertaken. Simulations were carried out in which spectra spanning a wide range of signal variability were generated (Figure 3-8) using the multiple-ray summation theoretical model (EQ 3.2). This multiple-ray model is ideal for simulating echo spectra variability, since it is capable of describing a vast range of signals ranging from a coherent two-ray interference pattern (e.g. the echo from an elongated fluid-like zooplankter at broadside incidence) to a chaotic Gaussian-distributed white noise-like signal (Stanton *et al.* 1994b).

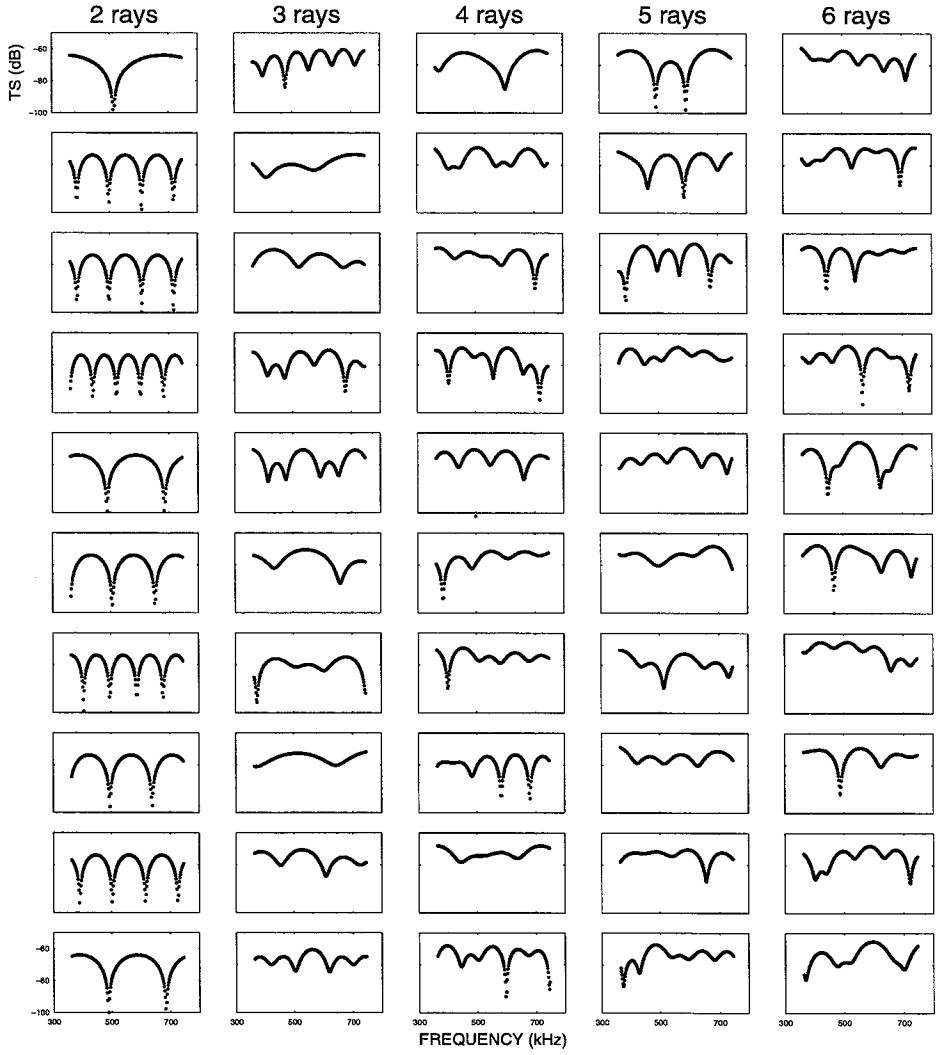

Figure 3-8 Multiple-ray model (EQ 3.2) predictions (magnitude of the Fourier transform, plotted as *TS* in dB) for fluid-like zooplankton with $N = 2, 3, 4, 5$, and 6 randomly spaced scattering features. Examples given for each case show a wide range of signal variability in the simulated spectra.

The ray-summation model has been used to predict scattering from fluid-like zooplankton containing an arbitrary number of randomly spaced scattering features, as well as the scattering contribution of the tissue of gas-bearing zooplankton. It models the scattering from a fluid-like animal as the sum of rays reflected from a number of randomly spaced scattering glints on the body of the animal. It is a simplified summation of phasors to account for the phase differences between ray reflections from the various glints. For the purposes of this simulation, the multiple-ray model (EQ 3.2) was employed with $N = 2$ through 6 to simulate variable acoustic returns in the **FL** class corresponding to the presence of two, three, four, five and six randomly-spaced scattering features on the animal body.

A preliminary assessment was made of the performance of the MPC with these simulated **FL** class signals. Only those returns that were identified as **FL** were considered correctly classified. The MPC did not perform well with these highly variable realisations, misclassifying about 40% of the signals overall (Table 3-5). For spectra generated with $N = 2$, almost half of the realisations were misclassified as **ES** since their null-spacings were more consistent with those of **ES** model space spectra than with **FL** model space spectra. About half of the misclassified realisations predicted using more than 2 rays in the summation were classed as **GB**, indicating that their SSR was comparable to that of spectra observed from gas-bearing animals. The MPC was shown to be quite sensitive to signal variability in the **FL** class, and was subject to ambiguity problems when faced with spectra that did not correlate well with those contained in the **FL** model space. Ambiguity in both null-spacing and SSR resulted in poor performance with these variable signals.

Table 3-5 MPC results (% classified as each scatterer type, n=50) with high-variability signals generated using the multiple-ray summation model (EQ 3.2) with the number of rays N ranging from 2 to 6.

	$N = 2$	$N = 3$	$N = 4$	$N = 5$	$N = 6$	average
%correct:	56%	58%	58%	64%	72%	62%
% classed as GB:	0%	30%	20%	24%	20%	19%
% classed as ES:	44%	12%	22%	12%	8%	19%

The sensitivity of the MPC to variability in the echo spectra may explain its inconsistent performance with the 1993 cruise data. To further improve upon the performance of the MPC, more sophisticated theoretical model based classification techniques that are better able to contend with signature variability have been developed (Chapter 4). These more advanced classifiers, collectively referred to as the Covariance Mean Variance Classifiers (CMVC), were designed to account for a wide range of echo spectra variability by incorporating into the model spaces the full

breadth of signals predicted by the theoretical models for each scattering class. Incorporating the variability alone will not necessarily improve classification success, since broadening the possible signatures for each class will result in ambiguity (overlap) between the model spaces of different classes. Successful classification then depends upon the ability of the classifier to resolve these ambiguities. To ensure more robust classification in the face of between-class overlap in both the observed spectra and in the model spaces, the CMVC were also designed to account for this ambiguity as part of the classification process. In addition, these more sophisticated classifiers are able to easily incorporate *a priori* information to constrain the inverse. With the CMVC, the classification choices themselves can be limited by eliminating certain answers or assigning probabilities to them based on available *a priori* information. *A priori* knowledge may also be employed to constrain the model spaces themselves based on a validity measure, which indicates the representativity of each member of the model spaces relative to data from known classes. Incorporating these capabilities into a theoretical model based classifier has the potential to significantly improve classification success over that obtained with the MPC.

CHAPTER 4

THEORETICAL MODEL BASED CLASSIFICATION: COVARIANCE MEAN VARIANCE CLASSIFIERS (CMVC)

Model based Covariance Mean Variance Classification (CMVC) techniques:

Algorithm development and application to the acoustic classification of zooplankton

Linda V. Martin Traykovski, Timothy K. Stanton, Peter H. Wiebe, and James F. Lynch.

ABSTRACT

For inversion problems where the theoretical or empirical basis from which to construct a relationship between observed data and model parameters is well-characterised, a promising approach to the classification problem is the application of techniques that can capitalise on the predictive power of class-specific models. For the zooplankton classification problem, there exist reasonably well-developed theoretical scattering models for three scattering classes (hard elastic-shelled, e.g. pteropods; fluid-like, e.g. euphausiids; gas-bearing, e.g. siphonophores), providing a sound basis for a model based classification approach. The model based Covariance Mean Variance Classification (CMVC) techniques rely on comparisons of observed echo spectra to theoretical-model-generated model spaces to classify broadband echoes from zooplankton into scattering classes based on similarities in covariance, mean, and variance, while accounting for ambiguity between model spaces as well as model validity (representativity). Three different classification algorithms have been developed based on the CMVC techniques. The Integrated Score Classifier (ISC) and the Pairwise Score Classifier (PSC) have some flexibility in terms of incorporating ambiguity and validity weightings, whereas the Bayesian Probability Classifier (BPC) accounts for ambiguity inherently in its expression of conditional probability, while validity is accounted for via empirically derived probability distributions. These three classification algorithms are capable of assigning observations to a class either based on class scores or based on matches to particular model realisations. Classifier performance was evaluated with several hundred echoes collected in a ship-board tank from 24 different individuals on two cruises to Georges Bank and the Gulf of Maine. All three classification algorithms had a very high rate of success with a high-quality, high SNR subset of the data (n=25 echoes from each class): between

80% and 90% of echoes were correctly classified based on the maximum class score criterion. With the entire dataset, the PSC yielded the best results overall, with a high percentage of correct classifications for echoes from gas-bearing and fluid-like animals. Echoes from hard elastic-shelled animals, which were not well classified by the maximum score PSC, were better classified by the maximum score **TYPE I** BPC. Best match PSC classification results (based on assigning an observation to the class containing the best match model realisation) were better than those based on the maximum score criterion, with an overall success rate of close to 85%. Inversions for animal size based on best match model realisation were promising; further work is necessary to quantify the other parameter values so that size may be determined more robustly. Overall, the three CMVC-based classification algorithms were able to successfully invert a high percentage of experimentally collected echoes from individual zooplankton for scattering class, particularly for the highest quality subset of data. The CMVC technique also shows promise in inverting for specific zooplankter characteristics, such as animal size, within a scattering class. Such accurate acoustic classification of zooplankton species is essential if reliable estimates of zooplankton biomass are to be made from acoustic backscatter measurements of the water column.

L.V. Martin Traykovski: Massachusetts Institute of Technology / Woods Hole Oceanographic Institution, Joint Program in Oceanography and Applied Ocean Sciences and Engineering; present address: Woods Hole Oceanographic Institution, MS 34, Woods Hole, MA 02543 USA. P.H. Wiebe: Department of Biology, Woods Hole Oceanographic Institution, Woods Hole, MA 02543. T.K. Stanton and J.F. Lynch: Department of Applied Ocean Physics and Engineering, Woods Hole Oceanographic Institution, Woods Hole, MA 02543. Correspondence to Martin Traykovski [email: lmartin@whoi.edu, phone (508) 289-2750, fax (508) 457-2134].

List of Symbols

a	radius of sphere or cylinder
$\bar{a}$	average radius
α_{wc}	within-class representativity weighting factor
α_{bc}	between-class representativity weighting factor
b_j	scattering amplitude of local facet that is broadside to incident acoustic wave
$b_m^{(f)}$	modal series coefficient for homogeneous fluid sphere
β_{tilt}	tilt angle of tangent to axis a particular point on the axis
β_l	attenuation coefficient of Lamb wave on an elastic shelled sphere
$\mathbf{C}$	Covariance Mean Variance (CMV) metric matrix
c	sound speed
c_l	sound speed of Lamb wave
$\mathbf{D}$	observed data matrix
η_l	phase shift due to partial circumnavigation (i.e. path between $\pm\theta_l$ points) of Lamb waves
ε_j	distance between the point of scatter and the zero phase reference plane
$\mathbf{f}^{(p)}$	empirically constructed probability mass function (PMF) for class p
f_{bs}	scattering amplitude in the backscattering direction
F_l	factor ranging from 0 to 1 to account for loss of Lamb wave due to discontinuity in shell
F_{spec}	factor ranging from 0 to 1 to account relative contribution of specular reflection
g	density contrast ρ_2/ρ_1
γ_κ, γ_ρ	material property parameters in DWBA formulation: $\gamma_\kappa = (\kappa_2 - \kappa_1)/\kappa_1$, $\gamma_\rho = (\rho_2 - \rho_1)/\rho_2$
γ	phase term to account for attenuation of Lamb wave due randomness of shell irregularities
G_l	coupling coefficient for combination of landing and launching of Lamb waves on the shell

h sound speed contrast c_2/c_1

h_{ij} height assigned to jth model realisation for each observation i in $\mathbf{V}$

i $\sqrt{-1}$ unless used as a summation index or subscript to $\hat{k}$

J_1 Bessel function of the first kind of order 1

$\mathbf{K}$ covariance matrix between data and model space (= $\mathbf{D}^T\mathbf{M}$)

k acoustic wavenumber (= $2\pi/\lambda$)

κ compressibility (= $1/(\rho c^2)$)

$\hat{k}_i$ wavenumber vector of incident field

λ acoustic wavelength

$\mathbf{M}_F^{(p)}$ full model space matrix for class p

$\mathbf{M}^{(p)}$ reduced model space matrix for class p

$p_a^{(p)}$ *a priori* probability for class p

Φ_l phase shift of Lamb wave heuristically added for non-ideal body

ρ mass density

r_S scattering distance, i.e. distance between transducer and animal

r_C calibration distance, i.e. distance between transmit and receive transducers

$\hat{r}_{pos}$ position vector of axis of deformed cylinder

$\Re$ plane wave/plane interface reflection coefficient (= $(gh-1)/(gh+1)$)

S_{ISC} Integrated Score Classifier (ISC) score matrix

S_{PSC} Pairwise Score Classifier (PSC) score matrix

S_{BPC} Bayesian Probability Classifier (BPC) score matrix

σ standard deviation of effective radius (relative to mean radius) of rough sphere

t	CMV threshold
t_R	redundancy threshold
t_f	probability mass function (PMF) threshold
TS	target strength (= $20\log\lvert f_{bs}\rvert$)
θ_l	launch/land angle for Lamb wave
$\mathbf{U}$	variance similarity matrix
$\mathbf{V}^{(p)}$	validation set (matrix) of observations of echo spectra known to be from class p
$\tilde{\mathbf{W}}_A^{(p)}$	integrated ambiguity weighting function for class p
$\tilde{\mathbf{W}}_A^{(qp)}$	pairwise ambiguity weighting function
$\tilde{\mathbf{W}}_R^{(p)}$	redundancy weighting function for class p
$\tilde{\mathbf{W}}_V^{(p)}$	integrated validity weighting function for class p
$\tilde{\mathbf{W}}_V^{(qp)}$	pairwise validity weighting function
$\mathbf{X}$	mean similarity matrix
1,2	subscripts indicating medium "1" (surrounding fluid) and medium "2" (body medium)

4.1 Introduction

The use of high-frequency acoustics to make volume backscatter measurements of the water column has made it possible to do rapid, high-resolution, broad-scale synoptic surveys of zooplankton abundance over the spatial and temporal scales important for populations of macrozooplankton. Attempts to use volume backscatter measurements of the ocean as indicators of zooplankton type, size and biomass rely on the accurate acoustic characterisation of various species of zooplankton. Traditional acoustic biomass estimation methods have employed single-frequency acoustic measures in conjunction with either theoretical models (e.g. Greenlaw 1979) or empirical regression relationships between the acoustic backscatter data and the biomass collected in simultaneous net samples (e.g. Flagg and Smith 1989a, 1989b). Biomass estimates based on simple regression curves or on single-frequency echo energy measurements may be subject to large errors, since oceanic zooplankton populations often consist of multiple-species assemblages of different sized organisms with drastically different acoustic scattering properties. For example, Wiebe *et al.* (1996) found that although volume scattering at 420 kHz was 4-7 times higher at two stratified sites versus a mixed site on Georges Bank, MOCNESS-collected biovolumes at these sites were not significantly different. This may be explained by the fact that the echo energy scattered per unit biomass varies significantly across species, with the relative echo energy per unit of biomass measured from animals ranging from elastic-shelled gastropods to fluid-like salps varying by a factor of ~19,000 to 1 (Stanton *et al.* 1994a). This huge species-dependent variability has important implications for the interpretation of acoustic survey data; equating larger acoustic returns to the presence of more or larger animals (thereby concluding that the higher the echo energy, the greater the biomass in the insonified region) could lead to gross errors in zooplankton biomass estimates by several orders of magnitude.

Much effort has been put toward characterising the acoustic target strength of zooplankton for the purposes of species identification, animal size classification, abundance estimation and acoustic signal separation. The echo integration method for acoustic biomass estimation, which measures the acoustic backscatter from a volume of water which may contain multiple scatterers, relies on accurate knowledge of the species of scatterers in the insonified volume and their respective scattering characteristics. Some attempts have been made to bridge the gap between acoustic backscatter measurements of the water column and the animal biomass present, while accounting for the vast species differences in scattering strength per unit biomass. Stanton *et al.* (1987) used existing theoretical and empirical scattering models for different classes of zooplankton in

combination with the species composition in net tows to predict the expected acoustic backscatter over a transect in the Gulf Stream, and compared this prediction to the measured acoustic backscatter. Due to net avoidance and inadequate scattering models, the predictions were only accurate to within an order of magnitude of the measured values, with discrepancies of up to 30 dB. Wiebe *et al.* (1996) performed a similar analysis on data from Georges Bank using more recently developed theoretical scattering models, and found reasonable agreement between observed and predicted values, to within about 4 dB. These studies have demonstrated that a solid understanding of the dependence of zooplankton target strength on animal size, shape, material properties and behaviour is necessary to convert integrated backscattered energy to numerical densities and apportion these densities to individual species of zooplankton, thereby obtaining an estimate of biomass in the water column.

The Forward Problem

The solution to the forward problem involves predicting the properties of the acoustic return from a scatterer based on knowledge of the physical and geometric properties of the scatterer as well as the specifications of the sonar system used to insonify it. Most of the progress in zooplankton bioacoustics has been made in this area, via the development of both theoretical and empirical models which describe the scattering from these animals in terms of their morphology and material properties. Various theoretical models have been developed to predict acoustic scattering from zooplankton based on animal morphology (Anderson 1950; Greenlaw 1977,1979; Johnson 1977; Love 1977; Penrose and Kaye 1979; Stanton 1988a,b 1989a,b 1990a,b; Chu *et al.* 1993; Stanton *et al.* 1993a,b; 1994a). To develop and corroborate scattering models, single-frequency target strength measurements have been made of zooplankton, both experimentally constrained (e.g. Greenlaw 1977; Kristensen and Dalen 1986; Wiebe *et al.* 1990; Foote *et al.* 1990; Stanton *et al.* (1993b, 1994a; Demer and Martin 1995) and *in situ* (e.g. Hewitt and Demer 1991, 1996). These measurements were taken at a single frequency, or a small number of discrete frequencies, and although they provide information about the scattering strength of the organisms, it is not possible to quantify the frequency dependence of the scattering over a continuous range of frequencies with these types of measurements. Recently, Chu *et al.* (1992) were able to insonify the decapod shrimp (*Palaemonetes vulgaris*) with a broad spectrum of frequencies simultaneously using a broadband chirp sonar. Following this work, Stanton *et al.* (1993b; 1994a,b; 1996) have been making target strength measurements of single organisms over a broad range of frequencies simultaneously by insonifying tethered zooplankton with broadband chirps. Comparison of the broadband echoes

received from these animals to theoretical scattering models (Figure 4-1) has resulted in a division of the insonified zooplankton into 3 acoustic types (Stanton *et al.* 1994a; Martin *et al.* 1996; Stanton *et al.* in press b): (i) **ES** hard elastic-shelled (e.g. pteropods); (ii) **FL** fluid-like (e.g. euphausiids); (iii) **GB** gas-bearing (e.g. siphonophores). Several representatives from each of the three scattering classes have been insonified in this manner, demonstrating that the frequency response is characteristic of the scatterer class. As a result, it should be possible to invert acoustic backscatter data for the class of scatterer.

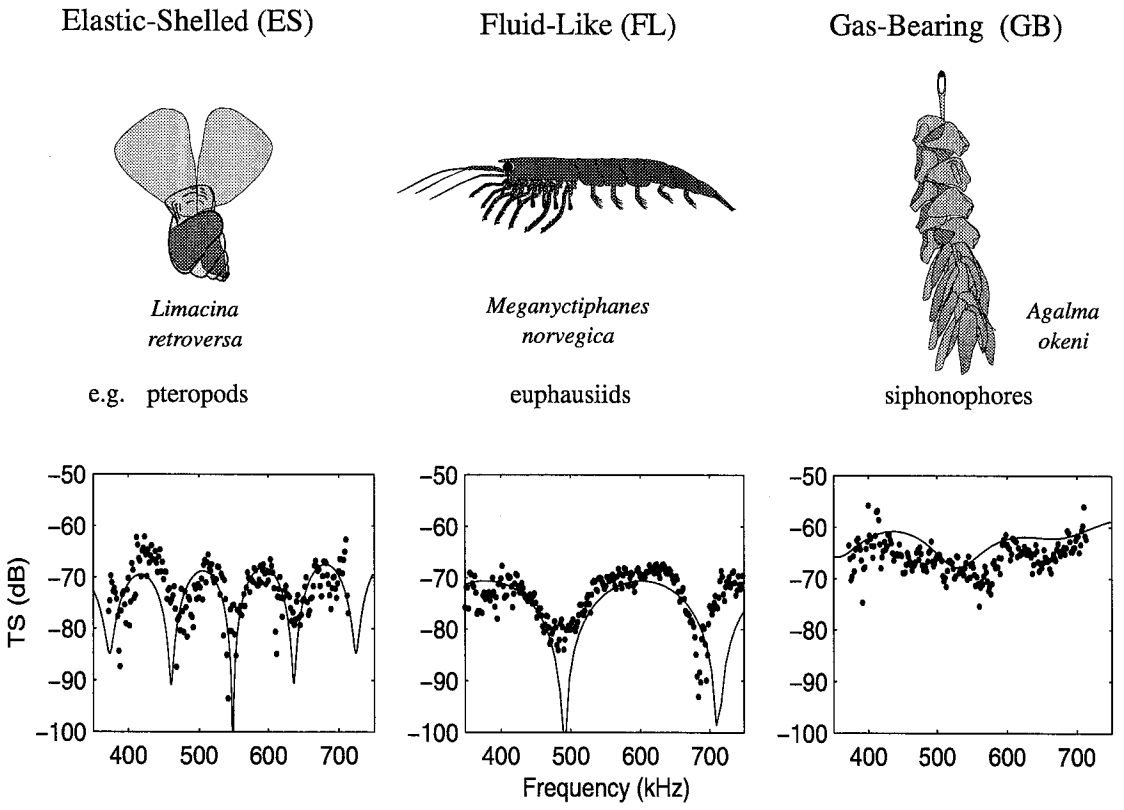

Figure 4-1 Representative zooplankton from the three scattering classes. Echoes collected from broadband insonifications of animals in each class are plotted (points) together with theoretical models (solid line) that describe the acoustic scattering from these three classes of animals under certain conditions. Details of these models are included in Stanton *et al.* (1996).

The Inverse Problem

The inverse problem is concerned with predicting the properties of the scatterer based on knowledge of the acoustic return from that object. The solution to this inverse problem has been

investigated for several applications within the discipline of acoustical oceanography, and success has been achieved with geoacoustic bottom inverses (e.g. Lynch *et al.* 1991; Rajan *et al.* 1987), acoustic tomographic inverses for measuring mesoscale variability of ocean temperature (e.g. Munk and Wunsch 1979; Brown 1984; Chiu *et al.* 1987), and acoustic inverses to measure the temperature field of turbulence microstructure (Goodman *et al.* 1992). In bioacoustical oceanography, some work has been done on identifying fish and fish schools from both single-frequency and multiple-frequency acoustic returns (e.g. Deuser *et al.* 1979; Holliday 1980; Zakharia and Sessarego 1982; Vray *et al.* 1990; Simmonds *et al.* 1996). For zooplankton, the size distribution of an assemblage has been estimated based on volume scattering data from a multifrequency sonar system using several discrete frequencies (Holliday 1977; Holliday *et al.* 1989; Pieper *et al.* 1990). If acoustic sampling of the ocean is broadband, it is possible to perform an inversion of acoustic returns for scatterer properties (Figure 4-2). If echoes from individual zooplankton are resolvable, and include a continuous sweep of frequencies (e.g. Stanton *et al.* 1994a), a classification inversion is possible (e.g. Martin *et al.* 1996). In this type of inversion, a spectral decomposition is performed on the echo time series from each individual scatterer, allowing each zooplankter to be classified according to its frequency-dependent scattering characteristics.

A classification inversion strives to categorise individual zooplankton into distinct scatterer types based on the signature information contained in the return spectra of broadband insonifications of the animals. Inversion schemes can be of two general types, those based on intrinsic features in the data and those based on an empirical or theoretical forward model of the scattering process. The first feature based and theoretical model based classification inversion techniques for zooplankton were developed by Martin *et al.* (1996). The feature based Empirical Orthogonal Function Classifier (EOFC) discriminates scatterer types based on differences in the variability in the echoes, exploiting only the inherent characteristic structure of the acoustic signatures without relying on theoretical scattering model predictions. The model based Model Parameterisation Classifier (MPC), which is the fully-damped least squares formulation of the generalised linear inverse (Aki and Richards 1980), depends on comparison of acoustic signatures with simplifying parameterisations of the theoretical scattering models for each scatterer type, assigning a given acoustic return to one of three classes based on its correlation with model realisations representing each class. The Covariance Mean Variance Classifiers (CMVC) developed in this paper are a set of more advanced model based techniques which exploit the full complexity of the theoretical models

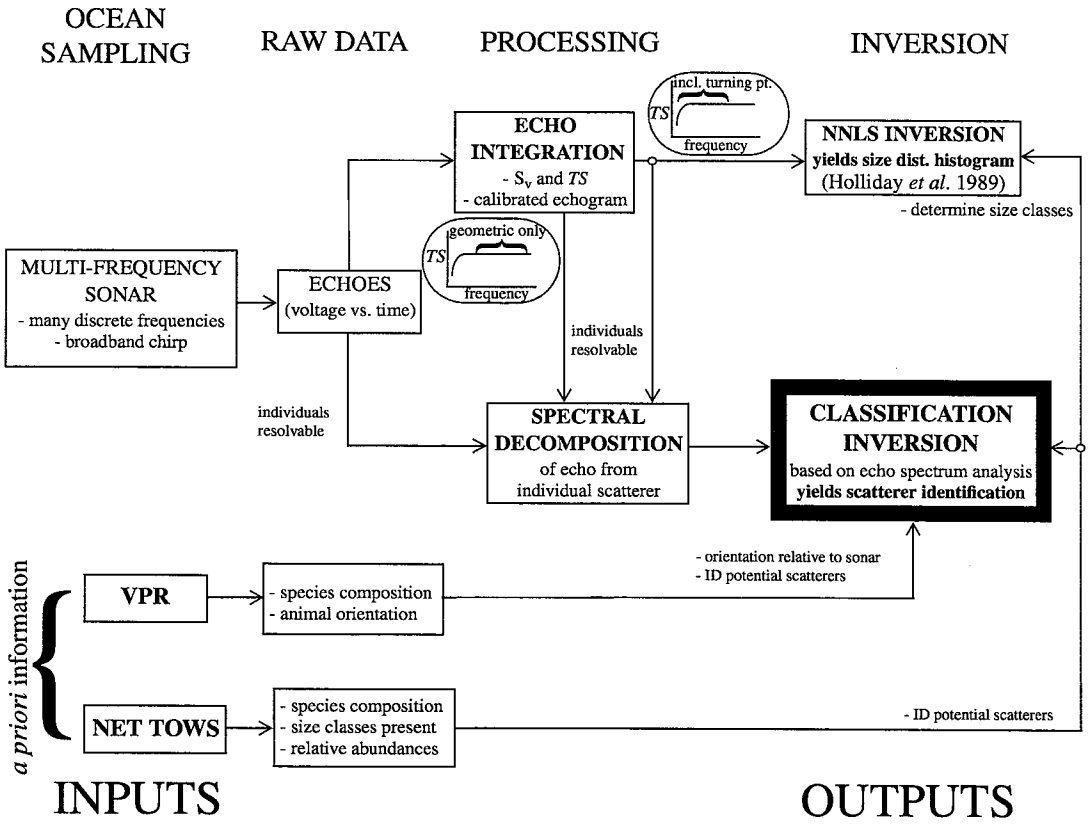

Figure 4-2 Approaches to solving the inverse problem for zooplankton. If frequency sampling brackets the turning point between the Rayleigh and geometric regimes, a non-negative least-squares (NNLS) inversion can be used to estimate the size distribution of a zooplankton assemblage. If echoes from individual zooplankton are resolvable and frequency sampling is virtually continuous, a CLASSIFICATION INVERSION can be performed to categorise individual zooplankton according to their frequency-dependent scattering characteristics. *A priori* information may be obtained via simultaneous net samples and/or VPR (Video Plankton Recorder) samples.

by searching the entire physical model parameter space without employing simplifying parameterisations. This more sophisticated approach aims to account for the ambiguity between the model spaces for different scattering classes as well as to quantify the validity of each theoretical model in predicting acoustic returns from known scatterers.

This paper is organised as follows. The collection and processing methods for the acoustic data used in classifier evaluation are outlined. The central portion of the paper, which describes the development of the CMVC, is divided into four main sections. First, the ideology behind the classification techniques is described, and the CMVC algorithms are given. Second, the details of the classifiers are presented, drawing on examples using simplified model spaces to elaborate on the design and mechanics of the algorithms. Next, the physics governing acoustic scattering for

each zooplankton class is reviewed, and the theoretical models which constitute the CMVC model spaces are outlined. Last, the performance of the CMVC algorithms is evaluated with experimentally collected data. Following this, the final discussion addresses the strengths and shortcomings of each classifier, as well as of the CMVC approach itself.

4.2 Data Collection and Processing

The data used in classifier development were collected on two separate cruises to Georges Bank and the Gulf of Maine: the Oceanus cruise 262 (27 September - 6 October 1993) and the Endeavor cruise 253 (18 September - 29 September 1994). Organisms were captured in both vertical and oblique tows with a meter net (335 μm mesh) with a cod end bucket (32 cm diameter by 46 cm tall), and sorted into large containers for short-term live storage under refrigeration to maintain seawater temperature. Prior to insonification, a detailed sketch was made of each animal and measurements were made of animal length, width, size of shell (pteropods) and size of gas inclusion (siphonophores). After each live animal was insonified, excess water was removed from the body and it was frozen. Wet weight was measured on land following the cruises. Individual organisms were tethered with an acoustically transparent monofilament strand and suspended in a 2.44 m diameter by 1.52 m high tank filled with filtered (through 64 μm mesh) seawater on-board the ship. Acoustic experiments included broadband insonification (center frequency 500 kHz, ~350 kHz - 750 kHz) of each live animal, as well as narrowband insonification at several other frequencies. Only the 500 kHz broadband data were used in classifier development. Insonifications were made with a pulse-echo acoustic data acquisition system. The transmit/receive transducer pair was mounted in an upward-looking transducer bank sitting on the bottom of the experimental tank, and the tethered animal was positioned at the focal point of the transducer pair, approximately 50 cm above the transducer bank (see Stanton *et al.* in press a for a detailed description of the experimental setup). During the two cruises, 50 individuals representing 15 different species of zooplankton were insonified, and the return echoes from over 36,000 acoustic transmissions were collected. A subset of these data, including representatives of the numerically abundant species found in the Northwest Atlantic (the pteropod gastropod *Limacina retroversa*, the euphausiid *Meganyctiphanes norvegica*, and the physonect siphonophores *Agalma okeni* and *Nanomia cara*), was used in classifier development and evaluation (Table 4-1).

Table 4-1 Acoustic data used in the development and evaluation of the CMVC.

scattering class	species and number	# echoes used
hard elastic-shelled (**ES**)	8 *Limacina retroversa* (1993) 2 *Limacina retroversa* (1994)	50 each 200 each
fluid-like (**FL**)	1 *Meganyctiphanes norvegica* (1993) 2 *Meganyctiphanes norvegica* (1994)	700 200/250
gas-bearing (**GB**)	9 *Agalma okeni* (1993) 1 *Agalma okeni* (1994) 1 *Nanomia cara* (1994)	50 each 200 200

To obtain the echo spectrum representing the actual acoustic return from the animal, the results of calibration measurements were combined with the raw received signals. During calibration (subscript C), the transmit and receive transducers were focused on each other with no target in the beam, and a calibration signal was transmitted. During the scattering experiments (subscript S), the transducers were aimed at the animal, and for each received acoustic return the calibrated echo spectrum was computed as:

$$|f_{bs}| = \left(\frac{Vrec_S}{Vrec_C}\right)\cdot\left(\frac{Vxmit_C}{Vxmit_S}\right)\cdot\left(\frac{r^2_S}{r_C}\right) \qquad \textbf{(EQ 4.1)}$$

In (EQ 4.1), f_{bs} is the acoustic backscattering amplitude of the animal, and is a measure of the efficiency with which an object scatters sound back toward the sound source (f_{bs} is related to σ_{bs}, the differential backscattering cross section, by $\sigma_{bs} = |f_{bs}|^2$). $Vrec_C$ and $Vxmit_C$ were computed by taking the absolute value of the FFT of the received and transmitted voltage time series for calibration, measured at the beginning and again at the end of the experiments each year. $Vxmit_S$ was computed as the absolute value of the FFT of the transmitted voltage time series for scattering measured at the end of each run (every 50 or 200 pings). To compute $Vrec_S$, a fixed rectangular window was applied to the received voltage time series for each return (to capture only the echo from the animal) before applying the FFT. The scattering and calibration distances were $r_S \approx 51$ cm and $r_C \approx 60$ cm respectively.

The acoustic returns of the zooplankton studied exhibit a very large dynamic range over the frequency band, and are often characterised by the occurrence of deep nulls at certain frequencies (where σ_{bs} is ~1/1000 of peak values). The echo spectrum, conventionally represented by TS (where $TS = 20\log|f_{bs}|$) on a logarithmic scale, is a convenient and widely-accepted means of compressing this huge dynamic range. This representation has the advantage of emphasising the

peak-and-null structure in the acoustic signatures, and the dynamic range compression also improves the suitability of the signals for numerical classification inversion schemes. The echo spectrum of each acoustic return was sampled at 241 points between 348.33 kHz and 748.33 kHz (1993 data), or at 152 points between 348.33 kHz and 600 kHz (1994 data; the reduced bandwidth of these data is the result of using a different transducer characterised by a non-ideal frequency response above 600 kHz). It is this sampled version of the echo spectrum that is used as the basis for classifier development and evaluation.

4.3 The CMVC Approach

A model based classification scheme strives to classify observations into a particular category based on the correspondence between the observations and theoretical or empirical model predictions for each category. The model based acoustic classification inversion for zooplankton described herein classifies the frequency spectrum of an acoustic return resulting from the broadband insonification of an individual zooplankter (echo spectra) into one of three classes representing acoustic scattering types as predicted by theoretical models for each class. The classification result for a single echo spectrum can be based on a global maximum "best match", which reveals the theoretical model which best predicts the observation. The observed echo spectrum is thus assigned to the class predicted by the best match theoretical model. Sub-optimal matches (local maxima) can also be taken into account, and a certainty score or probability for each class may be computed based on a subset of these matches. In this case, the observed echo spectrum may be assigned to the class with the highest score or probability. Alternatively, the inversion may consist of the certainty or probability that the observed echo spectrum belongs to each class, based on the relative class scores or probabilities themselves. If several echo spectra are observed for a single animal, these class scores/probabilities may be averaged over the observations.

All the classification techniques developed with the Covariance Mean Variance Classification (CMVC) approach incorporate three basic components: a *model space* for each class, a means by which to account for the *redundancy, ambiguity,* and *validity* of these model spaces, and a *CMV metric* with which to measure correspondence between the observations and the model spaces, as well as to quantify redundancy, ambiguity, and validity (Figure 4-3).

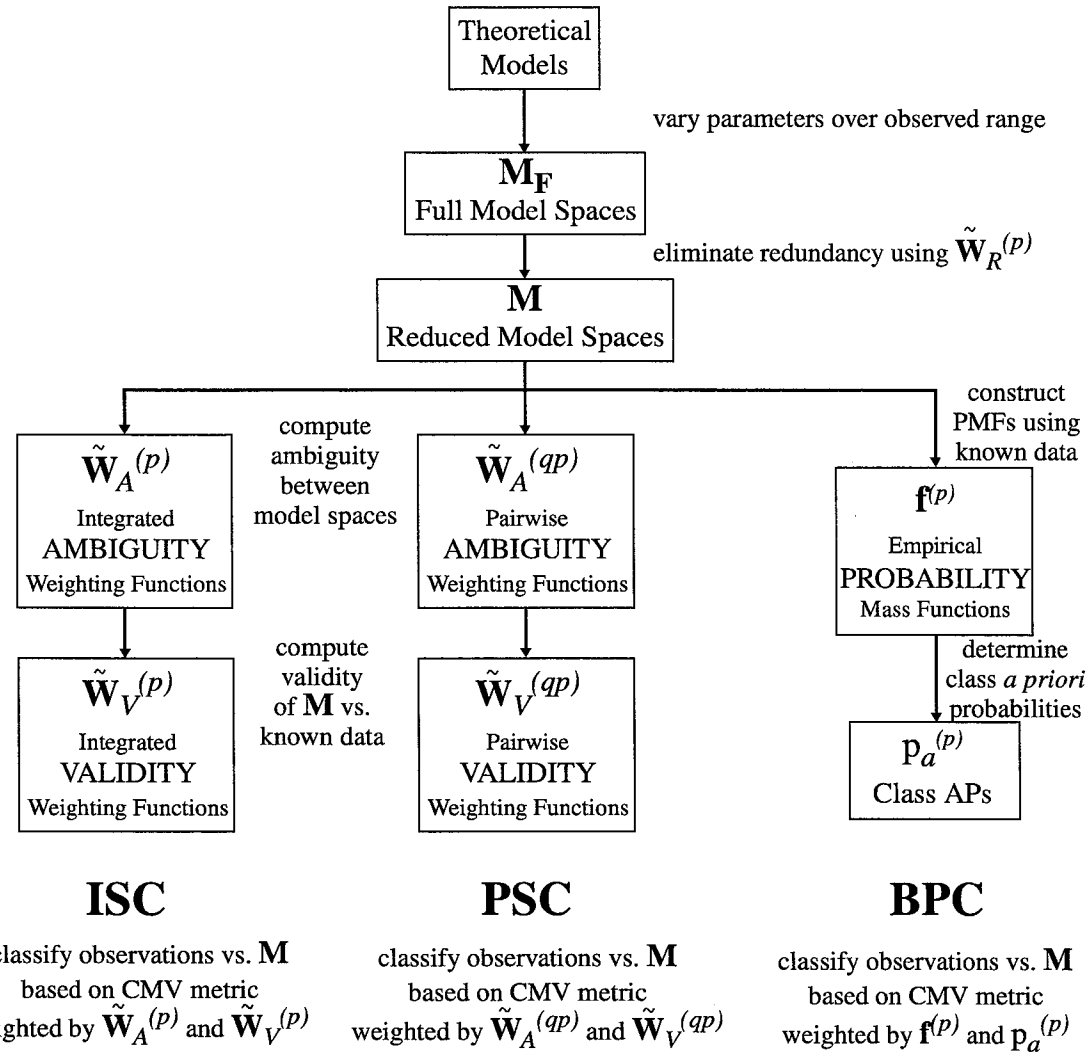

Figure 4-3 Diagram of the CMVC approach. Model spaces for each class p are constructed based on the theoretical models, and redundancy is eliminated by applying the redundancy weighting function $\tilde{\mathbf{W}}_R^{(p)}$. Ambiguity and validity are accounted for via ambiguity and validity weighting functions, $\tilde{\mathbf{W}}_A^{(p)}$ and $\tilde{\mathbf{W}}_V^{(p)}$ in the **ISC** (Integrated Score Classifier), $\tilde{\mathbf{W}}_A^{(qp)}$ and $\tilde{\mathbf{W}}_V^{(qp)}$ in the **PSC** (Pairwise Score Classifier), or the probability mass function $\mathbf{f}^{(p)}$ and the *a priori* probabilities $p_a^{(p)}$ in the **BPC** (Bayesian Probability Classifier). The CMV metric for classification is given in (EQ 4.2).

First, the theoretical scattering models are used to construct a model space for each class, consisting of model realisations which represent predictions of the theoretical models for particular parameter values spanning the entire parameter space. A model space may contain redundancy if there does not exist a one-to-one mapping between parameter values and predicted model realisations, for example, if different combinations of parameter values predict similar or virtually identical model realisations. Ambiguity between model spaces can arise if the theoretical models representing different scattering classes are non-unique over any part of the parameter

space, for example, if the theoretical model for a particular class predicts model realisations which are similar or identical to model realisations predicted by the theoretical model for another class. The validity of theoretical models in predicting known data can vary considerably; observed echo spectra may resemble some model realisations frequently, whereas other model realisations are scarcely or never observed in real data.

Elimination of redundant realisations within the model spaces (through the application of the redundancy weighting function $\tilde{\mathbf{W}}_R$) can increase classifier efficiency; this is particularly beneficial in cases where significant size reduction of model spaces can be achieved (drastically increasing computational efficiency) with minimal resolution cost. More importantly, to maximise the effectiveness of the classifier, overlap between model spaces must be accounted for by quantifying ambiguity (via the ambiguity weighting functions $\tilde{\mathbf{W}}_A$) and incorporating it into the classification scheme. In addition, by applying the validity weighting functions $\tilde{\mathbf{W}}_V$, rewards for high within-class validity for a model space can be incorporated into the classification by quantifying the representativity of a model space in predicting data known to be from that class; penalties may also be incurred for good representativity of data from outside that class. Finally, the CMV metric ($\mathbf{C}$) quantifies the correspondence between observed echo spectra ($\mathbf{D}$) and model realisations ($\mathbf{M}$) based on their covariance ($\mathbf{K}$, which compares their spectral structure), weighted by the similarity of mean echo levels ($\mathbf{X}$) and the variance similarity ($\mathbf{U}$), so that for class p:

$$\mathbf{C}^{(p)} = CMV(\mathbf{M}^{(p)}, \mathbf{D}) = \mathbf{K}^{(p)} \cdot \mathbf{X}^{(p)} \cdot \mathbf{U}^{(p)} \qquad \textbf{(EQ 4.2)}$$

Note that in (EQ 4.2), $\mathbf{C}_{ij}^{(p)} = \left(\sum_{k=1}^{n_p} \mathbf{D}_{ik}^{\mathrm{T}} \mathbf{M}_{kj}^{(p)} \right) \cdot \mathbf{X}_{ij}^{(p)} \cdot \mathbf{U}_{ij}^{(p)}$, since $\mathbf{K}^{(p)} = \mathbf{D}^{\mathrm{T}}\mathbf{M}^{(p)}$ is the covariance ($0 \le \mathbf{K}_{ij}^{(p)} \le 1$, see Papoulis 1991) between the observed data matrix $\mathbf{D}$ and the model space $\mathbf{M}^{(p)}$ (each column of $\mathbf{D}$ contains a mean-subtracted, energy-normalised observed echo spectrum, whereas each column of $\mathbf{M}^{(p)}$ contains a mean-subtracted, energy-normalised model realisation for class p); $\mathbf{X}^{(p)}$ and $\mathbf{U}^{(p)}$ are the mean and variance similarity matrices ($0 \le \mathbf{X}_{ij}^{(p)}, \mathbf{U}_{ij}^{(p)} \le 1$, where $\mathbf{X}_{ij}^{(p)} = 1$ indicates that the ith observation and the jth model realisation have identical mean echo levels, and $\mathbf{U}_{ij}^{(p)} = 1$ indicates that the ith observation and the jth model realisation have the same variance); n_p is the number of points in each echo spectrum; "$\cdot$" indicates element-wise multiplication of matrices.

Three distinct classification techniques (Figure 4-3) have been developed with the CMVC approach; the Integrated Score Classifier (ISC), the Pairwise Score Classifier (PSC) and the Bayesian Probability Classifier (BPC). Although they are based on the same CMV metric (EQ 4.2), the means by which ambiguity and validity are accounted for differs between classifiers. Details of

the calculation of $\tilde{\mathbf{W}}_R^{(p)}$, $\tilde{\mathbf{W}}_A^{(p)}$, $\tilde{\mathbf{W}}_V^{(p)}$, $\tilde{\mathbf{W}}_A^{(qp)}$, $\tilde{\mathbf{W}}_V^{(qp)}$, $\mathbf{f}^{(p)}$, and $\mathrm{p}_a{}^{(p)}$ are given in Section 4.4. The general algorithms for these three techniques are presented here.

4.3.1 Integrated Score Classifier (ISC)

For each observed echo spectrum, the Integrated Score Classifier computes a score for each class based on the CMV metric weighted by the integrated ambiguity $\tilde{\mathbf{W}}_A^{(p)}$ and validity $\tilde{\mathbf{W}}_V^{(p)}$ weightings for that class. The score matrix $S_{ISC}^{(p)}$ for each class p is computed as:

$$S_{ISC}^{(p)} = \frac{sum(\mathbf{C}^{(p)} \cdot \tilde{\mathbf{W}}_A^{(p)} \cdot \tilde{\mathbf{W}}_V^{(p)})}{sum_k(\mathbf{C}^{(k)} \cdot \tilde{\mathbf{W}}_A^{(k)} \cdot \tilde{\mathbf{W}}_V^{(k)})} \qquad \textbf{(EQ 4.3)}$$

where *sum* indicates element-wise summation. For each observed echo spectrum i, this classifier yields a relative score ($0 \le S_{ik}^{(p)} \le 1$) for each class k, which gives a measure of the certainty that the observation belongs to that class. For all data, the matrix of scores for class 1 is computed as the element-wise ratio of the sum of the elements of $\mathbf{C}^{(1)}$ weighted by the integrated ambiguity and validity weightings for class 1 model realisations ($\tilde{\mathbf{W}}_A^{(1)}$, $\tilde{\mathbf{W}}_V^{(1)}$) to the sum over all N classes (k = 1..N) of the element-wise sum of the weighted $\mathbf{C}^{(k)}$. The $\tilde{\mathbf{W}}_A^{(p)}$ and $\tilde{\mathbf{W}}_V^{(p)}$ for a given class are not other-class-specific, i.e. they are integrated measures of these properties over all model realisations in all other classes.

4.3.2 Pairwise Score Classifier (PSC)

The Pairwise Score Classifier computes a score for each class based on a weighted CMV metric, as does the **ISC**. However, in the **PSC**, the $\mathbf{C}^{(p)}$ are weighted by the pairwise ambiguity and validity weightings. This classifier is based on ideas from classical signal detection theory, where a "hit" is defined as a target detection when the target is present, whereas a "miss" occurs if the target is present but not detected. Extending this logic to a classification problem with N possible classes, this classifier computes both "hit" scores and "miss" scores for the observed echo spectra, based on an assumption of the *a priori* class membership. For observed echo spectra assumed to be in class m, the overall score matrix $S_{PSC}^{(p,m)}$ for class p is computed as the element-wise ratio of the hit score matrix for that class to the element-wise sum of the hit and miss score matrices, as follows:

$$S_{PSC}^{(p,m)} = \frac{\overline{\mathbf{S}^{(mp)}}}{\sum_{k=1}^{N} \overline{\mathbf{S}^{(mk)}}} \qquad \textbf{(EQ 4.4)}$$

In general, $\overline{\mathbf{S}^{(pq)}} = mean(\mathbf{C}^{(q)} \cdot \tilde{\mathbf{W}}_A^{(qp)} \cdot \tilde{\mathbf{W}}_V^{(qp)})$ is a matrix of mean scores for class p for all observations in class q; the numerator on the right-hand side of (EQ 4.4) is computed by setting $p = m$ and $q = p$, whereas the denominator is computed by setting $p = m$ and $q = k$. The **PSC** has better resolution than the **ISC** as a result of incorporating the more specific pairwise weighting functions ($\tilde{\mathbf{W}}_A^{(qp)}$, $\tilde{\mathbf{W}}_V^{(qp)}$) instead of the integrated weighting functions employed in the **ISC**. The particular pairwise weighting functions employed by the **PSC** are determined based on an assumption regarding the class membership of an observation. *A priori* information (e.g. from net tows) may be used to guide this assumption; alternatively, the classification may be run N times assuming a different *a priori* class membership each time, so that the results of each classification run can be taken into consideration.

4.3.3 Bayesian Probability Classifier (BPC)

An alternative approach to model based classification involves determining the probability that an observation belongs to a given class based on its correspondence with the model space for that class and an understanding of the underlying probability distribution of observations in that class. Given an observed echo spectrum d_i, the probability that d_i was received from an animal that belongs to scattering class p can be computed using Bayes rule (see Papoulis 1991):

$$P(d_i \in p | d_i) = \frac{\mathrm{p}_a^{(p)} \mathrm{f}^{(p)}(d_i | d_i \in p)}{\sum_{k=1}^{N} \mathrm{p}_a^{(k)} \mathrm{f}^{(k)}(d_i | d_i \in k)} \qquad \textbf{(EQ 4.5)}$$

In (EQ 4.5), $\mathrm{p}_a^{(p)}$ is the *a priori* probability of the occurrence of an observation from class p, and $\mathrm{f}^{(p)}$ is the probability mass function (PMF) for class p so that $\mathrm{f}^{(p)}(d_i | d_i \in p)$ is the probability associated with the occurrence of d_i given that it is in class p. In general, $\mathrm{f}^{(p)}$ may be the true probability distribution for each class, or it may be estimated, either from a probability distribution predicted by theoretical models for each class, or empirically from data. To determine the score for class p for an observed echo spectrum d_i, first the probabilities associated with the class p model realisations ($\mathbf{f}_i^{(p)}$) are weighted by the CMV metrics associated with the comparison of the observation (d_i) and those model realisations ($\mathbf{C}_i^{(p)}$). The score is then computed as the ratio of the sum of these weighted probabilities for class p to the sum over all N classes:

$$S_{iBPC}^{(p)} = \frac{sum(\mathbf{C}_i^{(p)} \cdot \mathbf{f}_i^{(p)} \mathrm{p}_a^{(p)})}{\sum_{k=1}^{N} sum(\mathbf{C}_i^{(k)} \cdot \mathbf{f}_i^{(k)} \mathrm{p}_a^{(k)})} \qquad \textbf{(EQ 4.6)}$$

so that each row of the score matrix $S_{BPC}^{(p)}$ contains N scores (one for each class) for a given observation. For the **BPC**, these scores are proportional to the probability that an observation belongs to a class, and are based on the underlying probability mass functions describing the model spaces for each class as well as the *a priori* probability associated with each class.

All three classification techniques (ISC, PSC, BPC) can be implemented in several configurations. For example, the resolution of each of these classifiers may be adjusted by choosing the range of values of the CMV metric to include in the classification. If the desired classification result is the "best match", then only the global maximum $\mathbf{C}_{ij}$ is included for each observation d_i. Alternatively, including all $\mathbf{C}_{ij}$ in the classification incorporates information about the correspondence between the observation and all model realisations representing all classes into the classification result. Computational considerations may render it impractical to include all this information in the classification decision, and in fact, better results are often achievable by considering some subset of the CMV correspondence values which includes local maxima (i.e. $t \leq \mathbf{C}_{ij}^{(p)} \leq max(\mathbf{C}_{ij}^{(p)})$); the threshold t may be adjusted according to the range appropriate for the classification problem. The CMV classification techniques are also flexible in terms of accounting for ambiguity and validity; the ISC and PSC may be implemented with or without $\tilde{\mathbf{W}}_A$ and/or $\tilde{\mathbf{W}}_V$, and the relative importance of these weightings may be adjusted depending upon the specific classification problem. In the BPC, if the probability distribution is empirically determined, the structure of $\mathbf{f}$ can be configured to account only for within-class validity, or to include outside-class representativity as well.

4.4 CMVC Mechanics with Simplified Model Spaces

To illustrate the mechanics of the CMVC techniques, the computational details involved in the determination of the redundancy weighting functions ($\tilde{\mathbf{W}}_R^{(p)}$), the ambiguity weighting functions ($\tilde{\mathbf{W}}_A^{(p)}$, $\tilde{\mathbf{W}}_A^{(qp)}$), the validity weighting functions ($\tilde{\mathbf{W}}_V^{(p)}$,$\tilde{\mathbf{W}}_V^{(qp)}$) and the PMFs ($\mathrm{p}_a^{(p)}$) are elaborated by employing a set of three highly-simplified model spaces for the zooplankton classification problem. These first-order model spaces consist of a small number of alternative model realisations (n_m = 100) for each of the three classes, thereby reducing the dimensionality of the problem for illustrative purposes. The simplified model realisations making up the first-order model spaces were derived from parameterisations of the theoretical models describing each scattering class. By choosing a range of simplifying parameters that encompassed some of the variability present in the echoes from scatterers in each class, a manageable set of reasonably

simple model spaces was constructed (Figure 4-4). The model parameterisation technique is similar to that used for the Model Parameterisation Classifier (MPC), and is described in Martin *et al.* 1996. The resulting simplified model spaces incorporate parameterisations of the subset of theoretical model predictions plotted in Figure 4-1; details of these models are given in Stanton *et al.* (1996; in press b). Although these simple model spaces do not encompass the complete range of variability in echo spectra predicted by the full theoretical model description of each class, they provide a good first-order representation of the more complex complete model spaces.

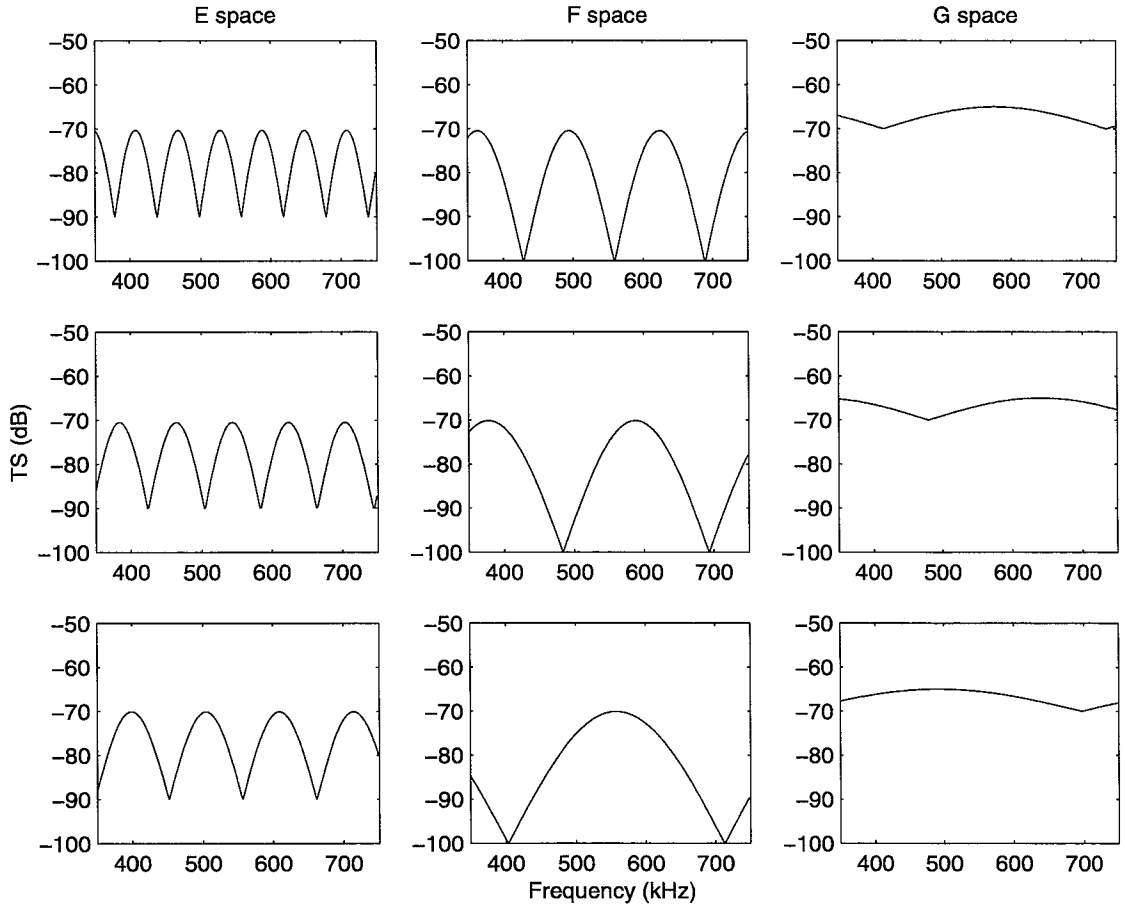

Figure 4-4 Example model realisations from the three first-order model spaces (E, F and G, $n_m = 100$). These simplified model realisations were derived from parameterisations of the theoretical scattering models describing the three classes of zooplankton, and are used to illustrate the computational details of the determination of $\tilde{\mathbf{W}}_R^{(p)}$, $\tilde{\mathbf{W}}_A^{(p)}$, $\tilde{\mathbf{W}}_V^{(p)}$, $\tilde{\mathbf{W}}_A^{(qp)}$, $\tilde{\mathbf{W}}_V^{(qp)}$, and $\mathbf{f}^{(p)}$.

4.4.1 Redundancy Weighting Functions

To maximise classifier efficiency, it is desirable to eliminate the redundancy within the model spaces for each class p. This may be accomplished by computing the redundancy weighting

function $\mathbf{W}_R^{(p)}$ for the full model space $\mathbf{M}_F^{(p)}$, and applying it to obtain a reduced model space $\mathbf{M}^{(p)}$ for that class:

$$\mathbf{M}_{F_R}^{(p)} = \mathbf{M}_F^{(p)} \cdot \tilde{\mathbf{W}}_R^{(p)} \qquad \text{(EQ 4.7)}$$

The redundancy weighting function acts as a mask filter, where the jth column of $\tilde{\mathbf{W}}_R^{(p)}(j)$ contains either 0s for $\mathbf{C}_R^{(p)}(i, j) \geq t_R$, or 1s otherwise (Figure 4-5). To obtain $\mathbf{M}^{(p)}$, the zero-valued realisations of $\mathbf{M}_{F_R}^{(p)}$ are eliminated so that the dimensionality of $\mathbf{M}^{(p)}$ is smaller than that of $\mathbf{M}_F{}^{(p)}$. The redundancy threshold t_R may be adjusted to optimise the tradeoff between resolution and numerical tractability for the specific classification problem. $\mathbf{C}_R^{(p)} = CMV(\mathbf{M}_F^{(p)}, \mathbf{M}_F^{(p)})$ is the matrix of CMV metrics for the model space compared to itself, and is computed as described in (EQ 4.2).

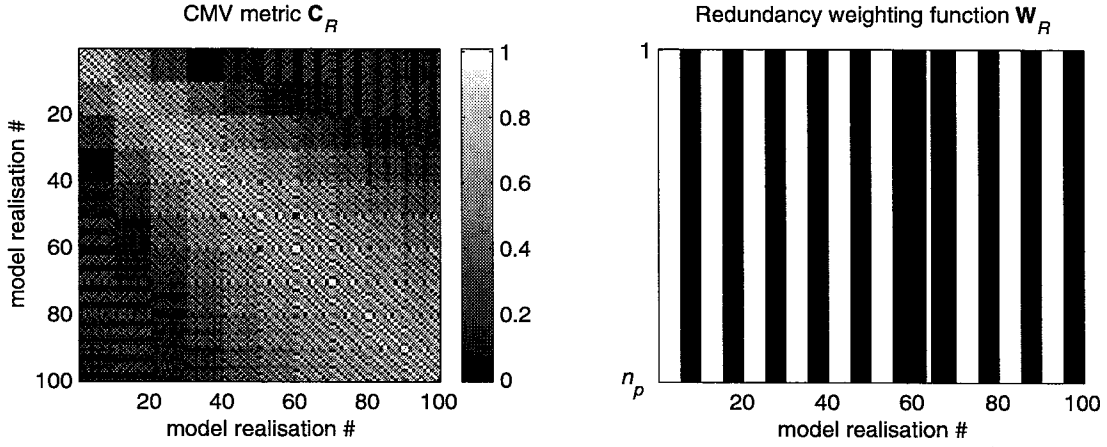

Figure 4-5 Matrix of CMV metrics $\mathbf{C}_R$ and the redundancy weighting function $\tilde{\mathbf{W}}_R$ for the simplified model space F (a first-order representation of the model space for the **FL** scattering class). In this simplified model space, $\mathbf{M}_F$ contains 100 realisations. Application of $\tilde{\mathbf{W}}_R$ with $t_R = 0.95$ reduces the dimensionality so that $\mathbf{M}$ contains only 46 realisations. n_p is the number of frequency samples in each model realisation.

4.4.2 Ambiguity Weighting Functions

For the CMV classifiers, the degree of overlap between the model spaces of different classes is determined by the extent to which the theoretical models representing different scattering classes are non-unique over any part of the parameter space. If different theoretical models predict similar or identical model realisations for the different classes, the classification result will be ambiguous unless the ambiguity in the model spaces can be accounted for by weighting the individual realisations according to their uniqueness. By implementing such an ambiguity weighting function, similarity of an observed echo spectrum with realisations in class p that are ambiguous

between classes will not contribute to $S^{(p)}$ as much as similarity with unambiguous class p realisations (e.g. see (EQ 4.3) for the **ISC**). The ambiguity weighting functions are computed as:

$$\tilde{\mathbf{W}}_A^{(pq)} = \overline{\mathbf{W}_A^{(pq)}} = mean(\mathbf{W}_A^{(pq)}) \qquad \textbf{(EQ 4.8)}$$

$$\tilde{\mathbf{W}}_A^{(p)} = \prod_{q \neq p} \overline{\mathbf{W}_A^{(pq)}} \qquad \textbf{(EQ 4.9)}$$

where $\mathbf{W}_A^{(pq)} = 1 - \mathbf{C}_A^{(pq)}$ (Figure 4-6) with $\mathbf{C}_A^{(pq)} = CMV(\mathbf{M}^{(q)}, \mathbf{M}^{(p)})$, computed as detailed in (EQ 4.2). The pairwise ambiguity weighting functions $\tilde{\mathbf{W}}_A^{(pq)}$ represent the average degree of ambiguity between each model realisation in the model space for class p and all the class q model space realisations (*mean* indicates a row-wise average); $0 \leq \tilde{\mathbf{W}}_A^{(pq)} \leq 1$ with values near 1 indicating high uniqueness (low ambiguity). The integrated ambiguity weighting function for class p $\tilde{\mathbf{W}}_A^{(p)}$ is computed as the element-wise product of the pairwise weightings and represents the net ambiguity for each realisation in class p relative to all other classes; for example, applying (EQ 4.9) for $p = 1$ yields $\tilde{\mathbf{W}}_A^{(1)} = \tilde{\mathbf{W}}_A^{(12)} \cdot \tilde{\mathbf{W}}_A^{(13)}$.

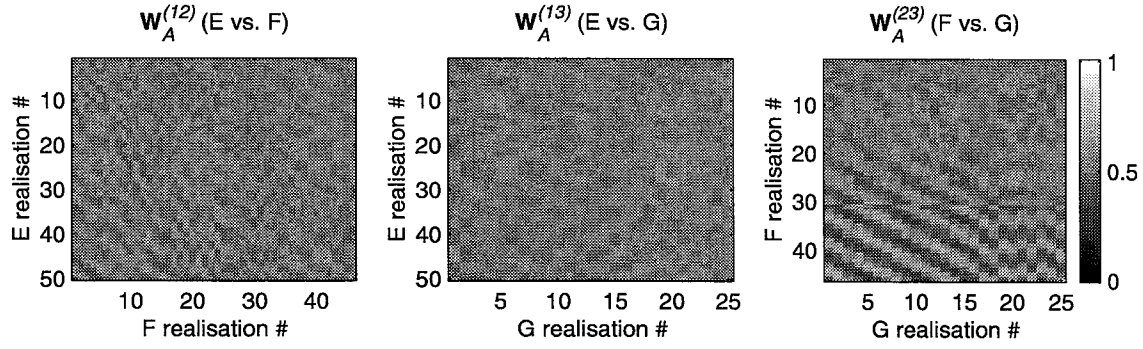

Figure 4-6 $\mathbf{W}_A^{(pq)}$ for the three first-order model spaces (E, F and G), from which the pairwise ambiguity functions $\tilde{\mathbf{W}}_A^{(pq)}$ are computed (EQ 4.8) and the integrated ambiguity functions $\tilde{\mathbf{W}}_A^{(p)}$ are derived (EQ 4.9). Ambiguity between class 2 (F) realisations and class 3 (G) realisations is highest, particularly for class 2 realisation numbers 25 through 46 (as reflected by low values of $\mathbf{W}_A^{(23)}$).

4.4.3 Validity Weighting Functions

The effectiveness of a model based classifier depends to a great extent upon the accuracy of the model spaces in representing observations from each class. For the zooplankton classification problem, if the theoretical model predictions that make up the model space for a particular class do not correspond well with echo spectra received from animals in that scattering class, the model space will have low validity. For example, observed echo spectra from class p may resemble some model realisations in the model space for class p, whereas other model realisations in the class p

model space are scarcely or never observed in class p data. For this reason, it is desirable to credit highly representative realisations with a high validity weighting. Alternatively, observed echo spectra from class q may resemble some model realisations in the model space for class p, in which case a penalty may be assigned to those class p realisations for their high representativity of class q data. The validity weighting functions quantify the validity of each model realisation by considering both within-class and between-class representativity, and are computed as:

$$\tilde{\mathbf{W}}_V^{(pq)} = \overline{\mathbf{W}_V^{(pq)}} = mean(\mathbf{W}_V^{(pq)}) \qquad \textbf{(EQ 4.10)}$$

$$\tilde{\mathbf{W}}_V^{(p)} = \alpha_{wc}\overline{\mathbf{W}_V^{(pp)}} - \overline{\alpha_{bc}\frac{1}{(N-1)}\sum_{q\neq p}\mathbf{W}_V^{(pq)}} \qquad \textbf{(EQ 4.11)}$$

where $\mathbf{W}_V^{(pq)} = \mathbf{C}_V^{(pq)}$ (Figure 4-7), with $\mathbf{C}_V^{(pq)} = CMV(\mathbf{M}^{(p)}, \mathbf{V}^{(q)})$ ($\mathbf{V}^{(q)}$ is a validation set of observations of known echo spectra from class q); $\mathbf{C}_V^{(pq)}$ is computed as detailed in (EQ 4.2). The pairwise validity weighting functions $\tilde{\mathbf{W}}_V^{(pq)}$ represent the average validity between each model realisation in the model space for class p in terms of its representativity of all the observed data in the validation set for class q, and are dependent on both the number of representative realisations and the degree to which they are representative; $0 \leq \tilde{\mathbf{W}}_V^{(pq)} \leq 1$ with values near 1 indicating high validity. The integrated validity weighting function for class p $\tilde{\mathbf{W}}_V^{(p)}$ is computed as an element-wise weighted sum of the pairwise weightings and represents the net validity for each realisation in class p. α_{wc} and α_{bc} are chosen to reflect the importance of within-class representativity relative to between-class representativity for the particular classification problem.

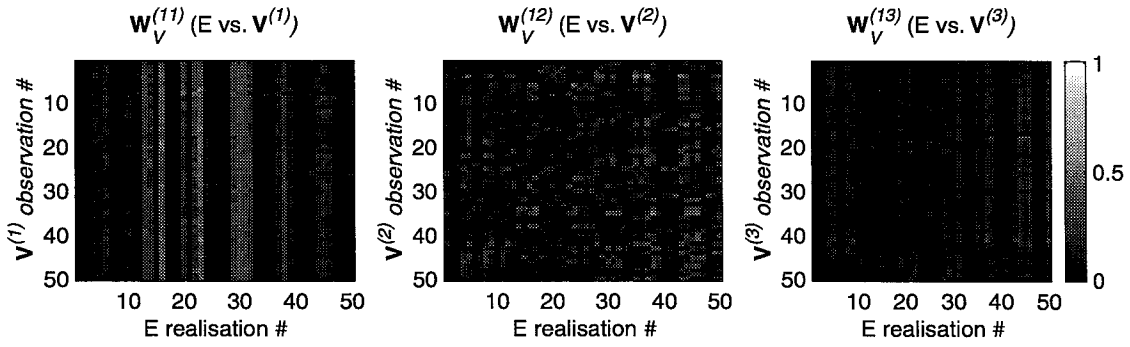

Figure 4-7 $\mathbf{W}_V^{(1q)}$ for the simplified model space E (a first-order representation of the model space for the **ES** scattering class), from which the pairwise validity functions $\tilde{\mathbf{W}}_V^{(pq)}$ are computed (EQ 4.10) and the integrated validity function $\tilde{\mathbf{W}}_V^{(1)}$ is derived (EQ 4.11). Within-class representativity of the validation set is higher than between-class representativity for the E model space. Some E class model realisations are more representative of $\mathbf{V}^{(1)}$ (the validation set for class 1 (E)) than others. For these calculations, the validation sets each contain 50 observed echo spectra: $\mathbf{V}^{(1)}$ was collected from a single pteropod (*Limacina retroversa*), $\mathbf{V}^{(2)}$ from a single euphausiid (*Meganyctiphanes norvegica*), and $\mathbf{V}^{(3)}$ from a single siphonophore (*Agalma okeni*).

4.4.4 Probability Mass Functions

For the zooplankton classification problem, the underlying probability distribution of observations in a given class can be modelled empirically, whereas the *a priori* probabilities p_a must be determined using *a priori* information (Figure 4-2). The probability mass function (PMF) $\mathbf{f}^{(p)}$ for class p is constructed based on a validation set of observations $\mathbf{V}^{(p)}$ of known echo spectra, in much the same way as with the computation of the validity weighting functions. This validation set may then be compared to class p model realisations to construct a "class-support" PMF (which accounts only for within-class validity), or to the model realisations in all N model spaces to build a "full-support" PMF (which also considers between-class representativity). An empirical PMF is simply a histogram, for which the x-axis bins (support) are the model realisations; the histogram $\mathbf{f}^{(p)}$ is constructed as follows:

$$\mathbf{f}_j^{(p)} = \sum_{i=1}^{n_V} h_{ij} \qquad \text{(EQ 4.12)}$$

where $\mathbf{f}_j^{(p)}$ is the value of the PMF for the jth model realisation, computed as the sum of the h_{ij} over all n_V observations in $\mathbf{V}^{(p)}$. For each observation i in $\mathbf{V}^{(p)}$, the height assigned to the jth model realisation h_{ij} may be computed in one of three ways:

TYPE I: $h_{ij} = 1$ for model realisation j for which $\mathbf{C}_{f_{ij}}^{(p)} = max(\mathbf{C}_{f_{ij}}^{(p)})$, $h_{ij} = 0$ otherwise.

TYPE II: $h_{ij} = \mathbf{C}_{f_{ij}}^{(p)}$ for all model realisations j for which $t_f \le \mathbf{C}_{f_{ij}}^{(p)} \le max(\mathbf{C}_{f_{ij}}^{(p)})$, $h_j = 0$ for all other realisations.

TYPE III: $h_{ij} = \mathbf{C}_{f_{ij}}^{(p)} / \sum_{k=1}^{n_j} \mathbf{C}_{f_{ik}}^{(p)}$ where n_j is the number of model realisations for which $t_f \le \mathbf{C}_{f_{ij}}^{(p)} \le max(\mathbf{C}_{f_{ij}}^{(p)})$, $h_j = 0$ for all other realisations.

Here $\mathbf{C}_f^{(p)} = CMV(\mathbf{M}, \mathbf{V}^{(p)})$ is computed as shown in (EQ 4.2), with $\mathbf{M} = \mathbf{M}^{(p)}$ for the class-support PMF; $max(\mathbf{C}_{f_i}^{(p)})$ indicates the maximum value in row i of $\mathbf{C}_f^{(p)}$. In constructing a **TYPE I** PMF, only the best match (global maximum) model realisation for each observation is considered, whereas for **TYPE II** and **TYPE III**, a subset of the CMV correspondence values which includes local maxima are considered (Figure 4-8), and the threshold t_f may be adjusted according to the appropriate range for the particular classification problem. In the **TYPE II** PMF, the h_{ij} are proportional to the degree of similarity (as measured by the CMV metric) between realisation j and

observation i, whereas for **TYPE III**, the h_{ij} are normalised so that only the relative CMV of a particular observation to all the model realisations is considered; differences in CMV across observations are not accounted for.

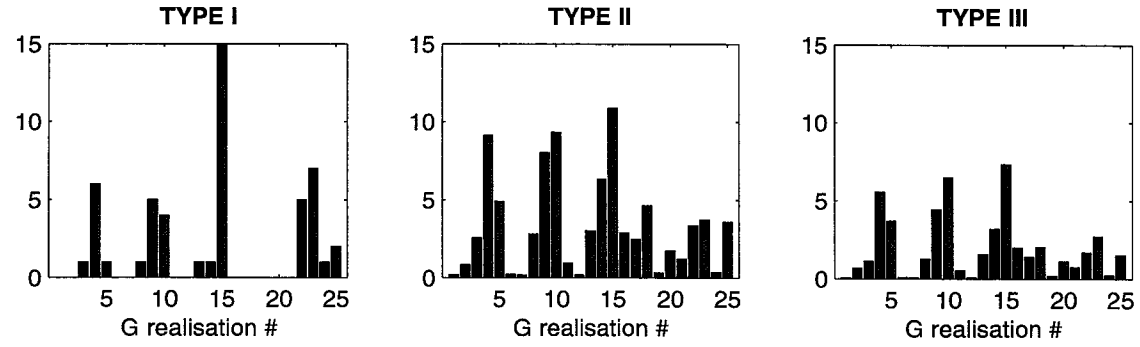

Figure 4-8 Class-support **TYPE I**, **TYPE II** and **TYPE III** PMFs $\mathbf{f}^{(3)}$, computed using (EQ 4.12), for the simplified model space G (a first-order representation of the model space for the **GB** scattering class). For **TYPE II** and **TYPE III** $\mathbf{f}, t_f = 0.5max(\mathbf{C}_{f_{ij}}^{(p)})$. The validation set $\mathbf{V}^{(3)}$ contains 50 observed echo spectra from a single siphonophore (*Agalma okeni*).

4.5 Zooplankton Scattering Physics

The CMVC are a set of advanced model based classification techniques designed to accommodate a wide range of potential model spaces, ranging from the simplifying parameterisations employed to illustrate computational mechanics in the last section, to the most sophisticated theoretical model representations for the acoustic backscattering of zooplankton available to date. To best evaluate the performance of the CMVC, it is desirable to construct model spaces which fully exploit the current knowledge of zooplankton scattering physics gained through the forward modelling of acoustic backscattering from several zooplankton types. Using empirical data collected from individual live zooplankton in combination with the basic physics governing the scattering from objects with simplified geometries, a number of theoretical model formulations have been developed to predict echoes from three classes of zooplankton. These sophisticated models, which provide the basis for the CMVC model spaces, are outlined here together with a review of the basic physics governing the scattering from these zooplankton classes.

In the following expressions for *TS* as a function of frequency for all three scattering classes, a is the equivalent spherical or cylindrical radius of the animal in m, k is the acoustic wavenumber $k = 2\pi f/c$, f is the acoustic frequency in Hz, c is the sound speed in m/s (i.e. $\lambda = c/f$), and $\Re$ is the reflection coefficient $\Re = (gh-1)/(gh+1)$ where $g = \rho_2/\rho_1$ is the density contrast of the organism (subscript 2) relative to water (subscript 1), and $h = c_2/c_1$ is its sound speed contrast.

For spherical hard elastic-shelled (**ES**) organisms (e.g. pteropods), a ray-based model which includes a summation of contributions from a direct return and a circumferential wave can be used to describe the scattering (Stanton *et al.* in press b). Although the circumferential wave contribution is generally represented by an infinite summation of terms representing multiple circumnavigations around the shell, for these organisms the series is truncated to include only the first partial circumnavigation, which is dominant:

$$TS_{ES} \cong 20\log\left|F_{spec}\frac{a}{2}\Re e^{-i2ka} - F_l\frac{\bar{a}}{2}G_l e^{i\Phi_l}e^{-2(\pi-\theta_l)\beta_l}\cdot e^{i\eta_l}e^{-(1/2)\gamma^2\sigma^2}\right| \qquad \textbf{(EQ 4.13)}$$

The first term in (EQ 4.13) represents the direct return (echo from the front interface of the body), assuming the shell can be modelled as a fluid sphere, with F_{spec} indicating the relative contribution of this specular reflection. The second term represents the scattering from a circumferential, antisymmetric Lamb wave l travelling at subsonic speeds along the surface of the shell (Marston 1988; Kargl and Marston 1989; Marston *et al.* 1990), with F_l indicating the relative contribution of this return. In this representation, the zeroth-order Lamb (flexural) wave dominates the scattering (Stanton *et al.* in press a), and $G_l = -8\pi\beta_l(c/c_l)$, $\Phi_l = -\pi/2$, $\theta_l = Re\{\text{asin}(c/c_l)\}$, $\eta_l = 2k\bar{a}[(c/c_l)(\pi-\theta_l) - \cos\theta_l] - \pi/2$, and $\gamma = 2k((c/c_l)(\pi-\theta_l) - \cos\theta_l)$ (where c_l is the speed of the Lamb wave, $c/c_l = (8ka+0.5)/(k\bar{a})$, and $\beta_l = 0.002ka$). The ray formulation for an idealised spherical shell has been modified to account for shell roughness (so that a is the average value of an ensemble of samples from a Gaussian distribution with mean $\bar{a}$ and standard deviation σ, with $\sigma = 0.025\bar{a}$) and discontinuities (Stanton *et al.* in press b). For example, if the animal is oriented in such a way that the opercular opening (aperture at top of shell in sketch of *Limacina retroversa* (Figure 4-1) through which animal body protrudes) interferes with the propagation of the flexural wave, the scattering will be dominated by the direct return, and the second term may be neglected ($F_l = 0$).

Scattering from elongated fluid-like (**FL**) crustacean zooplankton (euphausiids, shrimp) in the geometric regime may be approximated by a ray summation formula $\sum_{j=1}^{N} b_j \cdot e^{i2k\varepsilon_j}$ with each ray representing the scattering contribution from a different scattering feature of the fluid-like body (Stanton *et al.* 1994b, in press b). For each ray contribution, ε_j is the displacement of that scattering feature from a zero-phase reference plane, thereby accounting for the phase shift of each ray, and the b_j are the amplitude coefficients for the rays (e.g. for the ray associated with the front interface of the animal $b_j = (1/2)\Re\sqrt{\rho_j^{(1)}\cdot\rho_j^{(2)}}$ where $\rho_j^{(1)}$ and $\rho_j^{(2)}$ are the local radii of curvature of the point of scatter in two perpendicular planes (1) and (2)). In many cases, particularly when

the animal is oriented near broadside relative to the transducer, the scattering from these elongated fluid-like crustacean zooplankton is well-described by a simpler two-ray summation (e.g. the two-ray randomly oriented fluid bent cylinder model from Stanton *et al.* (1993a,b)), which models the constructive and destructive interference between the ray associated with scattering from the front interface of the animal and the ray associated with scattering from the back interface. Chu *et al.* (1993) and Stanton *et al.* (1993b) developed a more precise alternative to these ray models for weakly scattering elongated zooplankton at all angles of orientation using a formulation based on the distorted wave Born approximation (DWBA) volume integral (Morse and Ingard 1968). If the fluid-like body has a circular cross-section at every point along its length-wise axis, the DWBA integral may be reduced to a line integral along this axis (Stanton *et al.* in press b), yielding an exact expression for the scattering from an elongated, fluid-like zooplankter as a function of animal size, shape, material properties, and angle of orientation:

$$TS_{FL} = 20\log\left|\frac{k_1}{4}\int_{\hat{r}_{pos}} (\gamma_\kappa - \gamma_\rho) e^{i2(\hat{k}_i)_2 \cdot \hat{r}_{pos}} a \frac{J_1(2k_2 a\cos\beta_{tilt})}{\cos\beta_{tilt}} |d\hat{r}_{pos}|\right| \qquad \textbf{(EQ 4.14)}$$

In (EQ 4.14), J_1 is a Bessel function of the first kind of order 1, $\gamma_\rho = (\rho_2 - \rho_1)/\rho_2$, $\gamma_\kappa = (\kappa_2 - \kappa_1)/\kappa_1$, with compressibility κ defined as $\kappa_i = 1/(\rho_i c_i^2)$; subscript 1 refers to the surrounding medium (seawater), subscript 2 refers to the fluid-like medium of the zooplankton body, so that $(\gamma_\kappa - \gamma_\rho) = (1/gh^2) + (1/g) - 2$. Here, $(\hat{k}_i)_2 = \hat{k}_2 = \hat{k}_1/h$ and $0 < \beta_{tilt} < \pi$. This formulation accurately predicts the scattering from a deformed fluid-like cylindrical body of arbitrary shape (i.e. the cylindrical radius can vary along the length-wise axis) for any angle of orientation relative to the incident acoustic wave.

For gas-bearing (**GB**) fluid-like plankton (siphonophores) with a single gas inclusion (located at the top of the stem above the animal body in the sketch of *Agalma okeni* (Figure 4-1)), the general scattering properties are described by a spherical gas bubble plus fluid-like tissue model. In the formulation given in Stanton *et al.* (in press b), scattering from the gas inclusion is modelled using the modal series solution for a fluid sphere $-\frac{i}{k}\sum_{m=0}^{\infty}(2m+1)\cdot(-1)^m \cdot b_m^{(f)}$, where the $b_m^{(f)}$ are the modal series coefficients for a sphere (Anderson 1950). Scattering from the gas bubble may alternatively be modelled as a single ray contribution from a spherical gas inclusion, in a similar manner to the model for the direct return from a hard elastic spherical shell (term 1 in (EQ 4.13)). The gas bubble plus tissue model then becomes:

$$TS_{GB} \cong 20\log\left|\frac{1}{2}a\Re e^{-i2ka} + \sum_{j=1}^{N} b_j \cdot e^{i2k\varepsilon_j}\right| \qquad \text{(EQ 4.15)}$$

The first term in (EQ 4.15) represents the scattering from the gas inclusion (which at high ka is dominated by the echo from the front interface), assuming the bubble can be modelled as a fluid sphere, whereas the second term represents the scattering from the fluid-like body as a summation of the rays due to the major scattering features of the fluid-like tissue. As described for the ray summation for elongated fluid-like animals, the ε_j are the displacements of each scattering feature from a zero-phase reference plane, and are computed for the gas-bearing animal as $\varepsilon_j = (j-1)\cdot\bar{\varepsilon}_j + s\cdot\Delta\varepsilon_j$ with $\Delta\varepsilon_j$ varying randomly between 0 and $0.1\cdot\bar{\varepsilon}_j$, and s alternating randomly between +1 and -1. The ray amplitude coefficients b_j are difficult to determine for the siphonophore body, which is composed of many bracts and gastrozooids. Stanton *et al.* (in press b) estimated these coefficients based on the echo statistics of the scattering measured from a gas-bearing zooplankter before and after removal of the gas inclusion, so that the b_j for the tissue may be expressed in terms of the amplitude of the scattering from the gas inclusion and a ratio F_{tiss} of the energy scattered by the tissue relative to the bubble: $b_j = (\sqrt{F_{tiss}/2N})a\Re$, where N is the number of tissue rays. The echo from the gas bubble is believed to dominate the scattering from siphonophores; however, weaker echoes from the tissue may contribute measurably to the structure of the echo spectra in some cases.

4.6 CMVC Performance

The performance of the CMVC techniques was evaluated against over one thousand experimentally collected echoes, using the best theoretical models to date (without simplification) as a basis for the model spaces. For each class, a model space was constructed from the theoretical models described in the previous section by varying the values of the model parameters to generate several hundred model realisations, which represent theoretical scattering predictions spanning the entire chosen parameter space (Figure 4-9). Only a subset of the parameters were varied for each model, while the rest were fixed (values as indicated in the figure caption). For the **ES** model space, the mean shell radius $\bar{a}$, and the relative contributions of the specular F_{spec} and Lamb wave F_l were varied in (EQ 4.13); for the **FL** model space, the cylindrical radius a, the orientation angle β_{tilt} and the animal shape (as digitised from video images of several different animals and expressed by $\vec{r}_{pos}$) were varied in (EQ 4.14); for the **GB** model space, the bubble radius a, the mean

displacement for each ray $\bar{\varepsilon}_j$, and the relative tissue scattering contribution F_{tiss} were varied in (EQ 4.15). To ensure that the model spaces spanned the full extent of the parameter space, these parameter values were varied either over or their entire range (e.g. F_{spec}, F_l, β_{tilt}, F_{tiss}) or over the range observed in the experimentally measured animals (e.g. a). The resulting full model spaces contained 600, 700, and 800 model realisations for the **ES**, **FL**, and **GB** model spaces respectively.

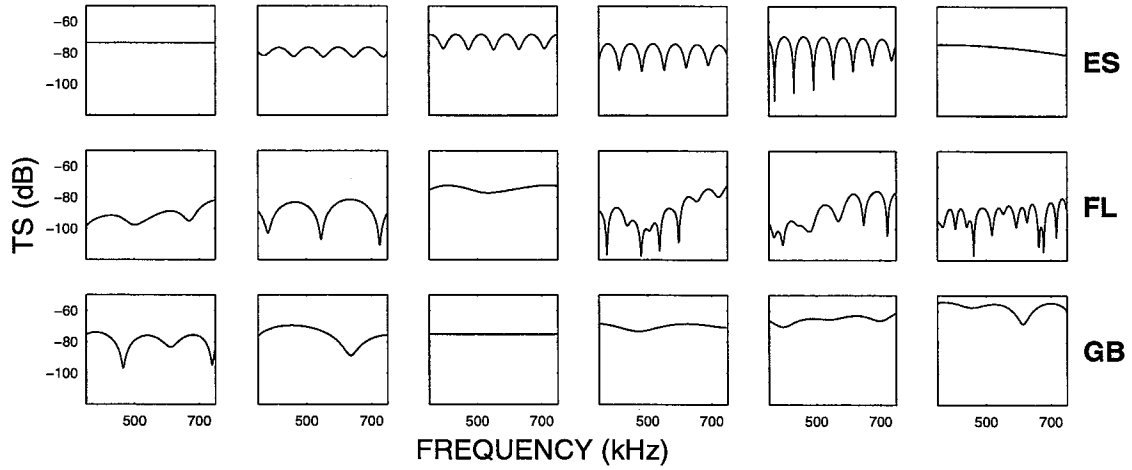

Figure 4-9 Selected examples of model realisations from the three model spaces **ES** (top row), **FL** (second row) and **GB** (bottom row) as generated by varying the parameters of the theoretical scattering models. The 600 realisations in the full **ES** model space $\mathbf{M}_F^{(1)}$ were generated using (EQ 4.13) with $c/c_l = 8$, $\Re = 0.84$, varying F_{spec} and F_l between 0 and 1, and $\bar{a}$ between 0.5 and 1 mm. $\mathbf{M}_F^{(2)}$ is composed of 700 **FL** realisations, generated using (EQ 4.14) with $g = 1.0357$ and $h = 1.0279$, varying β_{tilt} between 0 and 180°, a between 1 and 3 mm, and using 5 different shapes (digitised from actual video images of euphausiids). The 800 realisations in the full **GB** model space $\mathbf{M}_F^{(3)}$ were generated using (EQ 4.15) with $g = 0.0012$, $h = 0.22$, and $N = 6$, and varying F_{tiss} between 0 and 1, a between 0 and 1.75 mm, and $\bar{\varepsilon}_j$ between $\min(\lambda)/(N-1)$ and $\max(\lambda)/(N-1)$.

Redundancy was eliminated from the full model spaces $\mathbf{M}_F^{(p)}$ for each class using (EQ 4.7) with $t_R = 0.95$. The resulting reduced model spaces contained 237 (**ES** space, $\mathbf{M}^{(1)}$), 663 (**FL** space, $\mathbf{M}^{(2)}$), and 561 (**GB** space, $\mathbf{M}^{(3)}$) model realisations, so that a relatively minor sacrifice of within-class resolution was accompanied by a significant increase in computational efficiency. Ambiguity weighting functions $\tilde{\mathbf{W}}_A^{(p)}$ and $\tilde{\mathbf{W}}_A^{(qp)}$, validity weighting functions $\tilde{\mathbf{W}}_V^{(p)}$ and $\tilde{\mathbf{W}}_V^{(qp)}$, and class-support probability mass functions $\mathbf{f}^{(p)}$, were computed using (EQ 4.8) through (EQ 4.12) for each class. The validation set $\mathbf{V}^{(p)}$ used in the computation of $\tilde{\mathbf{W}}_V^{(p)}$, $\tilde{\mathbf{W}}_V^{(qp)}$, and $\mathbf{f}^{(p)}$ consisted of half the data for each class (every other echo from Table 4-1). Classification of the other half of the dataset was then carried out to evaluate the performance of the ISC (EQ 4.3), the PSC (EQ 4.4), and the BPC (EQ 4.6).

To assess classifier performance with the best quality data available, a 75-observation sample was extracted from the 1993 dataset. This subset consists of 25 acoustic returns each from an elastic-shelled pteropod *Limacina retroversa* (Animal 93-29), a fluid-like euphausiid *Meganyctiphanes norvegica* (Animal 93-33e) and a gas-bearing siphonophore *Agalma okeni* (Animal 93-18), and represents the highest signal-to-noise ratio (SNR) data collected. For all three classifiers, **ES** class scores ($S_{ISC}^{(1)}$, $S_{PSC}^{(1,1)}$, $S_{BPC}^{(1)}$) were high for the *L. retroversa* echoes, accompanied by low **FL** and **GB** class scores (Figure 4-10). Similarly, **GB** class scores were consistently high for *A. okeni* echoes.

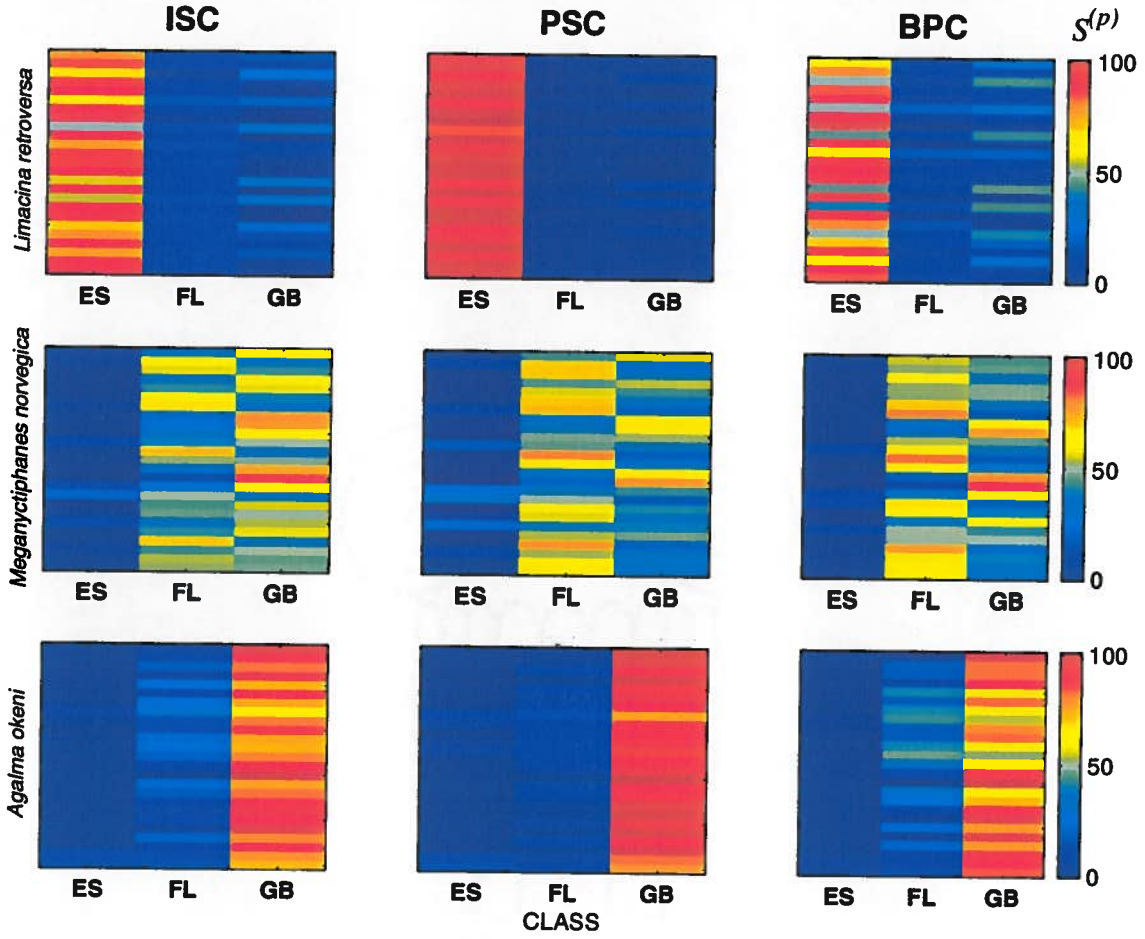

Figure 4-10 Classification scores for the Integrated Score Classifier (ISC; left, $S_{ISC}^{(p)} \times 100$), Pairwise Score Classifier (PSC; center, $S_{PSC}^{(p,p)}$) and Bayesian Probability Classifier (BPC; right, $S_{BPC}^{(p)}$) for a selected subset of the highest quality data (25 acoustic returns each (y-axis) from an elastic-shelled pteropod *Limacina retroversa*, top row, a fluid-like euphausiid *Meganyctiphanes norvegica*, middle row, and a gas-bearing siphonophore *Agalma okeni*, bottom row). Scores $S^{(p)}$ colour-coded according to the legend (right). ISC and PSC implemented including both ambiguity and validity weightings ($\tilde{\mathbf{W}}_A$, $\tilde{\mathbf{W}}_V$); BPC implemented using a class-support **TYPE II** $\mathbf{f}^{(p)}$ with $t_f = 0.5max(\mathbf{C}_{f_{ij}}^{(p)})$. Validation set **V** included half of the 1550 observations from the 1993 dataset. Classification threshold t was adjusted to include all CMV within the 3 dB-down range: $t = 0.5max(\mathbf{C}_{ij}^{(p)})$.

On the other hand, **FL** and **GB** class scores for the *M. norvegica* echoes were similar, so that assigning each echo to the class with the maximum score resulted in a high mis-classification rate for Animal 93-33e (Table 4-2). For this 75-echo dataset, the ISC correctly classified 80% of these echoes overall, whereas the PSC and BPC performed better, correctly classifying about 90% of the echoes. Alternatively, if the classification is made by assigning an observation to the class containing the best match model realisation (global maximum), the success rate with the *M. norvegica* echoes is increased, with the PSC achieving 100% correct classifications.

Table 4-2 Summary of ISC, PSC and BPC results for the high-quality subset of data (25 acoustic returns each from a pteropod *Limacina retroversa* (93-29), a euphausiid *Meganyctiphanes norvegica* (93-33e), and a siphonophore *Agalma okeni* (93-18)). Mean class scores (n=25) for each classifier ($\overline{S_{ISC}^{(p)}}$, $\overline{S_{PSC}^{(p,p)}}$, $\overline{S_{BPC}^{(p)}}$) are shown, followed by the % correctly classified based on assigning each observation to the class with the maximum score. Last 3 columns show % correctly classified based on assigning each observation to the class containing the best match.

		MEAN CLASS SCORES									% CORRECT (based on max S)			% CORRECT (based on max **C**)		
		$\overline{S_{ISC}^{(p)}}$			$\overline{S_{PSC}^{(p,p)}}$			$\overline{S_{BPC}^{(p)}}$			ISC	PSC	BPC	ISC	PSC	BPC
ANIMAL	n	**ES**	**FL**	**GB**	**ES**	**FL**	**GB**	**ES**	**FL**	**GB**						
93-29	25	.79	.09	.12	95	2	3	74	8	18	100%	100%	96%	96%	100%	12%
93-33e	25	.03	.44	.53	5	54	41	2	53	45	40%	64%	76%	68%	100%	84%
93-18	25	.02	.14	.84	2	7	91	1	21	79	100%	100%	100%	96%	100%	32%
Overall	75		-			-			-		80%	88%	91%	77%	100%	43%

Classifier performance was also assessed with the complete dataset for 1993 and 1994 (non-validation portion; n=775 for 1993, n= 625 for 1994). These data included echoes from 10 different pteropods *L. retroversa*, 3 euphausiids *M. norvegica*, and 11 siphonophores *A. okeni* (10), and *Nanomia cara* (1; another species of physonect (gas-bearing) siphonophore commonly found in the N.W. Atlantic Ocean). Each of the classifiers was implemented in two different configurations: for the ISC and PSC, ambiguity and validity weighting functions were either included or neglected; for the BPC, either **TYPE I** or **TYPE II** class-support PMFs were used (Figure 4-11). *A. okeni* echoes were correctly classified most often, while the *L. retroversa* data was generally poorly classified. The PSC showed the best performance overall, both when classifying based on the class with the maximum score, as well as based on the class with the best match model realisation. The PSC performed considerably better when the weighting functions were included, particularly for the *M. norvegica* data. Notably, PSC classifications based on the global maximum best match model realisation were best overall, although for the *L. retroversa* data, BPC classification with a **TYPE I** PMF yielded the most favourable results.

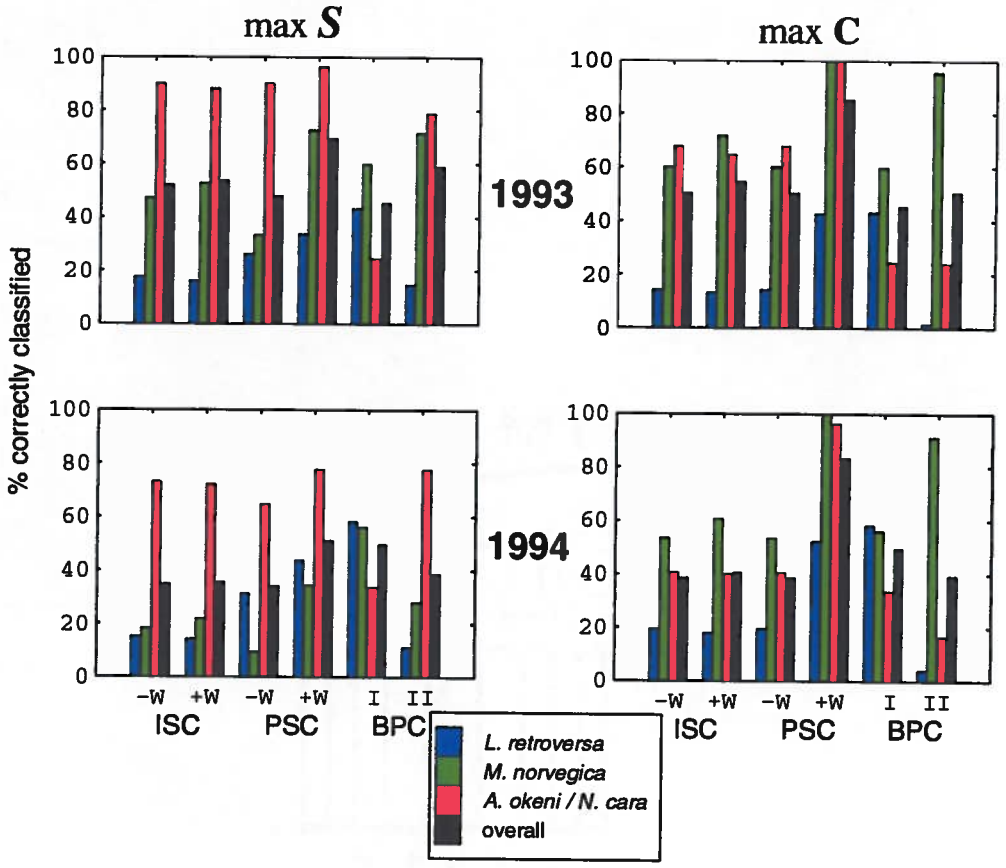

Figure 4-11 Classification results (% correct) for complete 1993 (top row, n = 200 for *L. retroversa*; n = 350 for *M. norvegica*; n = 225 for *A. okeni*) and 1994 (bottom row, n = 200 for *L. retroversa*; n = 225 for *M. norvegica*; n = 200 for *A. okeni / N. cara*) dataset. Classifications based on assigning observations to the class with maximum score (max S) are shown at left; those based on assigning echoes to the class containing the best match model realisation (max **C**) are shown at right. ISC and PSC implemented with (+W) and without (-W) $\tilde{\mathbf{W}}_A$ and $\tilde{\mathbf{W}}_V$; BPC implemented with both **TYPE I** (I) and **TYPE II** (II) class-support $\mathbf{f}^{(p)}$. For 1993 classifications, validation set **V** included half of the 1550 1993 observations; for 1994 classifications, **V** included half of the 2800 1993 plus 1994 observations. In all cases, $t = 0.5max(\mathbf{C}_{ij}^{(p)})$.

In addition to inverting echoes for scattering class, the classifiers were also designed to invert for scatterer characteristics within a class. This may be accomplished by considering the global maximum best match model realisation for each echo; since a given model realisation arises from a theoretical model prediction for a particular combination of parameters, it is possible to invert each echo for these "best-fit" parameter values. For classification of echoes based on the best match model realisation, the PSC demonstrated the best performance (Figure 4-11). The high success rate of the global maximum best match PSC is attributable to its excellent between-class resolution; however, sufficient within-class resolution is necessary in order to invert for individual

scatterer characteristics (as related to theoretical model parameters). To evaluate the within-class resolution of the PSC, the parameter values associated with the best match model realisation are compared to known characteristics of the animal (selected examples are shown in Figure 4-12). Of the model parameters that were varied to create the model realisations for each class, only animal size was measured for the experimental animals. For all 25 *L. retroversa* echoes in the high quality data subset, the inversions predicted the mean shell size reasonably well (a = 0.7 mm as compared to an experimentally measured average shell size of about 0.75 mm). Interestingly, the predicted F_l varied slightly (around a central value of 0.67) from echo to echo, probably as a result of small changes in the position of the opercular opening relative to the transducer during insonification (caused by very slight orientational changes in the animal due to ship motion). For the *M. norvegica* echoes, animal size is fairly well-predicted for echoes where the predicted angle of orientation β_{tilt} is near broadside (90°) (a=1.65 mm as compared to the experimentally measured radii of about 1.5 mm (dorso-ventral) and 2 mm (lateral)). For these elongated, actively-swimming animals, the sound wave was often incident at off-broadside angles, changing the apparent size of the animal (projection of the animal radius onto the acoustic axis) significantly. Since animal size and angle of orientation for these elongated fluid-like animals are confounded, it will be difficult to accurately invert for individual animal size without knowing the angle of orientation. For the *A. okeni* data, the inversions predicted a smaller bubble size (e.g. a = 0.75 mm) for some echoes and a larger bubble size for others (e.g. a = 1.25 mm) as compared to the experimentally measured dimensions of the elongated bubble (about 0.6 mm - 1 mm). In general, the PSC is able to identify the best match between echoes and model realisations by relying on the CMV metric, and shows promise in inverting for specific animal characteristics as represented by the theoretical model parameters.

4.7 Discussion

The CMVC techniques provide a comprehensive framework within which to perform classification inversions based on theoretical or empirical models for each class. Three different classification algorithms (ISC, PSC, BPC) have been developed using the CMVC approach, and these were applied to the classification of broadband acoustic echoes received from several species of zooplankton with good success. For a given observed echo spectrum, these classifiers provide a relative weighted measure of similarity to each model realisation in each of the model spaces ($\mathbf{C}$), as well as a relative score for each class (S). If the classification is based on matches to particular

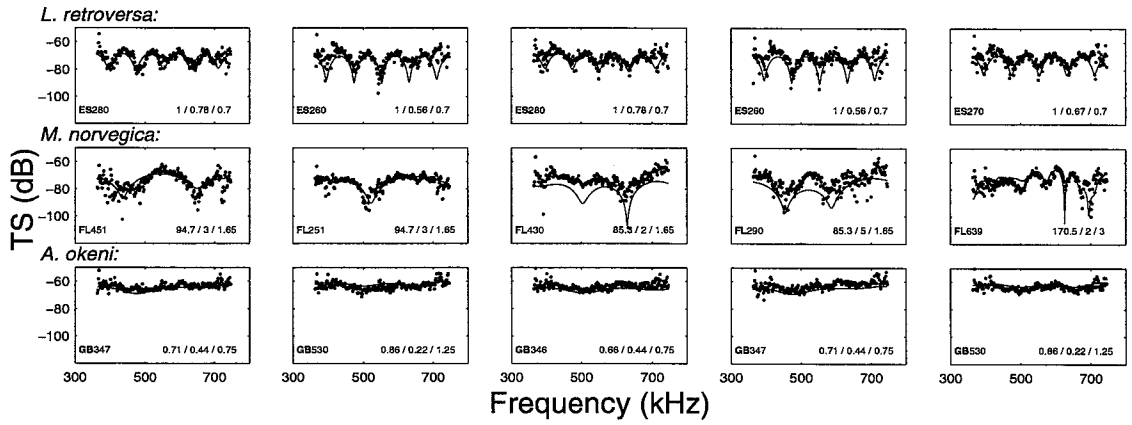

Figure 4-12 Selected examples of PSC-inverted best match echo classifications for five observations each of a pteropod *L. retroversa* ($\bar{a} \cong 0.75$ mm, top), a euphausiid *M. norvegica* ($a \cong 1.5$ - 2 mm, middle), and a siphonophore *A. okeni* ($a \cong 0.6$ - 1 mm, bottom), from the high-quality subset of 1993 data. Observations (points) plotted together with best match model realisations (solid line); best match scattering class and model realisation number shown at bottom left, parameter inversions given at bottom right (**ES**: $F_{spec}/F_l/\bar{a}$; **FL**: β_{tilt}/shape#/a; **GB**: $F_{tiss}/\bar{\varepsilon}_j/a$; $\bar{a}$ and a in mm, β_{tilt} in degrees). PSC implemented including both ambiguity and validity weightings ($\tilde{\mathbf{W}}_A$, $\tilde{\mathbf{W}}_V$). Validation set **V** included half of the 1550 1993 observations. Classification threshold t was adjusted to include all CMV within the 3 dB-down range: $t = 0.5max(\mathbf{C}_{ij}^{(p)})$.

model realisations, the observation may then be assigned to the class containing the best match model realisation ($max(\mathbf{C})$ criterion). Alternatively, if the class scores are used as a basis for classification, the observation may be assigned to the class with the highest score ($max(S)$ criterion); the class scores themselves provide error bounds on that decision. It may not always be desirable to assign an observation to one of the classes, particularly when two or more class scores are similar. In this case, although the class scores give an indication of the relative certainty that the observation belongs to a given class, it may not be assignable to any particular class if the class scores do not exceed some minimum threshold, or if they are not separated by some minimum difference.

One of the fundamental components of the CMVC techniques is their ability to account for the ambiguity between the model spaces as well as the validity of each model space in representing known data from that class. For example, for the three scattering classes of zooplankton, the highest degree of ambiguity occurred between theoretical model predictions for the **FL** and the **GB** model spaces. This ambiguity was accompanied by a slightly lower within-class validity for the **GB** class. One result of this could be that echoes from fluid-like animals are incorrectly classified as **GB**. In fact, when the classifiers were implemented without accounting for ambiguity

or validity (-W in Figure 4-11), the **GB** class scores for the fluid-like *M. norvegica* echoes were often higher, resulting in misclassification of these echoes as **GB**. Incorporating both ambiguity and validity weightings into the classifications (+W) improved the *M. norvegica* classification results considerably (e.g. for 1993 data, PSC (-W): 33% correctly classified; PSC (+W): 73% correctly classified, based on assigning an observation to the class with the maximum score). PSC classification results for the other animals also improved with the incorporation of $\tilde{\mathbf{W}}_A$ and $\tilde{\mathbf{W}}_V$. Clearly, accounting for both ambiguity and validity allows for fine-tuning of the resolution of the classifiers, leading to better classification results.

Depending on the model spaces for the particular classification problem, and the relative importance of between-class versus within-class overlap, as well as between-class representativity of the model realisations, the ISC and PSC techniques can be implemented with ambiguity weightings, validity weightings, both, or neither. With the BPC, ambiguity is inherently accounted for in the expression for conditional probability (EQ 4.5), since if the model spaces for two classes (e.g. 1 and 2) are highly ambiguous, $\mathbf{f}^{(1)}$ and $\mathbf{f}^{(2)}$ will be similar for a particular observation. The BPC relies on the PMFs to account for model representativity. Both within-class validity and between-class representativity (as reflected by $\mathbf{f}_j^{(p)}$, the value of the PMF for the jth model realisation) are confounded with other issues. For example, in addition to indicating that model realisation j has low validity in representing data from class p, a small $\mathbf{f}_j^{(p)}$ could also indicate that observations represented by model realisation j occur very infrequently, or that the observations are outside the parameter range of the model space (i.e. that the model space as constructed fails to span the entire range of observable echo spectra). The ISC and PSC provide a flexible means by which to incorporate ambiguity and validity weightings, whereas with the BPC there is no explicit way in which to condition the classification to favour certain less-ambiguous model realisations based on the degree of ambiguity, nor is there a mechanism for penalising a model realisation which represents data outside its class well.

The three different classification algorithms offer implementation alternatives depending upon the classification problem at hand. For example, the PSC has greater between-class resolution due to the incorporation of pairwise ambiguity and validity weightings. However, unlike the ISC which requires no *a priori* information, the PSC is based on an assumption of the *a priori* class membership of the data; if good *a priori* information is available (as it was for the experimental data with which these classifiers were tested), the PSC has a performance advantage over the ISC,

yielding more accurate classifications. *A priori* information regarding species composition for field-collected data may be obtained via simultaneous net or pump samples. A sensitivity analysis was carried out to assess the impact of an incorrect assumption of *a priori* class membership on the PSC results. It revealed that echoes from some animals (*L. retroversa* and *A. okeni*) are just as well-classified (using the maximum score criterion) even if the wrong *a priori* class membership assumption is made, whereas the *M. norvegica* data can be much more poorly classified under the wrong class membership assumption. If good *a priori* information is not available, the ISC may be the more robust alternative, depending upon the species composition of the data to be classified.

In the BPC, two types of PMFs can be constructed depending on the relative importance of within-class versus between-class model representativity. A class-support PMF incorporates a measure of within-class validity, whereas a full-support PMF can also provide a measure of the validity of model realisations in a given class for representing data in other classes. The computationally less expensive class-support PMFs were used in the classifications, since a preliminary sensitivity analysis with a test dataset indicated that the classification results based on the full-support PMFs were no better overall than those obtained with class-support PMFs. Specifically, classification results (based on maximum score criterion) for the *L. retroversa* echoes remained the same, while the success rate with *M. norvegica* echoes increased considerably (100% correct vs. 72% with the class support PMFs), likely as a result of the full-support PMFs accounting for between-class representativity. However, classification results with *A. okeni* echoes using the full-support PMFs deteriorated (68% correct vs. 100% with class-support PMFs), probably because the full-support PMFs do not provide flexibility in conditioning the impact of high between-class representativity the way the validity weightings for the ISC and PSC do.

Classification with the BPC is based on the underlying probability distribution describing how the model space of each class is represented by known data collected from that class, as well as the *a priori* probability of that class. Ideally, the true probability distribution of echo spectra for the three scattering classes of zooplankton would be used as the $\mathbf{f}^{(p)}$, but the true distribution is not known. Furthermore, although the theoretical models are able to predict realisations of individual echo spectra for a specific set of parameter values, they do not predict the probability distribution for these realisations. If a distribution was known for each of the parameters in the models, the probability distribution of the model realisations for each class could be generated from the theoretical models based on the multivariate probability distribution of the parameters. In the

absence of a true distribution, or a multivariate expression based on theoretically predicted distributions of the parameter values, the $\mathbf{f}^{(p)}$ must necessarily be constructed empirically. This empirical PMF is built using data from known class, and reflects the frequency of occurrence of each model realisation in the real data; in this way, it is similar to the validity weighting functions for the ISC and PSC. Constructing $\mathbf{f}^{(p)}$ in this manner relies on the assumption that the theoretical models, and therefore the model spaces, accurately predict the entire range of echo spectra observable for a given class, and that the available known data used to construct the probability distribution are representative and span the entire range of observable echo spectra. To the extent that these assumptions are met, the empirical PMFs are good estimators of the true probability distributions of echo spectra for the three scattering classes.

The application of model based classification techniques is only possible if there exist theoretical or empirical forward models which express the relationship between the observed data and the model parameters. For the zooplankton classification problem, theoretical model predictions were used to generate the model spaces, but empirical models may also be employed, particularly when the theoretical basis from which to construct a sound relationship between data and model is not well-characterised. In the absence of good theoretical or empirical models, feature based classification techniques provide another alternative. Feature based inversions (e.g. distance based classifiers, principal components analysis, and the EOFC (Martin *et al.* 1996)) are based only on the inherent characteristics of the observed data; they operate independently of theoretical or empirical models since they capitalise on measurable features of the data belonging to each class, exploiting class-specific differences in these features.

The model spaces are an integral component of the model based CMVC approach. The success of any model-based inversion scheme depends upon the degree to which the forward model adequately describes the relationship between the observed data and the model parameters, and whether features predicted by the model can be resolved in the data. Although the theoretical models for each scattering class ((EQ 4.13),(EQ 4.14),(EQ 4.15)) will not accurately predict all possible observed echoes, these sophisticated models describe the general scattering characteristics of zooplankton in each class sufficiently to allow discrimination between classes. A model based classification scheme that incorporates the full detail of the theoretical model predictions into the model spaces for each class can be designed, but such a design would be very complex due to the number of model parameters, and may not classify robustly, particularly in the case where the

values of many of these parameters are unknown or unmeasurable. It may in fact be desirable to design a scheme that can exploit the predictive power of the theoretical models for echo classification without being encumbered by the details in the models. In constructing the model spaces for the zooplankton scattering classes, only a small subset of the model parameters was varied, while the rest (usually those that have been empirically determined, such as β_l and (c/c_l) in (EQ 4.13), or g and h in (EQ 4.14) as measured by Foote (1990)) remained fixed. The resulting model spaces provided sufficient resolution to discriminate between the scattering classes.

Depending upon the particular classification problem, if model spaces derived from the most sophisticated theoretical models are too complex or too large, so that the classification problem becomes computationally intractable, simplified model spaces can offer a good alternative. For the zooplankton classification problem, the model spaces can be simplified by parameterising the theoretical model predictions into simpler forms; one such simplification is the parameterisation which resulted in the first-order model spaces (Section 4.4) used to illustrate $\tilde{\mathbf{W}}_R$, $\tilde{\mathbf{W}}_A$, and $\mathbf{f}^{(p)}$ algorithm development. These first-order, simplified model spaces for the three zooplankton scattering classes consist of model realisations that are very crude representations of a subset of the theoretical model predictions; they do not encompass the variability predicted in the most sophisticated model spaces. Notwithstanding, using these first-order model spaces to classify the high quality data subset yields classification results that are comparable to those achieved with the more comprehensive, sophisticated theoretical model representations (e.g. overall % correctly classified (n=75) based on maximum score criterion for ISC: 78%; PSC: 85%; BPC: 84%; as compared to Table 4-2). It becomes more advantageous to employ the sophisticated model space when classifying the entire dataset, since echoes collected in different experiments from different animals exhibit considerably greater echo variability.

Inversion for individual zooplankter characteristics based on best match model realisations was limited to animal size (mean shell radius $\bar{a}$ for **ES**, equivalent cylindrical or spherical radius a for **FL** and **GB**) with this dataset. Inversion for the other model parameters used to generate the model spaces for the three classes was not attempted, since parameters such as F_{spec} and F_l for the elastic-shelled animals (*L. retroversa*), and F_{tiss} and $\bar{\varepsilon}_j$ for the gas-bearing animals (*A. okeni*), are difficult, if not impossible, to measure. Stanton *et al.* (in press b) have in fact adjusted these parameters to match empirical data, both for single echoes and statistically. For the elastic-shelled animals, it is certain that F_{spec} and F_l depend on the orientation of the opercular opening in the

shell relative to the incoming sound wave, but this dependence remains uncharacterised. For the fluid-like animals (*M. norvegica*) however, animal shape and angle of orientation β_{tilt} during insonification can be measured using a high-magnification, underwater video camera; by marking the video footage corresponding to individual insonifications, correlations between echo spectra and animal shape, size, and orientation may be investigated. This analysis has been carried out, including an inversion of echo spectra for animal orientation, with excellent results for another species of euphausiid, the Antarctic krill, *Euphausia superba* (Martin Traykovski *et al.* submitted; see also McGehee *et al.* accepted, for the use of video techniques in the interpretation of single-frequency target strength measurements). For field-collected data, *a priori* information about animal size, shape, and probability of occurrence may be obtained via simultaneous net or pump samples, whereas video techniques such as the VPR (Video Plankton Recorder) can provide information about size, shape, probability of occurrence, and orientation.

Matching observations to individual model realisations based on the CMV metric may also prove to be a useful tool in further theoretical model development and fine-tuning. To date, forward model development, which has involved fitting theoretical model predictions to data and adjusting parameter values, has relied on judging the correspondence between the observations and the model predictions by eye (e.g. Stanton *et al.* 1993b; 1994a; 1996; in press a; etc.). Instead of assessing the goodness of fit of a particular model prediction to empirical data by visual inspection, the CMV metric provides an opportunity to quantify the fit between data and model. In addition, the CMVC techniques provide a framework within which the parameter space for a particular theoretical model may be searched exhaustively to determine the best matches to observed echo spectra. In this manner, further theoretical model development could be focused on better quantifying some of the parameter values, possibly leading to prediction of probability distributions for these parameters. In addition, more effort must be put toward empirically quantifying the measurable parameters (e.g. animal size, orientation, sound speed contrast, density contrast etc.) so that inversions may be ground-truthed.

Field implementation of the CMVC inversion techniques for broadband echoes, in conjunction with single-frequency acoustic surveys of zooplankton populations, has the potential to drastically improve estimates of animal biomass. A classification inversion of broadband echo spectra for scatterer type allows for correct apportionment of acoustic volume backscattered energy to animals in each scattering class. The material properties of animals within a scattering class are

similar, leading to a strong relationship between scattering class and animal biomass. In addition, inverting for animal size within each class could further improve the accuracy of zooplankton biomass estimates. Technological challenges that must be overcome to permit field implementation of a classification inversion based on broadband echo spectra include variable beam width and variable SNR over the bandwidth of current broadband sources suitable for field use; development of constant beam width broadband transducers is underway by others. Solving the inverse problem of identifying a scatterer from its acoustic signature in the field will enable biological oceanographers to make more reliable estimates of zooplankton type, size, and biomass from acoustic backscatter data.

4.8 Summary

The CMVC techniques rely on comparisons of observed echo spectra to theoretical-model-generated model spaces to classify broadband echoes from zooplankton into scattering classes based on similarities in covariance, mean, and variance, while accounting for ambiguity between model spaces as well as model validity (representativity). Three distinct classification algorithms (ISC, PSC and BPC) were developed, and their performance was evaluated with several hundred echoes collected in a ship-board tank from 24 different individuals on two cruises to Georges Bank and the Gulf of Maine. All three classifiers had a very high rate of success with the high-quality, high SNR subset (n=75) of the data (between 80% and 90% of echoes correctly classified based on the maximum score criterion). With the entire dataset, the PSC with both ambiguity and validity weightings yielded the best results overall (96% of *A. okeni* echoes (n = 225) and 73% of *M. norvegica* (n = 350) echoes from 1993 correctly classified). However, the BPC with class-support **TYPE I** PMF performed best for the *L. retroversa* echoes. For the PSC, classification results based on assigning an observation to the class containing the best match model realisation were better than those based on the maximum score criterion (85% of 1993 data (n = 775) and 83% of 1994 data (n = 625) correctly classified overall). Best match classifications for the ISC and BPC tended to be poorer overall than those based on the maximum class score, with the exception of *M. norvegica* echoes, which the BPC with **TYPE II** PMF classified much more accurately by the best match criterion (95% of 1993 (n = 350) and 91% of 1994 (n = 225) *M. norvegica* data correctly classified) than by the maximum score criterion. Inversions for animal size based on best match model realisation showed promise; further work is necessary to quantify the other parameter values so that size may be inverted for more robustly. Overall, the three CMVC-based

classification algorithms were able to successfully invert a good percentage of experimentally collected echoes from individual zooplankton for scattering class, particularly for the highest quality subset of data. The CMVC technique also shows promise in inverting for specific zooplankter characteristics, such as animal size, within a scattering class.

ACKNOWLEDGEMENTS

The authors are indebted to the Caswell lab, Dezhang Chu, Nancy Copley, Bob Eastwood and Andy Solow of the Woods Hole Oceanographic Institution, Mark Benfield of Louisiana State University, Baton Rouge, Louisiana, Duncan McGehee of Tracor Applied Sciences, San Diego, California, Lori Scanlon of the University of Southern California, Los Angeles, California, and the captains and crews of the "RV Oceanus" and the "RV Endeavor" for making this research possible. The research was supported by the Ocean Acoustics, Oceanic Biology and URIP programs of the Office of Naval Research grant numbers N00014-89-J-1729, N00014-95-1-0287 and N00014-92-J-1527, the Biological Oceanography program of the National Science Foundation grant number OCE-9201264 and the WHOI/MIT Joint Program Education Office. This work was completed in partial fulfillment of the requirements for a Ph.D., and LVMT would like to thank her thesis committee, including co-authors TKS, PHW and JFL, as well as Penny Chisholm of the Massachusetts Institute of Technology, for their support, encouragement and advice over the last five years. This is Woods Hole Oceanographic Institution contribution number 9597.

REFERENCES

Aki, K. and P.G. Richards. 1980. Quantitative Seismology. Theory and Methods Vol. II. Chapter 12. W.H. Freeman and Co. San Francisco.

Anderson, V.C. 1950. "Sound scattering from a fluid sphere". J. Acoust. Soc. Am., 22: 426-431.

Brown, M.G. 1984. "Linearized travel time, intensity, and waveform inversions in the ocean sound channel - A comparison". J. Acoust. Soc. Am., 75: 1451-1461.

Chiu, C.S., J.F. Lynch and O.M. Johannessen. 1987. "Tomographic resolution of mesoscale eddies in the marginal ice zone: A preliminary study". J. Geophys. Res., 92(C7): 6886-6902.

Chu, D., T.K. Stanton and P.H. Wiebe. 1992. "Frequency dependence of sound backscattering from live individual zooplankton". ICES J. Mar. Sci., 49: 97-106.

Chu, D., K.G. Foote and T.K. Stanton. 1993. "Further Analysis of target strength measurements of Antarctic krill at 38 and 120 kHz: Comparison with deformed cylinder model and inference of orientation distribution". J. Acoust. Soc. Am., 93: 2855-2988.

Demer, D.A. and Martin, L.V. 1995. "Zooplankton target strength: Volumetric or areal dependence?". J. Acoust. Soc. Am., 98: 1111-1118.

Deuser, L.M., D. Middleton, T.D. Plemons and J.K. Vaughan. 1979. "On the classification of underwater acoustic signals. II. Experimental applications involving fish". J. Acoust. Soc. Am. 65: 444-455.

Flagg, C.N. and S.L. Smith. 1989a. "On the use of the acoustic Doppler current profiler to measure zooplankton abundance". Deep-Sea Res., 36: 455-474.

Flagg, C.N. and S.L. Smith. 1989b. "Zooplankton abundance measurements from acoustic Doppler current profiling". Proceedings of Ocean '89, Mar. Tech. Soc. and I.E.E.E., Seattle, WA, September 18-21, 1989.

Foote, K.G. 1990. "Speed of sound in *Euphausia superba*". J. Acoust. Soc. Am., 87: 1405-1408.

Foote, K.G., I. Everson, J.L. Watkins and D.G. Bone. 1990. "Target strengths of Antarctic krill (*Euphausia superba*) at 38 kHz and 120 kHz". J. Acoust. Soc. Am., 87: 16-24.

Greenlaw, C.F. 1977. "Backscattering spectra of preserved zooplankton". J. Acoust. Soc. Am., 62: 44-52.

Greenlaw, C.F. 1979. "Acoustical estimation of zooplankton populations". Limnol. Oceanogr., 24: 226-242.

Goodman, L., J. Oeschger and D. Szargowicz. 1992. "Ocean acoustics turbulence study: acoustic scattering from a buoyant axisymmetric plume". J. Acoust. Soc. Am., 91: 3212-3227.

Hewitt, R.P. and D.A. Demer. 1991. "Krill Abundance". Nature, 353: 310.

Hewitt, R.P. and D.A. Demer. 1996. "Lateral target strength of Antarctic krill". ICES Journal of Marine Science, 53: 297-302.

Holliday, D.V. 1977. "Extracting bio-physical information from the acoustic signatures of marine organisms" In N.R. Andersen and B.L. Zahuranec (eds.) Oceanic Sound Scattering Prediction. Plenum Press, N.Y.

Holliday, D.V. 1980. "Use of acoustic frequency diversity for marine biological measurements". Pp. 423-460 in F.P. Diemer, F.J. Vernberg and D.Z. Mirkes (eds.) Advanced Concepts in Ocean Measurements for Marine Biology. Belle W. Baruch Library in Marine Science #10, University of South Carolina Press, Columbia, S.C.

Holliday, D.V., R.E. Pieper and G.S. Kleppel. 1989. "Determination of zooplankton size and distribution with multifrequency acoustic technology". J. Cons. int. Explor. Mer, 46: 52-61.

Johnson, R.K. 1977. "Sound scattering from a fluid sphere revisited". J. Acoust. Soc. Am., 61: 375-377.

Kargl, S.G. and P.L. Marston. 1989. "Observations and modeling of the backscattering of short tone bursts from a spherical shell: Lamb wave echoes, glory, and axial reverberations". J. Acoust. Soc. Am., 85: 1014-1028.

Kristensen, A. and J. Dalen. 1986. "Acoustic estimation of size distribution and abundance of zooplankton". J. Acoust. Soc. Am., 80: 601-611.

Love, R.H. 1977. "Target strength of an individual fish at any aspect". J. Acoust. Soc. Am., 62: 1397-1403.

Lynch, J.F., S.D. Rajan and G.V. Frisk. 1991. "A comparison of broadband and narrow-band modal inversions for bottom geoacoustic properties at a site near Corpus Christi, Texas". J. Acoust. Soc. Am. 89: 648-665.

Marston, P.L. 1988. "GTD for backscattering from elastic spheres and cylinders in water and the coupling of surface elastic waves with the acoustic field". J. Acoust. Soc. Am., 83: 25-37.

Marston, P.L., S.G. Kargl., and K.L. Williams. 1990. "Rayleigh, Lamb, and Whispering Gallery wave contributions to backscattering from smooth elastic objects in water described by a generalization of GTD". Pp. 211-216 in S.K. Datta, J.D. Achenback, and Y.S. Rajapakse (eds.) Elastic Wave Propagation and Ultrasonic Nondestructive Evaluation. Elsevier, Amsterdam.

Martin, L.V., T.K. Stanton, P.H. Wiebe, and J.F. Lynch. 1996. "Acoustic classification of zooplankton". ICES Journal of Marine Science, 53: 217-224.

Martin Traykovski, L.V., R.L. O'Driscoll, and D.E. McGehee. submitted. "Effects of orientation on broadband acoustic scattering of Antarctic krill (*Euphausia superba*): implications for inverting zooplankton spectral acoustic signatures for angle of orientation". Limnol. Oceanogr.

McGehee, D.E., R.L. O'Driscoll, and L.V. Martin Traykovski. accepted. "Effects of orientation on acoustic scattering from Antarctic Krill". Deep-Sea Res.

Morse, P.M. and K.U. Ingard. 1968. Theoretical Acoustics. Princeton University Press, Princeton, N.J. 927 p.

Munk, W. and C. Wunsch. 1979. "Ocean acoustic tomography: a scheme for large scale monitoring". Deep-Sea Res., 26: 123-161.

Papoulis, A. 1991. Probability, Random Variables, and Stochastic Processes. Third Edition, McGraw-Hill, Inc., New York. 666 p.

Penrose, J.D. and G.T. Kaye. 1979. "Acoustic target strengths of marine organisms". J. Acoust. Soc. Am., 65: 374-380.

Pieper, R.E., D.V. Holliday and G.S. Kleppel. 1990. "Quantitative zooplankton distributions from multifrequency acoustics". J. Plankton Res., 12: 433-441.

Rajan, S.D., J.F. Lynch and G.V. Frisk. 1987. "Perturbative inversion methods for obtaining bottom geoacoustic parameters in shallow water". J. Acoust. Soc. Am., 82: 998-1017.

Simmonds, E.J., F. Armstrong and P.J. Copeland. 1996. "Species identification using wideband backscatter with neural network and discriminant analysis". ICES J. Mar. Sci., 53: 189-195.

Stanton, T.K. 1988a. "Sound scattering by cylinders of finite length. I. Fluid cylinders". J. Acoust. Soc. Am., 83: 55-63.

Stanton, T.K. 1988b. "Sound scattering by cylinders of finite length. II. Elastic cylinders". J. Acoust. Soc. Am., 83: 64-67.

Stanton, T.K. 1989a. "Sound scattering by cylinders of finite length. III. Deformed cylinders". J. Acoust. Soc. Am., 86: 671-705.

Stanton, T.K. 1989b. "Simple approximate formulas for backscattering of sound by spherical and elongated objects". J. Acoust. Soc. Am., 86: 1499-1510.

Stanton, T.K. 1990a. "Sound scattering by zooplankton". Rapp. P.-v. Reun. Cons. int. Explor. Mer, 189: 353-362.

Stanton, T.K. 1990b. "Sound scattering by spherical and elongated shelled bodies". J. Acoust. Soc. Am., 88: 1619-1633.

Stanton, T.K., R. D. M. Nash, R.L. Eastwood, and R.W. Nero. 1987. "A field examination of acoustical scattering from marine organisms at 70 kHz". IEEE Journal of Oceanic Engineering, OE-12(2): 339-348.

Stanton, T.K., C.S. Clay, and D. Chu. 1993a. "Ray representation of sound scattering by weakly scattering deformed fluid cylinders: Simple physics and application to zooplankton". J. Acoust. Soc. Am., 94: 3454-3462.

Stanton, T.K., D. Chu, P.H. Wiebe and C.S. Clay. 1993b. "Average echoes from randomly oriented random-length finite cylinders: Zooplankton models". J. Acoust. Soc. Am., 94: 3463-3472.

Stanton, T.K., P.H. Wiebe, D. Chu, M.C. Benfield, L. Scanlon, L.V. Martin and R.L. Eastwood. 1994a. "On acoustic estimates of biomass". ICES J. Mar. Sci., 51: 505-512.

Stanton, T.K., P.H. Wiebe, D. Chu, and L. Goodman. 1994b. "Acoustic characterization and discrimination of marine zooplankton and turbulence". ICES J. Mar. Sci., 51: 469-479.

Stanton, T.K., D. Chu and P.H. Wiebe. 1996. "Acoustic scattering characteristics of several zooplankton groups." ICES J. Mar. Sci., 53: 289-295.

Stanton, T.K., D. Chu, P.H. Wiebe, L.V. Martin and R.L Eastwood. in press a. "Sound scattering by several zooplankton groups I: Experimental determination of dominant scattering mechanisms". J. Acoust. Soc. Am.

Stanton, T.K., D. Chu, and P.H. Wiebe. in press b. "Sound scattering by several zooplankton groups II: Scattering models". J. Acoust. Soc. Am.

Vray, D., G. Gimenez and R. Person. 1990. "Attempt at classification of echo-sounder signals based on the linear discriminant function of Fisher". Rapp. P.-v. Reun. Cons. int. Explor. Mer., 189: 388-393.

Wiebe, P.H., C.H. Greene, T.K. Stanton, J. Burczynski. 1990. "Sound scattering by live zooplankton and micronekton: Empirical studies with a dual-beam acoustical system". J. Acoust. Soc. Am. 88(5): 2346-2360.

Wiebe, P.H., D. Mountain, T.K. Stanton, C.H. Greene, G. Lough, S. Kaartvedt, J. Dawson and N. Copley. 1996. "Acoustical study of the spatial distribution of plankton on Georges Bank and the relationship between volume backscattering strength and the taxonomic composition of the plankton". Deep-Sea Res. II, 43:1971-2001

Zakharia, M. and J.P. Sessarego. 1982. "Sonar target classification using a coherent echo processing". Proc. IEEE International Conference on Acoustics, Speech and Signal Processing, Paris, France.

CHAPTER 5

EFFECT OF ANIMAL ORIENTATION ON SPECTRAL SIGNATURES

Changes in animal orientation can impact the frequency response of the acoustic returns from zooplankton in all three scattering classes. Understanding of the variability in acoustic signatures resulting from differences in the angle of orientation of the animal relative to the incident acoustic wave will improve classification success. Measurements of artificially constrained zooplankton as well as *in situ* measurements have shown that the target strength of many zooplankton varies with animal orientation. A better understanding of this orientational dependence, coupled with a means by which to invert for animal orientation based on acoustic returns, could improve acoustic survey-based biomass estimates of zooplankton significantly.

This chapter is an investigation of the impact of animal orientation on the echo spectra received from broadband insonifications of zooplankton. To better understand natural animal orientation during feeding, swimming, and resting, the first section of this chapter (Section 5.1) presents a brief summary of a preliminary investigation into the *in situ* orientation of those species of zooplankton collected in the N.W. Atlantic for which acoustic scattering experiments have been conducted. This sort of understanding is necessary to apply the results of an orientational analysis to the interpretation of *in situ* acoustic survey data. Following this, the theoretical basis for variability in echo spectra due to differences in both animal size and orientation is summarised (Section 5.2). The bulk of the chapter, which is written as a manuscript (Section 5.3), is devoted to a detailed exploration of the effects of animal orientation on acoustic signature based on experimentally collected data from representatives of the fluid-like scattering class (Antarctic krill). To determine the impact of changes in orientation on the spectral structure of echoes received from the krill, video data of each animal (acquired simultaneously with the acoustic returns) were analysed in conjunction with the acoustic data. Angle of orientation of the animal at the time of insonification was compared on a ping-by-ping basis with the frequency spectrum of the corresponding acoustic return. Acoustic returns received from the krill were then compared to the spectra predicted by the distorted wave Born approximation theoretical model for the angle of orientation, size, and shape as measured for each animal. Finally, the Covariance Mean Variance Classification algorithms were employed to invert the observed echo spectra for angle of orientation, and a comparison of experimentally-observed and classifier-predicted orientations was made, with implications for application of the CMVC to *in situ* inversions for animal orientation.

5.1 INVESTIGATION OF *IN SITU* ORIENTATION

A preliminary investigation of the *in situ* orientation of representatives of each of the three zooplankton scattering classes is summarised here. Sources of data include the literature, as well as photographs and video footage from SCUBA divers, a submersible, and the Video Plankton Recorder. All video references (in quotes) are listed at the end of the Reference section (p. 185).

5.1.1 *Agalma okeni*

Physonect siphonophores possess a gas-filled float called a pneumatophore, which acts as an indicator of which direction is up, and may help to keep the animal nearly erect in the water (Fraenkel and Gunn 1940). Video footage of *A. okeni* reveals that this species can rest passively with tentacles retracted, floating about in the water column, the stem orientation drifting through about 180° (centered on vertical with the pneumatophore up) with equal time spent in all orientations ("Blue Water"). When this siphonophore is feeding however, the tentacles are extended (Purcell and Mills 1989) and it hangs motionless in the water column, the body held horizontally or at an angle with the gas float above it and the tentacles hanging down in a curtain (Madin 1988). In *A. okeni*, the pneumatophore is not big enough to constrain the orientation of the animal to vertical (Biggs 1977), so that it may hang at any angle, from vertical to nearly horizontal, surrounded by a haze of tentacles (Mackie and Boag 1963). *In situ* observations indicate that this species is usually inclined 15° - 40° from the vertical (Biggs 1977), thereby allowing it to extend its tentacles without tangling them (Figure 5-1). Video footage of *A. okeni* feeding indicate that it can also fish with the stem coiled up loosely ("Ocean Drifters").

5.1.2 *Meganyctiphanes norvegica*

Meganyctiphanes norvegica is an active, rapid swimmer. While swimming, the telson is usually flexed slightly downwards (ventrally), but may be straightened during quick movements (Macdonald 1927). *M. norvegica* undergoes diel vertical migrations, and is found below 100m during the day, where it is passive and lethargic (Mauchline and Fisher 1980). It has been found to feed only in the upper 100 m of water in the evening and at night (Lasker 1966), except in winter when the adults have been seen feeding most actively during the day (Mauchline and Fisher 1980). Upward swimming when rising to the surface is gyratory, and *M. norvegica* often makes several complete "somersaults" in rapid succession (Macdonald 1927). Video footage shows swarms of this euphausiid darting about rapidly, with the majority of individuals oriented head up and within ~20° of vertical, alternating between swimming in straight lines and spiralling, although some

Figure 5-1 *Agalma okeni* in typical fishing posture. Image captured from video footage ("Ocean Drifters").

individuals are oriented nearly horizontally ("Johnson Sea-Link 1987"). Video recordings made from a submersible with lights on demonstrate what may be a phototactic reaction; swarms of *M. norvegica* gather near the lights, swimming in spirals in all directions, but predominantly upward toward the sea surface ("Johnson Sea-Link CNN"). Analysis of images captured from this video footage revealed that most individuals appear to be oriented nearly vertically, head up as if swimming for the surface (Figure 5-2).

Photo camera observations have been made of free-swimming euphausiids *in situ* (Kristensen and Dalen 1986) to determine tilt angle (defined as the angle between the horizontal and a line drawn through the eyes and the longitudinal direction of the carapace). Two photos taken within 5 minutes of each other at 40 m depth at 0200 h contained 192 euphausiids whose mean angle of orientation was -9.8° (std. dev. 34.1°). Analysis of all their photos revealed that the mean tilt angle is slightly positive at night and slightly negative during the day, with standard deviations between 25° and 45°, and seems to be correlated with upward and downward diel vertical migration respectively. Although they do not describe their camera system in detail, it is likely that they used lights to capture images of euphausiids at night at 40 m depth. A limited number of video images recorded with visible red light (alleged not to illicit a phototactic response in euphausiids) show individual *M. norvegica* swimming by the camera in a variety of orientations, but almost always curled up with the telson tucked up toward the ventral surface of the animal ("VPR").

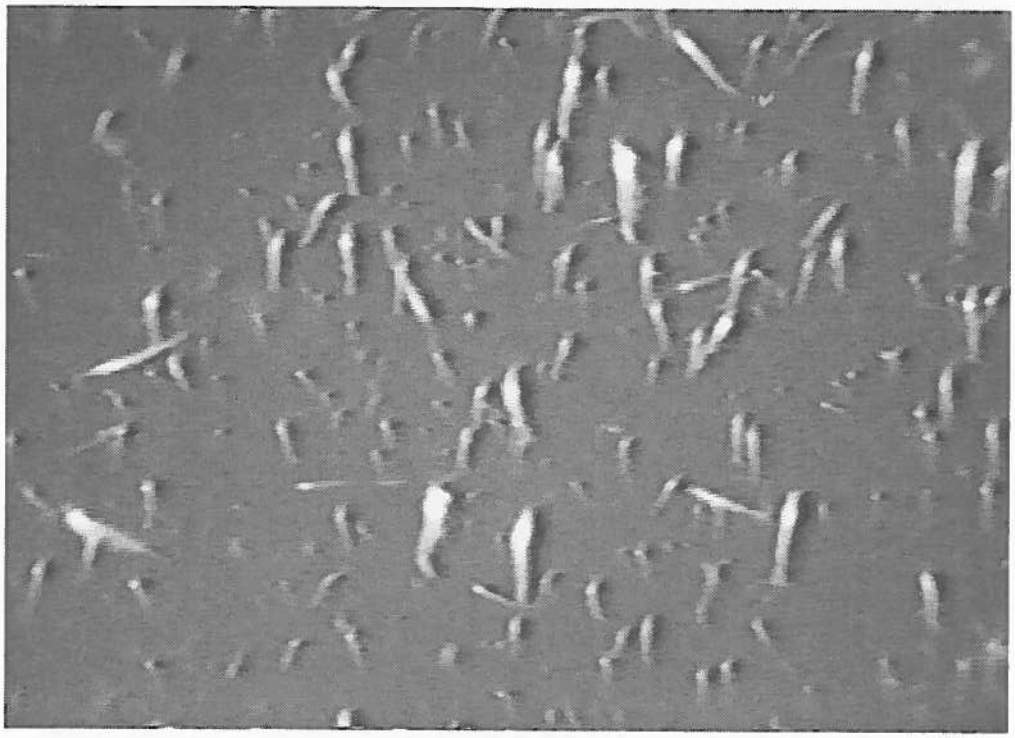

Figure 5-2 *Meganyctiphanes norvegica* filmed at night from a submersible with lights on ("Johnson Sea-Link CNN"). It is not known if this orientation is typical for upward swimming euphausiids.

5.1.3 *Limacina retroversa*

Swimming in *L. retroversa* is accomplished with the opercular opening pointing up and the wings exposed above the shell (Morton 1954). The wings flap in unison like oars, and the sharp, downward effector stroke propels the animal upward in a broadly spiral path (Morton 1964). The animal floats by extending its wings laterally, but sinks quickly if the wings are pulled together and held erect above the shell (Morton 1964). Fig. I of Morton (1954), reproduced here (Figure 5-3), shows the orientation of *L. retroversa* while swimming and sinking. Silhouette video photography ("VPR") has recorded several images of *L. retroversa* in natural orientations. Direct measurements from several frames of "VPR" footage indicate that for the most part, this species is oriented with the long axis of the shell at 45° (± 20°) from the horizontal, with the wings up (Figure 5-4). *L. retroversa* maintains neutral buoyancy while feeding, probably as a result of the large, spherical mucous web it deploys (Gilmer and Harbison 1986). When feeding, these pteropods must stop swimming; the wings remain expanded, but are motionless, and the ventral surface (including the opercular opening) faces upward (Gilmer and Harbison 1986), while the bulbous dorsal surface of the shell faces down. The long axis of the shell (from the end of the opercular opening to the spiral tip) appears to be inclined less than 45° to the horizontal, with the spiral tip at the lowest point.

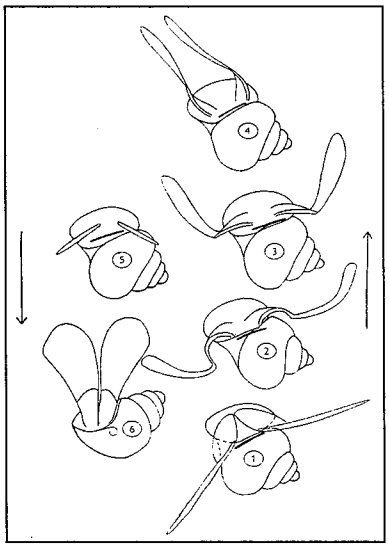

Figure 5-3 Sketches of *Limacina retroversa* showing typical the orientations while swimming upward (1-4) and sinking (5-top view, 6-side view). Reproduced from Fig. I of Morton (1954)

Figure 5-4 Image of *Limacina retroversa* captured with the Video Plankton Recorder; the long axis of the shell is oriented 45° from the horizontal.

A solid understanding of the natural orientations assumed by these zooplankton is necessary in order to improve biomass estimates made from acoustic survey data. A comprehensive knowledge-base of *in situ* animal orientation will assist in placing bounds on the values of some theoretical model parameters, as well as providing context for the data sets gathered from tethered animals. Information on the natural orientations of these zooplankton will help to constrain the classification inverse to include only reasonable animal orientations, thereby improving classification success.

5.2 LINK BETWEEN ANIMAL ORIENTATION AND SPECTRAL VARIABILITY

Different null spacings in the spectra of acoustic returns from fluid-like or elastic-shelled zooplankton arise as a result of different animal sizes and possibly orientations. There exists an inverse relationship between animal size and null spacing. To demonstrate this, consider a hard elastic-shelled animal with circular cross-section insonified at high frequency ($\lambda << a$). Scattering from this animal may be modelled using a two-ray formulation which accounts for the echo from the front interface of the animal as well as the echo resulting from energy shed by a circumferential wave travelling around the shell (Stanton *et al.* in press b). A null in the echo spectrum results when there is destructive interference, that is, when the phase difference $\phi_{d/c}$ between the ray scattered directly from the front interface of the animal (p_d) and the ray scattered from the circumferential wave (p_c) is π radians (Figure 5-5).

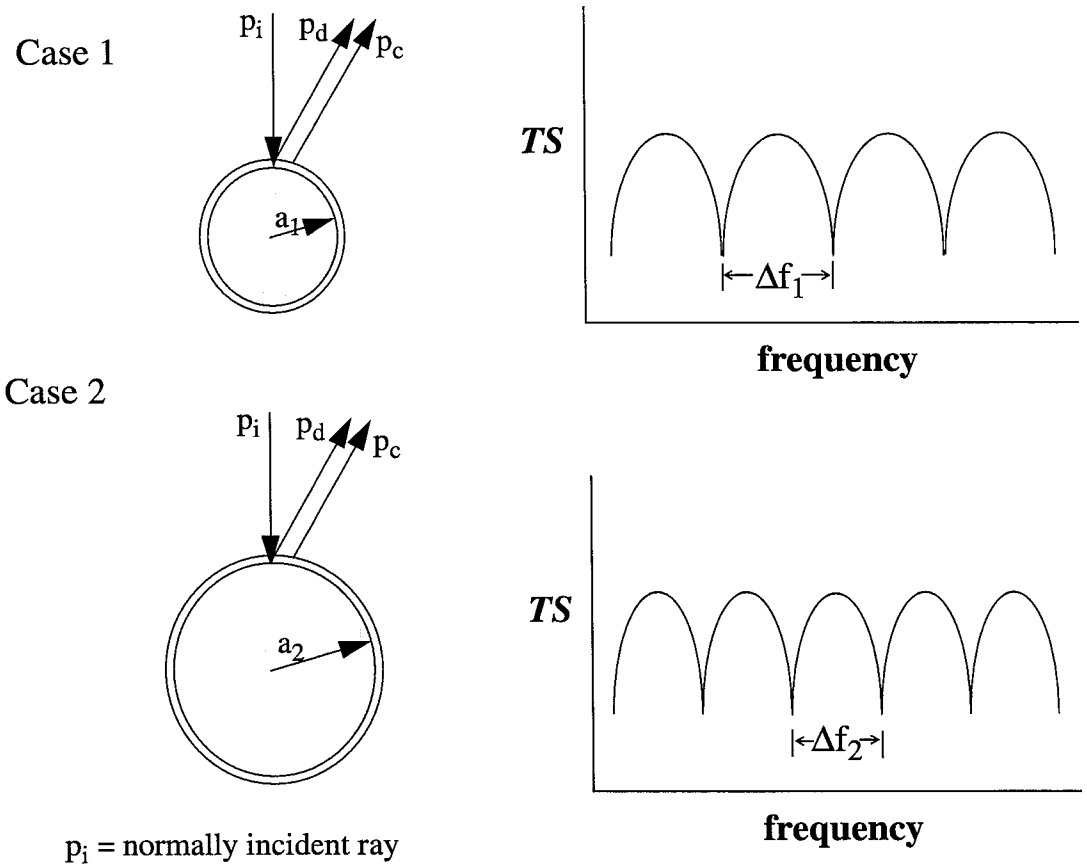

p_i = normally incident ray
p_d = ray scattered directly from the front interface (in the receiver direction)
p_c = ray scattered from the circumferential wave (in the receiver direction)

Figure 5-5 Schematic of an elastic-shelled animal insonified at high frequency ($\lambda >> a$), comparing spectra scattered from a small animal of radius a_1 (Case 1) vs. a larger animal of radius $a_2 > a_1$ (Case 2).

Setting the phase difference equal to π for the 2 cases yields: $\phi_{d/c} = \pi = k(2\pi a_1)\Delta f_1 = k(2\pi a_2)\Delta f_2$, where $2\pi a_n$ is the distance the circumferential ray travels around a body of radius a_n. This reduces to the relation $a_1\Delta f_1 = a_2\Delta f_2$, so that the echo spectra of bigger animals exhibit tighter null spacing.

For elongated animals, *apparent* size (relative to the acoustic wave) changes with the orientation of the animal relative to the incident acoustic beam. As a result, it is difficult to invert for scatterer size unless animal orientation is known *a priori*. To demonstrate this, consider a deformed cylindrical fluid-like animal insonified at high frequency ($\lambda << a$). Scattering from this animal may be modelled using a two-ray scattering model (Stanton *et al.* 1993a,b), which accounts for echoes reflected from the front and back interfaces of a weakly scattering target. Similar to the case of the elastic-shelled animal, a null in the echo spectrum results from destructive interference between the ray scattered from the front interface of the animal (p_f) and the ray scattered from the back interface (p_b), that is, when the phase difference $\varphi_{f/b}$ between these rays is π radians (Figure 5-6).

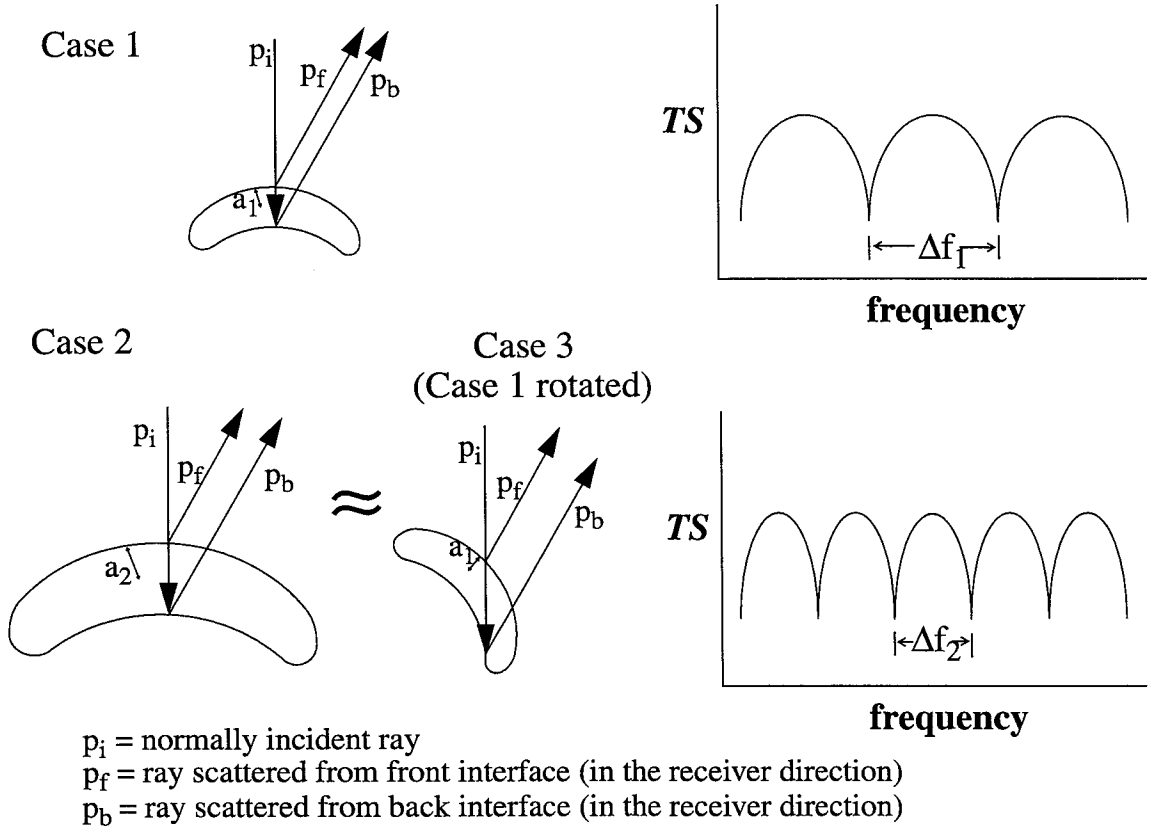

Figure 5-6 Comparison of echo spectra received from a deformed cylindrical fluid-like animal insonified at high frequency ($\lambda >> a$) for a small animal (radius a_1) at broadside incidence (Case 1) and off-broadside (Case 3), and a larger animal (radius $a_2 > a_1$) at broadside incidence (Case 2).

Equating $\phi_{f/b}$ for the 3 cases yields: $\phi_{f/b} = \pi = (2\pi\Delta f_1/c)d_1 = (2\pi\Delta f_2/c)d_2 = (2\pi\Delta f_3/c)d_3$, where d_n is the total distance the ray travels in the body in each case (n = 1, 2, 3) and c is the speed of sound in the body. When the body is at broadside incidence (Cases 1 and 2), $d_n \approx 4a_n$ where a_n is the equivalent cylindrical radius. Off-broadside (Case 3), the size of the rotated animal is a_1 but its *apparent* size (to the acoustic ray) is $>> a_1$, so that $d_3 \neq d_1$. Here $d_3 \approx d_2$ so that the null spacing of the echo spectra for Cases 2 and 3 are the same (i.e. $\Delta f_3 \approx \Delta f_2$).

Changes in spectral signature with changes in animal orientation have important implications for the classification inversion of zooplankton from broadband acoustic returns. If the impact of orientation on the echo spectra is well-characterised, it is possible to invert for orientation based on spectral signature. Combining orientation information derived from broadband acoustic data with data collected in single-frequency acoustic surveys has the potential to improve zooplankton biomass estimates considerably. A better understanding of orientational impacts on the acoustic returns can be gained via a combination of experimental and theoretical approaches. A powerful experimental approach involves combining acoustic data with high-magnification video footage which records the movement and orientation of the animal during insonification.

Such a video system was implemented in the ship-board tank experiments carried out during the Endeavor cruise 253 (18 September - 29 September 1994) to Georges Bank and the Gulf of Maine. Video footage was acquired for zooplankton representing all three scattering classes. A qualitative look at the correlation between the orientational video data and the acoustic data for a fluid-like animal (*Meganyctiphanes norvegica*) revealed that both the time series and the echo spectrum change significantly with changes in angle of orientation relative to the incident acoustic wave (Figure 5-7). Comparison of the time series reveals that the echo energy of returns received when the animal is at or near broadside incidence (i.e. when the long axis of the animal body is perpendicular to the incident acoustic wave) is generally considerably greater than the energy contained in off-broadside echoes. This observation is consistent with what is expected based on the physics of scattering from elongated objects, since at broadside incidence, an elongated animal presents a much larger backscattering cross-section to the incident acoustic wave than at any other angle of orientation. In addition, the echo spectrum at broadside incidence exhibits a wider null-spacing compared to the more erratic structure of the off-broadside echo spectrum. This qualitative analysis lead to a quantitative study of the effect of animal orientation on the echo spectra of fluid-like zooplankton, the details of which are presented in the following manuscript.

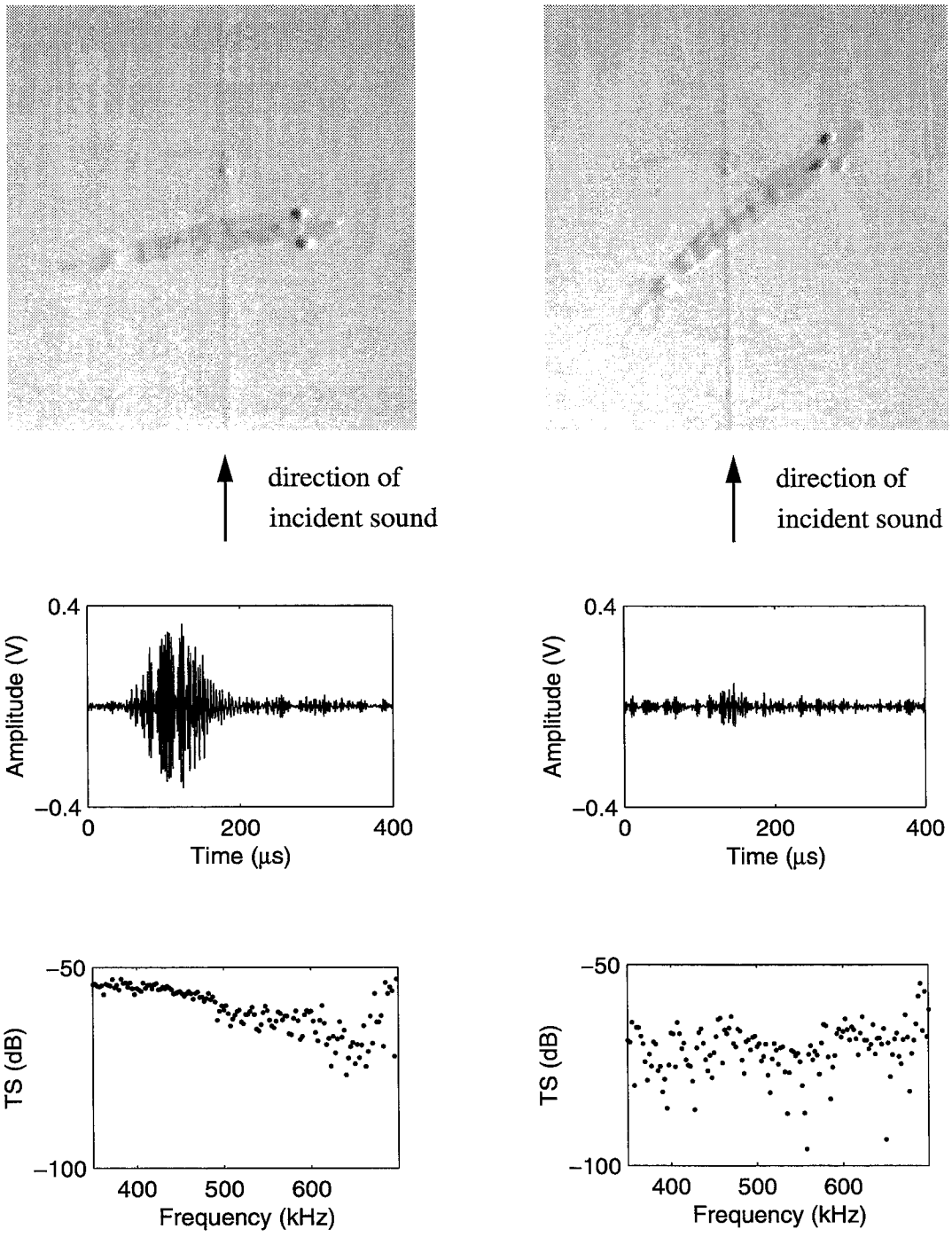

Figure 5-7 Video images of an elongated fluid-like zooplankter (30.5 mm long *Meganyctiphanes norvegica*) insonified at two different angles of orientation. Orientation significantly affects both the strength of the acoustic return (time series, top) and the shape of the frequency response (bottom).

5.3 EFFECT OF ORIENTATION ON ECHO SPECTRA OF FLUID-LIKE ANIMALS

Effect of orientation on broadband acoustic scattering of Antarctic krill *Euphausia superba*: Implications for inverting zooplankton spectral acoustic signatures for angle of orientation

Linda V. Martin Traykovski, Richard L. O'Driscoll, and Duncan E. McGehee.

ABSTRACT

Biomass estimates of Antarctic krill (*Euphausia superba*) stocks in the Southern Ocean are often based on high-frequency acoustic survey data. In order to make accurate estimates of zooplankton biomass from acoustic backscatter measurements, the acoustic characteristics of the species of interest must be well-understood. In particular, it has long been recognised that the target strength of elongated, fluid-like zooplankton such as *E. superba* varies with animal orientation. Acoustic scattering experiments were performed to elucidate the effect of animal orientation on the broadband scattering characteristics of Antarctic krill. During the experiments, several individual, live krill were tethered and suspended in a tank filled with filtered, chilled seawater. Several thousand echoes were collected from fourteen animals during insonification with a broadband chirp of center frequency 500 kHz (~350 kHz - 750 kHz), while their behaviour was simultaneously captured on video tape. A novel video analysis technique was applied to images for 11 of the animals to extract the angle of orientation of the krill corresponding to each insonification. This analysis revealed that echo spectra from krill near broadside incidence relative to the incident acoustic wave were characterised by widely-spaced (~200 kHz) deep nulls, whereas off-broadside echo spectra exhibited a more erratic structure, with several closely spaced (< 50 kHz) nulls of variable depth. Spectrally-averaged echo levels were found to be about 5 dB higher near broadside incidence as compared to off-broadside. The acoustic returns collected from the krill were compared to theoretical predictions for all angles of orientation based on a distorted wave Born approximation (DWBA) model for each animal. The pattern of changes in echo spectra with orientation is very similar for the experimentally measured data and the DWBA model predicted spectra for all 11 krill; however, the theoretical model predicts a much greater drop in *TS* (about 20 dB) as orientation changes from broadside incidence to off-broadside than was actually observed for these animals as they changed orientation (about a 5 dB drop going from broadside incidence to off-broadside). Information contained in the broadband echo spectra of the krill was used to

invert the acoustic returns for angle of orientation by applying a newly-developed Covariance Mean Variance Classification (CMVC) approach, using generic and animal-specific theoretical and empirical model spaces. The animal-specific empirical model space (based on data collected from the appropriate animal) was best able to invert for angle of orientation. Employing a generic empirical model space (based on data collected from an arbitrary krill) resulted in more accurate inversions overall than could be achieved using the appropriate animal-specific theoretical model space. By deploying a broadband sonar system in conjunction with single-frequency acoustic surveys of Antarctic krill, and implementing a classification inversion such as the CMVC technique with a generic empirical model space, it is possible to determine the angle of orientation of individual krill in the field. Extraction of this orientational information has the potential to improve the accuracy of krill biomass estimates significantly.

L.V. Martin Traykovski: Massachusetts Institute of Technology / Woods Hole Oceanographic Institution, Joint Program in Oceanography and Applied Ocean Sciences and Engineering; present address: Woods Hole Oceanographic Institution, MS 34, Woods Hole, MA 02543 USA. R.L. O'Driscoll: Department of Marine Science, University of Otago, P.O. Box 56, Dunedin, New Zealand. D.E. McGehee: Department of Applied Ocean Physics and Engineering, Woods Hole Oceanographic Institution, Woods Hole, MA 02543; present address: Tracor Applied Sciences, 4669 Murphy Canyon Road, Suite 102, San Diego, CA 92123 USA. Correspondence to Martin Traykovski [email: lmartin@whoi.edu, phone (508) 289-2750, fax (508) 457-2134].

5.3.1 Introduction

Marine zooplankton are of central importance to the ecology of the oceanic region in which they live, serving as a principal food source for the larval and adult stages of commercially important fish species (Turner 1984), and in the case of Antarctic krill, providing a direct trophic link between the primary producers and the top predators (seabirds, whales, seals) of the Southern Ocean (El-Sayed 1988; Nemoto *et al.* 1988; Permitin 1970). In addition, a commercially important krill fishery became established about twenty years ago, peaking in the early 1980s with landings of over 500,000 metric tons (Nicol and de la Mare 1993). Because *Euphausia superba* plays such a central ecological role in the Antarctic marine food web, affecting the breeding success of the top predators that rely on it as a food source (Croxall *et al.* 1988), it has become increasingly important to assess and manage the impact of the fishery on krill stocks. Consequently, accurate knowledge of krill distribution, abundance (biomass), and production is necessary in order to characterise the trophic interactions in the Southern Ocean food web, as well as to successfully manage krill stocks as a resource.

Conventional methods for estimating zooplankton biomass include measurement of displacement volume (Yentsch and Hebard 1957 cited in Wiebe *et al.* 1975), wet weight (Nakai and Honjo 1962 cited in Wiebe *et al.* 1975), dry weight (Lovegrove 1966 cited in Wiebe *et al.* 1975) or carbon (Curl 1962 cited in Wiebe *et al.* 1975) from net (e.g. MOCNESS - Wiebe *et al.* 1985) or pump (Miller and Judkins 1981) samples. As a result of the spatial patchiness of zooplankton populations in the ocean and extreme temporal variability in their abundance, it is estimated that biomass can vary over seven orders of magnitude on the spatial and temporal scales important for populations of macrozooplankton (Huntley and Lopez 1992). For example, Antarctic krill are distributed over a vast area of ocean, aggregating in patches, shoals, schools, swarms, and superswarms, which can cover many square km, extend to 200 m depth, and display complex, small-scale, horizontal and vertical structure (Nicol and de la Mare 1993). Conventional techniques for biomass estimation (nets, pumps, trawls) are not suited for simultaneous sampling of the entire water column over the relevant scales, nor to resolving ecologically important small-scale patterns of krill distribution. To make more accurate biomass estimates, high resolution (~1 m) instruments capable of mapping variation in zooplankton biomass on large vertical (10 - 100 m), horizontal (1 - 10 km), and temporal (days to months) scales are required. The use of high-frequency acoustics to make volume backscatter measurements of the water column has recently made it possible to do rapid, high-resolution, broad-scale synoptic surveys of krill abundance over the time and space scales of interest.

Traditional acoustic biomass estimation methods have employed single-frequency acoustic measures in conjunction with either theoretical models (e.g. Greenlaw 1979) or empirical regression relationships between acoustic backscatter and biomass collected in simultaneous net samples (e.g. Flagg and Smith 1989). Attempts to use volume backscatter measurements of the ocean as indicators of zooplankton type, size and biomass rely on the accurate acoustic characterisation of the zooplankton species of interest. Biomass estimates based on simple regression curves or on single-frequency echo energy measurements may be subject to large errors, particularly if important factors such as species-specific material properties, morphology and animal orientation are overlooked. Much effort has been put toward characterising the acoustic target strength of krill for the purposes of species identification, animal size classification, abundance estimation, and acoustic signal separation. Single-frequency target strength measurements have been made of krill and other elongated crustacean zooplankton (other euphausiids, shrimp), both experimentally constrained (by tethering or encagement, e.g. Greenlaw

representing predictions of the models for particular parameter values spanning the entire parameter space. For the *E. superba* data, the objective of this classification is to invert observed echo spectra for a specific parameter value: angle of orientation. The CMVC techniques can be implemented in several alternative configurations, one of which may be employed to search the entire physical model parameter space for the best-match model realisations for a set of observations, and report the parameter values of interest. Determination of the best match is based on the CMV metric (**C**), which quantifies the correspondence between an ensemble of observed echo spectra (**D**) and all the model realisations (**M**) based on their covariance (**K**, which compares their spectral structure), weighted by the similarity of mean echo levels (**X**) and the variance similarity (**U**), so that:

$$\mathbf{C} = CMV(\mathbf{M}, \mathbf{D}) = \mathbf{K} \cdot \mathbf{X} \cdot \mathbf{U} \qquad \textbf{(EQ 5.5)}$$

Note that in (EQ 5.5), $\mathbf{C}_{ij} = \left(\sum_{k=1}^{n_p} \mathbf{D}_{ik}^{\mathrm{T}} \mathbf{M}_{kj} \right) \cdot \mathbf{X}_{ij} \cdot \mathbf{U}_{ij}$, since $\mathbf{K} = \mathbf{D}^{\mathrm{T}}\mathbf{M}$ is the covariance ($0 \le \mathbf{K}_{ij} \le 1$) between the observed data matrix **D** and the model space matrix **M**. Each column of **D** contains a mean-subtracted, energy-normalised observed echo spectrum, whereas each column of **M** contains a mean-subtracted, energy-normalised model realisation. **X** and **U** are the mean and variance similarity matrices ($0 \le \mathbf{X}_{ij}, \mathbf{U}_{ij} \le 1$, where $\mathbf{X}_{ij} = 1$ indicates that the *i*th observation and the *j*th model realisation have the same mean echo levels, and $\mathbf{U}_{ij} = 1$ indicates that the *i*th observation and the *j*th model realisation have identical variance), n_p is the number of points in each echo spectrum, and "$\cdot$" indicates element-wise multiplication of matrices. The best-match model realisation for the *i*th observed echo spectrum is found by determining the column m in which the maximum value in row i of **C** occurs, for example, for the first observation, $i = 1$ and the best-match m is the realisation for which $\mathbf{C}_{1m} = max(\mathbf{C}_{1j})$ over all j. The inversion result for observation i is then the angle of orientation associated with the model realisation m that best predicts that observation.

The ability of the classifier to invert echo spectra for angle of orientation depends to a large extent upon the representativity of the model space, that is, whether it accurately predicts the scattering over the entire observed range of the parameter values with sufficient resolution. In this inversion of krill echo spectra for angle of orientation, two theoretical model spaces and two empirical model spaces were employed. The theoretical model spaces include a size-constrained generic model space for all animals, and 11 animal-specific model spaces, one for each animal; both types consist of model realisations generated from predictions of the DWBA model (EQ 5.4). For the generic model space, five distinct discretisations of the animal body, representing five different

1977; Kristensen and Dalen 1986; Everson *et al.* 1990; Foote 1990; Foote *et al.* 1990; Wiebe *et al.* 1990; Demer and Martin 1995) and *in situ* (e.g. Hewitt and Demer 1991; Hewitt and Demer 1996). To obtain target strength information over a wide range of frequencies simultaneously, as well as to elucidate the frequency dependence of the scattering from elongated crustacean zooplankton, broadband insonifications have been made of tethered decapod shrimp (*Palaemonetes vulgaris*) as well as a species of euphausiid (*Meganyctiphanes norvegica*) found in the Northwest Atlantic (Chu *et al.* 1992; Stanton *et al.* 1994a; 1996) using a broadband chirp sonar. These single-frequency and broadband measurements have been used to develop and corroborate empirical and theoretical scattering models.

Empirical models (e.g. Greene *et al.* 1991) have relied on relating a single parameter (e.g. zooplankton size or wet weight) to acoustic target strength through a simple regression relationship. Initial theoretical scattering models for zooplankton (including elongated crustacean zooplankton) were based on the Anderson (1950) fluid sphere model (e.g. Greenlaw 1977,1979; Johnson 1977; Penrose and Kaye 1979), which accounted for animal size and material properties. The first scattering model to consider the elongate and deformable morphology of some of the crustacean zooplankton was developed by Stanton (1988a,b and 1989a,b) to describe the scattering of sound by arbitrarily deformed cylinders of finite length. It became widely recognised that in addition to animal size and shape, animal orientation could have significant effects on the scattering from these elongated plankton (Greenlaw 1977; Sameoto 1980; Samovol'kin 1980; Everson 1982; Kristensen and Dalen 1986; Chu *et al.* 1993). The theoretical models were further developed and refined (Stanton *et al.* 1993a,b; 1994a,b; 1996), and this orientational dependence was incorporated by describing scattering from these elongated zooplankton at normal incidence and at a distribution of orientations near broadside incidence using an approximate ray summation model (which takes advantage of the fact that many crustacean zooplankton behave acoustically as weakly scattering bent fluid cylinders). A more precise alternative to these ray models was developed for weakly scattering elongated zooplankton of arbitrary shape at all angles of orientation using a formulation based on the distorted wave Born approximation (DWBA) volume integral (Chu *et al.* 1993; Stanton *et al.* 1993b; Stanton *et al.* in press a,b).

This paper summarises an analysis of the effect of animal orientation on acoustic scattering by Antarctic krill. Both single-frequency and broadband acoustic scattering measurements were made of several individual krill, and each animal was filmed during insonification with a high-

magnification underwater video system. A separate paper (McGehee *et al.* accepted) is devoted to investigating the orientation-dependence of the single-frequency (120 kHz) target strength measurements. The work summarised herein is focused on interpretation of the broadband (500 kHz center frequency) scattering measurements in light of orientational information extracted using a novel video analysis technique. By coupling the collected broadband echo spectra with orientation data from the video footage, the effect of animal orientation on the frequency-dependent scattering characteristics of elongated, fluid-like zooplankton such as krill may be elucidated. The echo spectra collected from krill in different orientations are presented. These echoes are compared to the theoretical model results of the DWBA volume integral, which predicts echo spectra for all angles of orientation. Subsequently, a classification inversion using the model based Covariance Mean Variance Classification (CMVC) technique (Martin Traykovski *et al.* submitted) is carried out, employing both theoretical and empirical models to invert the echo spectra backscattered from the krill for angle of orientation.

5.3.2 Methods

Scattering Experiment

Acoustic and video data were collected during a week-long experiment (17 August - 21 August 1995) at the Long Marine Laboratory of the University of California at Santa Cruz (UCSC). Antarctic krill (*Euphausia superba*) had been captured by Langdon Quetin and Robin Ross in the Southern Ocean near Palmer Station, Antarctica in February 1995, and placed in individual containers without food for long-term storage under refrigeration at the University of California at Santa Barbara, until transport to UCSC in August. Acoustic experiments included insonification of each live animal with a broadband chirp of center frequency 500 kHz (~350 kHz - 750 kHz). The animals were also insonified with narrowband 120 and 200 kHz transducers, as well as a 250 kHz broadband transducer (broadband insonification at 1 MHz was attempted, but the transducer was found to be too insensitive); only the results of the 500 kHz broadband work are summarised here. Insonifications of the krill were made with a pulse-echo acoustic data acquisition system. The transmit/receive transducer pair was mounted in an side-looking transducer bank, and the animal was positioned at the focal point of the transducer pair (Figure 5-8), approximately 51 cm away from the transducer array. During insonification, individual krill were suspended one at a time in the 2 m long by 0.8 m wide by 0.75 m deep tank (adapted from a fiberglass dolphin transporter) filled with filtered, chilled seawater (maintained between 2° and 5° C). Each animal was tethered to

a vertically suspended 0.12 mm monofilament line with a very fine, acoustically transparent, synthetic strand tied around the first or second abdominal segment. Animals tethered in this manner had considerable freedom of movement, while being constrained to remain in the acoustic beam. To allow investigation of correlations between the acoustic scattering of an organism and its orientation, each animal was filmed during insonification with a high-magnification underwater video system. The video camera was mounted directly above the transducer bank, looking across and slightly downward at the animal. Each insonification was marked with an acoustic pulse recorded on one audio track of the Hi-8 video tape, while a time code was continuously recorded on the other audio track. This allowed direct correlation between each acoustic return and the orientation of the animal at the time of insonification (to within 1/30 second).

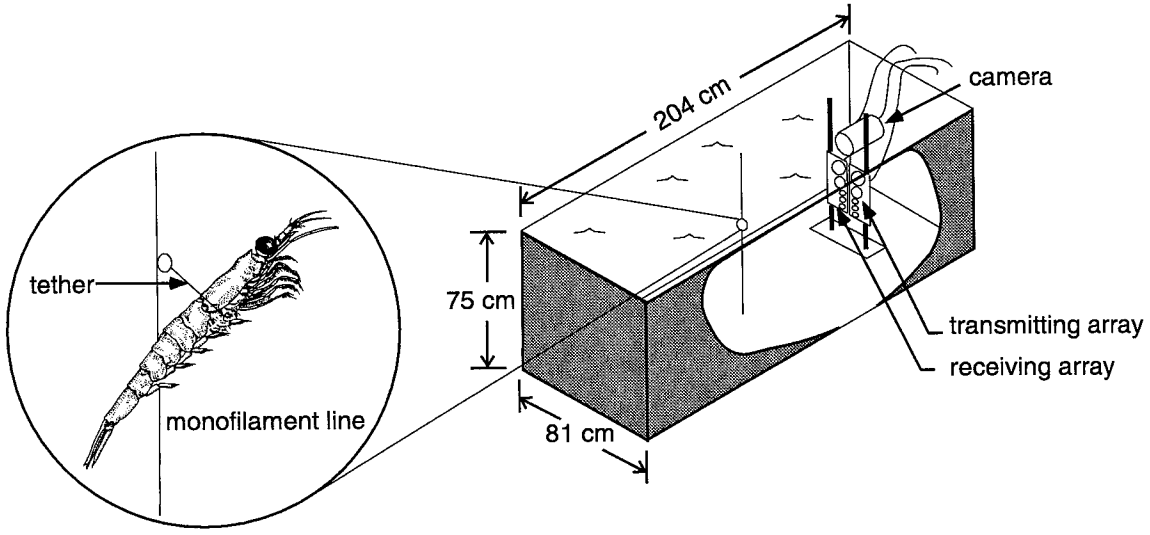

Figure 5-8 Scattering experiments were carried out in a portion of a modified fiberglass dolphin transporter. To permit freedom of movement during insonification, the animals were tethered to a vertical section of monofilament line with an acoustically transparent fine strand around the abdomen. The tethered animal was lowered to the focal point of a side-looking transducer pair. A high-magnification underwater video camera was mounted above the transducer array, looking slightly downward at the animal. Each insonification was marked with an acoustic pulse on the audio track of the video tape, so that animal orientation at the time of insonification could be determined.

After insonification, several measurements were made of each animal, including animal length, carapace height, carapace width, telson (central lobe of tail) length and wet weight (Table 5-1). Excess water was removed and each organism was frozen; dry weight was measured after oven-drying (at 60° C) at a later date. During the experiment, 14 individuals were insonified and the return echoes from 1000 acoustic transmissions were collected from each animal.

Table 5-1 Summary of measurements made of Antarctic krill. Total length measured from center of eye to tip of telson; carapace height measured at maximum dorso-ventral width; carapace width measured at maximum lateral width. * indicates animal had broken telson: total length (L2) estimated by scaling length to the end of uropods (L1) according to ratio (L2/L1) observed in other individuals of similar size; telson length also estimated by comparison to other animals of similar dimensions. Video analysis not possible for Animals 12-14 due to blurring of the video images caused by condensation on the inside of the camera housing. Dimensions in mm, weights in g.

animal #	total length	carapace height	carapace width	telson length	wet weight	dry weight	# echoes collected	# video images analysed
01	37.6	5.5	-	7.4	0.38	0.0872	1000	1000
02	42.2	5.9	-	8.6	0.51	0.1111	1000	400
03	41.4	5.4	4.4	8.4	0.55	0.1153	1000	400
04	38.9	4.8	4.35	7.7	0.38	0.0932	1000	400
05	41.4	5.3	4.4	7.1	0.56	0.1181	1000	1000
06	40.15	4.9	4.2	6.25	0.44	0.0916	1000	200
07*	33.3	4.4	3.65	6.2	0.24	0.0532	1000	1000
08	29.75	3.95	3.2	6.0	0.16	0.0363	1000	200
09	37.6	5.25	4.45	6.35	0.36	0.0702	1000	200
10	37.3	4.95	4.0	7.1	0.36	0.0689	1000	200
11	40.6	5.4	4.15	7.85	0.44	0.1016	1000	200
12	39.6	5.4	4.0	7.35	0.44	0.0884	1000	none
13*	42.9	6.0	4.9	8.1	0.55	0.1285	1000	none
14	42.45	6.15	4.6	7.7	0.58	0.1265	1000	none

Acoustic Data Processing

To obtain the echo spectrum representing the actual acoustic return from the animal, the raw signals received from the krill were combined with the results of calibration measurements, taken at the beginning (16 August 1995) and again at the end (24 August 1995) of the scattering experiments. During calibration, the transmit and receive transducers were focused on each other with no target in the beam, and a calibration signal was transmitted. The transmitted and received voltage time series were collected for these calibration measurements. During the scattering experiments, the transducers were aimed forward, focused at a range of about half a meter, and the animal was placed in this focal region. The transmitted and received voltage time series were

collected for the scattering measurements, and for each received acoustic return the calibrated echo spectrum was computed as:

$$|f_{bs}| = \left(\frac{Vrec_S}{Vrec_C}\right) \cdot \left(\frac{Vxmit_C}{Vxmit_S}\right) \cdot \left(\frac{r^2_S}{r_C}\right) \quad \text{(EQ 5.1)}$$

In (EQ 5.1), f_{bs} is the acoustic backscattering amplitude of the animal, and is a measure of the efficiency with which an object scatters sound back toward the sound source (f_{bs} is related to σ_{bs}, the differential backscattering cross section (Clay and Medwin 1977), by $\sigma_{bs} = |f_{bs}|^2$). $Vrec_C$ and $Vxmit_C$ were computed by taking the absolute value of the FFT of the received and transmitted voltage time series for calibration. $Vxmit_S$ was computed as the absolute value of the FFT of the transmitted voltage time series for scattering measured at the end of each run (every 200 pings). To compute $Vrec_S$, a fixed rectangular window was applied to the received voltage time series for each return (to capture only the echo from the animal) before applying the FFT. The scattering and calibration distances were $r_S \approx 51$ cm and $r_C \approx 60$ cm respectively. The echo spectrum ($TS = 20\log|f_{bs}|$) for each return was then sampled at 203 points between 348.33 kHz and 685 kHz (due to undesirable transducer frequency response characteristics in the upper end of its frequency range, the full bandwidth (~350-750 kHz) of the collected data was not used). It is this sampled echo spectrum that is used in analysing the effects of orientation on the frequency-dependent scattering characteristics of Antarctic krill.

Video Data Processing

Video images for 11 of the 14 animals were analysed to extract the angle of orientation of the krill corresponding to each echo spectrum (Table 5-1). For some animals, orientation was extracted from only a subset of the 1000 images, since the video analysis procedure was extremely time-consuming. Condensation inside the video camera housing obscured the images for Animals 12 through 14, so that video analysis was not possible for these individuals.

To determine the orientation of the animal corresponding to each received echo spectra, it was necessary to extract from the video tape only the frames captured at the time of each insonification, as indicated by the acoustic pulses recorded on the audio track. To accomplish this, the audio and video channels of the original Hi-8 video tapes were duplicated onto Betamax and VHS, and a screen-burn of the time code was made on the duplicates to allow easier identification and location of frames of interest. The tapes were advanced frame-by-frame using a video editing deck (e.g. for

VHS, Panasonic AG-7500, JVC BR-S525U or BR-S810U, which permit frame-by-frame advancement with an audible audio track), and the time code of each frame in which an acoustic pulse occurred was noted. The video frames of interest were then identified upon playback by the screen-burned time code, captured, digitised, and stored in TIFF format using the public domain image processing and analysis program NIH *Image* for the Macintosh.

For each image, the origin of a three-dimensional rectilinear coordinate system was situated at the base of the animal's telson (Figure 5-9**A**). In this coordinate system, the video image represents the projection of the animal onto the x-y plane, as the camera looks in the negative z-direction. The animal itself is then represented by a vector $\vec{\mathbf{a}}$ from the origin to the point midway between the center of the eyes. Measurements were made to determine the x- and y-coordinates of $\vec{\mathbf{a}}$ (a_x and a_y) for each image. Using a custom-built Matlab® measurement program, the location of the mid-point between the center of the eyes as well as the anterior edge of the conspicuous dark patch which marks the base of the telson were determined by clicking these points with a mouse; the colormap was adjusted to facilitate discrimination of these points on the images. The projected length of the animal a_{xy} (in the x-y plane) was computed as $a_{xy} = \sqrt{a_x^2 + a_y^2}$ directly from these measurements. The z-coordinate a_z of $\vec{\mathbf{a}}$ was determined using the fact that $a_z = \sqrt{|\vec{\mathbf{a}}|^2 - a_{xy}^2}$ (Figure 5-9**B**), where $|\vec{\mathbf{a}}|$ is the length of $\vec{\mathbf{a}}$, as measured from an image in which the animal was estimated to be broadside to the camera (i.e. perpendicular to the camera line of sight, $a_z = 0$). The sign of a_z was determined by noting whether the animal was head towards (a_z positive), broadside to (a_z 0), or head away from (a_z negative) the camera, as reflected by changes in the projected length of the animal a_{xy} for a succession of single images (a_{xy} attained its maximum $|\vec{\mathbf{a}}|$ when the animal was broadside to the camera). This was corroborated by watching the video in real time to estimate when broadside crossings occurred, and noting the head orientation before and after each crossing. Additional information was extracted from the images, including the x-y locations of the center of each eye, a coarse estimate of the axial roll of the animal (e.g. lateral, feet down; ventro-lateral, feet up; dorsal; etc.), and a subjective judgement of the degree of flex of the animal body (images in which the animal was very bent were discarded to minimise errors in a_{xy}).

The angle of orientation of the animal was then determined for each image by computing the angle φ between the animal vector $\vec{\mathbf{a}}$ and the incident acoustic wave vector $\vec{\mathbf{k}}$ (Figure 5-9**B**):

$$\varphi = \operatorname{acos}\left(\frac{\vec{\mathbf{k}} \cdot \vec{\mathbf{a}}}{|\vec{\mathbf{k}}||\vec{\mathbf{a}}|}\right) \qquad \textbf{(EQ 5.2)}$$

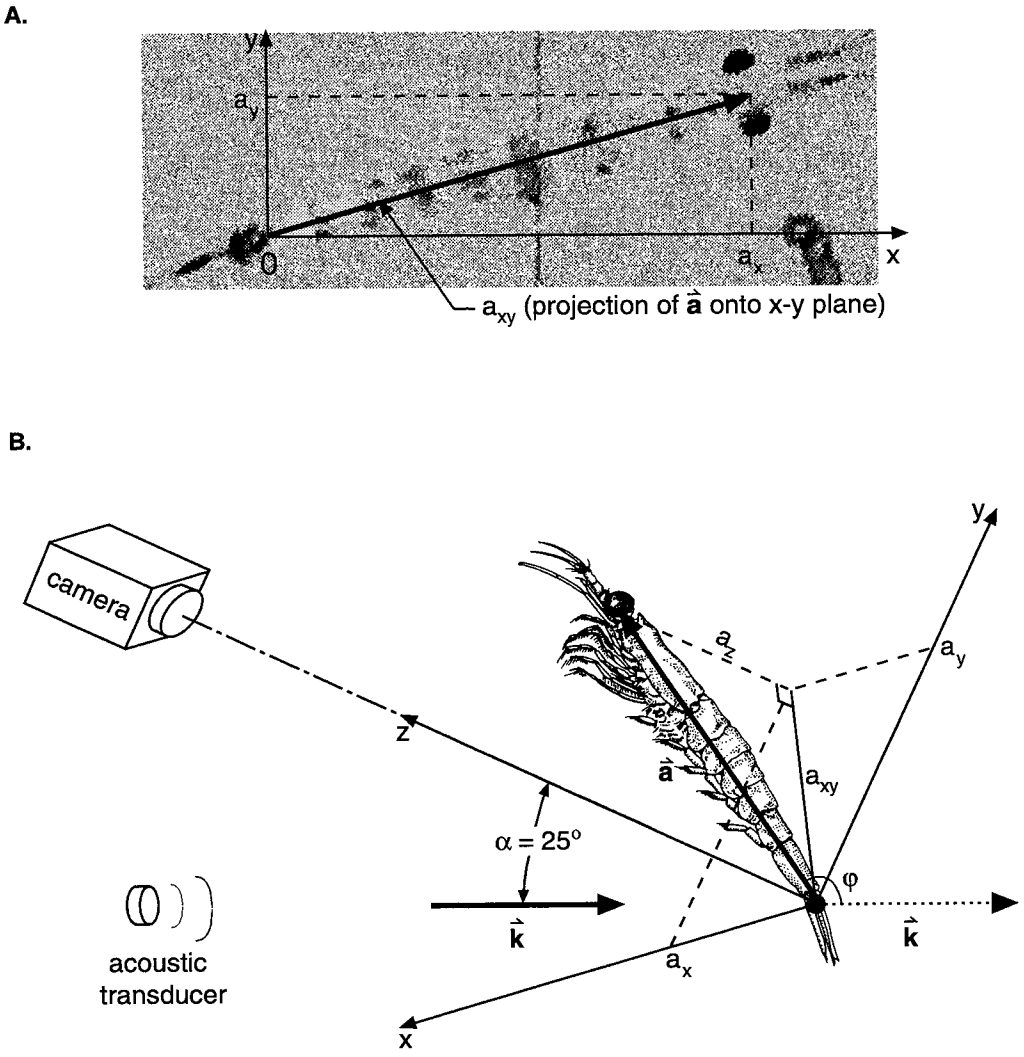

Figure 5-9 Geometry for determination of angle of orientation φ from the video images. **A.** Image gives the projection of the animal vector $\vec{a}$ onto the x-y plane of a 3-D coordinate system with origin situated at the base of the krill's telson. a_x and a_y computed directly from measurements made of the image; **B.** a_z determined from geometry shown; φ computed using (EQ 5.2); incident acoustic wave vector $\vec{k}$ is in the y-z plane, at an angle of $\alpha = 25°$ relative to the camera line of sight.

where $\vec{k} \cdot \vec{a}$ is the inner product (dot product) of the two vectors; (EQ 5.2) follows directly from the definition of the inner product: $\vec{k} \cdot \vec{a} = |\vec{k}||\vec{a}|\cos\varphi$, with $0 \le \varphi \le \pi$. For an animal located in the farfield of the transducers, the incident acoustic wave is locally planar over the body of the krill, and $\vec{k}$ is assumed to be perpendicular to the x-axis of the coordinate system, so that $k_x = 0$, and $\vec{k} = |\vec{k}|(k_x, k_y, k_z) = \frac{2\pi}{\lambda}(0, \sin\alpha, -\cos\alpha)$, where λ is the acoustic wavelength and α is the angle between the incident acoustic wave and the camera line of sight. With the animal positioned at the focal point of the transducer pair, this angle was measured as $\alpha = 25°$ (Figure 5-9**B**).

Theoretical Modelling

Acoustic backscattering from a finite-length, arbitrarily-shaped, weakly scattering (i.e. having density and sound speed similar to those of the surrounding medium) object in the farfield can be described by the general volume integral formulation (Morse and Ingard 1968) of the distorted wave Born approximation (DWBA):

$$f_{bs} = \frac{k_1^2}{4\pi}\iiint(\gamma_\kappa - \gamma_\rho)e^{i2(\vec{k}_i)_2 \cdot \vec{r}_0}dv_0 \qquad \textbf{(EQ 5.3)}$$

Recently, Chu *et al.* (1993) and Stanton *et al.* (1993b) developed a DWBA model to describe the frequency-dependent scattering characteristics of elongated, fluid-like zooplankton at all angles of orientation. If the body has a circular cross-section at every point along its length-wise axis, the DWBA volume integral (EQ 5.3) may be reduced to a line integral along this axis (Stanton *et al.* in press b), yielding an accurate expression for the scattering from an elongated, weakly-scattering fluid-like finite cylinder as a function of size, shape, material properties, and angle of orientation:

$$TS = 20\log\left|\frac{k_1}{4}\int_{\vec{r}_{pos}}(\gamma_\kappa - \gamma_\rho)e^{i2(\vec{k}_i)_2 \cdot \vec{r}_{pos}}a\frac{J_1(2k_2 a\cos\beta_{tilt})}{\cos\beta_{tilt}}|d\vec{r}_{pos}|\right| \qquad \textbf{(EQ 5.4)}$$

In (EQ 5.4), $TS = 20\log|f_{bs}|$, $k = 2\pi/\lambda$ is the acoustic wavenumber ($\lambda = c/f$ where c is the sound speed in m/s and f is the acoustic frequency in Hz), $(\vec{k}_i)_2 = \vec{k}_2 = \vec{k}_1/h$, J_1 is a Bessel function of the first kind of order 1, $\gamma_\rho = (\rho_2 - \rho_1)/\rho_2$, and $\gamma_\kappa = (\kappa_2 - \kappa_1)/\kappa_1$ with compressibility κ defined as $\kappa_i = 1/(\rho_i c_i^2)$; subscript 1 refers to the surrounding medium (seawater), subscript 2 refers to the fluid-like medium of the zooplankton body, so that $(\gamma_\kappa - \gamma_\rho) = (1/gh^2) + (1/g) - 2$, where $g = \rho_2/\rho_1$ is the density contrast of the organism relative to water, and $h = c_2/c_1$ is its sound speed contrast. This model predicts the scattering from a deformed fluid-like cylindrical body of arbitrary shape (i.e. the cross-sectional radius of the cylinder a can vary along the length-wise axis) for any angle of orientation relative to the incident acoustic wave by integrating the scattering contributions of each infinitesimally thin cross-section (located at $\vec{r}_{pos}$ along the length-wise axis, at an angle β_{tilt} relative to the incident acoustic wave) over of the entire animal body.

The line-integral DWBA formulation in (EQ 5.4) can be implemented in a numerical integration scheme to model the orientational dependence of the scattering from an animal of known size, shape, and material properties. The animal body may be discretised into several cylindrical cross-sections, each defined by a position $\vec{r}_{pos}$ along the length-wise axis of the animal body at an angle

β_{tilt} relative to the incident acoustic wave, a radius a, a density contrast g, and a sound speed contrast h. This discretisation was achieved by digitising the outline of the animal from a video image (in lateral aspect if possible), capturing several points along the dorsal and ventral surfaces (see Figures 5-11 and 5-12 A, B). This outline was then scaled to size using the measurements made of the animal after insonification (Table 5-1), and a and $\hat{r}_{pos}$ were computed for each discrete segment from each dorso-ventral pair of points. The sound speed contrast and density contrast were held constant over the animal body; values of g = 1.0357 and h = 1.0279 (as measured for *Euphausia superba* by Foote 1990) were used. For a particular angle of orientation of the animal, the backscatter at each of 203 acoustic frequencies (between 348.33 kHz and 685 kHz) was computed as the sum of the scattering contributions of each of the cylindrical cross-sections due to an incident acoustic wave vector $\hat{k}_1 = (|\hat{k}_1|\cos\beta_{tilt}, |\hat{k}_1|\sin\beta_{tilt})$. Since the orientational dependence of the scattering predicted by the DWBA model is symmetrical about 180° for an arbitrary shape with circular cross-section, the model was implemented by varying the angle of orientation in 1° increments between 0° and 180°. Appendix A of McGehee *et al.* (accepted) contains Matlab® code to implement this numerical integration scheme.

Inversion for Angle of Orientation

If the acoustic backscattered energy from elongated, fluid-like zooplankton exhibits a strong orientational dependence, biomass estimates for krill and other euphausiids based on the interpretation of acoustic survey data would be much improved by *in situ* determination of angle of orientation. Classification inversion schemes have been developed which can categorise individual zooplankton into distinct scatterer types (e.g. fluid-like, elastic-shelled, gas-bearing), as well as invert for specific parameters (e.g. animal size, animal orientation), based on the signature information contained in the return spectra of broadband insonifications of the animals (Martin *et al.* 1996; Martin Traykovski *et al.* submitted). Such a classification approach was applied to the echo spectra collected from *E. superba* during these scattering experiments to investigate the feasibility of inverting broadband acoustic returns for angle of orientation for these fluid-like zooplankton.

The Covariance Mean Variance Classifiers (CMVC) (Martin Traykovski *et al.* submitted) are a set of advanced model based techniques which classify observed echo spectra based on the correspondence between the observations and model predictions. Theoretical or empirical scattering models are used to construct a model space, which consists of model realisations

animal shapes (each approximately the size of the animal) were used as input into the DWBA, and model predictions were made as described in the previous section. The animal-specific theoretical model space generated for each animal consisted of realisations generated from the DWBA in the same manner, except the discretised shape was digitised from an image of that particular animal, so that it corresponded with the exact size and shape of that krill. The empirical model spaces included both a generic empirical model space, constructed by interpolating the echo spectra received from Animal 01 over angle of orientation (with 1° resolution), and four animal-specific empirical model spaces (for Animals 01, 03, 05 and 09), generated by interpolating the empirical data in the same manner, but based on the observed echo spectra for each animal. Only Animals 01, 03, 05 and 09 exhibited a sufficiently wide range of orientations to generate a model with nearly complete angular coverage (see orientation distribution histograms in Figure 5-10).

5.3.3 Results and Discussion

Variability in Echo Spectra with Angle of Orientation

Acoustic returns from the krill varied considerably with angle of orientation (Figure 5-10). Echo spectra from animals near broadside incidence relative to the incident acoustic wave ($\varphi = 90$) were characterised by widely-spaced deep nulls (often 20 dB or greater), usually separated by 200 kHz, whereas the frequency response of off-broadside echoes exhibited a more erratic structure, with several closely spaced (< 50 kHz) nulls of variable depth. The scattering from elongated, fluid-like zooplankton at broadside incidence is thought to be dominated by the constructive and destructive interference between the echo from the front interface and the echo from the back interface of the animal (see Figure 5-15 CASE 1). At off-broadside angles, contributions from other scattering features of the animal body are believed to become more significant, resulting in a more complicated/erratic interference pattern with many nulls (Stanton *et al.* 1994b; in press b).

The effect of orientation on average echo levels was investigated by computing the mean target strength (arithmetic mean over all frequencies) of the echo spectra received at each angle of orientation φ. Spectrally-averaged TSs (not shown) were found to be about 5 dB higher near broadside incidence vs. off-broadside for most animals. For the larger animals (e.g. Animals 02, 03, 05, 06, 11), average target strengths over the frequency band were approximately -70 dB at orientations near broadside vs. -75 dB off-broadside, whereas for the smaller animals (e.g. Animals 01, 08, 09, 10), the average *TS* near-broadside incidence was about -75 dB, versus off-broadside spectrally-averaged target strengths of approximately -80 dB. These observations are consistent

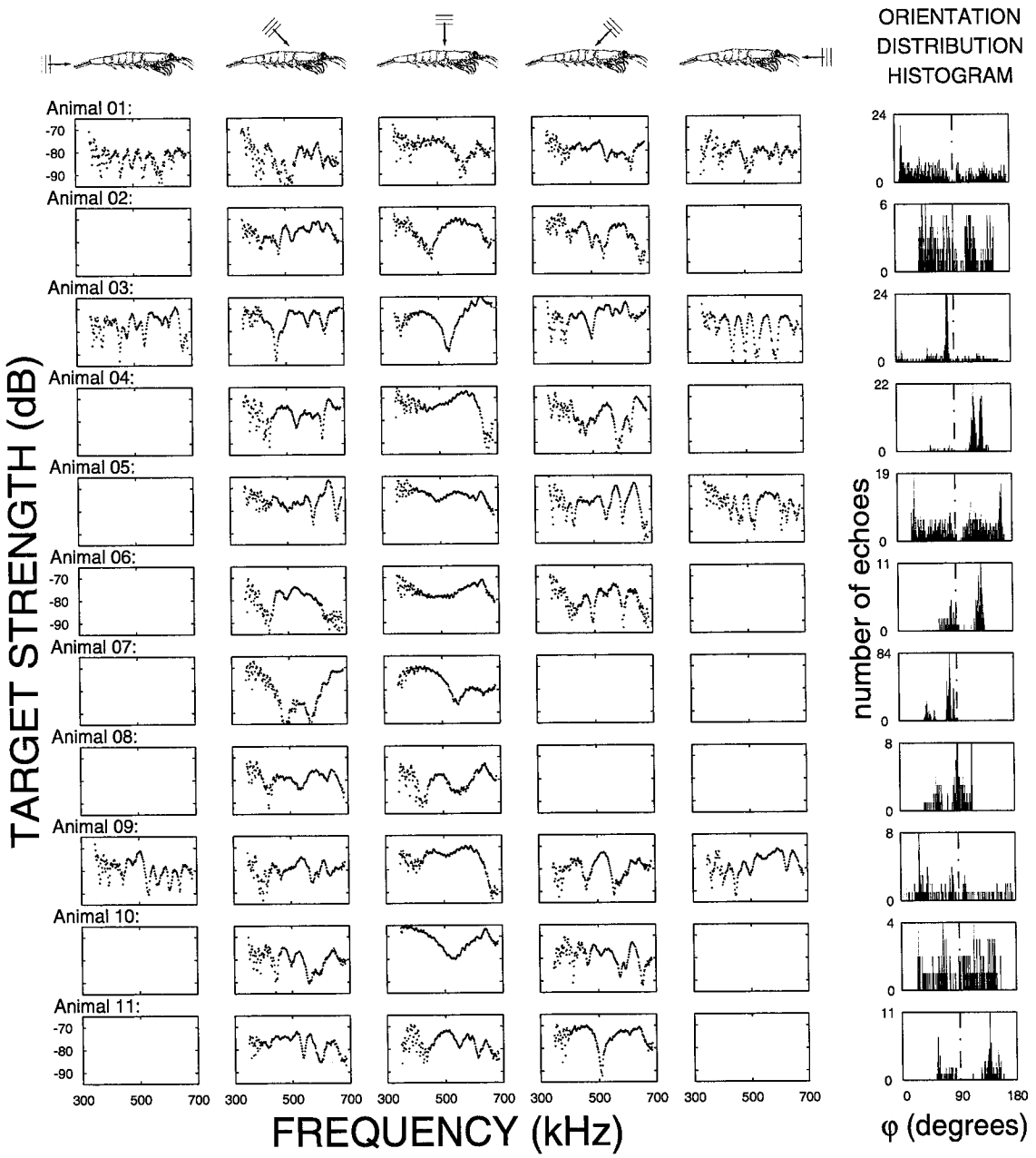

Figure 5-10 Examples of echo spectra received from 11 krill (Animals 01 through 11, rows) at 5 angles of orientation, with acoustic wave incident at $\varphi \cong 0°$, 45°, 90°, 135°, 180°(±15°) (first 5 columns); empty plots indicate that the animal did not assume that orientation during the experiment. Histogram of orientation distribution for each animal during insonification shown at right.

with what is expected based on the physics of scattering from elongated objects (Stanton 1988a,b; 1989a, 1993a,b) since at broadside incidence, an elongated krill presents a much larger backscattering cross-section to the incident acoustic wave than at any other angle of orientation.

There is a maximum of ±15° uncertainty in the calculation of φ using the video analysis method described to extract angle of orientation from two-dimensional images of the animal. Some of this uncertainty arises from possible error during measurement of the video frames, as a result of the limited pixel resolution of the image and the curvature of the animal body, both of which can affect the measured projected length of the animal. Measurement error is greatest when the animal is broadside to the camera and decreases non-linearly at angles off-broadside, since very small changes (errors) in the measured length when the projected length is maximum result in greater changes in computed angle relative to measurement errors made when the animal is off-broadside relative to the camera. An additional source of error in the calculation of φ arises from small changes in the value of α (the angle between the camera line of sight and the transducer line of sight, see Figure 5-9 B) due to uncertainty in the exact fore-aft camera position relative to the transducer bank. The maximum uncertainty of ±15° is a conservative estimate based on a sensitivity analysis of the effect of these sources of error on the calculated values of φ. In the experiment, not all animals assumed all orientations during insonification, as is evident from the histograms of the orientation distribution measured for each animal (Figure 5-10); Animals 01, 03, 05 and 09 were insonified at the widest range of angles φ. As a result of the extreme sensitivity of the measurement technique to very small changes in projected length near broadside incidence, many of the histograms exhibit low echo counts at or near $\varphi = 90°$. It should be noted that for an animal oriented broadside to the camera, φ can take on values between $90° + \alpha$ and $90° - \alpha$, so that the animal is not necessarily at broadside incidence relative to the acoustic wave.

Comparison to DWBA model theoretical predictions

Experimentally measured echo spectra versus angle of orientation φ were compared to theoretical model predictions based on a DWBA model for each animal. Two examples are presented: Animal 01 (Figure 5-11) and Animal 03 (Figure 5-12). Results for these animals are shown because they assumed the widest range of orientations during insonification, providing the best angular coverage over which to visualise the comparison between observations and theory. The pattern of changes in echo spectra with φ is very similar for the experimentally measured data and the DWBA model predicted spectra for all 11 krill, with only one or two nulls apparent in the frequency responses near broadside incidence, whereas the spectra become much more oscillatory (more peaks and nulls) off-broadside. Although the patterns agree qualitatively, the DWBA model predicts a much greater drop in *TS* (about 20 dB) as orientation changes from broadside incidence

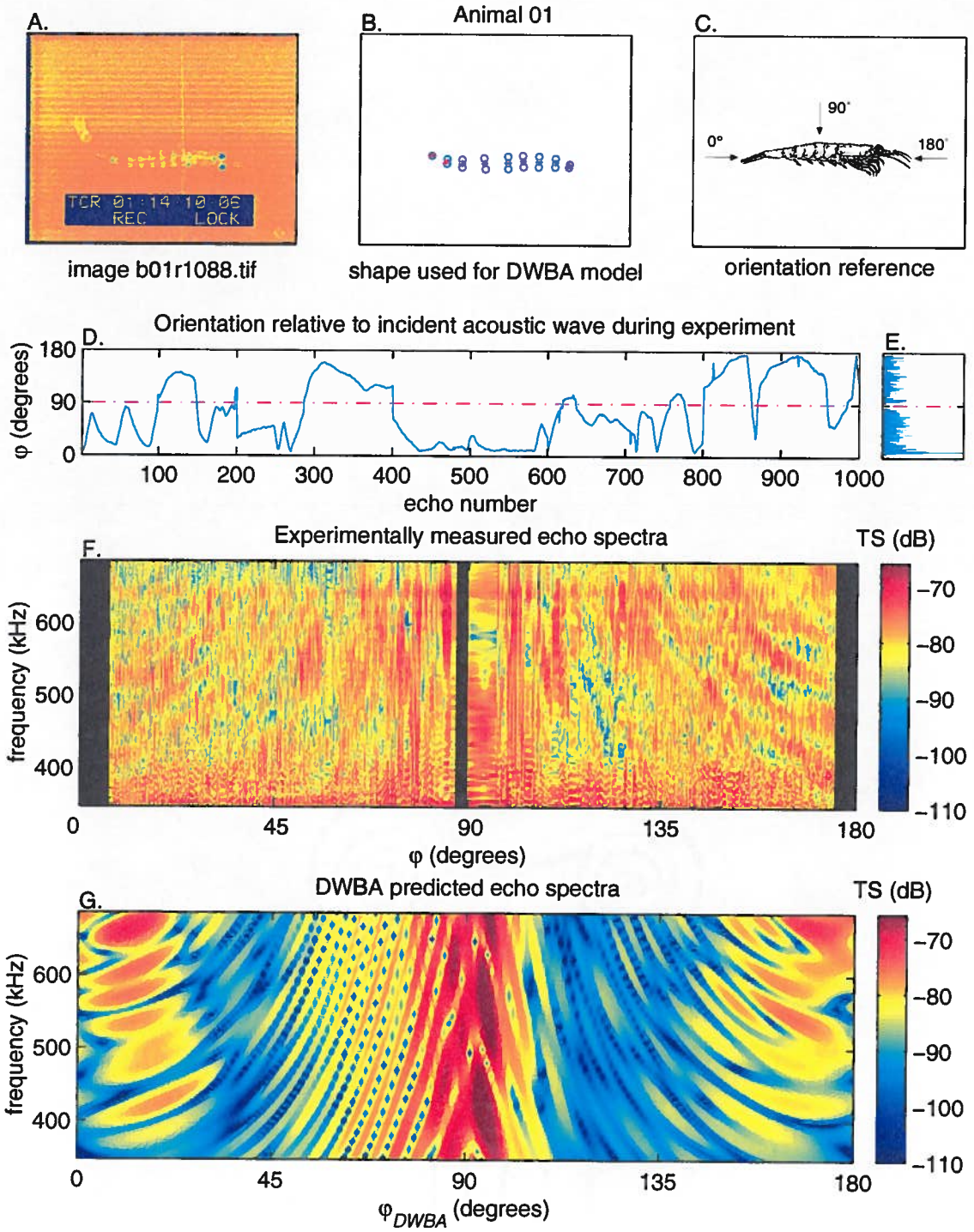

Figure 5-11 Experimentally measured echo spectra vs. DWBA model predictions for Animal 01: A. video image used to digitise animal shape; B. discretisation of animal body; C. orientation reference for DWBA modeling; D. time series of φ during insonification; E. orientation distribution histogram (n = 1000); F. measured echo spectra (y-axis, *TS* in colour) vs. angle of orientation φ (x-axis, interpolation over more than 1.5° is blacked-out); G. echo spectra predicted by DWBA model.

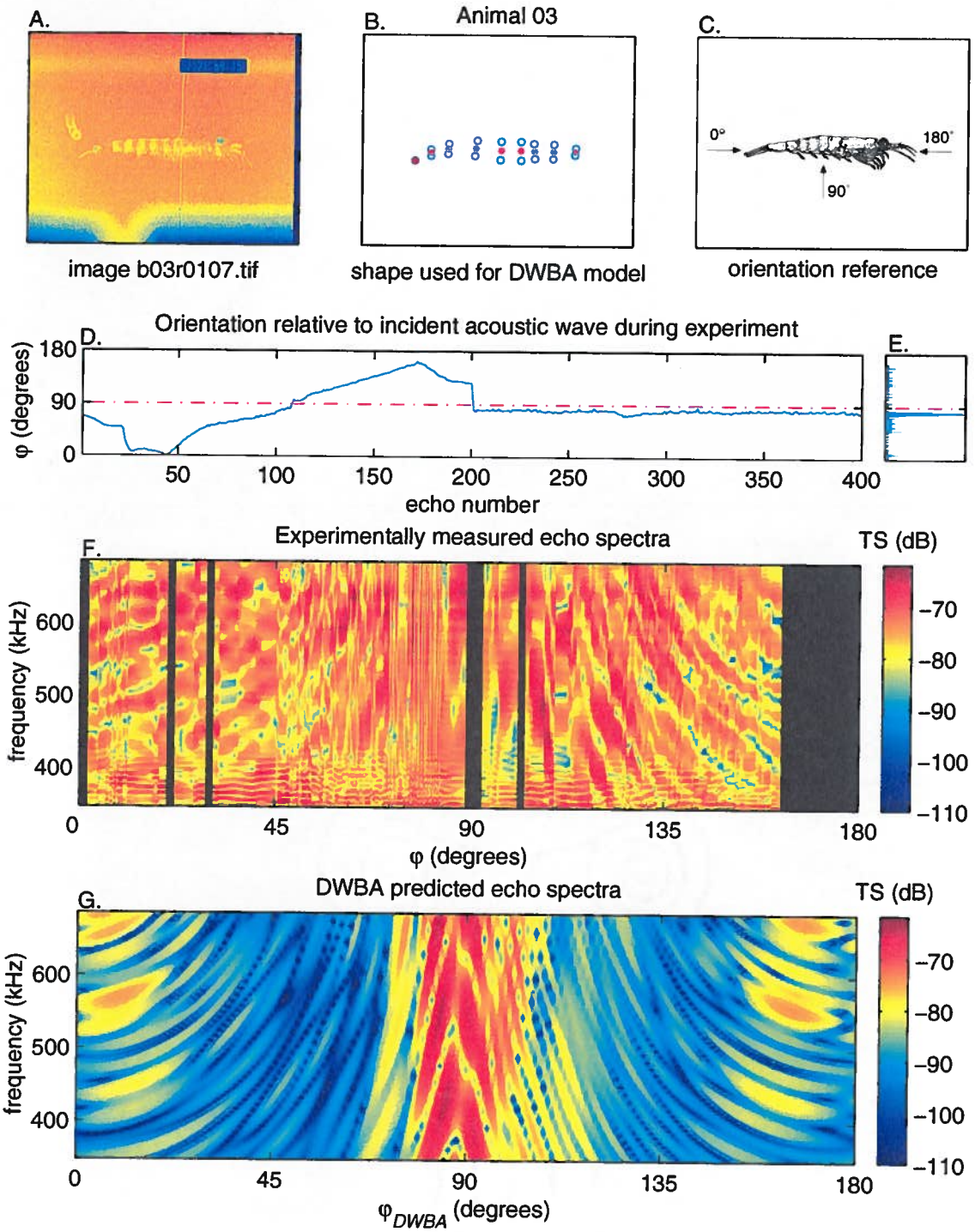

Figure 5-12 Experimentally measured echo spectra vs. DWBA model predictions for Animal 03: A. video image used to digitise animal shape; B. discretisation of animal body; C. orientation reference for DWBA modeling; D. time series of φ during insonification; E. orientation distribution histogram (n = 400); F. measured echo spectra (y-axis, *TS* in colour) vs. angle of orientation φ (x-axis, interpolation over more than 1.5° is blacked-out); G. echo spectra predicted by DWBA model.

to off-broadside (i.e. 20° - 60°, and 120° - 160°) than was actually observed for these animals as they changed orientation (about a 5 dB drop going from broadside incidence to off-broadside). Another feature of the theoretical model predictions not observed in the data is a subsequent increase in echo-levels closer to end-on (head-on and tail-on). In fact, the DWBA model consistently under-predicted off-broadside echo levels for all 11 animals, but model predictions of *TS* values near end-on were more consistent with the observations.

The DWBA theoretical model, which predicts scattering based on a highly simplified outline of the animal body by approximating it as a deformed cylinder, does not account for contributions of other scattering features of the complex animal body (e.g. rapidly moving legs). These unaccounted-for scattering features appear to make significant contributions to the observed echo levels at off-broadside angles of incidence for these krill. Examination of the time series of angle of orientation throughout the experiment revealed that for some animals orientation was rapidly varying (e.g. Animals 01 (see Figure 5-11 D), 02 and 05), whereas other krill changed orientation slowly (e.g. Animal 03 (see Figure 5-12 D), 09 and 10)), and still others (especially Animal 07) remained close to the same orientation throughout the experiment. Constraining the krill by tethering around the mid-section likely affects their activity level by eliciting an escape response. The impact of animal activity on echo levels is unknown, although some correlation between rapid swimming and elevated echo levels has been observed by the authors.

Inversion for angle of orientation

The information contained in the broadband echo spectra collected from the krill was used to invert the acoustic returns for animal angle of orientation. To accomplish this, a classification inversion using the Covariance Mean Variance Classification approach was performed on the krill echo spectra. This model based inversion was applied using both theoretical and empirical model spaces (Figure 5-13 shows raw and bin-averaged Animal 03 inversion results for both theoretical and empirical model spaces). The raw inversion results tended to be quite variable, particularly for the theoretical model spaces, whereas the bin-averaged results (obtained by averaging over five nearest neighbours) were less sensitive to outliers, and more clearly delineated how each model space performed in inverting for angle of orientation. Surprisingly, inversions obtained for most of the 11 krill using the animal-specific DWBA model space were no more accurate than could be achieved with the size-constrained generic DWBA model space. This indicates that the frequency response of the acoustic return, although sensitive to animal size, is relatively insensitive to animal

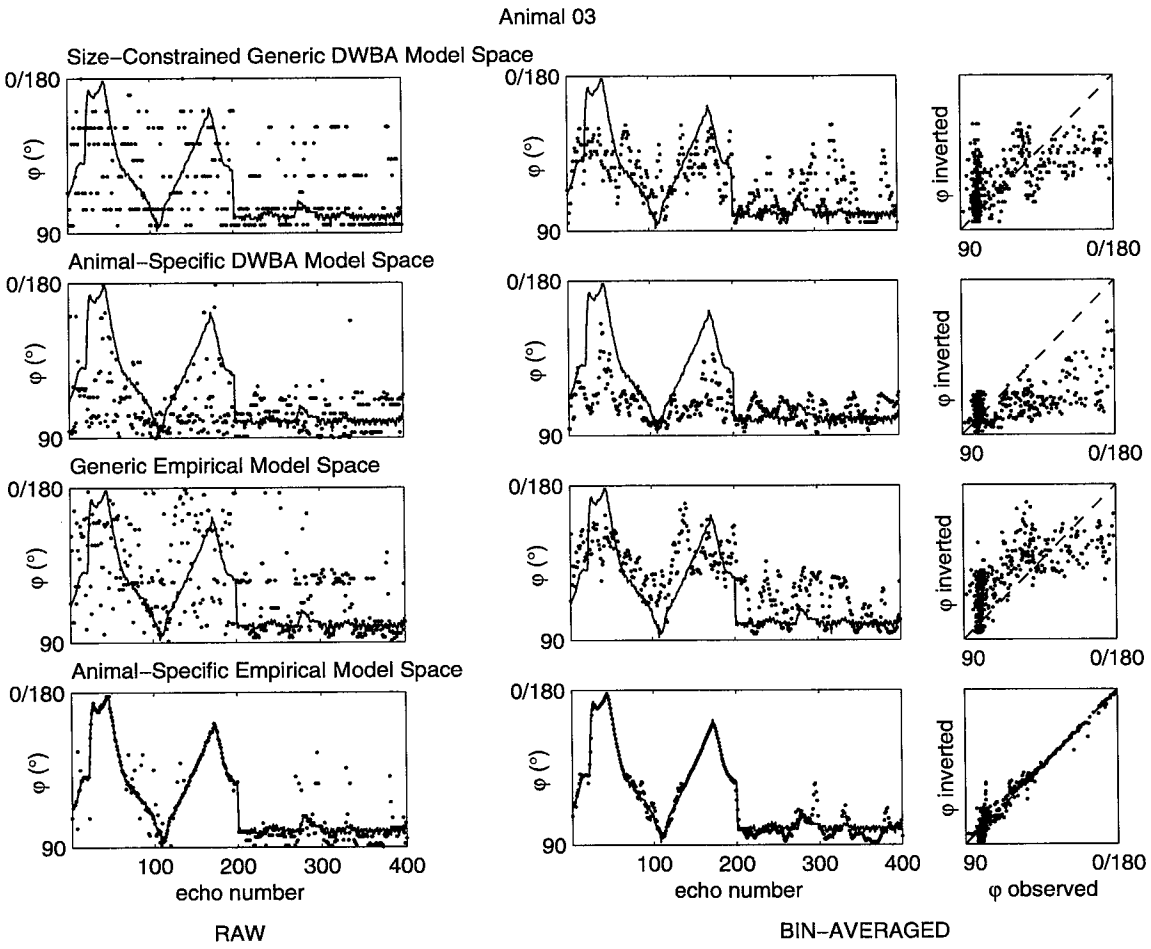

Figure 5-13 Inversion of echo spectra from Animal 03 for angle of orientation using the CMVC inversion technique, assuming symmetry about broadside incidence (90°). Observed angle of orientation φ (solid line) shown together with inversion results (points) achieved using four different model spaces: generic DWBA model space constrained to approximate size of Animal 03 (top); animal-specific DWBA model space for Animal 03 (2nd row); generic empirical model space (based on data from Animal 01, 3rd row); animal-specific empirical model space (based on data from Animal 03, bottom). Raw results shown at left, bin-averaged (over 5 echoes) results shown at right, including scatter plot of inverted vs. observed angle of orientation (dashed 45° line indicates perfect correspondence between inversion results and observations).

shape; the animal-specific model space was generated using the digitised shape of each animal scaled to the exact measured size, whereas the generic DWBA model space, although constrained to be approximately the same size as the animal, was generated using five arbitrary shapes digitised from different euphausiid zooplankton. Although the generic DWBA theoretical model space was not able to accurately invert for angle of orientation for these animals, this generic theoretical model space has been shown to be quite powerful in discriminating between different types of scatterers; the DWBA model has been employed in conjunction with two other theoretical

model spaces to classify several different species of zooplankton into three scattering classes (i.e. elastic-shelled, fluid-like, gas-bearing) based on broadband echo spectra (Martin Traykovski *et al.* submitted). While the resolution of the generic DWBA theoretical model space is sufficient for identifying krill and other euphausiids as elongated, fluid-like scatterers, it is possible that modelling these animals as simple deformed cylinders is not adequate if the goal is to invert single broadband echoes for a particular parameter (e.g. angle of orientation).

For most of the krill, the animal-specific DWBA theoretical model space did not perform as well as the generic empirical model space (which was based on acoustic returns collected from Animal 01); it would appear that a generic empirical model space based on data collected from an arbitrary krill is better able to invert for angle of orientation than an animal-specific theoretical model space, which predicts the scattering based on the actual size and shape of that particular animal. Although the generic empirical model space was based on data collected from an animal of different size and shape, it did account for contributions of other scattering features of the complex animal body not included in the simplifying theoretical model. Orientations predicted using the animal-specific empirical model space were the most accurate overall for Animals 01, 03, 05 and 09, providing a more robust inversion than that achieved with the generic empirical model space (Figure 5-14 shows generic and animal-specific empirical model space inversion results for these animals).

For these inversions (which are based on choosing the global maximum best-match echo spectra), symmetry about broadside incidence was assumed since both the observations and the theoretical model predictions for all animals exhibited considerable symmetry around 90° (see Figures 5-11 F, G and 5-12 F, G), so that a good match to a 45° model realisation will likely also be a good match to the similar 135° model realisation. In applying the CMVC inversion algorithm, the mean similarity (as represented by **X** in (EQ 5.5)) was included only for inversions using the animal-specific empirical model space. This mean comparison was suppressed when classifying with the other three model spaces, since the theoretical models had been shown to under-predict mean echo levels at many angles of orientation, and an empirical model based on a different-sized animal will exhibit different mean echo levels. In these cases, the inversion was based only on correlation in spectral structure between the observed echo spectra and the model realisations in the model space, as well as the variance similarity of the observations and the model realisations.

For elongated, fluid-like zooplankton such as krill, the structure of the frequency response depends on both size and orientation, so that it is not possible to invert broadband echo spectra for angle of

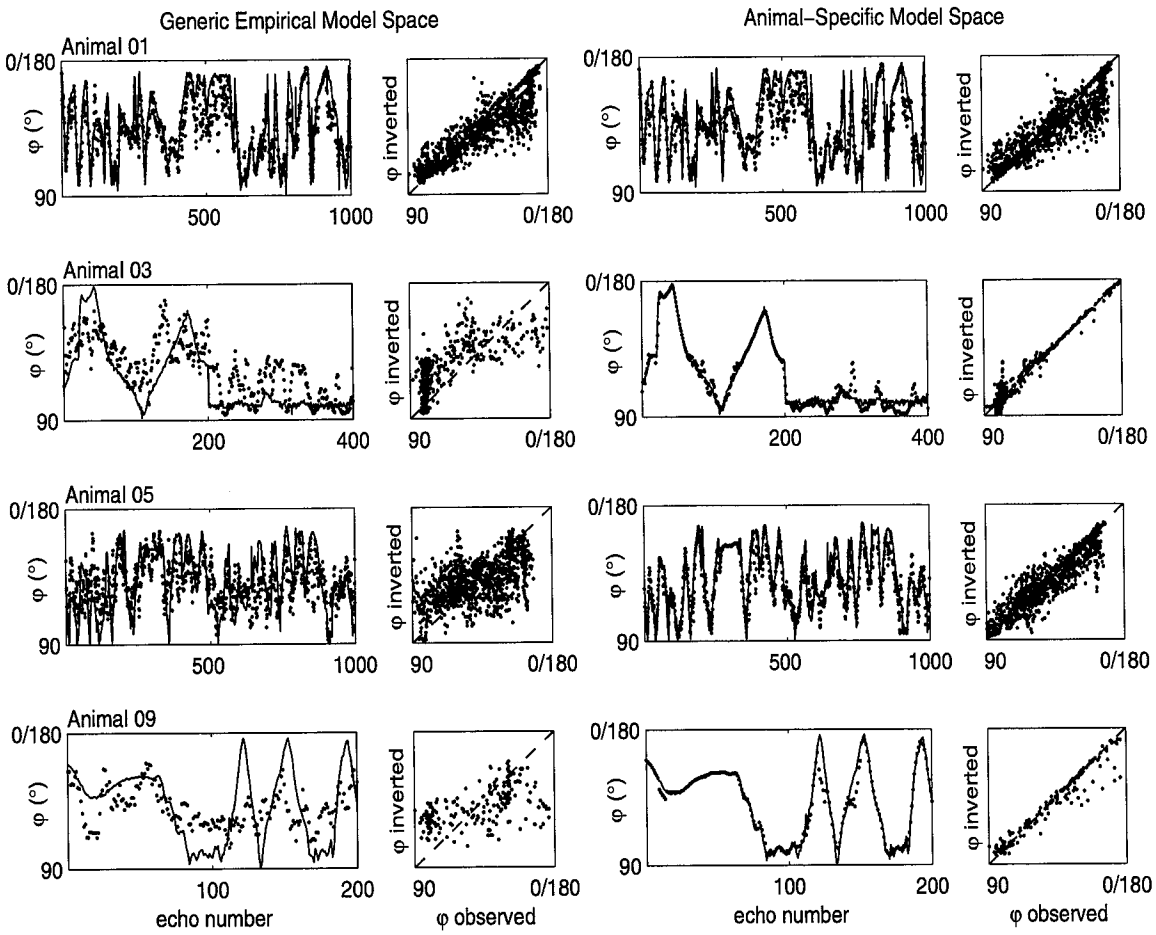

Figure 5-14 Bin-averaged (over 5 echoes) inversion results for Animals 01, 03, 05, and 09 (top to bottom) using the CMVC inversion technique (assuming symmetry about 90°) with the generic empirical model space (based on data from Animal 01, left) and the animal-specific empirical model space (right). Observed orientation φ (solid line) shown together with inversion results (points); 45° dashed line in scatter plot indicates perfect agreement between inversion results and observations.

orientation without some *a priori* information regarding animal size. In fact, animal size and angle of orientation are confounded, so that the frequency response of an echo received from a large animal may have a structure similar to that received from a much smaller animal at a different orientation relative to the incident acoustic wave. To illustrate this, consider a simple scattering model which includes a summation of only two rays (Stanton *et al.* 1993a,b), accounting for the constructive and destructive interference between the rays reflected from the front and back interfaces of a weakly scattering target such as a krill. The null spacing of the frequency response predicted by this two-ray model depends on the *apparent* size of the animal, that is, the distance the acoustic wave travels between the front and back interfaces of the animal. Apparent size is a

function of both animal radius and angle of orientation, so that the echo spectrum of a large krill at broadside incidence can exhibit the same structure as that of a smaller animal oriented off-broadside relative to the direction of insonification (Figure 5-15).

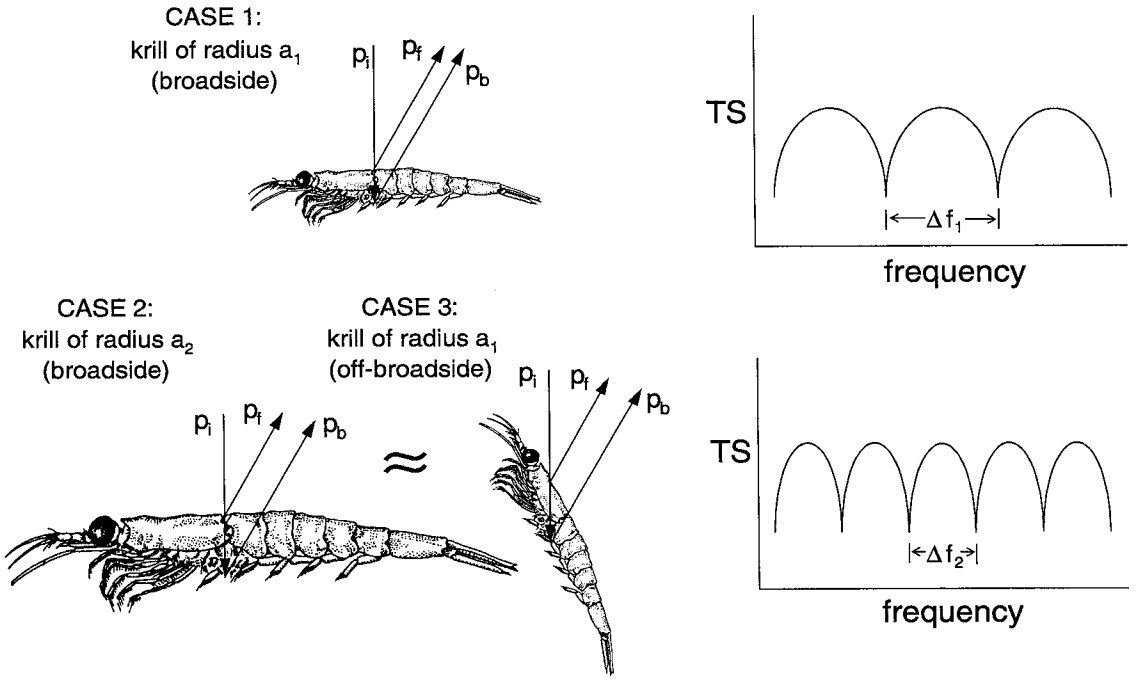

Figure 5-15 Comparison of echo spectra received from krill insonified at high frequency ($\lambda << a$) for a small animal (radius a_1) at broadside incidence (CASE 1) and off-broadside (CASE 3), and a large animal (radius $a_2 > a_1$) at broadside incidence. Nulls in the echo spectra result from destructive interference between the echo from the front interface p_f and the echo from the back interface p_b of the animal, which occurs when the phase difference between them $\phi_{f/b}$ is π radians; for the three cases shown: $\phi_{f/b} = \pi = (2\pi\Delta f_1/c)d_1 = (2\pi\Delta f_2/c)d_2 = (2\pi\Delta f_3/c)d_3$, where d is the distance the ray travels inside the body in each case, and c is the speed of sound in the body. When an animal is at broadside incidence (CASE 1 and CASE 2), $d_1 = 4a_1$ and $d_2 = 4a_2$, but off-broadside (CASE 3), the *apparent* size (to the acoustic wave) of the small krill is greater than a_1, so that $d_3 \neq d_1$. Here $d_3 \approx d_2$ so that the null spacing is the same for CASE 3 as for CASE 2 (i.e. $\Delta f_3 \approx \Delta f_2$).

Knowledge of animal orientation during insonification could significantly improve acoustic biomass estimates of zooplankton, particularly for aggregations of similarly-sized individuals of a single species, for example, swarms of Antarctic krill in the Southern Ocean. The *in situ* orientation distribution of *Euphausia superba* has not been measured quantitatively. Observations of freely-swimming *E. superba* in an aquarium indicated that they assumed a wide range of orientations (corresponding to φ varying between 40° and 180°), but spent most of the time

swimming upward at a steep angle, so that they would most often be oriented within 60° of end-on incidence relative to a downward-looking echosounder (Kils 1981). It is probable that the animals in Kils' aquarium (as well as the tethered krill insonified in these scattering experiments) assumed a much wider range of orientations than would be observed in the field by a downward-looking sonar system. In fact, qualitative *in situ* observations of *E. superba* by Hamner *et al.* (1983) revealed that all individuals in a school assumed the same orientation, and that krill in an aggregation usually swam horizontally; descending at angles of less than approximately 10° relative to the horizontal.

Information obtained via broadband insonification of individual zooplankton in the field, combined with ground-truthing of animal size (from net samples), could be inverted for angle of orientation with the CMVC inversion technique using a generic empirical model space (e.g. the one constructed based on data collected from Animal 01, or alternatively, one based on data collected from krill at known orientations *in situ*). Technological challenges that must be overcome to permit field implementation of a classification inversion based on broadband echo spectra include variable beam width and variable SNR over the bandwidth of current broadband sources suitable for field use; development of constant beam width broadband transducers is underway by others. Orientational information obtained through inversion of the frequency response of broadband echoes may then be used in conjunction with single-frequency acoustic survey data to make more accurate biomass estimates of Antarctic krill stocks in the Southern Ocean.

5.3.4 Summary

Acoustic scattering experiments involving simultaneous acquisition of broadband echoes and video footage from several Antarctic krill were carried out to determine the effect of animal orientation on echo spectral structure. Video images were analysed to determine the angle of orientation of the krill corresponding to each insonification. This analysis revealed that echo spectra from animals near broadside incidence relative to the incident acoustic wave were characterised by widely-spaced (~200 kHz) deep (>20 dB) nulls, whereas the frequency response of off-broadside echoes exhibited a more erratic structure, with several closely spaced (< 50 kHz) nulls of variable depth. Spectrally-averaged *TS* was found to be about 5 dB higher near broadside incidence vs. off-broadside for most animals. Experimentally measured echo spectra versus angle of orientation were compared to theoretical model predictions based on a DWBA model for each animal. The orientation-dependence pattern exhibited by the experimentally measured echo

spectra for all 11 krill is very similar to the pattern predicted by the DWBA model for each animal; however, the theoretical model predicts a much greater (by about 15 dB) drop in echo levels as orientation changes from broadside incidence to off-broadside than was actually observed for these animals as they changed orientation. Information contained in the broadband echo spectra of the krill was exploited to invert the acoustic returns for angle of orientation by applying the Covariance Mean Variance Classification approach, using generic and animal-specific theoretical and empirical model spaces. The animal-specific empirical model space (based on data collected from the appropriate animal) was best able to invert for angle of orientation. Notably, the generic empirical model space (based on data collected from an arbitrary krill) was better able to invert for angle of orientation than the animal-specific theoretical model space (which predicts the scattering based on the actual size and shape of that particular animal). The CMVC inversion technique can be implemented using a generic empirical model space to determine angle of orientation based on broadband echoes from individual zooplankton in the field. Pending technological development of a broadband sonar for deployment in conjunction with single-frequency acoustic surveys of Antarctic krill, extraction of this orientational information has the potential to significantly improve biomass estimates of krill stocks in the Southern Ocean.

ACKNOWLEDGEMENTS

The authors would like to thank Chuck Greene for coordinating the 1995 and 1996 Bioacoustical Oceanography Workshops, funded by the National Science Foundation and the Office of Naval Research, during which the scattering experiments and some of the data analysis were conducted. Many people contributed significantly to this work during the workshops, especially Karen Fisher, Janice Jones, Andrew Remsen, and Kathy Vigness. Thanks also to Langdon Quetin and Robin Ross of UCSB for providing the krill, Dan Costa, Bernie LeBoeuf and Betsy Steele for providing laboratory space at UCSC, and Bill Lange at the Woods Hole Oceanographic Institution for providing the video equipment. This work was completed in partial fulfillment of the requirements for a Ph.D., and LVMT would like to thank her thesis committee: Tim Stanton (who also provided the pulse-echo acoustic data acquisition system and guidance regarding the theoretical models), Peter Wiebe and Jim Lynch at WHOI, and Penny Chisholm of the Massachusetts Institute of Technology, for their support, encouragement and advice over the last five years. LVMTs research was supported by the Ocean Acoustics, Oceanic Biology and URIP programs of the Office of Naval Research grant numbers N00014-89-J-1729, N00014-95-1-0287 and N00014-92-J-1527, the Biological Oceanography program of the National Science Foundation grant number OCE-9201264 and the WHOI/MIT Joint Program Education Office. RLO would like to thank Television New Zealand and the Claude McCarthy Fellowship Foundation for supporting his participation in the workshops. DEM would like to thank Tracor and the WHOI Post-doctoral Fellowship program for support. This is Woods Hole Oceanographic Institution contribution number 9596.

REFERENCES

Anderson, V.C. 1950. "Sound scattering from a fluid sphere". J. Acoust. Soc. Am., 22: 426-431.

Chu, D., T.K. Stanton and P.H. Wiebe. 1992. "Frequency dependence of sound backscattering from live individual zooplankton". ICES J. Mar. Sci., 49: 97-106.

Chu, D., K.G. Foote and T.K. Stanton. 1993. "Further Analysis of target strength measurements of Antarctic krill at 38 and 120 kHz: Comparison with deformed cylinder model and inference of orientation distribution". J. Acoust. Soc. Am., 93: 2855-2988.

Croxall, J.P., T.S. McCann, P.A. Prince, P. Rothery. 1988. "Reproductive performance of seabirds and seals at South Georgia and Signy Island, South Orkney Islands, 1976-1987: Implications for Southern Ocean monitoring studies". pp. 261 - 285 *in* D. Sahrhage ed. Antarctic Ocean and Resources Variability. Springer-Verlag, N.Y.

Demer, D.A. and Martin, L.V. 1995. "Zooplankton target strength: Volumetric or areal dependence?". J. Acoust. Soc. Am., 98: 1111-1118.

El-Sayed, S.Z. 1988. The BIOMASS program. Oceanus, 31: 75-79

Everson, I., J.L. Watkins, D.G. Bone, and K.G. Foote. 1990. "Implications of a new acoustic target strength for abundance estimates of Antarctic krill". Nature, 345: 338-340.

Everson, I. 1982. "Diurnal variations in mean volume backscattering strength of an Antarctic krill (*Euphausia superba*) patch". Journal of Plankton Research, 4: 155-162.

Flagg, C.N. and S.L. Smith. 1989. "On the use of the acoustic Doppler current profiler to measure zooplankton abundance". Deep-Sea Res., 36: 455-474.

Foote, K.G. 1990. "Speed of sound in *Euphausia superba*". J. Acoust. Soc. Am., 87: 1405-1408.

Foote, K.G., I. Everson, J.L. Watkins and D.G. Bone. 1990. "Target strengths of Antarctic krill (*Euphausia superba*) at 38 kHz and 120 kHz". J. Acoust. Soc. Am., 87: 16-24.

Greene, C.H., T.K. Stanton, P.H. Wiebe and S. McClatchie. 1991. Acoustic estimates of Antarctic krill. Nature, 349:110.

Greenlaw, C.F. 1977. "Backscattering spectra of preserved zooplankton". J. Acoust. Soc. Am., 62: 44-52.

Greenlaw, C.F. 1979. "Acoustical estimation of zooplankton populations". Limnol. Oceanogr., 24: 226-242.

Hamner, W.M., P.P. Hamner, S.W. Strand and R.W. Gilmer. 1983. "Behaviour of Antarctic krill, *Euphausia superba*: chemoreception, feeding, schooling and molting." Science, 220: 433-435.

Hewitt, R.P. and D.A. Demer. 1991. "Krill Abundance". Nature, 353: 310.

Hewitt, R.P. and D.A. Demer. 1996. "Lateral target strength of Antarctic krill". ICES Journal of Marine Science, 53: 297-302.

Huntley, M.E. and M.D.G Lopez. 1992. "Temperature dependent production of marine copepods: a global synthesis". The American Naturalist, 140: 201-242.

Johnson, R.K. 1977. "Sound scattering from a fluid sphere revisited". J. Acoust. Soc. Am., 61: 375-377.

Kils, U. 1981. "The swimming behaviour, swimming performance and energy balance of Antarctic krill, *Euphausia superba*". BIOMASS Scientific Series, 3: 122pp.

Kristensen, A. and J. Dalen. 1986. "Acoustic estimation of size distribution and abundance of zooplankton". J. Acoust. Soc. Am., 80: 601-611.

Martin, L.V., T.K. Stanton, P.H. Wiebe, and J.F. Lynch. 1996. "Acoustic classification of zooplankton". ICES Journal of Marine Science, 53: 217-224.

Martin Traykovski, L.V., J.F. Lynch, T.K. Stanton, and P.H. Wiebe. submitted. "Model based Covariance Mean Variance Classification techniques: Algorithm development and application to the acoustic classification of zooplankton". IEEE J. Oceanic Eng.

McGehee, D.E., R.L. O'Driscoll, and L.V. Martin Traykovski. accepted. "Effects of orientation on acoustic scattering from Antarctic Krill". Deep-Sea Res.

Miller, C.B. and D.C. Judkins. 1981. "Design of pumping systems for sampling zooplankton, with descriptions of two high-capacity samplers for coastal studies". Biol. Ocean., 1: 29-56.

Morse, P.M. and K.U. Ingard. 1968. Theoretical Acoustics. Princeton University Press, Princeton, N.J. 927 p.

Nemoto, T., M. Okiyama, N. Iwasaki and T. Kikuchi. 1988. "Squid as predators on krill (*Euphausia superba*) and prey for sperm whales in the Southern Ocean". pp. 292 - 296 *in* D. Sahrhage ed. Antarctic Ocean and Resources Variability. Springer-Verlag, N.Y.

Nicol, S. and W. de la Mare. 1993. "Ecosystem Management and the Antarctic Krill". American Scientist, 81: 36-47.

Penrose, J.D. and G.T. Kaye. 1979. "Acoustic target strengths of marine organisms". J. Acoust. Soc. Am., 65: 374-380.

Permitin, Y.E. 1970. "The consumption of krill by Antarctic fishes". pp. 177 - 182 *in* M.W. Holdgate ed. Antarctic Ecology Vol. I. Academic Press, N.Y.

Sameoto, D.D. 1980. Quantitative measurements of euphausiids using a 120 kHz sounder in their *in situ* orientation. Canadian Journal of Fisheries and Aquatic Science, 37: 693-702.

Samovol'kin, V.G. 1980. Backscattering of ultrasonic waves by shrimps. Oceanology, 20: 667-670.

Stanton, T.K. 1988a. "Sound scattering by cylinders of finite length. I. Fluid cylinders". J. Acoust. Soc. Am., 83: 55-63.

Stanton, T.K. 1988b. "Sound scattering by cylinders of finite length. II. Elastic cylinders". J. Acoust. Soc. Am., 83: 64-67.

Stanton, T.K. 1989a. "Sound scattering by cylinders of finite length. III. Deformed cylinders". J. Acoust. Soc. Am., 86: 671-705.

Stanton, T.K. 1989b. "Simple approximate formulas for backscattering of sound by spherical and elongated objects". J. Acoust. Soc. Am., 86: 1499-1510.

Stanton, T.K., C.S. Clay, and D. Chu. 1993a. "Ray representation of sound scattering by weakly scattering deformed fluid cylinders: Simple physics and application to zooplankton". J. Acoust. Soc. Am., 94: 3454-3462.

Stanton, T.K., D. Chu, P.H. Wiebe and C.S. Clay. 1993b. "Average echoes from randomly oriented random-length finite cylinders: Zooplankton models". J. Acoust. Soc. Am., 94: 3463-3472.

Stanton, T.K., P.H. Wiebe, D. Chu, M.C. Benfield, L. Scanlon, L.V. Martin and R.L. Eastwood. 1994a. "On acoustic estimates of biomass". ICES J. Mar. Sci., 51: 505-512.

Stanton, T.K., P.H. Wiebe, D. Chu, and L. Goodman. 1994b. "Acoustic characterization and discrimination of marine zooplankton and turbulence". ICES J. Mar. Sci., 51: 469-479.

Stanton, T.K., D. Chu and P.H. Wiebe. 1996. "Acoustic scattering characteristics of several zooplankton groups." ICES J. Mar. Sci., 53: 289-295.

Stanton, T.K., D. Chu, P.H. Wiebe, L.V. Martin and R.L Eastwood. in press a. "Sound scattering by several zooplankton groups I: Experimental determination of dominant scattering mechanisms". J. Acoust. Soc. Am.

Stanton, T.K., D. Chu, and P.H. Wiebe. in press b. "Sound scattering by several zooplankton groups II: Scattering models". J. Acoust. Soc. Am.

Turner, J.T. 1984. The Feeding Ecology of Some Zooplankters That are Important Prey Items of Larval Fish. NOAA Technical Report NMFS 7, July 1984.

Wiebe, P.H., S. Boyd and J.L. Cox. 1975. "Relationships between zooplankton displacement volume, wet weight, dry weight and carbon:. Fishery Bulletin, 73: 777-786.

Wiebe, P.H., A.W. Morton, A.M. Bradley, R.H. Backus, J.E. Craddock, T.J. Cowles, V.A. Barber and G.R. Flierl. 1985. "New developments in the MOCNESS, an apparatus for sampling zooplankton and micronekton". Mar. Biol., 87: 313-323.

Wiebe, P.H., C.H. Greene, T.K. Stanton, J. Burczynski. 1990. "Sound scattering by live zooplankton and micronekton: Empirical studies with a dual-beam acoustical system". J. Acoust. Soc. Am. 88(5): 2346-2360.

CHAPTER 6

CONCLUSIONS AND RECOMMENDATIONS

This final chapter includes a first-order comparison of the performance of the different classification techniques developed in this thesis. Some guidelines are given for the implementation of these classification approaches based on the strengths and weaknesses of each technique. Some thoughts on the requirements for implementation of these classifiers with field-collected data are outlined, and recommendations for future research arising from this thesis work are made. The final section includes a summary of the contributions of this thesis.

6.1 COMPARISON OF CLASSIFICATION TECHNIQUES

In the course of this thesis work, a feature based classifier and several model based classifiers were developed for the purposes of classifying broadband acoustic echoes from zooplankton. The feature based Empirical Orthogonal Function Classifier (EOFC) discriminates scatterer types based on differences in echo variability without relying on the predictions of theoretical scattering models. The majority of this thesis work was focused on developing and refining model based approaches in order to best exploit the existing set of theoretical forward models, which express the relationship between backscattered echo spectra from individual zooplankton and the physical model parameters. The Model Parameterisation Classifier (MPC) depends on comparison of observed echo spectra with simplifying parameterisations of the theoretical scattering models for each class, assigning a given acoustic return to one of the three scattering classes. The Covariance Mean Variance Classifiers (CMVC), which include the Integrated Score Classifier (ISC), the Pairwise Score Classifier (PSC) and the Bayesian Probability Classifier (BPC), are a set of more advanced model based techniques which exploit the full complexity of the theoretical models by searching the entire physical model parameter space without employing simplifying parameterisations. This more sophisticated CMVC approach not only allows inversion for scatterer class, it also has the potential to invert for certain physical characteristics of the scatterer represented by the model parameters (e.g. size, orientation).

The performance of the various classifiers was evaluated with data collected during scattering experiments conducted in a ship-board tank on animals collected from Georges Bank and the Gulf of Maine. Classification results achieved with the different approaches for the entire 1993 dataset, as well as for a selected subset of the highest quality 1993 data, are compared (Table 6-1). The

high quality (high SNR) 1993 data subset consisted of 50 echoes each from a single representative of each class: for **ES** a pteropod *Limacina retroversa* 93-29; for **FL** a euphausiid *Meganyctiphanes norvegica* 93-33; for **GB** a siphonophore *Agalma okeni*. With this high quality data, feature based and model based classifiers both gave excellent results overall. The EOFC and MPC were better able to correctly classify data from the **FL** class than were the CMVC classifiers, with the exception of the best-match (max C) CMVC-PSC classifier, which produced 100% correct classifications for the high-quality data from all three classes. For both CMVC-ISC and PSC, using the best match (max C) criterion yielded better results overall than those achieved using the maximum score (max S) criterion; however, the opposite is true with the BPC, for which the maximum score results were considerably better than the best-match results.

Table 6-1 Comparative performance of classification techniques developed in this thesis. Results (% correctly classified) shown for entire 1993 dataset (right) as well as for selected subset of highest quality 1993 data (left, same subset as that shown in Figure 2-3, Figure 3-4 and Figure 4-10). For the entire 1993 dataset, spectra from the **ES** class were collected from 8 individual pteropods *Limacina retroversa*, **FL** spectra were collected from a single euphausiid *Meganyctiphanes norvegica*, and spectra from the **GB** class were collected from 9 individual siphonophores *Agalma okeni*, as described in Section 1.3. For the CMVC techniques, max S results are those based on assigning observations to the class with maximum score; max C results are those based on assigning echoes to the class containing the best match model realisation. ISC and PSC implemented with $\tilde{\mathbf{W}}_A$ and $\tilde{\mathbf{W}}_V$; BPC implemented with **TYPE II** class-support $\mathbf{f}^{(p)}$. For the high quality data, n=10 (EOFC), n=50 (MPC), n=25 (CMVC) for **ES**, **FL**, and **GB**. For all 1993 data, EOFC: n=80 (**ES**), n=200 (**FL**), n=90 (**GB**); MPC: n=400 (**ES**), n=1000 (**FL**), n=450 (**GB**); CMVC: n=200 (**ES**), n=350 (**FL**), n=225 (**GB**) (1993 validation dataset).

	1993 HIGH QUALITY DATA				ALL 1993 DATA			
CLASSIFIER:	**ES**	**FL**	**GB**	OVERALL	**ES**	**FL**	**GB**	OVERALL
M1-EOFC	100%	100%	80%	93%	95%	88%	73%	86%
MPC	100%	94%	92%	95%	37%	85%	40%	64%
CMVC-ISC: max S	100%	40%	100%	80%	16%	53%	88%	53%
max C	96%	68%	96%	87%	13%	72%	64%	54%
CMVC-PSC: max S	100%	64%	100%	88%	34%	73%	96%	69%
max C	100%	100%	100%	100%	43%	100%	100%	85%
CMVC-BPC: max S	96%	76%	100%	91%	15%	71%	79%	59%
max C	12%	84%	32%	43%	2%	95%	24%	50%

Comparing the results for the entire 1993 dataset, which includes data of variable quality (some with considerably lower SNR than the high-quality subset), the best classification performance is achieved with the feature based EOFC. The lower overall success rates of the model based MPC and CMVC result from poor performance with the *L. retroversa* data (**ES**); much of this data

exhibited a greater degree of noise contamination compared to data from the other 2 classes. The CMVC techniques represent an improvement over the MPC for some data (e.g. **GB**, **FL**), since the CMVC model spaces encompass a wider range of signal variability for each class than the MPC model spaces, resulting in more accurate classifications. Although a high overall success rate was achieved with the best-match (max C) CMVC-PSC, classification of **ES** data for this classifier was quite poor.

Those acoustic returns that are not as well-predicted by the theoretical models, particularly those with significant noise contamination, are expected to be more difficult to invert correctly with a theoretical model based inversion scheme. Although the MPC and CMVC performed very well with the high-quality sub-sample, these model based classifiers were less successful in classifying the complete dataset, in which many of the echoes had lower SNR than the high-quality subset. In particular, the model based classifiers were less successful with the *Limacina retroversa* data; this is most likely due to the presence of sufficient noise contamination so that the data did not closely resemble the theoretical model predictions. Since the MPC and CMVC rely on matching the acoustic return to predictions of the theoretical models, noise contamination is particularly troublesome for this type of classifier.

A feature based classifier such as the EOFC has the advantage of not relying on model predictions to guide the classification, and has been found to be less sensitive to noise contamination in the signal. Better results may be achieved by discriminating based on the intrinsic features of the echoes, particularly if some of these features remain unaffected by noise contamination, or can be easily distinguished from noise features (as in the case of the EOFC, where signal modes are often quite distinct from noise modes). The overall performance of the feature based EOFC was considerably better than the model based MPC, particularly for **ES** and **GB** returns. The modal feature, which represents the dominant variability in the signal, appears to be much stronger than the noise contamination in the *L. retroversa* data, contributing to the improved performance of the EOFC over the model based MPC and CMVC (EOFC: 88% correct vs. MPC: 37% correct; CMVC-PSC (max C): 43% correct). In fact, with the EOFC, most of the 5-ping ensembles for a given *L. retroversa* were assigned to the same dominant mode, indicating that returns from an individual share the same signature components. For *A. okeni* returns, the EOFC was able to discriminate the oscillatory spectra as **GB** even though the MPC classed them as **FL**, indicating that the dominant mode of variability for *A. okeni* was different than that for *M. norvegica*. Since

the EOFC classifies based on the modes of variability present in small ensembles of echoes, it may perform better than the model based classifiers when there is a high degree of within-class variability in the echoes; by considering a small group of echoes at a time instead of only one, some of the ping-to-ping variability will be captured in the modal features derived from this ensemble of echoes.

6.2 GUIDELINES FOR IMPLEMENTATION

Several approaches have been developed in this thesis for the classification inversion of zooplankton based on broadband echo spectra from individuals. Evaluation of the classification algorithms involved assessing the ability of each classifier to discriminate signatures in the presence of noise, as well as to handle the inherent ping-to-ping and animal-to-animal variability in the acoustic returns from individuals in the same scattering class. It is expected that no single inversion approach will provide the best answer under all circumstances. Some guidelines for the implementation of the various classifiers are outlined here. These guidelines are based on the relative strengths and shortcomings of each classification approach, taking into account the success rate of each classification algorithm with known data. Some of the factors considered include the differential performance of each of the classifiers with noise-contaminated or bandwidth-reduced data, success with highly variable echoes within a class, as well as differential ability to discriminate echoes from members of each of the three scattering classes (as shown in Table 6-1). Other considerations include whether or not a sound theoretical basis exists from which to develop a scattering model for each class, what type of inversion result is desired, and the computational resources available to perform the classification. The implementation guidelines are summarised in the form of a decision matrix (Table 6-2).

In order to best make use of these guidelines to arrive at a decision regarding which classification approach to implement in a particular situation, some *a priori* information is required. For example, some knowledge of the presence and degree of noise contamination, the variability of echoes expected from animals within a particular scattering class, the scatterer types present, and/ or the size and orientation of the scatterers, will serve as important *a priori* information, affecting the choice of the most appropriate inversion technique for the problem at hand. In the absence of any *a priori* information regarding data quality and/or scatterer types and attributes, the classifiers must be considered equally effective in those regards, and the implementation decision must be based solely on other criteria, such as the type of answer desired, or computational considerations.

The guidelines given in Table 6-2 can be used to preferentially weight some approaches over others in the presence of *a priori* information, while ruling out those alternatives that do not meet the requirements for a particular classification problem.

Table 6-2 Decision matrix for implementation of the classifiers developed in this thesis. Criteria/constraints listed at left. A circle "O" indicates the preferred option(s) for the criteria listed. A cross "X" indicates that classifier does not meet criteria listed, and cannot be implemented for that purpose. A dash "-" indicates that classifier was not evaluated with respect to the criterion. EOFC: Empirical Orthogonal Function Classifier; MPC: Model Parameterisation Classifier; CMVC: Covariance Mean Variance Classification techniques; ISC: Integrated Score Classifier; PSC: Pairwise Score Classifier; BPC: Bayesian Probability Classifier; max S: classification based on maximum class score; max C: classification based on best-match model realisation.

CRITERIA / CONSTRAINTS:		EOFC	MPC	CMVC	
				max S	max C
Forward model for each class:	theoretical	O	O	O	O
	empirical	O			O
	none	O	X	X	X
Type of answer desired:	assign each echo to a class	O	O	O	O
	error bounds on class assignment	X	X	O[1]	
	probability/certainty echo in each class	X	X	O[1]	
	invert for particular parameter value	X	X		O[2]
Data quality:	considerable noise contamination	O			
	high signal variability within a class	O		O	O
	reduced bandwidth	O		-	-
	single echo per individual only	X	O	O	O
A priori information:	predominantly **ES** individuals present	O			
	predominantly **FL** individuals present	O	O		O[1]
	predominantly **GB** individuals present			O[3]	O[2]
Computational power (speed, RAM, storage) available:	limited		O		
	moderate	O	O		
	high	O	O	O	O

1. PSC or BPC preferred over ISC
2. PSC only
3. ISC or PSC preferred over BPC

For inversion problems where the theoretical or empirical basis from which to construct a relationship between observed data and model parameters is not well-characterised, it is necessary to employ a feature based inversion technique, such as the EOFC, which can operate independently of a forward model. If the goal of the classification is to assign an echo to a particular scattering class, any of the classifiers are capable of producing this result; however, only

the maximum score CMVC approaches (max S) can provide error bounds on this answer, as well as giving an indication of the probability or certainty that the echo belongs to each class. The EOFC and MPC are not capable of inverting an echo spectrum for particular parameter values such as animal orientation; for this application, the best-match (max C) Pairwise Score Classifier (PSC) is the best choice. The EOFC is the preferred alternative for classification problems where there is significant noise contamination, whereas both the EOFC and the CMVC techniques perform better than the MPC in cases where there is considerable echo variability within a class. Notably, the EOFC relies on the availability of several echoes from each individual to assign it to a class, so that the availability of only a single echo per individual precludes classification with the EOFC. As summarised in Section 6.1 (see Table 6-1 for details), some of the inversion techniques give better classification results with certain scatterer types. As a result, an *a priori* estimate of the relative abundance of the different scatterers (e.g. from net tows) would be very useful in guiding classifier selection. Finally, computational considerations may place constraints on classifier choice. The CMVC approaches, for example, are computationally intensive algorithms which require a significant amount of memory (at least 100 megabytes of RAM) to implement, as well as a fast processor, and sufficient disk space for storage of the model spaces, weighting functions, and CMV metric matrices. On the other hand, the EOFC and MPC are more streamlined approaches, and although they will run faster with a faster processor, these algorithms do not have the RAM or storage requirements of the CMVC. The EOFC is more demanding of RAM and disk space (due to the modal computations) than is the MPC, which requires only a small amount of disk space to store the compact, parameterised model spaces. The decision of the most appropriate inversion approach to implement for a particular classification problem may be arrived at by weighing each of these factors based on the guidelines given in Table 6-2.

6.3 CONSIDERATIONS FOR FIELD DATA COLLECTION

The successful implementation of a classification scheme which will result in a more accurate estimate of animal biomass in the water column through the inversion of acoustic returns from zooplankton relies on the mode and quality of ocean sampling. Specific considerations include the type of acoustic data required to apply the classification scheme successfully, including the minimum data set on which these inversions could be carried out, as well as the technological developments necessary to acquire this data set. Field application of some approaches may require more than one single-target broadband insonification per individual. Spatial resolution adequate to

resolve individuals may be achieved by casting the echosounder through zooplankton aggregations in a tow-yo mode. Technological challenges that must be overcome to permit field implementation of a classification inversion based on broadband echo spectra include variable beam width and variable SNR over the bandwidth of current broadband sources suitable for field use; development of constant beam width broadband transducers is underway by others. These issues must be addressed to drive acoustic sampling technology in a direction that will facilitate the implementation of this acoustic classification approach for the purposes of increasing the accuracy of *in situ* zooplankton biomass estimates.

The classification techniques presented herein were developed using acoustic data collected from captured animals, tethered and suspended in an experimental tank. There is a possibility that the experimental conditions may have resulted in some acoustic returns, or features of these returns, that rarely would occur under natural conditions *in situ*. For example, animal behaviour and orientation *in situ* differs significantly from tethered behaviour, and it is likely that individuals insonified in the scattering experiments exhibited a much wider range of orientations than they would *in situ*. Certain artifacts may be introduced by removing the organisms from their natural environment, including multiple bubbles resulting from embolism of the single gas inclusion of siphonophores, and the retraction of pteropod feet and mucous web when captured. In the case of animals kept in long-term storage before insonification, such as the Antarctic krill, which were stored without food for about six months prior to the scattering experiments, the material properties (sound speed contrast, density contrast) of the laboratory animals may differ from those of animals under natural conditions. In addition, the experimental conditions may have introduced noise contamination that is not necessarily representative of the noise likely to be present in field-collected data. For example, many of the scattering measurements were made in a ship-board tank while cruising at normal boat speed in sea states as high as 5; sources of electrical noise from ship operations, as well as turbulence-induced temperature microstructure due to sloshing and/or stratification of the tank water, may have introduced artifacts that would not be observed under natural conditions. Although the laboratory data set may not be fully representative of *in situ* acoustic echoes from these zooplankton, the classification inversion approaches outlined in this thesis illustrate the potential of exploiting class-specific and individual-specific differences in broadband echo spectra acoustic signatures for the purposes of automatic acoustic classification of zooplankton.

The ultimate goal of acoustic sampling of the ocean is to elucidate the broad-scale distribution and abundance of animal taxa, as well as the relationship between biological distributions and the physical properties of the water column. As a result, approaches to the collection and analysis of acoustic backscatter data for the purposes of zooplankton biomass estimation are evolving toward a more integrated approach that will encompass a variety of acoustical, optical and standard physical oceanographic measurements (see Wiebe *et al.* 1997). Complementary data sets are being acquired using video techniques such as the Video Plankton Recorder (VPR), net tows with coarse depth resolution such as the Mutiple Opening/Closing Net and Environmental Sensing System (MOCNESS), as well as via environmental sensors for the measurement of micro-scale features (e.g. conductivity, index of refraction, turbulence microstructure), and fine- to coarse- scale features (e.g. temperature, salinity, optical beam transmittance, flourescence, downwelling irradiance) of the water column. Acoustic sampling now includes measurements made at a variety of frequencies, using both upward-looking and downward-looking transducers, towed at a constant depth, and tow-yowed throughout the water column. Incorporation of broadband acoustic single-target measurements into this integrated sampling regime will provide the data necessary to solve the inverse problem. Application of the classification inversion techniques developed in this thesis, in combination with the *a priori* information available from simultaneously acquired VPR imges and net tow samples, will allow identification of scatterers based on their acoustic signatures. Information about scattering class, animal orientation, and size obtained through inversion of the frequency responses of broadband echoes may then be used in conjunction with simultaneous single-frequency acoustic volume backscatter survey data to make more reliable, accurate estimates of zooplankton biomass.

6.4 RECOMMENDATIONS FOR FUTURE RESEARCH

This thesis work will serve as a departure point for future research into techniques for solving the inverse problem in zooplankton bioacoustics. A natural extension of the classification approaches developed herein is the application of these techniques to field-collected data. Pending technological development of suitable broadband acoustic transducers, each of the classification algorithms should be evaluated with data collected from known individuals *in situ*. Depending on the representativity of the tank-collected data, application of the classifiers to field data may necessitate some "re-training", particularly with respect to the validation sets used in the CMVC techniques, and possibly the modal libraries for the EOFC, since these were based exclusively on

tank-collected echoes. For example, the probability mass functions (PMF) employed in the Bayesian Probability Classifier (BPC) may need to be re-constructed based on the the underlying probability distribution of a field-observed validation set of echoes from animals in a given class, since differences between tethered and natural orientation distributions may cause this field distribution to differ from the tank-observed probability distribution. Upon field implementation, each of the classifiers should also be evaluated in light of the particular signal-to-noise (SNR) considerations experienced during field deployment, as these may differ considerably from the types and levels of noise contamination experienced in the tank. It is anticipated that classifier implementation on *in situ* echoes will be accompanied by ongoing algorithm development and refinement, so that the techniques may be fine-tuned for particular classification applications as they arise.

The preliminary results achieved with the feature based EOFC are very promising, particularly in terms of its performance in the presence of significant noise contamination and signal variability. The modal libraries for the EOFC could be supplemented using data collected during the 1994 cruise as well as the 1995 UCSC scattering experiment (for the fluid-like class only). Field deployment of this classifier may also require further development of these libraries based on the echoes collected from each scattering type *in situ*. With a large enough data set, the modal libraries should be constructed using half the data, and the other half should be employed for classifier evaluation and fine-tuning. Further investigation into alternative feature based classifers is likely to prove productive, given the success achieved with the EOFC. The development of a suite of feature based classification techniques will complement the model based classifiers, since the two approaches have different strengths. Future work should involve seeking other characteristics of the signatures (in addition to the modes of variability) that have the potential to uniquely identify a particular scattering class. Features that are the most discriminating may then be selected to be used in the classification.

Distance based classification techniques should be explored further, since a comprehensive statistical framework exists for the development and implementation of such classifiers. These techniques will allow exploration of a wider range of features, from which the best discriminators may be identified by means of a rigorous feature extraction process. Based on an extensive clustering analysis, statistical decision rules may be derived. These decision rules could be based on the multivariate probability density functions for the features for each class, as well as derived

directly from the distribution of known samples in feature space. The possibility of using ensemble-type features (possibly based on statistical analysis of several echoes) should also be explored, so that if several echoes from a single individual were available, the information contained in this ensemble of echoes could be exploited to best advantage.

In preparation for applying the classification inversion techniques on data collected *in situ*, further understanding of the limitations of each classifier in terms of sensitivity to signal degradation may be useful. In particular, the CMVC techniques could be evaluated more rigorously in this regard by applying them to simulated echoes possessing different known levels and types of noise contamination or bandwidth reduction, in much the same way the EOFC and MPC were evaluated in Sections 2.4 and 3.4. The effects of other types of signal degradation, for example, correlated additive noise, or signal contamination due to the presence of multiple zooplankton scatterers in the insonified volume, could also be investigated. The synergistic impact of the presence of more than one source of signal degradation bears investigation; for example, the effects of simultaneous bandwidth reduction and decreasing SNR (due to additive uncorrelated noise contamination) on classifer performance could be evaluated. Armed with this understanding of the performance of each classification technique under a suite of signal degradation conditions, the most suitable inversion approaches for *in situ* data may be chosen based in part on the particular signal degradation issues that arise in the field.

Another issue that has important implications for field application of these classifiers involves the data requirements for successful classifier implementation. In addition to the minimum bandwidth and SNR requirements for signature discrimination already discussed, other considerations include the number of echoes required per individual, as well as the spectral resolution necessary to sample the signatures. For the EOFC for example, although the classifier was evaluated based on an ensemble size of 5 echoes, a sensitivity analysis could be carried out to determine the effect of ensemble size on classifier performance, so that the suitability of this approach for applications with smaller or larger ensemble sizes may be judged. The EOFC, MPC and CMVC techniques were developed for application to broadband echoes for which sampling across the frequency band is continuous. To assess their applicability to situations in which only a finite number of discrete samples of the echo spectrum are available, the effect of decreasing spectral resolution on classifier performance should be evaluated to determine the degree to which classification performance degrades as the echo spectra are increasingly under-sampled.

Acoustic sampling platforms have been deployed that provide a number of discrete frequency samples, for example, MAPS (Multifrequency Acoustic Profiling System), which uses 21 frequencies from 0.1 MHz to 10 MHz (Pieper *et al.* 1990). The advanced version of BIOMAPER has 5 frequencies from 43 kHz to 1 MHz (Wiebe *et al.* 1997), but sampling in the 350-750 kHz band is limited to the data from a 420 kHz transducer. Even if the single-echo theoretical models could be extended down into the Rayleigh scattering regime for all three classes of scatterers, it is probably not possible to successfully invert for scatterer class with only these 5 frequency samples of the echo spectra (spanning approximately 5 octaves) using the model based MPC and CMVC classification approaches. The feature based EOFC is also unlikely to resolve different scatterer types from BIOMAPER data, since the structure in the echo spectra observed for the animals in the three scattering classes varies over a fairly narrow frequency range (nulls can be less than 50 kHz apart), so that the spectral resolution achievable with BIOMAPER is probably insufficient to adequately sample the modes of variability of the echoes. It is possible to chose the 5 frequencies to minimise the power aliased, but this will not guarantee an optimal signal for classification. For classification problems in which the available information content of the data is limited (e.g. with only 5 frequencies, the signal will be aliased), distance based classification techniques (as described in Section 2.1.1) are the most promising. The target strength at each of the 5 frequencies may be projected in five-dimensional feature space, and following feature extraction, decision rules can be applied to classify the echoes using classical statistical pattern recognition approaches. Preliminary work with this distance based approach has shown promise for identifying different water types and classifying waters containing different phytoplankton species based on satellite-derived water-leaving radiances in only three narrow spectral bands (Martin Traykovski and Sosik in prep.). It is likely that similar success could be achieved using this approach for the inversion of zooplankton echo spectra for scatterer type based on only a few discrete frequency samples.

Inversion for particular model parameter values (e.g. animal size or orientation) using the CMVC techniques has proven quite successful, particularly for elongated, fluid-like zooplankton. However, in order to further evaluate and refine the techniques developed to invert echo spectra for angle of orientation, more accurate orientational data needs to be collected during insonification. The single-camera video system used record animal orientation during the 1994 cruise and the 1995 workshop scattering experiments cannot provide the same accuracy as that obtainable by measuring animal orientation with a two-camera or a stereo-camera system. Future measurements of all three scatterer types would benefit from the implementation of a more sophisticated camera

system. The time required for analysis of the video data could be reduced significantly if the camera system were triggered by the outgoing acoustic signal. In this manner, every frame captured would give the orientation of the animal at the time of an insonification, eliminating the time-consuming task of sorting through thousands of frames to locate those of interest. It may be desirable to record the experiment on conventional video also, to provide a continuous record of animal movement, which in some cases can serve to resolve ambiguities.

Although the 1995 workshop experiment at UCSC focused on individuals from the fluid-like class, video data are available for individuals representing the other scattering classes from the experiments performed on the 1994 cruise. In particular, analysis of the video data for the elastic-shelled animals would be a valuable first step toward quantifying the relationship between shell orientation relative to the incident acoustic wave and changes in acoustic signature. The shape of the echo spectrum received from this animal is largely influenced by the relative contributions of the specular reflection and the energy shed by the circumferential wave, as parameterised by F_{spec} and F_l respectively in (EQ 4.13). It should be possible to quantify the relationship between these parameters and shell orientation using video data, particularly for F_{spec}, which is dependent upon the point of incidence of the acoustic wave on the shell (e.g. if the animal is oriented in such a way that the acoustic wave is incident on the opercular opening instead of the hard shell, F_{spec} is much reduced). Correlations between F_l and shell orientation may be more difficult to establish, since this parameter is largely dependent on the manner in which the circumferential wave propagates around the shell, including whether or not it experiences attenuation due to intersection with the opercular opening, which may not be obvious from orientational information obtained from the video. Detailed analysis of the effect of animal orientation on echo spectra for all three scattering classes should be accompanied by an analysis of the effects of other factors, for example, the impact of changes in density contrast g and sound speed contrast h on the acoustic signatures.

Finally, implementing the CMVC (as described in Section 5.3) for the inversion of echo spectra for specific parameter values such as angle of orientation *in situ* may require implementation of an empirical model space representative of natural conditions, particularly if the *in situ* orientation distribution differs from that observed in the tank. In general, a much better understanding of *in situ* zooplankton orientation is necessary. This will require dedicated studies of natural animal behaviour. Quantification of the orientation distribution of the scatterers of interest under natural conditions would provide important *a priori* information to help constrain the classification inverse, contributing to improvements in the accuracy of zooplankton biomass estimates.

6.5 CONTRIBUTIONS OF THIS THESIS WORK

- Establishment of a comprehensive framework for the development of feature based and model based classification techniques for the inversion of broadband echo spectra for zooplankton scatterer class.

- Development of a feature based classifier, the Empirical Orthogonal Function Classifier (EOFC), which discriminates between scatterer classes by identifying the characteristic modes of variability in the echo spectra for each class.

- Development of a streamlined theoretical model based classification approach, the Model Parameterisation Classifier (MPC), which exploits the predictive power of the theoretical models for each scatterer class, distinguishing the echo spectra by relying on simplified parameterisations of the theoretical model predictions.

- Detailed study of the sensitivity of the feature based (EOFC) and simplified model based (MPC) classifiers to signal degradation, including the effects of contaminating noise and bandwidth reduction on classifier performance.

- Development of a suite of sophisticated theoretical model based classification techniques, the Covariance Mean Variance Classifiers (CMVC), which rely on comparisons of observed echo spectra to theoretical model generated model spaces (encompassing theoretical model predictions for particular parameter values spanning the entire parameter space) to classify broadband echoes from zooplankton into scattering classes based on similarities in covariance, mean, and variance, while accounting for ambiguity between model spaces as well as model validity (representativity). The CMVC is a general formulation, applicable to a wide variety of classification problems in oceanography.

- Development of an approach for the determination of angle of orientation at the time of insonification employing a novel video data analysis technique, and application of this technique in combination with acoustic data analysis to elucidate the effects of animal orientation on acoustic signature.

- Development of theoretical and empirical model spaces for the inversion of broadband echoes from elongated fluid-like zooplankton for angle of orientation.

- Specification of guidelines for the implementation of the classification inversion techniques.

ACKNOWLEDGEMENTS

There are many individuals without whom this thesis work would not have been possible, and I would like to thank them by acknowledging their contributions to my work. My co-advisors Tim Stanton and Peter Wiebe, and my thesis committee Penny Chisholm and Jim Lynch, have supported me in this work over the last five years; their advice and encouragement is much appreciated.

There were many individuals involved in the collection of the data used in this thesis during the 1993 and 1994 cruises, as well as the 1995 Bioacoustics Workshop at UCSC. For the 1993 and 1994 cruises, my advisor Tim Stanton spearheaded the research program, lead every aspect of the experiment, and was fully involved in the data collection activities. Special thanks to Dezhang Chu, who was always happy to answer questions about the data. Many thanks also to Mark Benfield, Nancy Copley, Charlie Corwin, Bob Eastwood, Duncan McGehee, Lori Scanlon, and the captains and crews of RV "Oceanus" and RV "Endeavor" for helping to collect such a great data set. Thanks to Bill Lange for the underwater video camera equipment. A warm thank you to Chuck Greene from Cornell University for organising the three Bioacoustics Workshops I attended; these provided a stimulating, interactive, and productive atmosphere in which to accomplish experimental work and data analysis, and an opportunity to meet a group of talented colleagues, among whom are those who contributed to the krill experimental work: Karen Fisher, Kathy Vigness, Janice Jones, and Andrew Remsen; and those who provided resources: Langdon Quetin and Robin Ross (who provided the krill), and Dan Costa, Bernie LeBoeuf, and Betsy Steele (who provided laboratory space). A very special thank you to my co-authors Duncan McGehee and Richard O'Driscoll for all their hard work and their careful review of the manuscript.

Many people at WHOI were very generous with their time and resources, providing a welcoming and supportive environment in which to work. Special thanks to Hal Caswell for providing me with lab space, computer resources, and funding support over the last five years. Past and present members of the Caswell lab have been very kind in sharing their space, and have always been there to discuss my ideas with me: Mike Neubert, Mark Hill, Jesus Pineda, Mercedes Pascual-Dunlap, Myriam Barbeau and Sarah Little. Thanks also to Dan Smith, who has provided patient computer support, including solutions to any roadblocks I encountered in my data analysis. And a special thank you to Andy Solow, who has always been generous in his support, and in sharing his time and ideas, and Heidi Sosik, whose support and encouragement have been important to me.

Thanks to the WHOI/MIT Joint Program Education Office for partial funding, as well as their friendly staff; thanks also to the past and present educational coordinators for their dedication to helping the students. Other sources of funding for my thesis work include the Ocean Acoustics, Oceanic Biology and URIP programs of the Office of Naval Research grant numbers N00014-89-J-1729, N00014-95-1-0287 and N00014-92-J-1527, and the Biological Oceanography program of the National Science Foundation grant number OCE-9201264. Thanks to John Steele and Van Holliday for arranging funding for me to attend the ICES Bioacoustics Symposium in Aberdeen.

My friends and family have been a foundation of support for me over the last five years. Thanks to my dear friends Ewann Agenbroad-Berntson, Becky Coverdale, Dave Demer, and Lisa Garland, whose support has meant so much to me. A warm thank you to my parents, my brother Eric and his family, my Nonna, and my parents-in-law, who have been unfailing in their confidence in me. A pat on the head for my steadfast companion the Blue dog, who attended lectures with me, took excellent notes, and still loves me despite the walks I missed when I put this work ahead of him. Finally, a very special thank you to my husband Peter for all his love, patience and encouragement over these past five years.

REFERENCES

Aki, K. and P.G. Richards. 1980. Quantitative Seismology. Theory and Methods Vol. II. Chapter 12. W.H. Freeman and Co. San Francisco.

Anderson, V.C. 1950. "Sound scattering from a fluid sphere". J. Acoust. Soc. Am., 22: 426-431.

Backus, G. and F. Gilbert. 1967. "Numerical applications of a formalism for geophysical inverse problems". Geophys. J. R. Astron. Soc., 13: 247-276.

Biggs, D.C. 1977. "Field studies of fishing, feeding and digestion of siphonophores". Mar. Behav. Physiol., 4: 261-274.

Brown, M.G. 1984. "Linearised travel time, intensity, and waveform inversions in the ocean sound channel - A comparison". J. Acoust. Soc. Am., 75: 1451-1461.

Chiu, C.S., J.F. Lynch and O.M. Johannessen. 1987. "Tomographic resolution of mesoscale eddies in the marginal ice zone: A preliminary study". J. Geophys. Res., 92(C7): 6886-6902.

Chu, D., T.K. Stanton and P.H. Wiebe. 1992. "Frequency dependence of sound backscattering from live individual zooplankton". ICES J. Mar. Sci., 49: 97-106.

Chu, D., K.G. Foote and T.K. Stanton. 1993. "Further Analysis of target strength measurements of Antarctic krill at 38 and 120 kHz: Comparison with deformed cylinder model and inference of orientation distribution". J. Acoust. Soc. Am., 93: 2855-2988.

Clay, C.S. and H. Medwin. 1977. Acoustical Oceanography: Principles and Applications. John Wiley and Sons, N.Y. 544p.

Croxall, J.P., T.S. McCann, P.A. Prince, P. Rothery. 1988. "Reproductive performance of seabirds and seals at South Georgia and Signy Island, South Orkney Islands, 1976-1987: Implications for Southern Ocean monitoring studies". pp. 261 - 285 *in* D. Sahrhage ed. Antarctic Ocean and Resources Variability. Springer-Verlag, N.Y.

Demer, D.A. and Martin, L.V. 1995. "Zooplankton target strength: Volumetric or areal dependence?". J. Acoust. Soc. Am., 98: 1111-1118.

Deuser, L.M., D. Middleton, T.D. Plemons and J.K. Vaughan. 1979. "On the classification of underwater acoustic signals. II. Experimental applications involving fish". J. Acoust. Soc. Am. 65: 444-455.

El-Sayed, S.Z. 1988. The BIOMASS program. Oceanus, 31: 75-79

Everson, I. 1982. "Diurnal variations in mean volume backscattering strength of an Antarctic krill (*Euphausia superba*) patch". Journal of Plankton Research, 4: 155-162.

Everson, I., J.L. Watkins, D.G. Bone, and K.G. Foote. 1990. "Implications of a new acoustic target strength for abundance estimates of Antarctic krill. Nature, 345: 338-340.

Flagg, C.N. and S.L. Smith. 1989a. "On the use of the acoustic Doppler current profiler to measure zooplankton abundance". Deep-Sea Res., 36: 455-474.

Flagg, C.N. and S.L. Smith. 1989b. "Zooplankton abundance measurements from acoustic Doppler current profiling". Proceedings of Ocean '89, Mar. Tech. Soc. and I.E.E.E., Seattle, WA, September 18-21, 1989.

Foote, K.G. 1990. "Speed of sound in *Euphausia superba*". J. Acoust. Soc. Am., 87: 1405-1408.

Foote, K.G. 1991. "Summary of methods for determining fish target strength at ultrasonic frequencies". ICES J. Mar. Sci., 48: 211-217.

Foote, K.G., I. Everson, J.L. Watkins and D.G. Bone. 1990. "Target strengths of Antarctic krill (*Euphausia superba*) at 38 kHz and 120 kHz". J. Acoust. Soc. Am., 87: 16-24.

Fox, C.G., R.P. Dziak, H. Matsumoto and A.E. Schreiner. 1994. "Potential for monitoring low-level seismicity on the Juan de Fuca Ridge using military hydrophone arrays". Marine Technology Society Journal, 27: 22-30.

Fraenkel, G.S. and D.L. Gunn. 1940. The Orientation of Animals. Oxford University Press.

Fukunaga, K. 1972. Introduction to Statistical Pattern Recognition. Academic Press, N.Y.

Gilmer, R.W. and Harbison, G.R. 1986. "Morphology and field behavior of pteropod molluscs: feeding methods in the families Cavoliniidae, Limacinidae and Peraclididae (Gastropoda, Thecosomata)". Marine Biology, 91: 47 - 57.

Goodman, L., J. Oeschger and D. Szargowicz. 1992. "Ocean acoustics turbulence study: acoustic scattering from a buoyant axisymmetric plume". J. Acoust. Soc. Am., 91: 3212-3227.

Greene, C.H., T.K. Stanton, P.H. Wiebe and S. McClatchie. 1991. Acoustic estimates of Antarctic krill. Nature, 349:110.

Greenlaw, C.F. 1977. "Backscattering spectra of preserved zooplankton". J. Acoust. Soc. Am., 62: 44-52.

Greenlaw, C.F. 1979. "Acoustical estimation of zooplankton populations". Limnol. Oceanogr., 24: 226-242.

Hamner, W.M., P.P. Hamner, S.W. Strand and R.W. Gilmer. 1983. "Behaviour of Antarctic krill, *Euphausia superba*: chemoreception, feeding, schooling and molting." Science, 220: 433-435.

Haykin, S. 1988. Digital Communications. John Wiley & Sons, Inc., N.Y.

Hewitt, R.P. and D.A. Demer. 1991. "Krill Abundance". Nature, 353: 310.

Hewitt, R.P. and D.A. Demer. 1996. "Lateral target strength of Antarctic krill". ICES Journal of Marine Science, 53: 297-302.

Holliday, D.V. 1977. "Extracting bio-physical information from the acoustic signatures of marine organisms" In N.R. Andersen and B.L. Zahuranec (eds.) Oceanic Sound Scattering Prediction. Plenum Press, N.Y.

Holliday, D.V. 1980. "Use of acoustic frequency diversity for marine biological measurements". Pp. 423-460 in F.P. Diemer, F.J. Vernberg and D.Z. Mirkes (eds.) Advanced Concepts in

Ocean Measurements for Marine Biology. Belle W. Baruch Library in Marine Science #10, University of South Carolina Press, Columbia, S.C.

Holliday, D.V., R.E. Pieper and G.S. Kleppel. 1989. "Determination of zooplankton size and distribution with multifrequency acoustic technology". J. Cons. int. Explor. Mer, 46: 52-61.

Huntley, M.E. and M.D.G Lopez. 1992. "Temperature dependent production of marine copepods: a global synthesis". The American Naturalist, 140: 201-242.

Johnson, R.K. 1977. "Sound scattering from a fluid sphere revisited". J. Acoust. Soc. Am., 61: 375-377.

Kargl, S.G. and P.L. Marston. 1989. "Observations and modeling of the backscattering of short tone bursts from a spherical shell: Lamb wave echoes, glory, and axial reverberations". J. Acoust. Soc. Am., 85: 1014-1028.

Kils, U. 1981. "The swimming behaviour, swimming performance and energy balance of Antarctic krill, *Euphausia superba*". BIOMASS Scientific Series, 3: 122pp.

Kristensen, A. and J. Dalen. 1986. "Acoustic estimation of size distribution and abundance of zooplankton". J. Acoust. Soc. Am., 80: 601-611.

Lasker, R. 1966. "Feeding, growth, respiration and carbon utilization of a euphausiid crustacean". J. Fish. Res. Bd. Can., 23: 1291-1317.

Lebourges, A. 1990. "Utilisation de la spectroscopie ultrasonore en vue d'identifier les espèces de poisson". Thèse de doctorat de l'Université Paris VI.

Love, R.H. 1977. "Target strength of an individual fish at any aspect". J. Acoust. Soc. Am., 62: 1397-1403.

Lynch, J.F., S.D. Rajan and G.V. Frisk. 1991. "A comparison of broadband and narrow-band modal inversions for bottom geoacoustic properties at a site near Corpus Christi, Texas". J. Acoust. Soc. Am. 89: 648-665.

Macdonald, R. 1927. "Food and habits of *Meganyctiphanes norvegica*". J. Mar. Biol. Assoc. U.K., 14: 753-784.

Mackie, G.O. and D.A. Boag. 1963. "Fishing, feeding and digestion in siphonophores". Pubbl. staz. zool. Napoli, 33: 178-196.

Madin, L. P. 1988. "Feeding behaviour of tentaculate predators: *in situ* observations and a conceptual model". Bulletin of Marine Science, 43(3): 413-429.

Marston, P.L. 1988. "GTD for backscattering from elastic spheres and cylinders in water and the coupling of surface elastic waves with the acoustic field". J. Acoust. Soc. Am., 83: 25-37.

Marston, P.L., S.G. Kargl., and K.L. Williams. 1990. "Rayleigh, Lamb, and Whispering Gallery wave contributions to backscattering from smooth elastic objects in water described by a generalisation of GTD". Pp. 211-216 in S.K. Datta, J.D. Achenback, and Y.S. Rajapakse (eds.) Elastic Wave Propogation and Ultrasonic Nondestructive Evaluation. Elsevier, Amsterdam.

Martin, L.V., T.K. Stanton, P.H. Wiebe, and J.F. Lynch. 1996. "Acoustic classification of zooplankton". ICES Journal of Marine Science, 53: 217-224.

Martin Traykovski, L.V., J.F. Lynch, T.K. Stanton, and P.H. Wiebe. submitted a. "Model based Covariance Mean Variance Classification techniques: Algorithm development and application to the acoustic classification of zooplankton". IEEE J. Oceanic Eng.

Martin Traykovski, L.V., R.L. O'Driscoll, and D.E. McGehee. submitted b. "Effects of orientation on broadband acoustic scattering of Antarctic krill (*Euphausia superba*): implications for inverting zooplankton spectral acoustic signatures for angle of orientation". Limnol. Oceanogr.

Martin Traykovski, L.V. and H.M. Sosik. in prep. "Optical classification of water types from remotely-sensed water-leaving radiance data".

Mauchline, J. and L.R. Fisher. 1980. "The biology of Mysids and Euphausiids". Advances in Marine Biology, 18: 1-681.

McGehee, D.E., R.L. O'Driscoll, and L.V. Martin Traykovski. accepted. "Effects of orientation on acoustic scattering from Antarctic Krill". Deep-Sea Res.

Menke, W. 1989. Geophysical Data Analysis: Discrete Inverse Theory. Academic Press Inc. San Diego.

Miller, C.B. and D.C. Judkins. 1981. "Design of pumping systems for sampling zooplankton, with descriptions of two high-capacity samplers for coastal studies". Biol. Ocean., 1: 29-56.

Morse, P.M. and K.U. Ingard. 1968. Theoretical Acoustics. Princeton University Press, Princeton, N.J.. 927 p.

Morton, J.E. 1954. "The biology of *Limacina retroversa*". J. Mar. Biol. Ass. U.K., 33: 297-312.

Morton, J.E. 1964. "Locomotion". pp. 383-423 *In* K.M. Wilbur and C.M. Yonge. (eds.) Physiology of Mollusca. Academic Press, N.Y.

Munk, W. and C. Wunsch. 1979. "Ocean acoustic tomography: a scheme for large scale monitoring". Deep-Sea Res., 26: 123-161.

Nemoto, T., M. Okiyama, N. Iwasaki and T. Kikuchi. 1988. "Squid as predators on krill (*Euphausia superba*) and prey for sperm whales in the Southern Ocean". pp. 292 - 296 *in* D. Sahrhage ed. Antarctic Ocean and Resources Variability. Springer-Verlag, N.Y.

Nicol, S. and W. de la Mare. 1993. "Ecosystem Management and the Antarctic Krill". American Scientist, 81: 36-47.

Nishimura, C.E. and D.M. Conlon. 1994. "IUSS dual use: monitoring whales and earthquakes using SOSUS". Marine Technology Society Journal, 27: 13-21.

Papoulis, A. 1991. Probability, Random Variables, and Stochastic Processes. Third Edition, McGraw-Hill, Inc., New York. 666 p.

Penrose, J.D. and G.T. Kaye. 1979. "Acoustic target strengths of marine organisms". J. Acoust. Soc. Am., 65: 374-380.

Permitin, Y.E. 1970. "The consumption of krill by Antarctic fishes". pp. 177 - 182 *in* M.W. Holdgate ed. Antarctic Ecology Vol. I. Academic Press, N.Y.

Pieper, R.E., D.V. Holliday and G.S. Kleppel. 1990. "Quantitative zooplankton distributions from multifrequency acoustics". J. Plankton Res., 12: 433-441.

Pugh, P.R. and G.R. Harbison. 1986. "New observations on a rare physonect siphonophore, *Lychnagalma utricularia* (Claus 1879)". J. Mar. Biol. Ass. U.K., 66: 695 - 710.

Pugh, P.R. and M.J. Youngbluth. 1988. "A new species of *Halistema* (Siphonophora: Physonectae: Agalmidae) collected by submersible". J. Mar. Biol. Ass. U.K., 68: 1 - 14.

Purcell, J.E. and C.M. Mills. 1989. "The correlation between nematocyst types and diets in pelagic hydrozoa" In D.A. Hessinger and H. Lenhoff. (eds.) The Biology of Nematocysts. Academic Press, N.Y.

Rajan, S.D., J.F. Lynch and G.V. Frisk. 1987. "Perturbative inversion methods for obtaining bottom geoacoustic parameters in shallow water". J. Acoust. Soc. Am., 82: 998-1017.

Sameoto, D.D. 1980. Quantitative measurements of euphausiids using a 120 kHz sounder in their *in situ* orientation. Canadian Journal of Fisheries and Aquatic Science, 37: 693-702.

Samovol'kin, V.G. 1980. Backscattering of ultrasonic waves by shrimps. Oceanology, 20: 667-670.

Scalabrin, C., N. Diner, A. Weill, A. Hillion and M.-C. Mouchot. 1996. "Narrowband acoustic identification of monospecific fish shoals". ICES J. Mar. Sci., 53: 181-188.

Shinozuka, M. and C.-M. Jan. 1972. "Digital simulation of random processes and its application". Journal of Sound and Vibration, 25(1): 111-128.Smith, S.L., R.E. Pieper, M.V. Moore, L.G. Rudstam, C.H. Greene, J.E. Zamon, C.H. Flagg and C.E. Williamson. 1992. "Acoustic techniques for the *in situ* observation of zooplankton". Arch. Hydrobiol. Beih. Ergebn. Limnol., 36: 23-43.

Simmonds, E.J., F. Armstrong and P.J. Copeland. 1996. "Species identification using wideband backscatter with neural network and discriminant analysis". ICES J. Mar. Sci., 53: 189-195.

Stanton, T.K. 1988a. "Sound scattering by cylinders of finite length. I. Fluid cylinders". J. Acoust. Soc. Am., 83: 55-63.

Stanton, T.K. 1988b. "Sound scattering by cylinders of finite length. II. Elastic cylinders". J. Acoust. Soc. Am., 83: 64-67.

Stanton, T.K. 1989a. "Sound scattering by cylinders of finite length. III. Deformed cylinders". J. Acoust. Soc. Am., 86: 671-705.

Stanton, T.K. 1989b. "Simple approximate formulas for backscattering of sound by spherical and elongated objects". J. Acoust. Soc. Am., 86: 1499-1510.

Stanton, T.K. 1990a. "Sound scattering by zooplankton". Rapp. P.-v. Reun. Cons. int. Explor. Mer, 189: 353-362.

Stanton, T.K. 1990b. "Sound scattering by spherical and elongated shelled bodies". J. Acoust. Soc. Am., 88: 1619-1633.

Stanton, T.K., R. D. M. Nash, R.L. Eastwood, and R.W. Nero. 1987. "A field examination of acoustical scattering from marine organisms at 70 kHz". IEEE Journal of Oceanic Engineering, OE-12(2): 339-348.

Stanton, T.K., C.S. Clay, and D. Chu. 1993a. "Ray representation of sound scattering by weakly scattering deformed fluid cylinders: Simple physics and application to zooplankton". J. Acoust. Soc. Am., 94: 3454-3462.

Stanton, T.K., D. Chu, P.H. Wiebe and C.S. Clay. 1993b. "Average echoes from randomly oriented random-length finite cylinders: Zooplankton models". J. Acoust. Soc. Am., 94: 3463-3472.

Stanton, T.K., P.H. Wiebe, D. Chu, M.C. Benfield, L. Scanlon, L.V. Martin and R.L. Eastwood. 1994a. "On acoustic estimates of biomass". ICES J. Mar. Sci., 51: 505-512.

Stanton, T.K., P.H. Wiebe, D. Chu, and L. Goodman. 1994b. "Acoustic characterization and discrimination of marine zooplankton and turbulence". ICES J. Mar. Sci., 51: 469-479.

Stanton, T.K., D. Chu and P.H. Wiebe. 1996. "Acoustic scattering characteristics of several zooplankton groups." ICES J. Mar. Sci., 53: 289-295.

Stanton, T.K., D. Chu, P.H. Wiebe, L.V. Martin and R.L Eastwood. in press a. "Sound scattering by several zooplankton groups I: Experimental determination of dominant scattering mechanisms". J. Acoust. Soc. Am.

Stanton, T.K., D. Chu, and P.H. Wiebe. in press b. "Sound scattering by several zooplankton groups II: Scattering models". J. Acoust. Soc. Am.

Tang, X. and Stewart, W.K. 1994. "Texture classification using principle component analysis techniques". Proceedings of the European Symposium on Satellite Remote Sensing, 26-30 September, 1994, Rome, Italy.

Turner, J.T. 1984. The Feeding Ecology of Some Zooplankters That are Important Prey Items of Larval Fish. NOAA Technical Report NMFS 7, July 1984.

Vray, D., G. Gimenez and R. Person. 1990. "Attempt at classification of echo-sounder signals based on the linear discriminant function of Fisher". Rapp. P.-v. Reun. Cons. int. Explor. Mer., 189: 388-393.

Wiebe, P.H., S. Boyd and J.L. Cox. 1975. "Relationships between zooplankton displacement volume, wet weight, dry weight and carbon:. Fishery Bulletin, 73: 777-786.

Wiebe, P.H., A.W. Morton, A.M. Bradley, R.H. Backus, J.E. Craddock, T.J. Cowles, V.A. Barber and G.R. Flierl. 1985. "New developments in the MOCNESS, an apparatus for sampling zooplankton and micronekton". Mar. Biol., 87: 313-323.

Wiebe, P.H., C.H. Greene, T.K. Stanton, J. Burczynski. 1990. "Sound scattering by live zooplankton and micronekton: Empirical studies with a dual-beam acoustical system". J. Acoust. Soc. Am. 88(5): 2346-2360.

Wiebe, P.H., D. Mountain, T.K. Stanton, C.H. Greene, G. Lough, S. Kaartvedt, J. Dawson and N. Copley. 1996. "Acoustical study of the spatial distribution of plankton on Georges Bank and the relationship between volume backscattering strength and the taxonomic composition of the plankton". Deep-Sea Res. II, 43:1971-2001.

Wiebe, P.H., T.K. Stanton, M.C. Benfield, D. G. Mountain, and C.H. Greene. 1997. "High-frequency acoustic volume backscattering in the Georges Bank coastal region and its interpretation using scattering models". IEEE J. Oceanic Eng., 22:445-464.

Zakharia, M. and J.P. Sessarego. 1982. "Sonar target classification using a coherent echo processing". Proc. IEEE International Conference on Acoustics, Speech and Signal Processing, Paris, France.

VIDEO REFERENCES

"Blue Water": 1984 dives 1188, 98; 1214, 19, 35, 41, 49; 1985 dives 1329, 71, 80, 84, 96, 97; 1519 from the Gulf Stream, the Florida Current and the Bahamas, obtained from Larry Madin.

"Johnson Sea-Link 1987": 9/29/87 from Gulf of Maine & S. New England canyons, obtained from Peter Wiebe.

"Johnson Sea-Link CNN": 9/87 from Gulf of Maine, used for CNN clip, obtained from Chuck Greene at Cornell University.

"Ocean Drifters": 1993 National Geographic Explorer program, obtained from Edie Widder at Harbor Branch Oceanographic Institution.

"VPR": 5/24/92 from Georges Bank, obtained from Mark Benfield, Cabell Davis, Scott Gallagher.